Dissertation zur Erlangung des Doktorgrades
der Fakultät für Chemie und Pharmazie
der Ludwig-Maximilians-Universität München

Study of the Fumaryl Scaffold under Lewis and Superacidic Conditions

Marie Corinne Bayer

aus München, Deutschland

2022

Erklärung

Diese Dissertation wurde im Sinne von § 7 der Promotionsordnung vom 28. November 2011 von Herrn Prof. Dr. Andreas J. Kornath betreut.

Eidesstattliche Versicherung

Diese Dissertation wurde eigenständig und ohne unerlaubte Hilfe erarbeitet.

München, den 04.01.2023

……..

Marie Bayer

Dissertation eingereicht am 05.10.2022

1. Gutachter: *Prof. Dr. Andreas Kornath*

2. Gutachter: *Prof. Dr. Konstantin Karaghiosoff*

Mündliche Prüfung am 12.12.2022

„In den kleinsten Dingen zeigt die Natur die allergrößten Wunder.“

Carl von Linné (1707 – 1778)

Danksagung

Ich möchte mich zuerst bei meinem Doktorvater Herrn Prof. Dr. Andreas J. Kornath für die interessante und anspruchsvolle Aufgabenstellung dieser Dissertation, für sein Vertrauen und konstruktive Unterstützung, sowie die wissenschaftliche Freiheit bei der Anfertigung dieser Arbeit, und die Möglichkeit über mich hinauszuwachsen, herzlich bedanken.

Des Weiteren möchte ich mich bei Herrn Prof. Dr. Konstantin Karaghiosoff für die Zweitbegutachtung der vorliegenden Arbeit bedanken.

Mein besonderer Dank gilt meiner Arbeitskollegin und Arbeitskollegen Alan, Alex, Basti, Chris, Dirk, Domi, Flo, Julian, Steffi, Ulli und Valentin für die einzigartige Arbeitsatmosphäre und die schöne Zeit, die wir miteinder verbracht haben.

Ich möchte meiner Praktikantin Johanna und meinen Praktikanten Christoph und Niko für ihren tatkräftigen Beitrag zu dieser Arbeit danken.

Besonders möchte ich mich bei Chris, Alex und Valentin bedanken für das Picken von Einkristallen und das Lösen ihrer Kristallstrukturen. Ihr habt einen großen Teil zum Gelingen dieser Doktorarbeit beigetragen.

Mein Dank gilt Frau Gabriele Schmeißer und Frau Irene Scheckenbach für die tolle Unterstützung in organisatorischen Angelegenheiten.

Abschließend möchte ich mich bei meinen Freundinnen und meinem Freund Alex bedanken, die mich während meines Studiums und meiner Promotion begleitet und unterstützt haben. Ein besonderer Dank gilt meiner Familie. Danke für eure bedingungslose Unterstützung, Zuspruch, Geduld und Verständnis.

Table of Contents

1. Introduction

Cis-trans-isomerism is a particular example of stereoisomerism, in which pairs of molecules reveal identical connectivities but differ in the orientations of their functional groups in space.[1,2] Double bonds represent one key element involved in *cis–trans*-isomers, which do not rotate, and only by breaking them, interconversion of the two isomers becomes possible.[2] One of the most famous representatives of *cis-trans*-isomerism in substituted *α,β*-unsaturated alkenes might be butenedioic acid. Considering the *cis*-isomer, the functional groups are oriented on the same side of the double bond.[1] Scheme 1 shows the *cis*-butenedioic acid, which is also called maleic acid. The respective *trans*-isomer, better known as fumaric acid, represents the more stable form because the functional groups are oppositely arranged without impeding each other.[3]

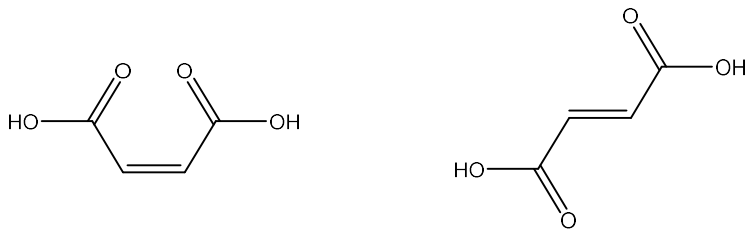

Scheme 1. Lewis structures of the two *cis-trans*-isomers maleic acid (left) and fumaric acid (right).

Fumaric acid was first isolated by *Braconnot* in 1810 from mushrooms,[4] however it received its name subsequently. In 1819 *Lassaigne* found among the decomposition products of malic acid, maleic, and paramaleic acid.[5,6] A few years later, *Winckler* isolated from the juice of common fumitory, fumaria officinalis, an acid, which was therefore named fumaric acid.[4,5,7] Finally, *Demarcay* identified paramaleic acid as fumaric acid.[5,6]

A picture together with a herbar specimen of fumaria officinalis is displayed in Figure 1. Presumably, the name “fumitory“ alludes to the visual nature of the plant, rising from the ground like fumes.[8] Common fumitory belongs to the family of papaveraceae also known as the poppy family. From the ancient world up to the present day, fumaria officinalis has played a role in human therapy.[8]

Regarding the molecular structure of fumaric acid in further detail, it reveals an alternating arrangement of double and single bonds, which is designated in literature as a conjugated system[3,9,10,11] and was first described in 1899 by *Thiele*.[12] Conjugation is referred to as the overlap of a p-orbital with the π-orbital of an adjacent double bond. In this way delocalization of the π-electrons across the adjacent aligned p-orbitals becomes possible, resulting in increased stabilization of the system due to a lowered overall energy of the molecule, a

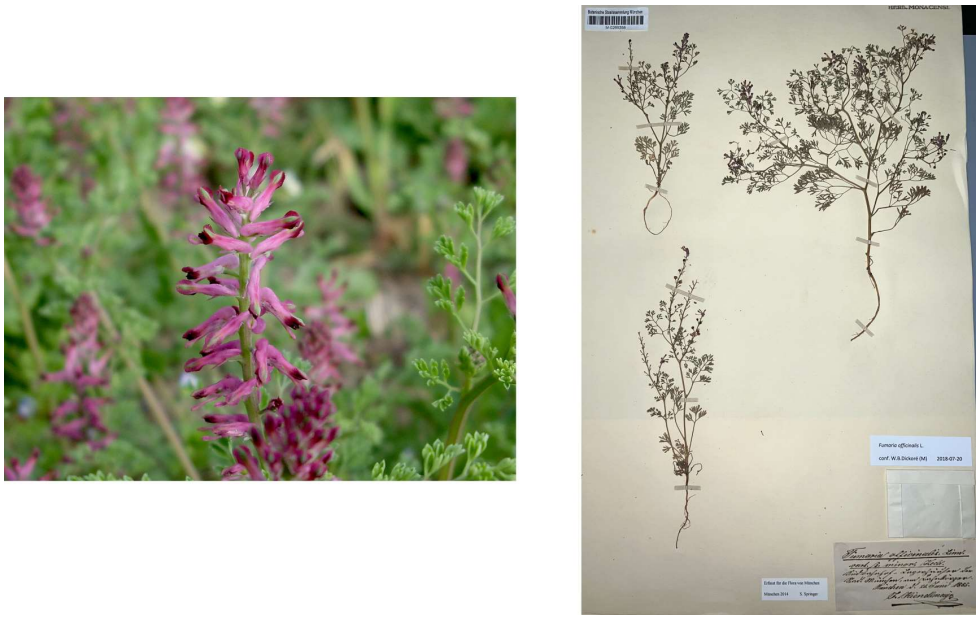

Figure 1. Fumaria officinalis (left) and its herbar specimen from 1883 of the Botanische Staatssammlung München (right).

shortening of the single bond lengths, and modified charge distribution.[9] The electron distribution of conjugated molecules is traced back to resonance stabilization and is best described using contributing structures, as described in Scheme 2 for fumaric acid.[9,10]

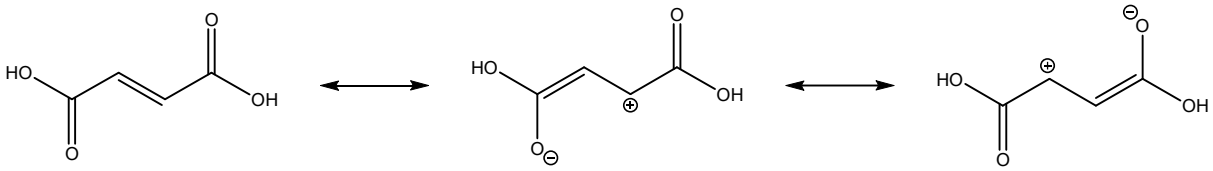

Scheme 2. Contributing structures of the conjugated molecule fumaric acid.

The conjugated system of fumaric acid provides a further special feature. A set of conformers arises from the limited rotation about the single bonds, which is established in the literature as rotational isomerism.[10,13] The three possible planar rotational isomers of fumaric acid are illustrated in Scheme 3. The *trans-trans* and the *cis-cis* conformer are both centrosymmetric, implying an inversion center as one of its symmetry elements.

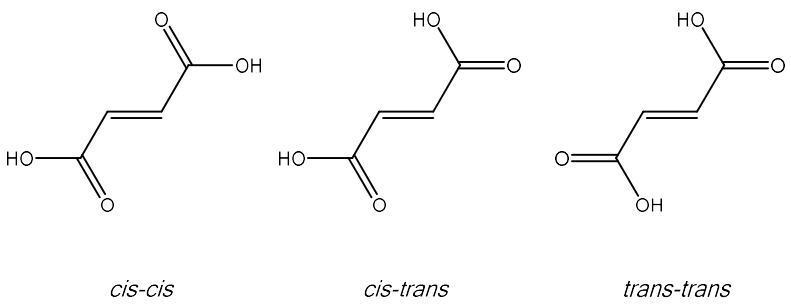

Scheme 3. Possible conformations of fumaric acid.

Since the rotational conformers are rapidly equilibrating,[2,14] the transformation of maleic to fumaric acid requires a catalyst.[3] This interconversion proceeds via c*is-trans* isomerization and is predicated on acid catalysis,[15,16] as it is described for several *α,β*-unsaturated carboxylic acids.[15,17] *Noyce et al.*[17] described the mechanism of the acid-catalyzed isomerization as an addition-elimination. The protonation of the ethylenic linkage displays the first step, followed by the hydration of the formed carbocation.[15,17] Besides, the electrophilic addition reaction, representing a typical reaction of alkenes, takes place at the C=C double bond. Thus, the ethylenic linkage of fumaric acid is attacked preferentially.[3]

The situation, however, becomes different under superacidic conditions, since they are formed in nonaqueous solutions.[18] Superacids were designated in 1927 by *Hall* and *Conant* [19] and defined in 1971 by *Gillespie* as an acid that is on the one hand capable of protonating weak bases, for instance, carbonyl compounds and on the other hand stronger than 100% sulfuric acid.[18,20] *Hammett* and *Deyrup* suggested a method to determine the strength of superacids using the Hammett acidity function H_0 (Equation (1)) referred to as the equilibrium in Equation (2).[18,21] Accordingly superacids exhibit values of H_0 less than –12.[18]

$$H_0 = pK_{BH^+} - \log\frac{BH^+}{B} \quad (1)$$

$$B + H^+ \rightleftharpoons BH^+ \quad (2)$$

Olah pioneered the use of superacids in order to stabilize carbocations, winning him the Nobel Prize in Chemistry in 1994.[22] He used for this the binary superacidic system consisting of fluorosulfuric acid and antimony pentafluoride HSO_3F/SbF_5 which was named “magic acid“ originated in Olah‘s laboratory at Case Western Reserve University.[18,22] The strongest liquid superacid is represented by the fluoroantimonic acid system HF/SbF_5, revealing H_o values of approximately –24.[18] Hence, these superacidic systems are 10^{16} times stronger compared to 100% sulfuric acid.[23]

This magic acid was used by *Larsen et al.*[15] to investigate fumaric acid under superacidic conditions. From their investigations they could not observe the protonation of the C=C double bond, instead, an O-diprotonation of fumaric acid was detected using NMR spectroscopy.[15] By substituting the functional groups of fumaric acid different molecules containing the fumaryl skeletal structure are generated, such as fumaryl halides and fumaramide, which are neither examined in Lewis acids nor superacids so far.

2. Objectives

The aim of this thesis is the investigation of different functional groups on the molecules in the fumarate series on the one hand under Lewis acidic conditions and on the other hand in superacidic media. The first topic of the thesis is engaged in the examination of the neutral compound fumaryl fluoride, illustrated in Scheme 4. The largely unknown structure and the possibility of detecting three rotational isomers attracted our attention. Moreover, investigations on fumaryl halides in strong Lewis acidic media will be carried out with the aim to examine whether a halide abstraction leads to acylium ions, or the formation of oxonium complexes occurs. For this purpose, fumaryl chloride (see Scheme 4) and fluoride will be examined in Lewis acidic media, using the Lewis acids AsF_5, SbF_5, and $SbCl_5$. The second topic of this thesis is concerned with the investigation of varying functional moieties on the conjugated system in the fumaryl scaffold in superacidic media regarding the impact of protonation on the structure of the resulting cation in combination with the respective electron distribution. Fumaric acid will be investigated in the binary superacidic media HF/MF_5 (M=As, Sb) at first to determine if the structural skeleton is transformed. Thereupon, the hydroxy groups of fumaric acid are replaced by amino groups, giving the molecule fumaramide (see Scheme 4), and furthermore exchanged for fluorines, resulting in the molecule fumaryl fluoride. The target is to investigate the effect of the protonation on the amide group and the acyl fluoride moiety, respectively, regarding the structure and the electron distribution of the fumaryl framework. Besides, the degree of protonation is considered a central aspect of these studies.

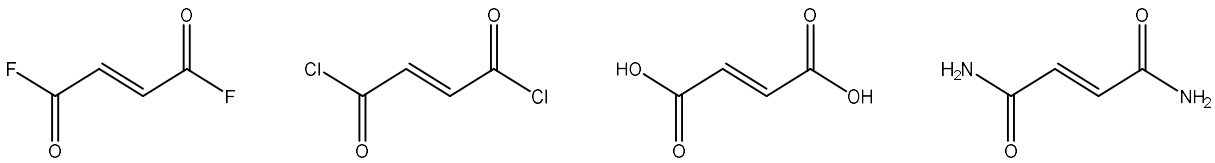

Scheme 4. Lewis structures of different molecules of the fumarate series.

3. Summary

3.1 Investigations in Lewis Acidic Media

The first subject of this thesis deals with the investigations of the molecule fumaryl fluoride. We were interested in determining the so far unknown structure and detecting three possible rotational isomers. Furthermore, we examined the behavior of fumaryl halides in Lewis acidic media with regard to the formation of acyl cations and oxonium complexes. The molecular structure, as well as the electron distribution of the resulting species, were central issues for this first part. The examination of fumaryl fluoride and chloride was conducted in the Lewis acidic media SO_2ClF/MF_5 (M=As, Sb) and $SO_2ClF/SbCl_5$. Low-temperature vibrational spectroscopy was employed for the characterization of the obtained compounds. For selected salts, a single-crystal X-ray structure analysis was performed additionally. Quantum chemical calculations were conducted to gain a comprehensive understanding of the structure and electron distribution of the formed species. Hereinafter, a summary of these studies is presented.

3.1.1 Fumaryl Fluoride

Fumaryl fluoride was synthesized by nucleophilic substitution with antimony(III) fluoride after *Vasileff et al.*[24] according to Equation (3).[25]

$$3\ C_4H_2Cl_2O_2 + 2\ SbF_3 \xrightarrow{100\ °C,\ 1h} 3\ C_4H_2F_2O_2 + 2\ SbCl_3 \quad (3)$$

With the help of low-temperature vibrational spectroscopy and single-crystal X-ray analysis, all of the possible planar rotational isomers *trans-trans*-, *cis-cis*- and *cis-trans*-fumaryl fluoride were detected, which are illustrated in Scheme 5.

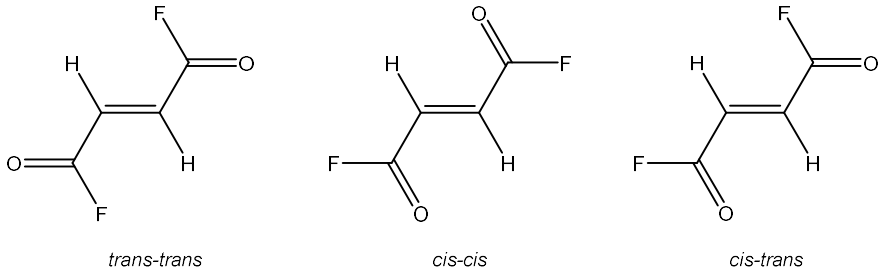

Scheme 5. Conformations of fumaryl fluoride.

Crystalline fumaryl fluoride is composed exclusively of centrosymmetric conformers. The formula unit of $C_4H_2F_2O_2$ is depicted in Figure 2. One half of the fumaryl fluoride molecules exist as *cis-cis* conformers. The other half reveals a disorder, comprising 82% *trans-trans*- and

18% *cis-cis*-fumaryl fluoride. The gaseous, liquid, and amorphous states exhibit additionally the *cis-trans* species.

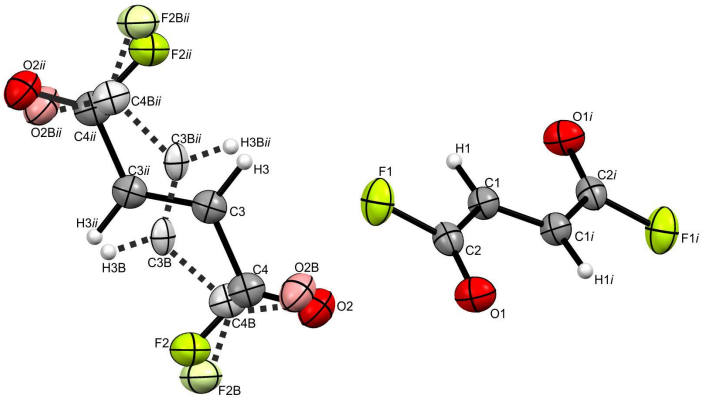

Figure 2. Formula unit of $C_4H_2F_2O_2$ (displacement ellipsoids with 50% probability). Symmetry operations: *i* = 1–x, 1–y, –z; *ii* = –x, 1–y, 1–z. *Cis-cis*-fumaryl fluoride (right) and *trans-trans*-fumaryl fluoride (left) with 18% disordered *cis-cis*-fumaryl fluoride (dashed line).

In order to compare the three rotational isomers, their energy differences were calculated at the CCSD-FC/aug-cc-pVTZ level of theory. The *trans-trans*, *cis-cis,* and *cis-trans* conformers in combination with their energy differences are shown in Figure 3.

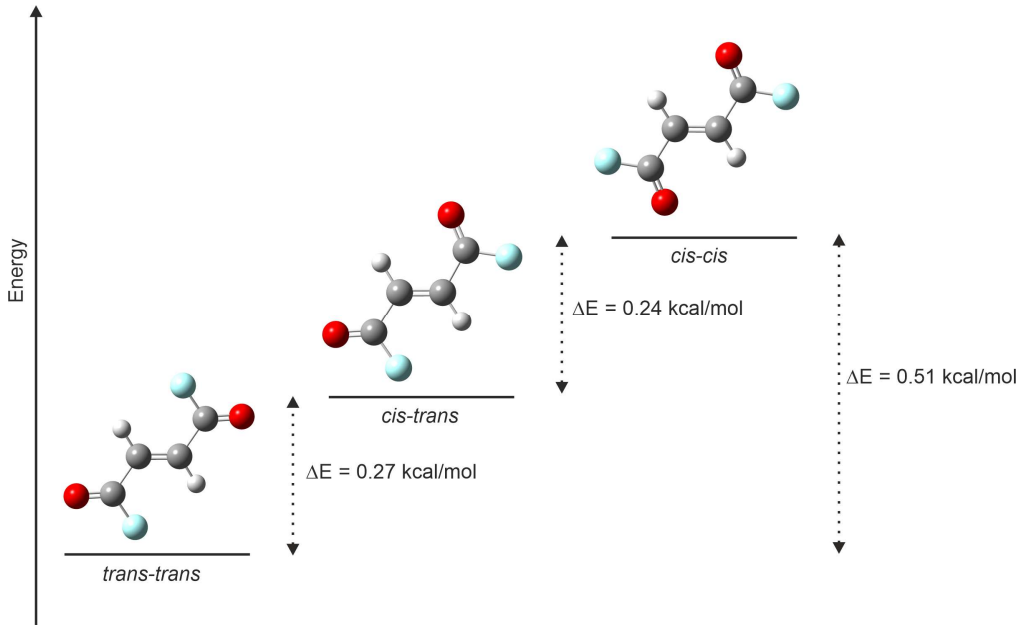

Figure 3. The three discrete conformers of fumaryl fluoride combined with their calculated energy differences.

The global energetic minimum is detected for the *trans-trans* conformer, contradicting the experimental results of crystalline fumaryl fluoride. The assumption arises that the introduction of a halogen atom must destabilize the low-energy *trans* conformer and stabilize the *cis* species.[26] One reason for this could be when conjugation is possible between the carbonyl

and the halogen substituent, the *cis* conformer is stabilized compared to the *trans* conformer,[27,28] primarily relating to the fluorine derivatives.

The comparison of fumaryl fluoride to related molecules like fumaryl chloride[29] and fumaraldehyde[30] showed that the substitution of a halogen atom for an aldehyde proton has a substantial effect on the relative order of stability of the *cis* and *trans* conformers.[27] In the case of the substituent being a halogen atom, the relative energies of the rotational isomers appear to be considerably reduced.[14,26]

3.1.2 Oxonium Complexes and Acyl Cations of Fumaryl Halides

Fumaryl halides were reacted in different Lewis acidic media in order to investigate the formation of complexes and acyl cations. Mono- and diadducts are formed according to Equations (4) and (5) for the reaction of fumaryl fluoride with AsF_5 in liquid SO_2ClF.[25]

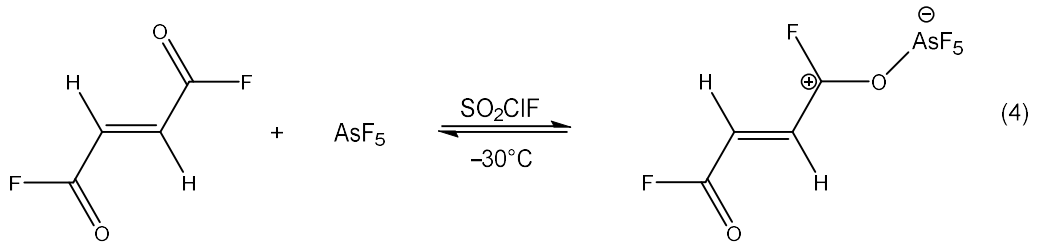

(4)

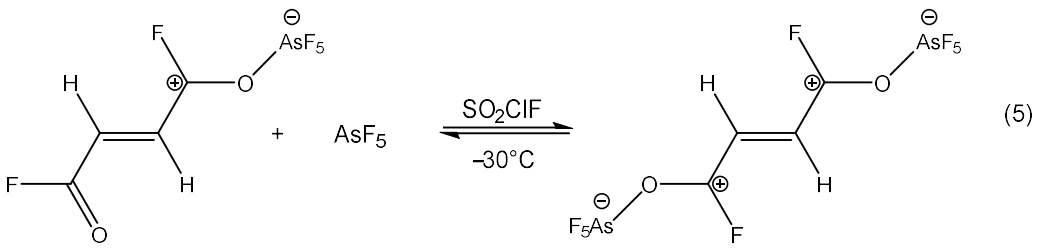

(5)

The oxygen-coordinated monoadducts of fumaryl fluoride with AsF_5 consist of the *cis-trans* conformers of fumaryl fluoride. The respective diadduct crystallizes as the centrosymmetric *trans-trans* conformer. A detail of the crystal structure of $C_4H_2F_2O_2$, 4 ($C_4H_2F_2O_2 \cdot AsF_5$), $C_4H_2F_2O_2 \cdot 2\ AsF_5$ comprising four different species is depicted in Figure 4.

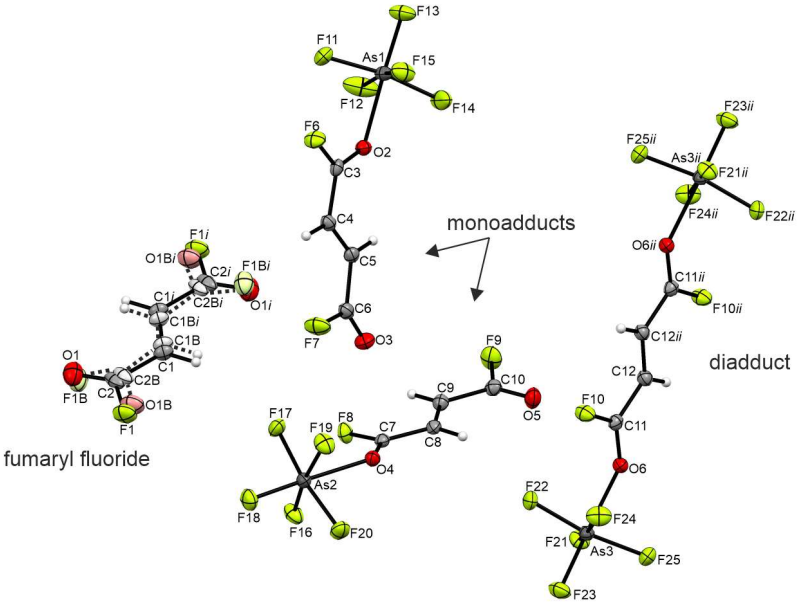

Figure 4. Detail of the crystal structure of $C_4H_2F_2O_2$, 4 ($C_4H_2F_2O_2 \cdot AsF_5$), $C_4H_2F_2O_2 \cdot 2\ AsF_5$ (displacement ellipsoids with 50% probability). Symmetry operations: *i = –x, 1–y, –z; ii = –x, –y, 2–z*. (*Cis-cis*-fumaryl fluoride with disordered *trans-trans*-fumaryl fluoride (dashed line)).

To investigate the Lewis basic characteristics of the higher homologous element, fumaryl chloride was reacted with $SbCl_5$ under the same conditions. This reaction led to a covalent donor-acceptor complex with oxygen-bonded $SbCl_5$ as per Equation (6). The formula unit of $C_4H_2Cl_2O_2 \cdot 2\ SbCl_5$ is shown in Figure 5.[31]

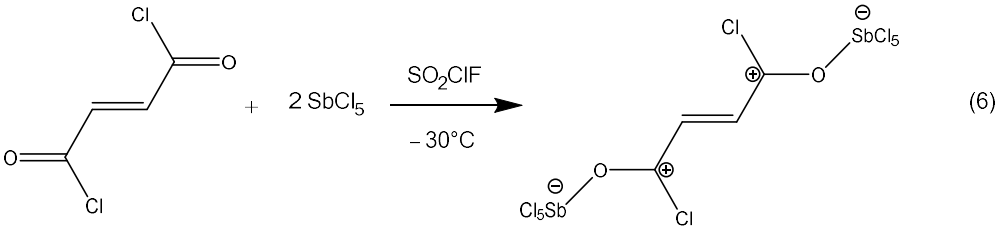

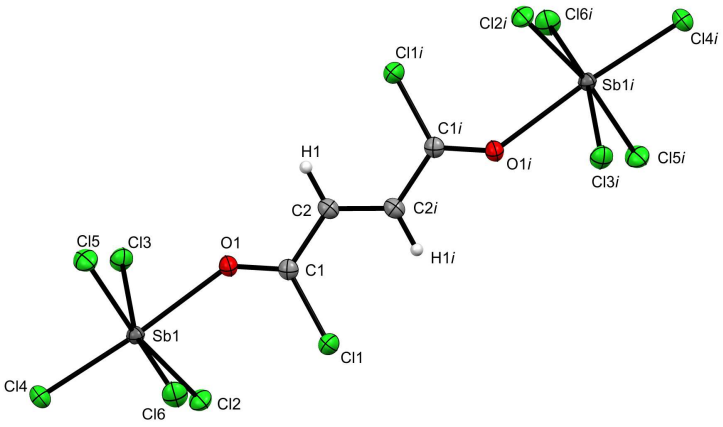

Figure 5. Formula unit of $C_4H_2Cl_2O_2 \cdot 2\ SbCl_5$ (displacement ellipsoids with 50% probability). Symmetry operation: *i = 1–x, –y, 1–z*.

Moreover, the reaction of fumaryl chloride with SbF_5 in SO_2ClF solutions was examined giving monoacylium ions. Surprisingly, the monoacylium ion contained fluorine, which is attributed to chlorine-fluorine exchange, under the terms of Equation (7).

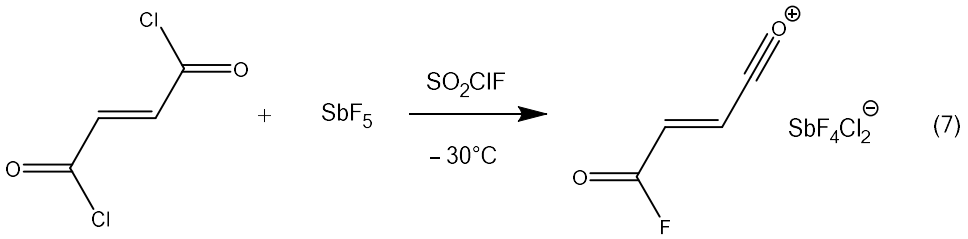

(7)

The reaction was repeated using fumaryl fluoride as starting material. The generation of monoacylium ions according to Equation (8) was observed. Vibrational spectroscopic studies confirm the formation of the acyl cation. The asymmetric unit of $[C_4H_2FO_2]^+[Sb_3F_{16}]^-$ is depicted in Figure 6. Diacyl cations were not obtained despite applying an eight-fold excess of SbF_5.

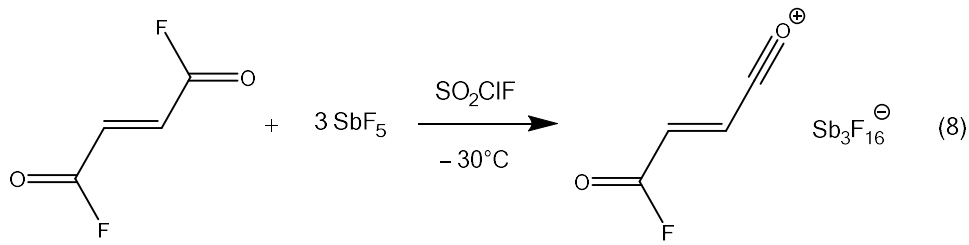

(8)

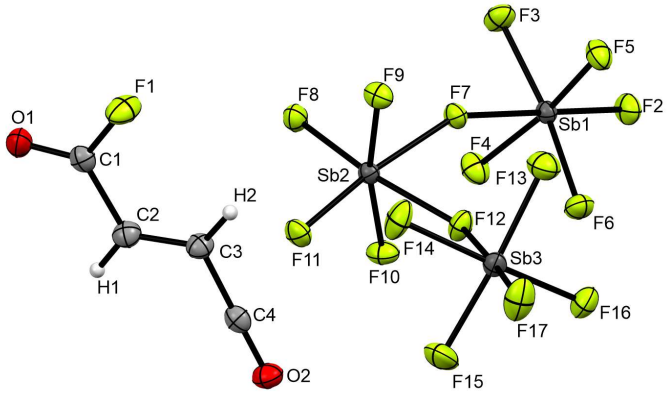

Figure 6. Asymmetric unit of $[C_4H_2FO_2]^+[Sb_3F_{16}]^-$ (displacement ellipsoids with 50% probability).

The crystal structure of $[C_4H_2FO_2]^+[Sb_3F_{16}]^-$ exhibits one C···O and three C···F contacts and the nature of these interactions is discussed with the aid of electrostatic potential maps, NPA charges, and NBO analysis, executed on the B3LYP/aug-cc-pVTZ level of theory. An illustration of the C···O and C···F contacts combined with the ESP map is depicted in Figure **7**. The region around the oxocarbenium center suffers from a depletion of electron density and provides a positive electrostatic potential designated in the literature as π-hole,[32] which is

observed in the ESP map. The π-hole is regarded as positive electrostatic potential on unpopulated π* orbitals, which are consequently able to interact with electron donors.[33] Due to the sp-hybridization of the carbon atom, confirmed by NBO analysis, the π-hole owns a ring structure. In conclusion, the stabilization of the monoacyl cation arises from electrostatic attraction[34] and electron back-donation[35,36] from oxygen and fluorine ligands (lp → π*(C4-O2)) to the π-hole at the oxocarbenium center.

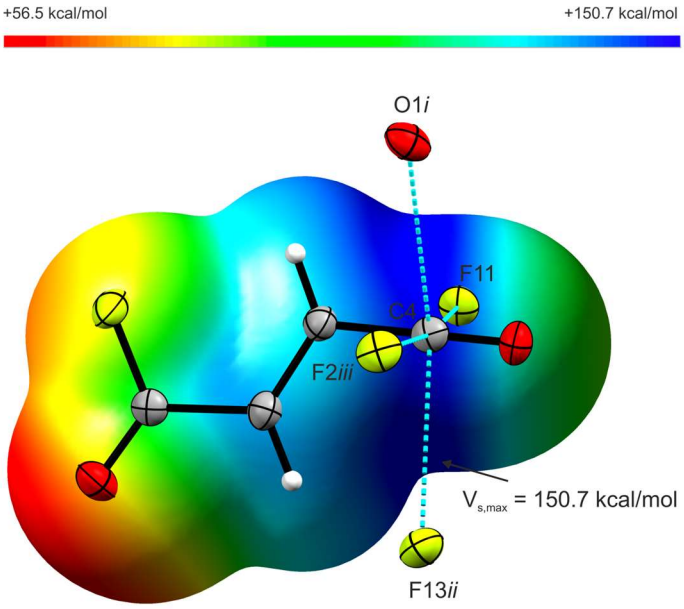

Figure 7. Intermolecular interactions in the crystal structure of $[C_4H_2FO_2]^+[Sb_3F_{16}]^-$ (displacement ellipsoids with 50% probability). C···O and C···F contacts are drawn as dashed blue lines. The calculated ESP surface mapped onto an electron density isosurface value of 0.0004 bohr^{-3} with the color scale range from 56.5 kcal mol^{-1} to 150.7 kcal mol^{-1}. Symmetry operations: *i = 2–x, 0.5+y, 0.5–z; ii = x, 1.5–y, –0.5+z; iii = 1+x, 1.5–y, –0.5+z.*

Furthermore, calculations of ESP maps including NPA charges for the diacyl cation $[C_4H_2O_2]^{2+}$ were performed on the B3LYP/aug-cc-pVTZ level of theory. Due to the small distances between the positive charges involving charge-charge repulsion, without the possibility of delocalization, the formation of the diacyl cation cannot be observed.[37]

3.2 Investigations in Superacidic Media

The second part of this thesis is concerned with the reaction behavior of different functional groups on the fumaryl scaffold in superacidic media in terms of the extent of protonation on the respective structure and electron distribution. To perform these investigations fumaric acid, fumaramide, and fumaryl fluoride were reacted in the binary superacidic systems XF/BF_3 and XF/MF_5 (X=H, D; M=As, Sb). The resulting compounds were characterized by low-temperature vibrational spectroscopy. Single-crystal X-ray structure analyses and low-temperature NMR spectroscopy were additionally carried out for selected salts. In order to acquire a deeper understanding of the structure and electron distribution of the protonated cations, quantum chemical calculations were executed. An overview of these studies is given in the following.

3.2.1 Protonation of Fumaric Acid

The diprotonation of fumaric acid was achieved by using an excess of the respective Lewis acid in the binary superacidic systems according to Equation (9). Figure 8 shows the formula unit of $[C_4H_6O_4]^{2+}([SbF_6]^-)_2$.[38]

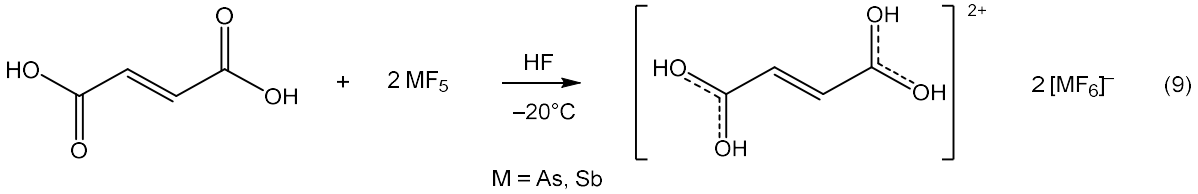

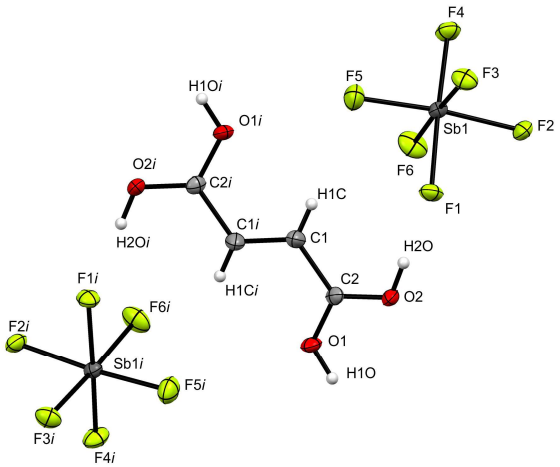

Figure 8. Formula unit of $[C_4H_6O_4]^{2+}([SbF_6]^-)_2$ (displacement ellipsoids with 50% probability). Symmetry operation: *i = 1–x, y, 0.5–z.*

The synthesis of the salt comprising the O-monoprotonated cation was performed after Equation (10). By having a closer look at the crystal structure of $[C_4H_5O_4]^+[SbF_6]^-$, it is noticeable that one proton is shared between two oxygen atoms and formally only half of a proton is connected to the respective oxygen atom. This results in the generation of a chain,

as illustrated in Figure 9. Thus, the formally monoprotonated fumaric acid is delineated more accurately as a double hemi-protonated fumaric acid.

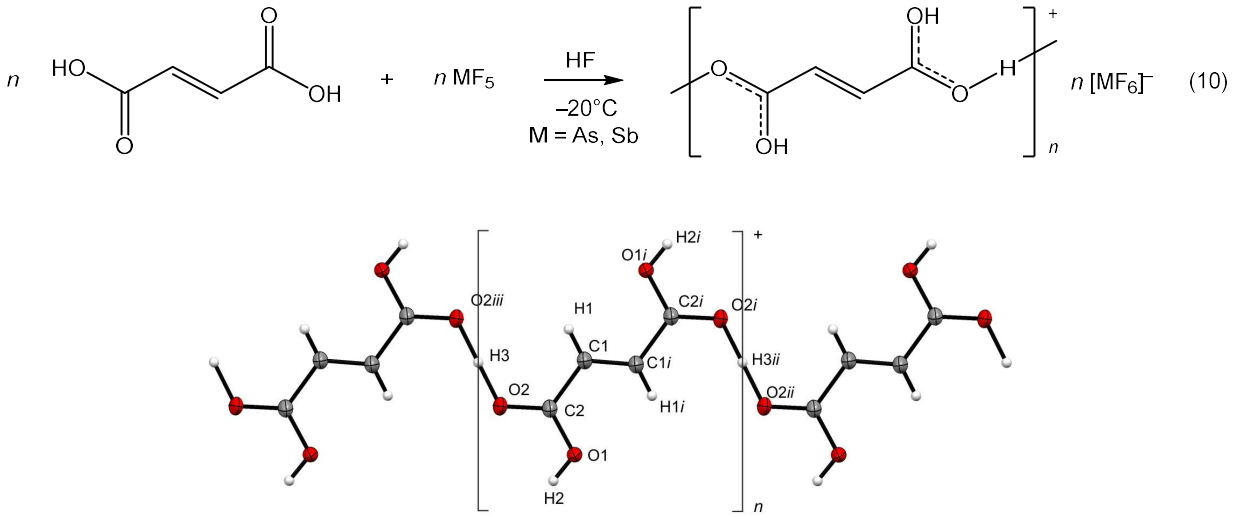

Figure 9. Cation chains in $[C_4H_5O_4]^+[SbF_6]^-$ based on the double hemi-protonation (displacement ellipsoids with 50% probability). Symmetry operations: *i = –x, 2 –y, 2 –z; ii = x, 1+y, z; iii = –x, 1 –y, 2–z.*

In order to calculate the structure of the double hemi-protonated fumaric acid, two protonated formaldehyde molecules together with two hydrogen fluoride molecules are added to one fumaric acid molecule, as shown in Figure 10. The adduct $[C_4H_6O_4 \cdot 2\ H_2CO \cdot 2\ HF]^{2+}$ was calculated on the ωB97XD/aug-cc-pVTZ level of theory.

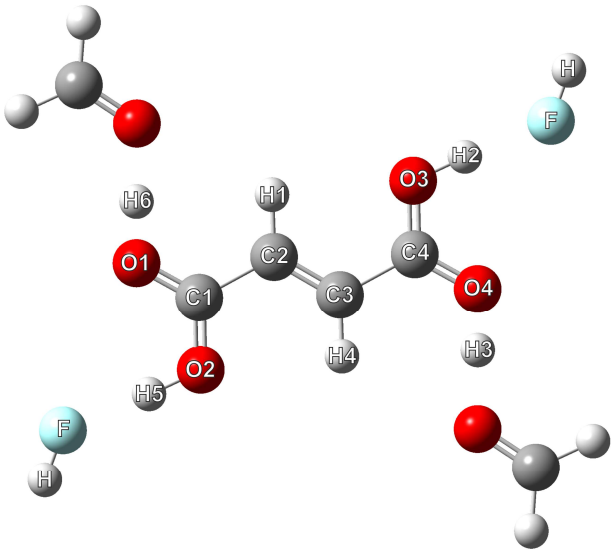

Figure 10. Calculated structure of simulated double hemi-protonated fumaric acid $[C_4H_6O_4 \cdot 2\ H_2CO \cdot 2\ HF]^{2+}$ under consideration of hydrogen bonds in the solid state.

A comparative analysis of some selected protonated and deprotonated salts of fumaric acid showed that the C–O and C–C bond lengths do not differ significantly from dication to dianion. Irrespective of protonation or deprotonation the carbon-oxygen scaffold remains constant.

3.2.2 Protonation of Fumaramide

For further investigations, fumaric acid was slightly changed by replacing the hydroxy groups with amino moieties resulting in the molecule fumaramide. One feature of amides, in general, is depicted by the high resonance stabilization, resting on the strong influence of the +M effect,[9] as illustrated by fumaramide in Scheme 6.

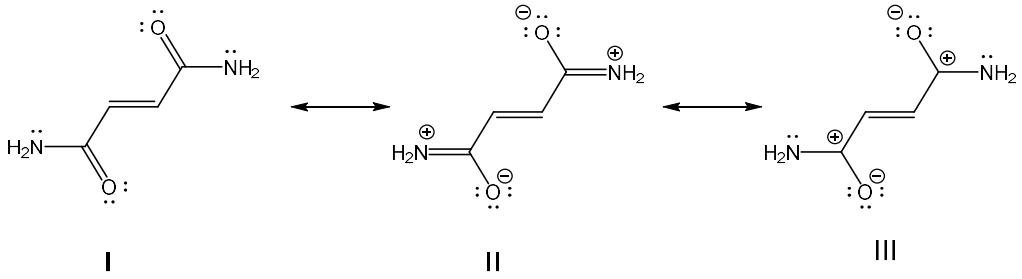

Scheme 6. Resonance structures of fumaramide.

An equimolar amount of the Lewis acids in reference to fumaramide was used with the aim of generating the monoprotonated species. Unexpectedly, a mixture of the diadduct with O-coordinated HF, $C_4H_6N_2O_2 \cdot 2\ HF$, and the diprotonated species was obtained. The formula unit of $C_4H_6N_2O_2 \cdot 2\ HF$ is shown in Figure 11.[39]

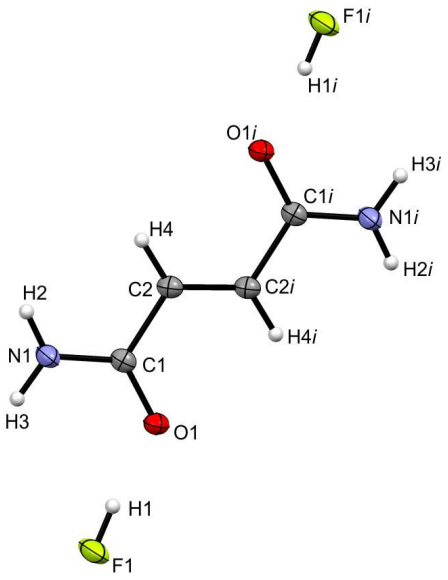

Figure 11. Formula unit of $C_4H_6N_2O_2 \cdot 2\ HF$ (displacement ellipsoids with 50% probability). Symmetry operation: *i* = *–x, 1–y, 1–z*.

The O-diprotonated species $[C_4H_8N_2O_2]^{2+}$ was formed under the terms of Equation (11) by employing an excess of the Lewis acids (SbF_5 or BF_3) in the binary superacidic systems. The crystal structure of $[C_4H_8N_2O_2]^{2+}[(BF_4)^-]_2$ reveals bifurcated, three- and four-center hydrogen bonds as shown in Figure 12.

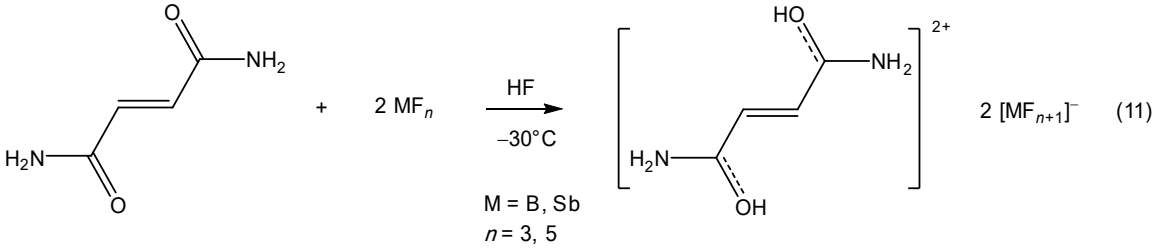

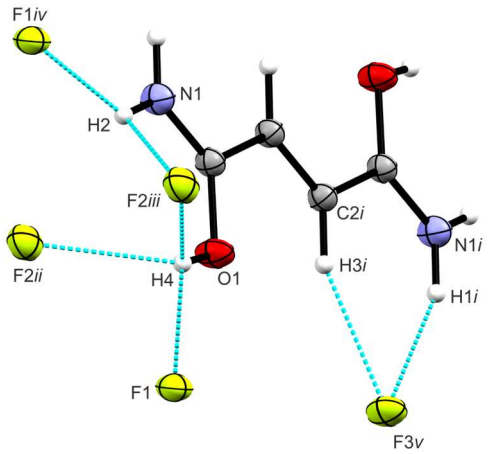

Figure 12. Selected hydrogen bonds in $[C_4H_8N_2O_2]^{2+}[(BF_4)^-]_2$ (displacement ellipsoids 50% probability). Symmetry operations: *i = –x, –y, 1–z; ii = –1+x, y, z; iii = 1–x, 1–y, 1–z; iv = –x, 1–y, 1–z; v = 1.5–x, –0.5+y, 1.5–z.* All contacts are drawn as dashed blue lines.

The vibrational frequencies and the crystal data portended that the protonation leads to an elongation of the C–O bond lengths in combination with a shortening of the C=N bond distances. The impact of the protonation on the resonance +M effect and the electron distribution concerning the conjugated system is examined by an ESP map calculated at the B3LYP/aug-cc-pVTZ level of theory, which is displayed in Figure 13. By reason of the protonation the electron density of the conjugated system shifts from the oxygen atoms to the nitrogen atoms thereby strengthening the C=N and simultaneously weakening the C–O bond. Aside from that, the nitrogen lone pair contributes entirely to the formation of the C=N π-bond, which is demonstrated by the NBO analysis, represented in Figure 14. The C=N double bond character is stabilized due to the O-diprotonation.

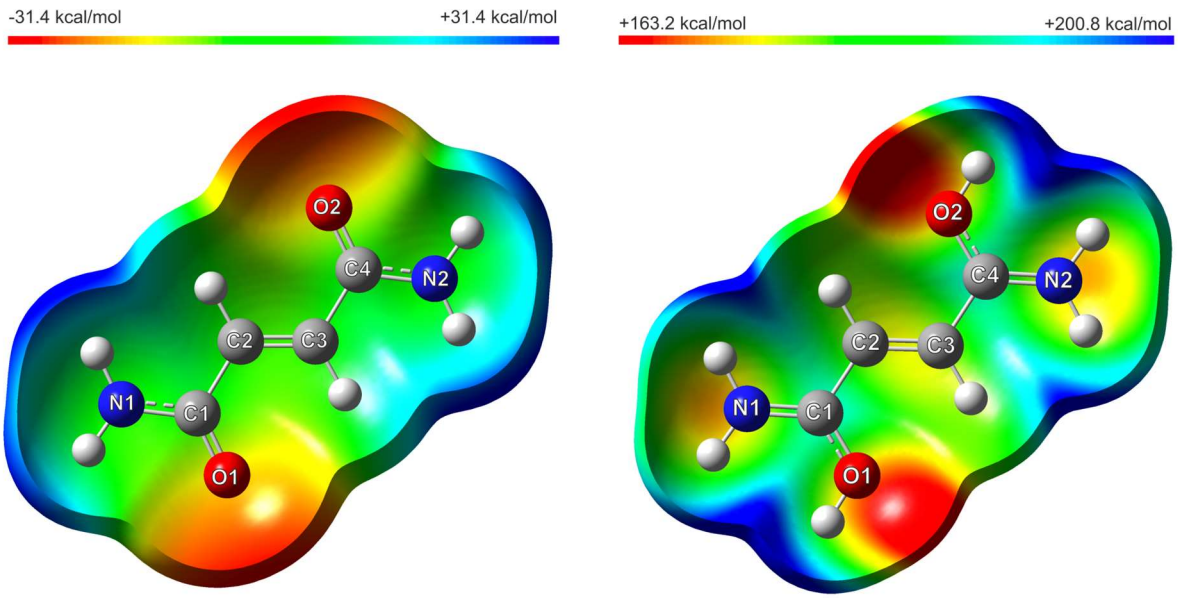

Figure 13. Left: Calculated ESP surface mapped onto an electron density isosurface value of 0.0004 bohr^{-3} with the color scale ranging from –31.4 kcal mol^{-1} to +31.4 kcal mol^{-1} of $C_4H_6N_2O_2$. Right: Calculated ESP surface mapped onto an electron density isosurface value of 0.0004 bohr^{-3} with the color scale ranging from +163.2 kcal mol^{-1} to +200.8 kcal mol^{-1} of $[C_4H_8N_2O_2]^{2+}$.

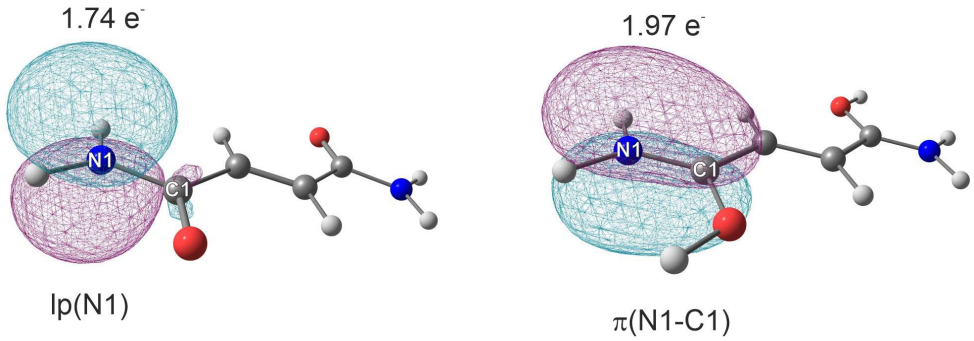

Figure 14. Selected NBOs for the nitrogen lone pair of fumaramide (left) and for the CN bond of $[C_4H_8N_2O_2]^{2+}$ (right) with corresponding occupancies.

3.2.3 Protonation of Fumaryl Fluoride

Another modification of the fumaryl scaffold was undertaken by exchanging the amino groups for fluorines, giving the molecule fumaryl fluoride. The acyl fluoride moiety was investigated in superacidic systems for the first time. An equimolar amount of the Lewis acids in reference to fumaryl fluoride is needed to form the salt containing the monoprotonated cation after Equation (12). The cation of $[C_4H_3F_2O_2]^+[SbF_6]^-$, which is shown in Figure 15, exists as the *trans-trans* conformer.[40]

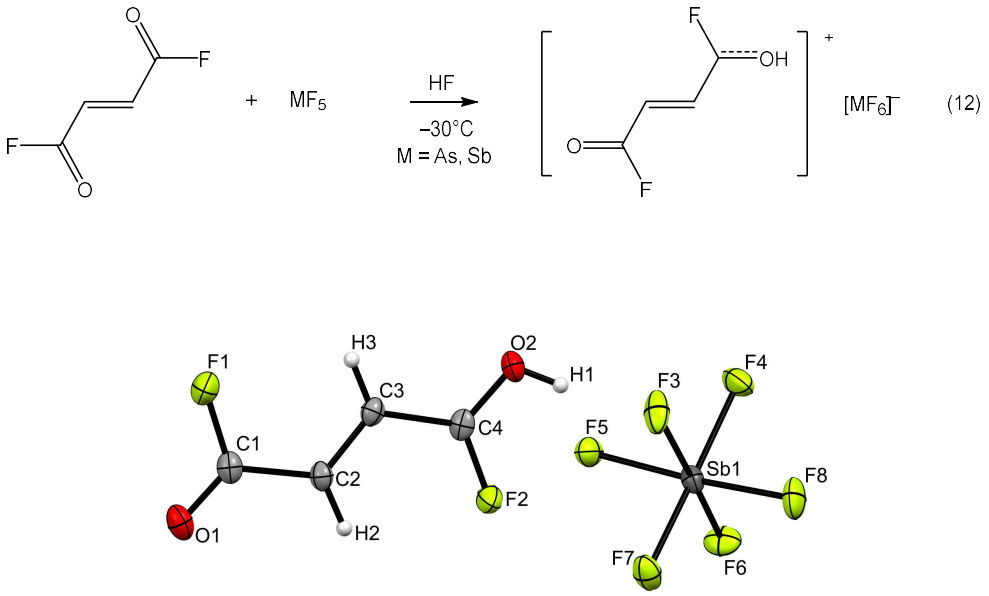

Figure 15. Asymmetric unit of $[C_4H_3F_2O_2]^+[SbF_6]^-$ (displacement ellipsoids with 50% probability).

An excess of the Lewis acids (AsF_5 or SbF_5) is required to synthesize the diprotonated fumaryl fluoride according to Equation (13). Figure 16 depicts a projection of the formula unit of $[C_4H_4F_2O_2]^{2+}([AsF_6]^-)_2$.

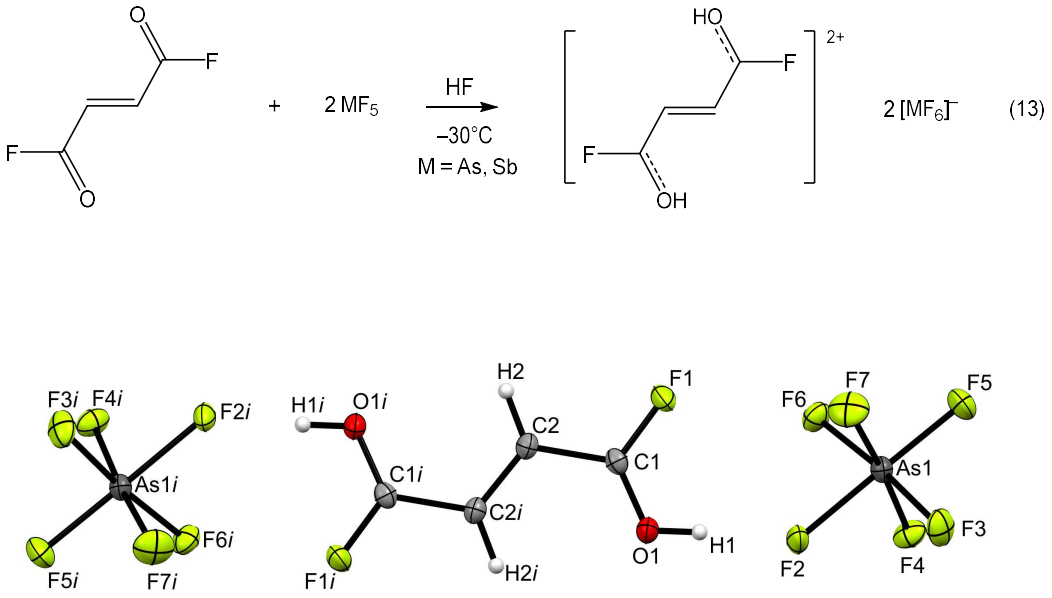

Figure 16. Formula unit of $[C_4H_4F_2O_2]^{2+}([AsF_6]^-)_2$ (displacement ellipsoids with 50% probability). Symmetry operation: *i = 1–x, y, 0.5–z.*

Vibrational spectra and single-crystal X-ray structure analyses show that the protonation leads to an elongation of the C=O bonds, whereas the C–F bond lengths are considerably reduced. To examine the electron distribution of the diprotonated species, an electrostatic potential (ESP) map combined with selected natural population analysis (NPA) charges was calculated on the B3LYP/aug-cc-pVTZ level of theory and is illustrated in Figure 17.

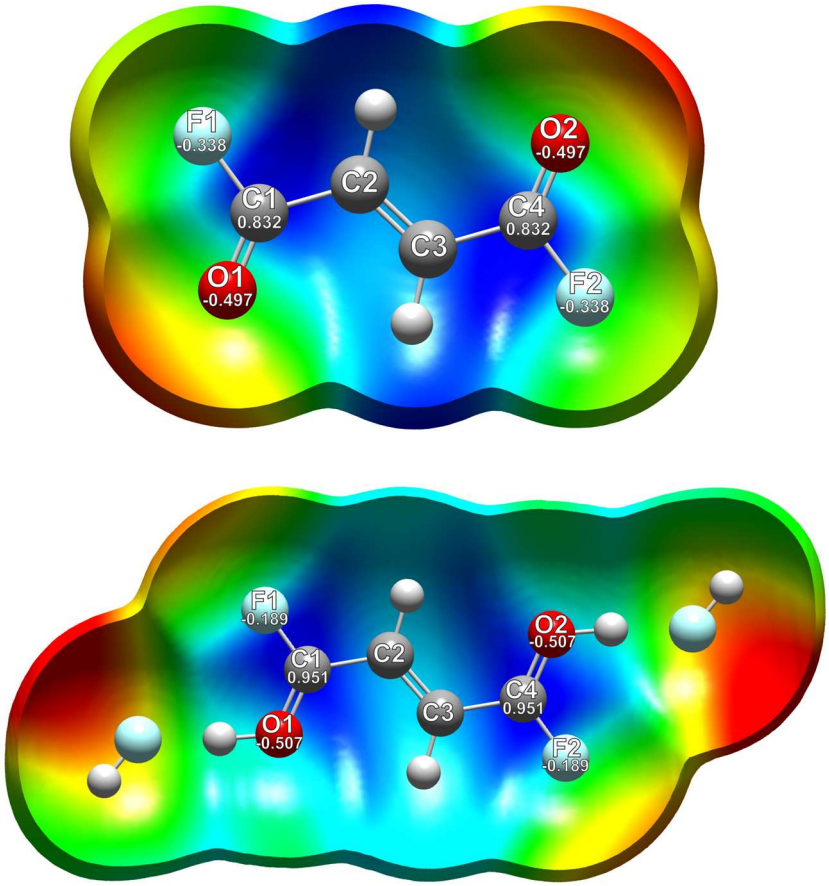

Figure 17. Top: Calculated ESP surface mapped onto an electron density isosurface value of 0.0004 bohr^{-3} with the color scale ranging from –18.2 kcal mol^{-1} (red) to 22.0 kcal mol^{-1} (blue) of *cis*-*cis*-$C_4H_2F_2O_2$. Bottom: calculated ESP map with an electron density isosurface value of 0.00004 bohr^{-3} and a color scale range from 138.1 kcal mol^{-1} (red) to 194.5 kcal mol^{-1} (blue) of $[C_4H_4F_2O_2 \cdot 2\ HF]^{2+}$. Selected NPA charges are given in [a.u.].

The electron distribution shifts from the fluorine atom, which is inductively electron withdrawing, and simultaneously electron donating by resonance[35,41] to the C–F bond in the diprotonated cation, established in the literature as the +R effect (see Scheme 7).[42]

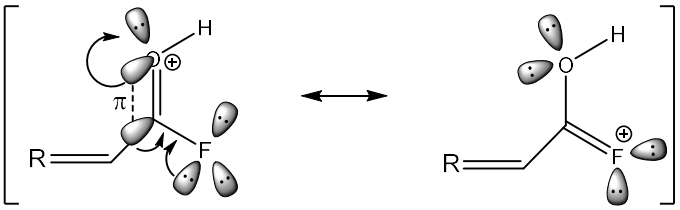

Scheme 7. Illustration of the +R effect by means of the protonated acyl fluoride moiety.

The NMR spectra of diprotonated fumaryl fluoride show the enhanced resonance-electron-donating ability in the increased proton–fluorine coupling constants. The bond between carbon and fluorine in the diprotonated cation exhibits a low double-bond character. In conclusion, it may be stated that the strongest bond in organic chemistry[43] is further strengthened by the protonation of the acyl fluoride moiety owing to the +R effect.

4. Conclusion

The aim of this thesis was the investigation of different functional groups on the fumaryl framework under Lewis acidic conditions and in superacidic media. The investigations considering the neutral compound fumaryl fluoride determined the largely unknown molecular structure and conformational composition. All of the three possible planar rotational isomers were detected. Comparison to related molecules demonstrated that the substitution of a halogen atom for an aldehyde proton has a considerable impact on the energy of conformation. The studies regarding the investigation of fumaryl halides in strong Lewis acidic media revealed oxonium complexes with the Lewis acids AsF_5 and $SbCl_5$. Merely SbF_5, known as one of the strongest Lewis acids and additionally a very strong fluoride acceptor[44] accomplished the abstraction of one halogen atom. In the case of fumaryl chloride, the respective monoacylium ion was formed under chlorine-fluorine exchange, giving an acyl cation containing one acyl fluoride moiety. The abstraction of both halogen atoms under the formation of the diacyl cation does not occur, which is explained by the small distances between the positive charges involving charge-charge repulsion,[37] without the possibility of delocalization. The observation that fumaryl chloride and fluoride, would not give diacylium ions can be considered a great advantage for the Friedel-Crafts synthesis of ketones keeping an acyl fluoride group because fluorine substituents are a common and essential drug component.

The studies in superacidic media resulted in the maintenance of the fumaryl scaffold and no addition to the C=C double bond was observed. The O-diprotonation was observed in fumaric acid, fumaramide as well as in fumaryl fluoride. However, when it comes to monoprotonation large differences emerge between the three target molecules. Formally monoprotonated fumaric acid reveals a double hemi-protonated chain structure, in which one proton is shared between two oxygen atoms, and formally only half of a proton is connected to the respective oxygen atom. With regard to fumaramide, no monoprotonation was observed. Fumaryl fluoride, however, crystallizes as monoprotonated cation when using an equimolar amount of the Lewis acids in reference to the reactant. Centrosymmetry represents one characteristic all regarded molecules have in common. Monoprotonation, certainly, leads to a lowered symmetry. In order to keep the centrosymmetry, fumaric acid builds up the double hemi-protonated chain structure while fumaramide is not able to stabilize the asymmetric monoprotonated form. Only fumaryl fluoride reveals clear monoprotonated species. The possibility of stabilizing the asymmetric monoprotonated form depends on the distinctiveness of each functional group. Aside from that, we were able to show that the C–F bond, known as the strongest bond in organic chemistry,[43] is further strengthened by the protonation of fumaryl fluoride on account of the +R effect.

[1] K. Schwetlick, *Organikum*. *Organisch-chemisches Grundpraktikum*, Wiley-VCH, Weinheim, **2001**.

[2] K. P. C. Vollhardt, N. E. Schore, *Organic chemistry*. *Structure and function*, Freeman, New York, Basingstoke, **2011**.

[3] H. K. A. Hädener, *Grundlagen der organischen Chemie*, Birkhäuser Basel, Basel, **2006**.

[4] W. Karrer, *Konstitution und Vorkommen der organischen Pflanzenstoffe (exclusive Alkaloide)*, Springer, Basel, **1976**.

[5] C. Marquart, *Lehrbuch der practischen und theoretischen Pharmacie*, Verlag von C. G. Kunze, Mainz, **1866**.

[6] H. Limpricht, *Lehrbuch der Organischen Chemie*, C. A. Schwetschke, Braunschweig, **1862**.

[7] E. O. von Lippmann, *Zeittafeln Zur Geschichte der Organischen Chemie*. *Ein Versuch*, Springer, Berlin, Heidelberg, **1921**.

[8] S. Bäumler, *Heilpflanzenpraxis Heute Arzneipflanzenporträts*, Elsevier, München, **2021**.

[9] T. Schirmeister, C. Schmuck, P. R. Wich, *Beyer/Walter Organische Chemie*, Hirzel Verlag, Stuttgart, **2016**.

[10] A. Wollrab, *Organische Chemie*, Springer Berlin Heidelberg, Berlin, Heidelberg, **2009**.

[11] a) I. Fleming, *Molecular orbitals and organic chemical reactions*, Wiley, Hoboken, **2009**; b) E. Breitmaier, G. Jung, *Organische Chemie*. *Grundlagen, Verbindungsklassen, Reaktionen, Konzepte, Molekülstruktur, Naturstoffe*, Thieme, Stuttgart, **2009**.

[12] J. Thiele, *Justus Liebigs Ann. Chem.* **1899**, *306*, 87.

[13] G. P. Moss, *Pure Appl. Chem.* **1996**, *68*, 2193.

[14] D. F. Koster, T. P. Vasileff, G. L. Carlson, *Spectrochim. Acta Part A: Mol. Spectrosc.* **1971**, *27*, 1633.

[15] J. W. Larsen, P. A. Bouis, *J. Org. Chem.* **1973**, *38*, 1415.

[16] a) R. Ugarte, C. Bustos, I. Moreno-Villoslada, *J. Chil. Chem. Soc.* **2011**, *56*, 656; b) K. Nozaki, R. Ogg, *J. Am. Chem. Soc.* **1941**, *63*, 2583.

[17] D. S. Noyce, P. A. King, F. B. Kirby, W. L. Reed, *J. Am. Chem. Soc.* **1962**, *84*, 1632.

[18] G. A. Olah, G. K. S. Prakash, Á. Molnár, J. Sommer, *Superacid chemistry*, Wiley, Hoboken, N.J., **2009**.

[19] N. F. Hall, J. B. Conant, *J. Am. Chem. Soc.* **1927**, *49*, 3047.

[20] R. J. Gillespie, T. E. Peel, *Adv. Phys. Org. Chem.* **1971**, *9*, 1.

[21] L. P. Hammett, A. J. Deyrup, *J. Am. Chem. Soc.* **1932**, *54*, 2721.

[22] T. Mathew, *Nature* **2017**, *544*, 162.

[23] G. A. Olah, G. K. Prakash, J. Sommer, *Science* **1979**, *206*, 13.

[24] T. P. Vasileff, D. F. Koster, *J. Org. Chem.* **1970**, *35*, 2461.

[25] M. C. Bayer, C. Jessen, A. J. Kornath, *Z. Anorg. Allg. Chem.* **2021**, *647*, 258.

[26] K. Hagen, *J. Mol. Struct.* **1985**, *128*, 139.

[27] A. Kulbida, M. N. Ramos, M. Rasanen, J. Nieminen, O. Schrems, R. Fausto, *Faraday Trans.* **1995**, *91*, 1571.

[28] D. F. Koster, *J. Am. Chem. Soc.* **1966**, *88*, 5067.

[29] J. M. Landry, J. E. Katon, *Spectrochim. Acta Part A: Mol. Spectrosc.* **1984**, *40*, 871.

[30] G. Paulen, M. Trætteberg, N. Nigri, A. Kjekshus, B. Klewe, D. L. Powell, *Acta Chem. Scand.* **1974**, *28a*, 1155.

[31] M. C. Bayer, N. Greither, C. Jessen, A. Nitzer, A. J. Kornath, *Eur. J. Inorg. Chem.* **2022**, e202200391.

[32] a) W. Zierkiewicz, M. Michalczyk, S. Scheiner, *Molecules* **2021**, *26*, 1740; b) H. Wang, W. Wang, W. J. Jin, *Chem. Rev.* **2016**, *116*, 5072.

[33] A. Bauzá, T. J. Mooibroek, A. Frontera, *ChemPhysChem* **2015**, *16*, 2496.

[34] a) J. S. Murray, P. Lane, T. Clark, K. E. Riley, P. Politzer, *J. Mol. Model.* **2012**, *18*, 541; b) O. Loveday, J. Echeverría, *Nat. Commun.* **2021**, *12*, 5030.

[35] K. O. Christe, X. Zhang, R. Bau, J. Hegge, G. A. Olah, G. K. S. Prakash, J. A. Sheehy, *J. Am. Chem. Soc.* **2000**, *122*, 481.

[36] T. Laube, *Chem. Rev.* **1998**, *98*, 1277.

[37] J. W. Larsen, P. A. Bouis, *J. Am. Chem. Soc.* **1975**, *97*, 6094.

[38] M. C. Bayer, C. Jessen, A. J. Kornath, *Z. Anorg. Allg. Chem.* **2020**, *646*, 333.

[39] M. C. Bayer, N. Greither, V. Bockmair, A. Nitzer, A. J. Kornath, *Eur. J. Inorg. Chem.* **2022**, e202200501.

[40] M. C. Bayer, C. Kremser, C. Jessen, A. Nitzer, A. J. Kornath, *Chem. Eur. J.* **2022**, *28*, e202104422.

[41] a) G. A. Olah, C. A. Cupas, M. B. Comisarow, *J. Am. Chem. Soc.* **1966**, *88*, 362; b) B. E. Smart, *J. Fluor. Chem.* **2001**, *109*, 3; c) G. A. Olah, G. K. S. Prakash, G. Rasul, *Proc. Natl.*

Acad. Sci. U.S.A. **2013**, *110*, 8427; d) E. Kraka, D. Cremer, *ChemPhysChem* **2009**, *10*, 686.

[42] T. Hiyama, *Organofluorine Compounds, Chemistry and Applications*, Springer-Verlag Berlin Heidelberg, Berlin, Heidelberg, **2000**.

[43] D. O'Hagan, *Chem. Soc. Rev.* **2008**, *37*, 308.

[44] A. F. Holleman, E. Wiberg, N. Wiberg, G. Fischer, *Anorganische Chemie*, De Gruyter, Berlin, Boston, **2017**.

5. Appendix

The following appendix contains a catalog of publications, conference contributions, cover pictures, manuscripts, and supporting information which are published within the framework of this dissertation. All of the manuscripts have been published in peer-reviewed scientific journals. The publications are listed topically in the same order as they are combined in this thesis.

5.1 Publications

1. M. C. Bayer, C. Jessen, A. J. Kornath, *Structure and Properties of Fumaryl Fluoride, Z. Anorg. Allg. Chem.* **2021**, *647*, 258–265.
   DOI: 10.1002/zaac.202000248 Cover: DOI: 10.1002/zaac.202170041

2. M. C. Bayer, N. Greither, C. Jessen, A. Nitzer, A. J. Kornath, *Intermediates in Friedel-Crafts Acylation of Fumaryl Halides*, *Eur. J. Inorg. Chem*. **2022**, e202200391 (1 of 9).
   DOI: 10.1002/ejic.202200391 Cover: DOI: 10.1002/ejic.202200540

3. M. C. Bayer, C. Jessen, A. J. Kornath, *Preparation and Characterization of Protonated Fumaric Acid, Z. Anorg. Allg. Chem.* **2020**, *646*, 333–339.
   DOI: 10.1002/zaac.202000091 Cover: DOI: 10.1002/zaac.202070071

4. M. C. Bayer, N. Greither, V. Bockmair, A. Nitzer, A. J. Kornath, *Stabilizing the C=N Double Bond Character in Fumaramide with the Aid of Superacids, Eur. J. Inorg. Chem*. **2022**, e202200501 (1 of 8).
   DOI: 10.1002/ejic.202200501

5. M. C. Bayer, C. Kremser, C. Jessen, A. Nitzer, A. J. Kornath, *Strengthening of the C−F Bond in Fumaryl Fluoride with Superacids, Chem. Eur. J.* **2022**, *28*, e202104422 (1 of 10).
   DOI: 10.1002/chem.202104422 Cover: DOI: 10.1002/chem.202200450

5.2 Conference Contributions

Poster Presentations

1. Preparation of Characterization of Protonated Fumaric acid, M. C. Bayer, A. J. Kornath, *19th European Symposium on Fluorine Chemistry*, Warsaw, Poland, 26.08.2019.
2. Shortening of the C–F Bond Length in Fumaryl Fluoride with the Aid of Superacids, M. C. Bayer, A. Kornath, *20th European Symposium on Fluorine Chemistry*, Berlin, Germany, 15.08.2022.

Oral Presentations

1. Intermediates in Friedel-Crafts Acylation of Fumaryl Halides, M. C. Bayer, A. J. Kornath, *19. Deutscher Fluortag*, Schmitten, Germany, 20.09.2022.

5.3 Cover Pictures, Articles and Supporting Information

Journal of Inorganic and General Chemistry

ZAAC

Zeitschrift für anorganische und allgemeine Chemie

2021

647/4

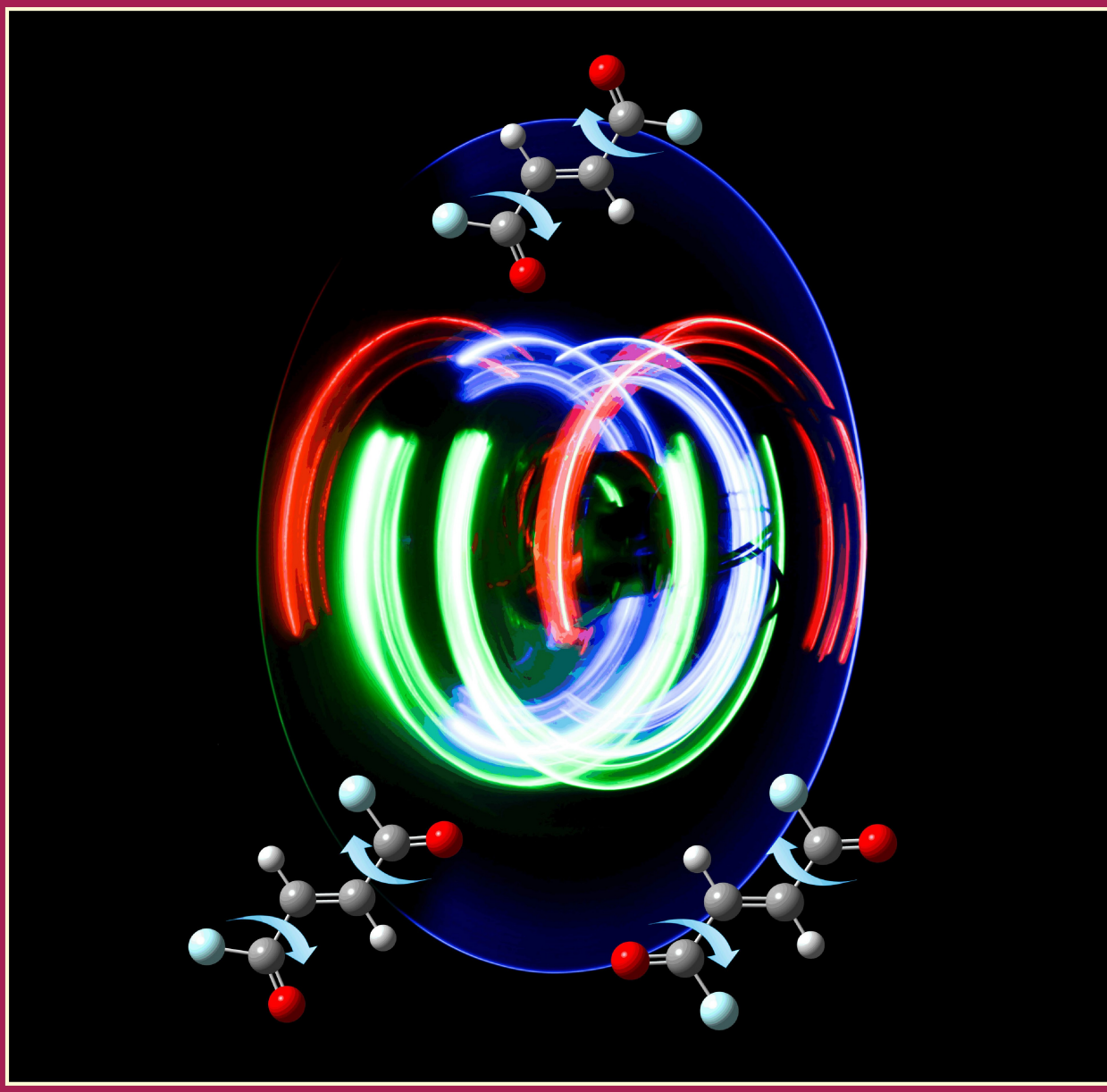

Front Cover: Structure and Properties of Fumaryl Fluoride

Marie C. Bayer, Christoph Jessen, and Andreas J. Kornath

WILEY-VCH

www.zaac.wiley-vch.de

Journal of Inorganic and General Chemistry
ZAAC
Zeitschrift für anorganische und allgemeine Chemie
DOI: 10.1002/zaac.202000248
ARTICLE

Structure and Properties of Fumaryl Fluoride

Marie C. Bayer,[a] Christoph Jessen,[a] and Andreas J. Kornath*[a]

Dedicated to Prof. Dr. Thomas M. Klapötke on the Occasion of his 60th Birthday

Abstract. The molecular structure and the conformational composition of fumaryl fluoride were determined by low-temperature vibrational spectroscopy and single-crystal X-ray structure analysis. Three planar rotational isomers, *trans-trans*-, *cis-cis*- and *cis-trans*-fumaryl fluoride were identified. $C_4H_2F_2O_2$ crystallizes in the monoclinic space group $P2_1/c$ with four formula units per unit cell. Besides, Lewis acid-base adducts between fumaryl fluoride and arsenic pentafluoride were synthesized. These adducts, which contain O–As bonding interactions, were found to crystallize as the monoadducts *trans-cis*-$C_4H_2F_2O_2{\cdot}AsF_5$ and *cis-trans*-$C_4H_2F_2O_2{\cdot}AsF_5$. Moreover, the diadduct *trans-trans*-$C_4H_2F_2O_2{\cdot}2\ AsF_5$ was determined by X-ray crystallography. The experimental data are discussed together with quantum chemical calculations of *trans-trans*-, *cis-cis*-, and *cis-trans*-fumaryl fluoride.

Introduction

Considering their unique properties, organofluorine compounds are of great importance in organic, bioorganic, and medicinal chemistry as well as materials sciences.[1,2] Since organofluorine compounds are notably rare in nature, they are only accessible artificially by fluorination of organic compounds.[3] Extensive progress in fluorine chemistry has been made with the fluorination of organic halides by nucleophilic substitution with antimony(III) fluoride, as discovered by *Swarts*.[3,4] In particular, acyl fluorides are versatile intermediates in organic syntheses, due to their high stability, in comparison to other acyl halides.[1] This is based on the unique stability of the carbon-fluorine bond.[5] An interesting representative of acyl fluorides is fumaryl fluoride [*trans*-F(O)C–CH=CH–C(O)F], owing to the presence of two acyl moieties. As a conjugated system, fumaryl fluoride can exist as three planar rotational conformers (Scheme 1).[6,7]

An equilibrium mixture of planar conformers in the liquid state of fumaryl fluoride has been reported,[6,7] which is in good agreement with results obtained for molecules in the fumarate series.[8,9] However, the three isomers have not yet been clearly distinguished. Only few investigations on fumaryl fluoride, which could prove useful as starting material for the synthesis of organofluorine compounds, have been reported yet. Fumaryl fluoride has not been explicitly characterized by vibrational spectroscopy and structural parameters are still unknown. As part of our research in the field of acyl fluorides, we herein present our results.

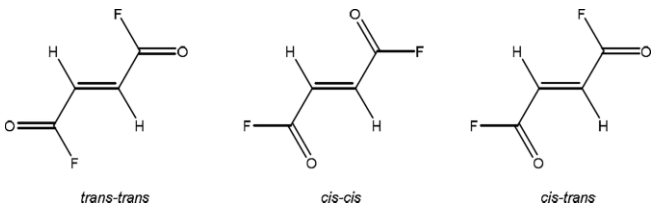

Scheme 1. Possible conformations of fumaryl fluoride.

Results and Discussion

Fumaryl fluoride was synthesized by nucleophilic substitution with antimony(III) fluoride [see Equation (1)].[3,4] The preparation procedure was previously reported by *Vasileff et al*.[7] We report a good reproducibility of this process and a yield of around 90 %. Fumaryl fluoride was obtained as a colorless liquid at 25 °C, which is stable up to 130 °C. The density of liquid fumaryl fluoride at 25 °C approximates 1.47 g·mL^{-1}.

$$3\ C_4H_2Cl_2O_2 + 2\ SbF_3 \xrightarrow{100°C,\ 1h} 3\ C_4H_2F_2O_2 + 2SbCl_3 \quad (1)$$

To elucidate the Lewis basic properties of fumaryl fluoride, we started its reaction with AsF_5 in liquid SO_2ClF. We observe only the formation of mono- and diadducts according to Equation (2) and Equation (3):

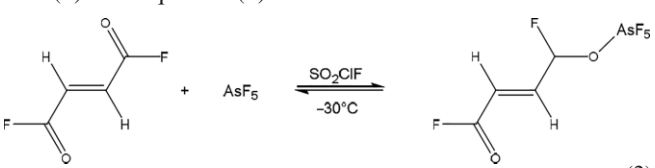

(2)

* Prof. Dr. A. J. Kornath
E-Mail: andreas.kornath@cup.uni-muenchen.de
[a] Department Chemie
Ludwig-Maximilians-Universität München
Butenandstr. 5–13(D)
81377 Munich, Germany
Supporting information for this article is available on the WWW under **http://dx.doi.org/10.1002/zaac.202000248** or from the author.

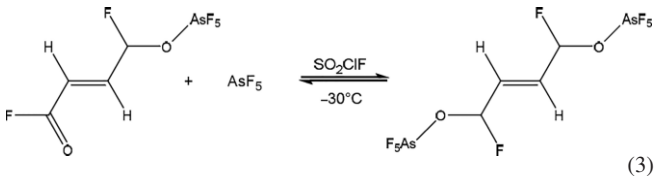

(3)

The crystallization of such reaction mixtures leads to colorless crystals containing fumaryl fluoride, the monoadducts and the diadduct. The crystal structure analysis is discussed later. A formation of acyl cations according to Equation (4) and Equation (5) has not been observed.

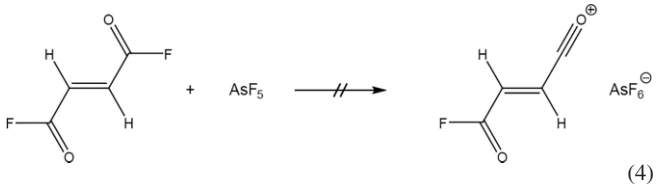

(4)

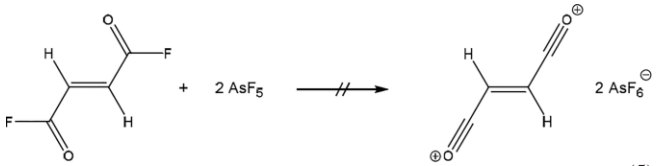

(5)

Vibrational Spectra of $C_4H_2F_2O_2$

Figure 1 illustrates the vibrational spectra of fumaryl fluoride in different states of matter. In Table 1 selected experimental vibrational frequencies of fumaryl fluoride in different states of matter in comparison with literature data[6] and calculated vibrational frequencies of *trans-trans*-, *cis-cis*- and *cis-trans*-fumaryl fluoride are summarized. The complete Table (Table S2) is listed in the Supporting Information. The vibrational spectra of fumaryl fluoride (**1**) and fumaryl chloride

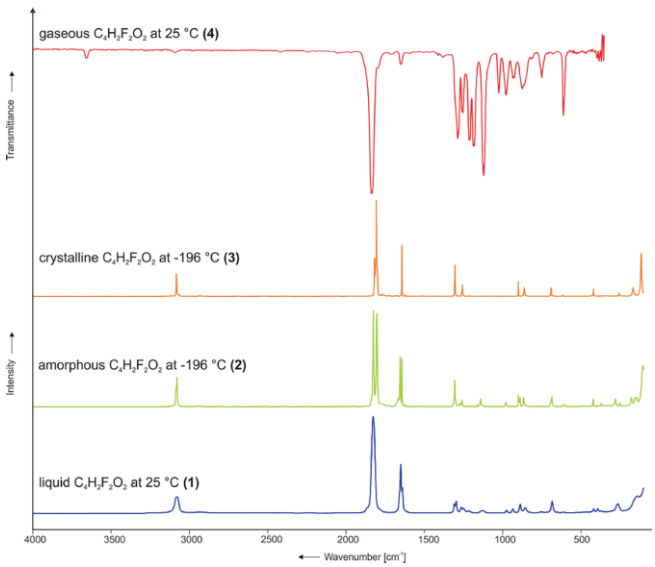

Figure 1. Vibrational spectra of liquid (**1**), amorphous (**2**), crystalline (**3**) and gaseous (5 mbar) (**4**) fumaryl fluoride at different temperatures.

are shown in Figure S1 (Supporting Information). A Table of the vibrational frequencies of fumaryl chloride (Table S1) in comparison with literature data[6,8] is listed in the Supporting Information.

By comparing the liquid (**1**), amorphous (**2**), and crystalline (**3**) phase spectra of fumaryl fluoride, it is apparent that the spectrum of (**3**) is conspicuously simpler than the spectra of (**1**) and (**2**). This agrees well with the presence of a rotational equilibrium in the liquid state with one rotational isomer preferentially crystallizing as the sample is slowly cooled.[6] The spectrum of (**2**) is obtained by quickly freezing the sample at –196 °C. As mentioned above, there are three planar conformers in liquid fumaryl fluoride possible (Scheme 1). The *cis-trans* conformer possesses C_s point group symmetry. The 24

Table 1. Selected experimental vibrational frequencies [cm^{-1}] of $C_4H_2F_2O_2$ in different states of matter in comparison with literature data[6] and calculated vibrational frequencies /cm^{-1} of *trans-trans*-, *cis-cis*- and *cis-trans*-fumaryl fluoride.

$C_4H_2F_2O_2$ exp. [a]				$C_4H_2F_2O_2$ Reference [6]	$C_4H_2F_2O_2$ calcd.[b,c]	Assignment	
Raman (liquid) (**1**)	Raman (amorphous) (**2**)	Raman (crystalline) (**3**)	IR (gaseous) (**4**)	Raman	IR/Raman		
			3097 vw		3207(3/0)	*cis-cis*	ν_{as}(C–H)
3079(17)	3080(31)	3084(23)			3203(0/96)	*cis-cis*	ν_{s}(C–H)
			1840 vs		1866(517/0)	*cis-cis*	ν_{as}(C=O)
1827(100)	1825(100)				1867(345/208)	*cis-trans*	$\nu(C=O)_t$
		1819(39)			1868(0/351)	*trans-trans*	ν_{s}(C=O)
	1803(97)	1806(100)			1871(0/154)	*cis-cis*	ν_{s}(C=O)
1651(51)	1655(52)		1655 vw	1650	1700(22/147)	*cis-trans*	ν(C=C)
1641(27)	1643(50)	1643(53)			1706(0/165)	*cis-cis*	ν(C=C)
1307(10)	1306(28)	1305(32)			1331(0/9)	*cis-cis*	δ_{s}(CCH)
1264(6)	1259(8)	1259(8)			1126(0/12)	*cis-cis*	ν_{s}(C–F)
		1257(12)			1247(0/29)	*trans-trans*	ν_{s}(C–F)
			1126 vs		1122(480/0)	*cis-cis*	ν_{as}(C–C)
975(3)	979(6)		984 w	978	939(52/3)	*cis-trans*	ν(C–F)
935(5)			932 w	931	936(1/5)	*cis-trans*	γ(CCH)
		862(9)			850(0/9)	*trans-trans*	ν_{s}(C–C)

a) Abbrevations for IR intensities: vs. = very strong, s = strong, m = medium, w = weak, vw = very weak. b) Calculated on the B3LYP/aug-cc-pVTZ level of theory. c) IR intensities in km·mol^{-1}; Raman intensities in $Å^4$ per u.

fundamental vibrations ($17A' + 7A''$) are both IR and Raman active. Both, the *trans-trans* and *cis-cis* conformers have C_{2h} symmetry ($9A_g + 3B_g + 4A_u + 8B_u$) and due to the centrosymmetry, the Rule of Mutual Exclusion will hold. Hence, the distinction between the *cis-trans* conformer and the conformers with a center of inversion is possible. The assignment of the vibrational modes was made by analyzing the Cartesian displacement vectors of the calculated vibrational modes of *trans-trans*-, *cis-cis*- and *cis-trans*-fumaryl fluoride and by comparison with literature data of fumaryl fluoride[6] and fumaryl chloride.[8]

For the *cis-cis* conformer the antisymmetric C–H stretching vibration is observed in the IR spectrum at 3097 cm^{-1} (**4**) and, as expected, is absent in the Raman spectra. The symmetric C–H stretching mode, which is absent in the IR spectrum, is detected in the Raman spectra at 3079 cm^{-1} (**1**), 3080 cm^{-1} (**2**), and 3084 cm^{-1} (**3**), respectively. In the IR spectrum, the antisymmetric C=O stretching vibration is observed at 1840 cm^{-1} (**4**) and the symmetric C=O stretching mode is detected in the Raman spectra at 1803 cm^{-1} (**2**) and 1806 cm^{-1} (**3**), respectively. In the Raman spectra the C=C stretching vibration is observed at 1643 cm^{-1} (**2**), (**3**) and 1641 cm^{-1} (**1**), respectively. The *cis-cis* conformer is present in all of the different states of matter.

In the spectrum of (**3**) the symmetric C=O stretching mode is observed at 1819 cm^{-1}, which is not detectable in (**1**), (**2**) and (**4**). The symmetric C–F stretching vibration [1257 cm^{-1} (**3**)] and the symmetric C–C stretching vibration [862 cm^{-1} (**3**)] are only observed in the Raman spectrum of the crystalline fumaryl fluoride. Consequently, the *trans-trans* conformer is only present in the crystallized sample, which consists of the *cis-cis* and the *trans-trans* conformer.

The C=O stretching vibration is observed in the Raman spectra at 1827 cm^{-1} (**1**) and 1825 cm^{-1} (**2**), respectively. This Raman line disappears in the Raman spectrum upon crystallization. The C=C stretching mode is detected at 1651 cm^{-1} (**1**), 1655 cm^{-1} (**2**) and at 1655 cm^{-1} (**4**), which agrees well with the literature.[6] The C–F stretching vibration is assigned to the bands at 984 cm^{-1} (**4**), at 975 cm^{-1} (**1**) and at 979 cm^{-1} (**2**), which conforms to literature data.[6] The vibrational spectra of the amorphous and liquid sample show clearly more lines than expected for a separate C_{2h} conformer. This indicates that the *cis-trans* conformer is present in the gaseous, the liquid and the amorphous state of matter, but not in the crystallized sample.

Crystal Structure of $C_4H_2F_2O_2$

The $C_4H_2F_2O_2$ (**3**) crystallizes in the monoclinic space group $P2_1/c$ with four formula units per unit cell. Figure 2 shows the formula unit of **3**, containing *cis-cis* and *trans-trans* conformers. One half of the molecules exist as *cis-cis* conformers. The other half holds a disorder, consisting of 82 % *trans-trans*- and 18 % *cis-cis*-fumaryl fluoride. Selected structural parameters of **3** are given in Table 2. The bond lengths and angles (except for the torsion angles) of the *trans-trans* and the *cis-cis* conformer do not differ significantly from one another.

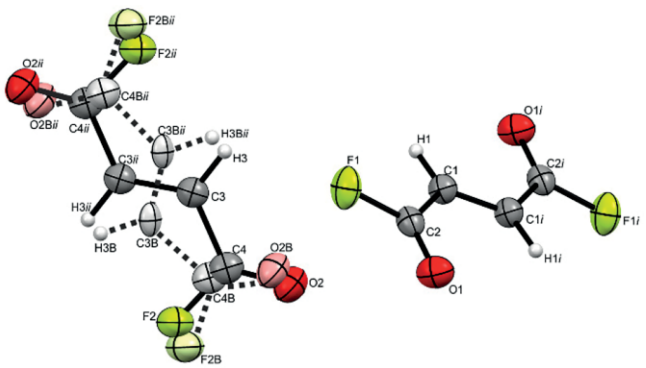

Figure 2. Formula unit of $C_4H_2F_2O_2$ (displacement ellipsoids with 50 % probability). Symmetry operations: *i* = 1–*x*, 1–*y*, –*z*; *ii* = –*x*, 1–*y*, 1–*z*. *Cis-cis*-fumaryl fluoride (right) and *trans-trans*-fumaryl fluoride (left) with 18 % disordered *cis-cis*-fumaryl fluoride (dashed line).

A comparison of the bond lengths and angles of fumaryl fluoride with fumaryl chloride[10] and fumaraldehyde[11] is

Table 2. Selected bond lengths and angles of $C_4H_2F_2O_2$.

	cis-cis-$C_4H_2F_2O_2$		*trans-trans*-$C_4H_2F_2O_2$
Bond lengths /Å			
C1–C1*i* (C=C)	1.314(2)	C3–C3*ii* (C=C)	1.322(6)
C1–C2 (C–C)	1.477(2)	C3–C4 (C–C)	1.473(4)
C2–O1 (C=O)	1.190(2)	C4–O2 (C=O)	1.177(4)
C2–F1 (C–F)	1.334(2)	C4–F2 (C–F)	1.349(3)
Bond angles /°			
O1–C2–F1	120.2(1)	O2–C4–F2	119.5(3)
O1–C2–C1	127.3(2)	O2–C4–C3	127.2(3)
F1–C2–C1	112.5(1)	F2–C4–C3	113.2(3)
C1*i*–C1–C2	120.3(2)	C3*ii*–C3–C4	123.1(3)
Angle of torsion /°			
O1–C2–C1–C1*i*	–4.6(3)	O2–C4–C3–C3*ii*	177.6(5)
F1–C2–C1–C1*i*	175.6(2)	F2–C4–C3–C3*ii*	–2.1(6)
Donor-acceptor distances /°			
		C3–H3···O1	3.528(3)

Symmetry operations: *i* = 1–*x*, 1–*y*, –*z*; *ii* = –*x*, 1–*y*, 1–*z*.

summarized in Table S3 (Supporting Information). Drawing comparisons of fumaryl fluoride with these two derivatives is very interesting, based on the atomic size of fluorine, lying in-between hydrogen and chlorine. The C=O bond lengths [1.190(2) Å (C2–O1)] of fumaryl fluoride agree well with formal C=O double bonds (1.19 Å)[12] and the C=O bond in fumaryl chloride.[10] However, this bond is significantly shorter than in fumaraldehyde [1.207(2) Å],[11] which is attributed to the strong electron-withdrawing effect of fluorine. The C–F bond lengths are with 1.334(2) Å slightly shorter than formal C–F bonds (1.36 Å).[12] The C–C single bond [1.477(2) Å], which is in good agreement with the C–C bonds in fumaryl chloride[10] and fumaraldehyde,[11] is slightly shorter than a formal C–C single bond (1.54 Å).[12] The C=C double bond [1.314(2) Å] is slightly shorter than formal C=C bonds (1.33 Å).[12] This conforms to the C=C bond in fumaraldehyde [1.336(5) Å],[11] which is significantly longer than the one in fumaryl fluoride. It can hence be assumed that the *X* atom of the CO*X* group has great influence on the carbon-carbon bond lengths in the conjugated molecules. The acyl fluoride groups are twisted against one another by 4° out of the carbon-skeleton plane, resulting in a slightly distorted planar structure. The crystal structure of **3** basically consists of the *cis-cis* conformer, indicating the most stable rotational isomer of $C_4H_2F_2O_2$. In the crystal packing of **3**, (Figure S2, Supporting Information) the conformers are connected via hydrogen bonds with C–H···O donor-acceptor distances of 3.528(3) Å, which can be categorized as weak hydrogen bonds in compliance with the classification of *Jeffrey*.[13] The *trans-trans* conformer builds up the hydrogen bond to the O1 oxygen atom of the *cis-cis* conformer. The disordered *cis-cis* species builds up a similar hydrogen bond to the same O1 oxygen atom of the *cis-cis* conformer, which is illustrated in Figure 3.

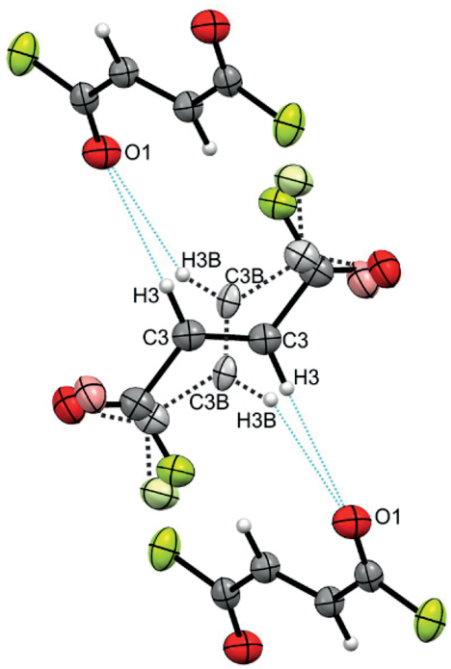

Figure 3. Hydrogen bonds in $C_4H_2F_2O_2$ (displacement ellipsoids with 50% probability).

Crystal Structure of $C_4H_2F_2O_2{\cdot}4(C_4H_2F_2O_2{\cdot}AsF_5){\cdot}(C_4H_2F_2O_2{\cdot}2AsF_5)$

The $C_4H_2F_2O_2{\cdot}4(C_4H_2F_2O_2{\cdot}AsF_5){\cdot}(C_4H_2F_2O_2{\cdot}2AsF_5)$ (**5**) crystallizes in the triclinic space group *P* with one formula unit per unit cell. Figure 4 shows a detail of the crystal structure of **5**, containing four different species. One component of the crystal structure holds a disorder, consisting of 76% *cis-cis*- and 24% *trans-trans*-fumaryl fluoride. Moreover, the crystal structure includes the two monoadducts with arsenic pentafluoride *trans-cis*-$C_4H_2F_2O_2{\cdot}AsF_5$ and *cis-trans*-$C_4H_2F_2O_2{\cdot}AsF_5$. The fourth species is the adduct of fumaryl fluoride with two arsenic pentafluoride molecules (*trans-trans*-$C_4H_2F_2O_2{\cdot}2AsF_5$). Selected structural parameters of **5** are listed in Table S4 in the Supporting Information. Table 3 summarizes selected bond lengths of **5**. The structural parameters of the disordered fumaryl fluoride in **5** are omitted for clarity.

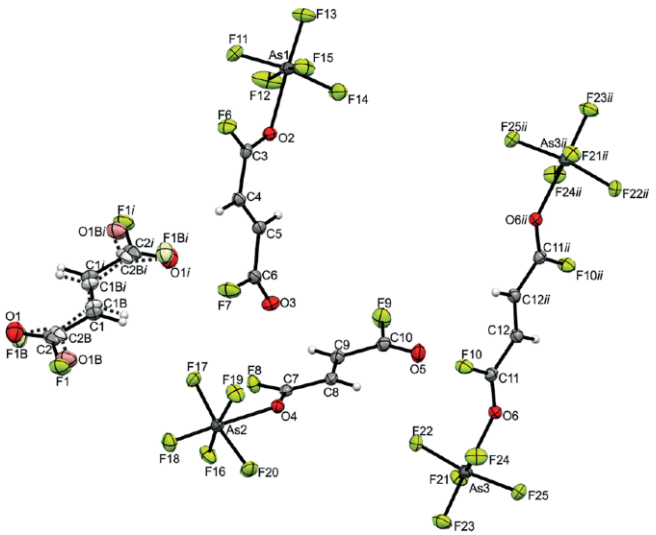

Figure 4. Detail of the crystal structure of **5** (displacement ellipsoids with 50% probability). Symmetry operations: *i* = –*x*, 1–*y*, –z; *ii* = –x, –y, 2–*z*. [*Cis-cis*-fumaryl fluoride with disordered *trans-trans*-fumaryl fluoride (dashed line)].

The coordination site for the Lewis acid is one of the oxygen atoms. The coordination of AsF_5 to fumaryl fluoride does not distort the overall planarity of the molecule. The largest deviations are observed for the carbonyl fluoride groups of *cis-trans*-$C_4H_2F_2O_2{\cdot}AsF_5$ which are twisted against one another by 8° out of the carbon skeleton plane. As might be expected, however, the formation of a monoadduct introduces asymmetry into the molecule so that bonds that were equivalent in **3** are no longer similar in the monoadduct. This effect is most distinct for the C=O bonds, which now have lengths of 1.221(2) Å (C3–O2) and 1.220(2) Å (C7–O4) for the oxygen bonded to AsF_5, respectively, and 1.177(3) Å (C6–O3) and 1.170(3) Å (C10–O5) for the uncoordinated oxygen atom, respectively. Considering the diadduct, the symmetry is rebuilt, leading to C=O distances of 1.215(3) Å (C11–O6). Since the C=O bonds get longer, the C–F bonds, on the other hand, are with 1.301(2) Å (C3–F6), 1.309(2) Å (C7–F8) and 1.304(2) Å (C11–F10) significantly shortened by the formation of the ad-

Table 3. Selected bond lengths of *trans-cis*-$C_4H_2F_2O_2{\cdot}AsF_5$, *cis-trans*-$C_4H_2F_2O_2{\cdot}AsF_5$ and *trans-trans*-$C_4H_2F_2O_2{\cdot}2\ AsF_5$.

Bbond lengths /Å	*trans-cis*-$C_4H_2F_2O_2{\cdot}AsF_5$		*cis-trans*-$C_4H_2F_2O_2{\cdot}AsF_5$		*trans-trans*-$C_4H_2F_2O_2{\cdot}2\ AsF_5$
C4–C5 (C=C)	1.316(3)	C8–C9 (C=C)	1.326(3)	C12–C12*ii* (C=C)	1.334(4)
C5–C6 (C–C)	1.474(3)	C9–C10 (C–C)	1.484(3)		
C3–C4 (C–C)	1.458(3)	C7–C8 (C–C)	1.451(3)	C11–C12 (C–C)	1.467(3)
C6–O3 (C=O)	1.177(3)	C10–O5 (C=O)	1.170(3)		
C3–O2 (C=O)	1.221(2)	C7–O4 (C=O)	1.220(2)	C11–O6 (C=O)	1.215(3)
C6–F7 (C–F)	1.342(2)	C10–F9 (C–F)	1.344(2)		
C3–F6 (C–F)	1.301(2)	C7–F8 (C–F)	1.309(2)	C11–F10 (C–F)	1.304(2)
As1–O2 (As–O)	2.037(2)	As2–O4 (As–O)	2.047(1)	As3–O6 (As–O)	2.044(1)

Symmetry operations: *ii* = –x, –y, 2 –*z*.

ducts. The C=C double bond in *trans-trans*-$C_4H_2F_2O_2{\cdot}2AsF_5$ is remarkably elongated by 0.02 Å, whereas the C=C bonds in the monoadducts are not affected.

However, the C–C bonds in the monoadducts are with 1.458(3) Å (C3–C4) and 1.451(3) Å (C7–C8) significantly shorter than in fumaryl fluoride, whereas the C–C bonds in the diadduct are not changed. The most pronounced effect on the bond angles is for the O–C–C and F–C–C angles. The O6–C11–C12 angle of the diadduct is most distinctively changed and is reduced to 122.5(2)° from 127.3(2)° in **3**. The As–O bond lengths range between 2.037(2) Å (As1–O2) and 2.047(1) Å (As2–O4), which are longer than formal As–O bond lengths (1.85 Å).[12] However, these bond lengths conform to calculated values in the literature of other O-coordinated adducts like $F_5As{-}O{=}C(CH_3)_2$ (2.065 Å).[14] The As–F bond lengths in all of the adducts are in the range between 1.703(1) Å and 1.684(1) Å, which are shorter than formal As–F bond lengths (1.78 Å).[12] These values are in good agreement with calculated and experimental bond lengths of arsenic pentafluoride adducts.[15] The bond angles of the AsF_5–O moiety of the adduct, indicate a slightly distorted octahedral structure. No hydrogen bonds are observed in the crystal structure of **5**.

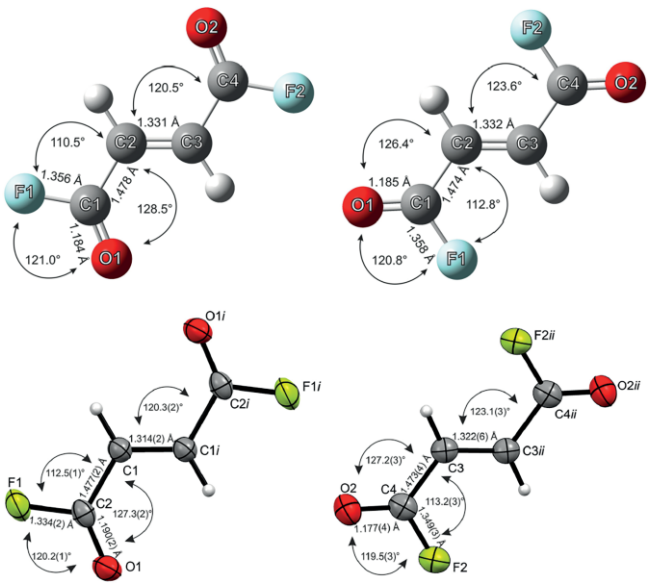

Figure 5. Calculated and experimental structures of $C_4H_2F_2O_2$. *Cis-cis*-fumaryl fluoride (left) and *trans-trans*-fumaryl fluoride (right). The disordered *cis-cis* conformer is omitted in the experimental structures for clarification. Symmetry operations: *i* = 1–*x*, 1–*y*, –z; *ii* = –*x*, 1–*y*, 1–*z*.

Quantum Chemical Calculations

The quantum chemical calculations of the *trans-trans*, *cis-cis* and *cis-trans* conformers were carried out using the B3LYP/aug-cc-pVTZ level of theory. Since the crystallized fumaryl fluoride (**3**) only consists of the centrosymmetric conformers, the *cis-trans* conformer is not discussed in detail in this section. A comparison of the calculated and the experimental structures of the *cis-cis* and *trans-trans* species is shown in Figure 5.

The structural parameters of the rotational isomers are in good agreement with the experimental values (Table S5, Supporting Information). To compare the three discrete rotational isomers, their energy differences were calculated on the CCSD-FC/aug-cc-pVTZ level of theory. The *trans-trans*, *cis-cis* and the *cis-trans* conformers are illustrated in Figure 6 together with their energy differences. All three geometries are real minima since they reveal no negative frequencies. The global energetic minimum is found for the *trans-trans* conformer.

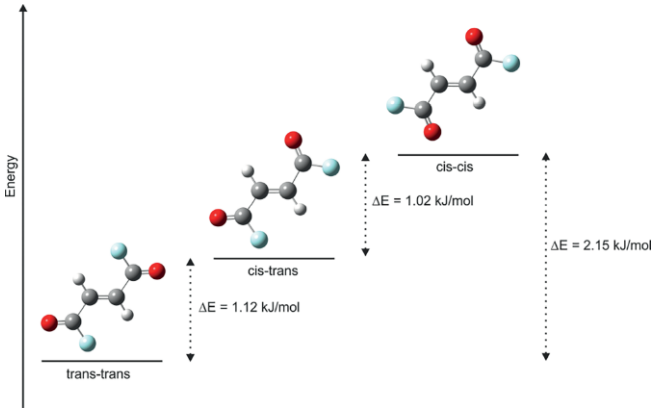

Figure 6. The three discrete conformers of fumaryl fluoride and their calculated energy differences.

In conjugated aldehydes, the energy difference between the two possible conformers is so high (>5.02 kJ·mol^{-1}) that only a very small quantity of the second isomer is present at ambi-

ent temperatures.[16,17] In acrolein e.g., the configuration of the lowest energy is the *trans*-position[17,18] with an energy difference to the *cis* conformer of 6.99 kJ·mol^{-1}.[19] This is consistent with fumaraldehyde[11,20] existing only as its *trans-trans* rotational isomer revealing an energy difference to the *cis-cis* species of 13.50 kJ·mol^{-1}.[20] The energy differences between the *cis* and the *trans* species for some molecules of the general formula RHC=CHC(O)*X* are summarized in Table 4. The nature of the substituent *X*, which is bound to the carbonyl carbon atom, has a great influence on the relative order of stability of the *cis* and the *trans* conformers.[21] In the case of a halogen atom as a substituent, the relative energies of the rotational isomers seem to be considerably reduced.[6,10] Therefore in fumaryl fluoride,[6] fumaryl chloride,[10] acrylyl fluoride,[22] and acrylyl chloride[23] there are additionally notable concentrations of the high-energy conformers present at room temperature.

Table 4. Energy differences for several molecules of the general formula RHC=CHC(O)*X*.

Molecule	Formula	Δ*E*(*cis* – *trans*)
Fumaryl fluoride	F(O)CHC=CHC(O)F	2.15 kJ·mol^{-1}
Fumaryl chloride	Cl(O)CHC=CHC(O)Cl	2.93 kJ·mol^{-1} [10]
Fumaraldehyde	H(O)CHC=CHC(O)H	13.50 kJ·mol^{-1} [20]
Acrylyl fluoride	H_2C=CHC(O)F	–0.95 kJ·mol^{-1} [23]
Acrylyl chloride	H_2C=CHC(O)Cl	1.76 kJ·mol^{-1} [23]
Acrolein	H_2C=CHC(O)H	6.99 kJ·mol^{-1} [19]

In contrast to fumaraldehyde, for which only one conformer (*trans-trans*) was found,[11] in fumaryl fluoride and fumaryl chloride, a mixture of different rotational isomers was observed, respectively.[6,8] Using the values in Figure 6, we find that the *cis-trans* conformer of fumaryl fluoride has an energy 1.12 kJ·mol^{-1} higher than the *trans-trans* conformer. In fumaryl chloride, the energy difference between these two conformers is with 2.51 kJ·mol^{-1} [10] considerably higher. The energy difference between the *cis-cis*-fumaryl fluoride and the *cis-trans* conformer is calculated to be 1.02 kJ·mol^{-1}, which is compared to fumaryl chloride (Δ*E* = 0.42 kJ·mol)[10] remarkably higher. The energy difference between the low-energy conformer (*trans-trans*) and the highest energy form (*cis-cis*) is with 2.93 kJ·mol^{-1} [10] higher than in fumaryl fluoride (2.15 kJ·mol^{-1}).

The quantum chemical calculations for fumaryl fluoride agree with the *trans-trans* conformer being thermodynamically preferred, which contradicts the experimental data of **3**. Since crystalline fumaryl chloride reveals only *trans-trans* conformers,[8] crystalline fumaryl fluoride principally consists of the *cis-cis* conformers. Similar observations have been made regarding the acrylyl derivatives. For the chloride, the *trans* conformer is clearly the more stable form, whereas the *cis* conformation is thermodynamically preferred for the fluoride molecule.[23] Therefore, the introduction of a halogen atom must destabilize the low-energy *trans* conformer and stabilize the *cis* species.[10] These observations can be interpreted by considering that when conjugation is possible between the carbonyl and the *X* substituent, the *cis* conformer is explicitly stabilized concerning the *trans* conformer,[21,24] which affects mostly the fluorine derivatives. Another essential factor that favors the *cis* conformers in the fluorine derivatives is the steric repulsions between RHC=CH and the oxygen atoms.[21]

The quantum chemically calcualted energy differences between the three conformers are in general very small, at the edge of accuracy of the theoretical method, and can be overcome easily. These small energy differences lead to the fact that at least two different conformers are present in each state of matter and an isolation of one conformer is not observed. This agrees well with the observation of the crystal structure of **5**. More than one conformer is present in the formation of the adducts with AsF_5.

Conclusions

The molecular structure and the conformational composition of fumaryl fluoride were determined by low-temperature vibrational spectroscopy and single-crystal X-ray analysis. All of the possible planar rotational isomers *trans-trans*-, *cis-cis*- and *cis-trans*-fumaryl fluoride were identified. Since crystalline fumaryl fluoride consists exclusively of the centrosymmetric conformers, principally of the *cis-cis* conformer, the gaseous, the liquid and the amorphous state reveal additionally the *cis-trans* species. Quantum chemical calculations at the B3LYP/aug-cc-pVTZ level of theory were considered for the assignment of the vibrational spectra. Comparing the three discrete rotational isomers, their energy differences were calculated at the CCSD-FC/aug-cc-pVTZ level of theory. Comparison to related molecules like fumaryl chloride[8] and fumaraldehyde[11] showed that the substitution of a halogen atom for an aldehyde proton has a considerable effect on the energy of the conformation. The same impact is observed, when comparing the conformation of acrolein[19] with that of acrylyl chloride[23] and acrylyl fluoride.[23]

Furthermore, oxygen-coordinated adducts of fumaryl fluoride with AsF_5 were prepared and characterized by X-ray crystallography. Monoadducts are formed out of the *cis-trans* conformers of fumaryl fluoride, whereas the diadduct crystallizes only as the centrosymmetric *trans-trans* conformer.

Experimental Section

Caution! Any contact with the components must be avoided. Arsenic pentafluoride is highly toxic and produces HF upon contact with water, such as fumaryl fluoride. Hydrogen fluoride can cause burns upon contact or inhalation and causes irreparable damage. Adequate safety measures must be implemented when handling these materials.

Apparatus and Materials: All experiments were executed on an electropolished stainless-steel vacuum line. For the synthesis of fumaryl fluoride, Young sample glass flasks with Young valves were employed. For the synthesis of the adducts with AsF_5, transparent FEP-reactors with PFA-adapters were utilized. The stainless-steel vacuum line and the reaction vessels were dried using fluorine. In a dynamic vacuum, excess fluorine was removed and absorbed by Sodalime. Low-temperature Raman spectroscopic measurements were performed on a Bruker® MultiRAMII FT-Raman spectrometer equipped with a Nd:YAG laser (λ = 1064 nm). The interpretation of the spectra was

conducted with the help of the software Advanced Chemistry Development, Inc.® (ACD/Labs 2015). Low-temperature IR spectra were recorded on a Bruker® Vertex-80V-FT-IR spectrometer. For the gas-phase IR spectra the optical path is 10 cm. The spectra were evaluated by using the same software as for the Raman spectra. The low-temperature single-crystal X-ray diffraction was carried out on an Oxford XCalibur3 diffractometer equipped with a Spellman generator (50 kV, 40 mA) and a Kappa CCD-detector, operating with Mo-K_α radiation (λ = 0.7107 Å) at 120 K. Data collection was performed using the CrysAlisCCD software[25] and for the reduction of the data set CrysAlisRED[26] was used. For the solution and refinement of the structure, the programs SHELXS-97[27] and SHELXL-97[28] integrated into the WinGX software package[29] were applied. The structures were checked with the help of the software PLATON.[30] The absorption correction was executed using the SCALE3 ABSPACK multiscan method.[31] Crystal data and structure refinement for the reported single-crystal structures are given in Tables S6 and S7 (Supporting Information). Quantum chemical calculations were carried out using the software package Gaussian09.[32] The quantum chemical calculations of the *trans-trans*-, *cis-cis*- and *cis-trans*-fumaryl fluoride were carried out using the B3LYP/aug-cc-pVTZ level of theory. To compare the three discrete rotational isomers, their energy differences were calculated on the CCSD-FC/aug-cc-pVTZ level of theory.

Synthesis of fumaryl fluoride: The preparation procedure was previously reported by *Vasileff et al.*[7] A glass flask with a grease-free stopcock was filled with the lewis acid SbF_3 (80 mmol) and $C_4H_2Cl_2O_2$ (40 mmol) in a nitrogen atmosphere. After the mixture was frozen at –196 °C, the glass flask was evacuated. Both components were warmed up, then stirred and heated at 100 °C for 1 h, in a static vacuum. The more volatile fumaryl fluoride was then condensed into another glass flask with a grease-free stopcock at –196 °C. A colorless liquid was formed in all of the experiments with a yield of around 90 %. The reaction of fumaryl chloride and antimony(III) fluoride leads to a very pure product of fumaryl fluoride. In the spectra of (**1**) (Figure S1, Supporting Information) no detectable impurities of the starting materials are observed. Therefore, fumaryl fluoride was used without further purification.

Synthesis of $C_4H_2F_2O_2$·4($C_4H_2F_2O_2$·AsF_5)·($C_4H_2F_2O_2$·2AsF_5): $C_4H_2F_2O_2$ (2.0 mmol) was condensed in a FEP-reactor vessel at –196 °C followed by the Lewis acid AsF_5 (2 mmol). Accordingly, SO_2ClF (2 mL) was added to the frozen mixture at –196 °C. The reaction mixture was warmed up to –30 °C and homogenized until a colorless solution was obtained. In a dynamic vacuum, excess solvent was slowly removed at –78 °C. In all of the experiments, with modified ratios of fumaryl fluoride to AsF_5, no crystals for single-crystal X-ray analysis were obtained. Colorless solids were formed in all of the experiments.

Supporting Information (see footnote on the first page of this article): The supporting information contains Raman and IR spectra of fumaryl fluoride (**1**) and fumaryl chloride (Figure S1); Experimental vibrational frequencies of fumaryl chloride in comparison with literature data[6,8] (Table S1); Experimental vibrational frequencies of fumaryl fluoride in different states of matter in comparison with literature data[6] and calculated vibrational frequencies of *trans-trans*-, *cis-cis*- and *cis-trans*-fumaryl fluoride (Table S2); Selected experimental bond lengths and angles of fumaryl fluoride in comparison with fumaryl chloride[10] and fumaraldehyde[11] (Table S3); Illustration of the crystal packing along the *b*-axis (50 % probability displacement ellipsoids) (Figure S2); Selected bond lengths and angles of *trans-cis*-$C_4H_2F_2O_2$·AsF_5, *cis-trans*-$C_4H_2F_2O_2$·AsF_5 and *trans-trans*-$C_4H_2F_2O_2$·2AsF_5. Symmetry operations: *ii* = *–x, –y, 2 –z* (Table S4); Selected experimental and calculated bond lengths and angles of $C_4H_2F_2O_2$ (Table S5); Crystal data and structure refinement of $C_4H_2F_2O_2$ (Table S6); Crystal data and structure refinement of $C_4H_2F_2O_2$·4($C_4H_2F_2O_2$·AsF_5)·($C_4H_2F_2O_2$·2AsF_5) (Table S7).

Acknowledgements

We gratefully acknowlegde the financial support of the Deutsche Forschungsgemeinschaft (DFG), the Ludwig-Maximilians-Universität (LMU) and the F-Select GmbH. Open access funding enabled and organized by Projekt DEAL.

Keywords: Fumaryl fluoride; Quantum chemical calculations; Vibrational spectroscopy; X-ray structure analysis; Rotational isomerism; Energy differences; AsF_5 adducts

References

[1] S. B. Munoz, H. Dang, X. Ispizua-Rodriguez, T. Mathew, G. K. S. Prakash, *Org. Lett.* **2019**, *21*, 1659.
[2] I. Ojima, *Fluorine in Medicinal Chemistry and Chemical Biology*, John Wiley & Sons, Ltd, Chichester, UK, **2009**.
[3] T. Hiyama, Organofluorine Compounds: Chemistry and Applications, Springer-Verlag, Berlin, **2000**.
[4] A. L. Henne, *Org. React.* **1944**, *2*, 49.
[5] R. Stephens, J. C. Tatlow, *Q. Rev. Chem. Soc.* **1962**, *16*, 44.
[6] D. F. Koster, T. P. Vasileff, G. L. Carlson, *Spectrochim. Acta Part A: Mol. Spectrosc.* **1971**, *27*, 1633.
[7] T. P. Vasileff, D. F. Koster, *J. Org. Chem.* **1970**, *35*, 2461.
[8] J. M. Landry, J. E. Katon, *Spectrochim. Acta Part A: Mol. Spectrosc.* **1984**, *40*, 871.
[9] a) W. O. George, A. J. Porter, *J. Chem. Soc., Perkin Trans. 1* **1973**, 954; b) C. Téllez, R. Knudsen, O. Sala, *J. Mol. Struct.* **1980**, *67*, 189; c) J. E. Katon, P.-H. Chu, *J. Mol. Struct.* **1982**, *78*, 141; d) J. E. Katon, P.-H. Chu, *J. Mol. Struct.* **1982**, *82*, 61.
[10] K. Hagen, *J. Mol. Struct.* **1985**, *128*, 139.
[11] G. Paulen, M. Trætteberg, N. Nigri, A. Kjekshus, B. Klewe, D. L. Powell, *Acta Chem. Scand. A* **1974**, *28*, 1155.
[12] A. F. Holleman, E. Wiberg, N. Wiberg, G. Fischer, *Anorganische Chemie*, De Gruyter, Berlin, Boston, **2017**.
[13] G. A. Jeffrey, *An introduction to hydrogen bonding. Topics in physical chemistry*, Oxford University Press, New York, **1997**.
[14] D. Stuart, S. D. Wetmore, M. Gerken, *J. Fluorine Chem.* **2019**, *221*, 9.
[15] a) B. Hoge, J. A. Boatz, J. Hegge, K. O. Christe, *Inorg. Chem.* **1999**, *38*, 3143; b) A. Apblett, T. Chivers, J. F. Richardson, *Can. J. Chem.* **1986**, *64*, 849.
[16] J. E. Katon, W. R. Feairheller, *J. Chem. Phys.* **1967**, *47*, 1248.
[17] M. S. de Groot, J. Lamb, *Proc. R. Soc. London A* **1957**, *242*, 36.
[18] E. A. Cherniak, C. C. Costain, *J. Chem. Phys.* **1966**, *45*, 104.
[19] L. A. Carreira, *J. Phys. Chem.* **1976**, *80*, 1149.
[20] L. K. Zen, H. H. Abdallah, C. S. Xian, W. Z. Xiang, *Science Int. (Lahore, Pakistan)* **2011**, *23*, 183.
[21] A. Kulbida, M. N. Ramos, M. Rasanen, J. Nieminen, O. Schrems, R. Fausto, *Faraday Trans.* **1995**, *91*, 1571.
[22] J. R. Durig, J. S. Church, D. A. C. Compton, *J. Chem. Phys.* **1979**, *71*, 1175.
[23] J. R. Durig, R. J. Berry, P. Groner, *J. Chem. Phys.* **1987**, *87*, 6303.
[24] D. F. Koster, *J. Am. Chem. Soc.* **1966**, *88*, 5067.
[25] CrysAlisCCD, Version 1.171.35.11 (release 16–05–2011 CrysAlis 171.NET), Oxford Diffraction Ltd, UK, **2011**.
[26] CrysAlisRED, Version 1.171.35.11 (release 16–05–2011 CrysAlis 171.NET), Oxford Diffraction Ltd, UK, **2011**.
[27] G. M. Sheldrick, *SHELXS-97*, Program for Crystal Structure Solution, University of Göttingen, Germany, **1997**.

[28] G. M. Sheldrick, *SHELXL-97*, Program for Crystal Structure Solution, University of Göttingen, Germany, **1997**.
[29] L. J. Farrugia, *J. Appl. Crystallogr.* **1999**, *32*, 837.
[30] A. L. Speck, *PLATON, A Multipurpose Crystallographic Tool*, Utrecht University, Utrecht, Netherlands, **1999**.
[31] SCALE3 ABSPACK, An Oxford Diffraction Program, Oxford Diffraction Ltd, UK, **2005**.
[32] M. J. Frisch, G. W. Trucks, H. B. Schlegel, G. E. Scuseria, M. A. Robb, J. R. Cheeseman, G. Scalmani, V. Barone, B. Mennucci, G. A. Petersson, H. Nakatsuji, M. Caricato, X. Li, H. P. Hratchian, A. F. Izmaylov, J. Bloino, G. Zheng, J. L. Sonnenberg, M. Hada, M. Ehara, K. Toyota, R. Fukuda, J. Hasegawa, M. Ishida, T. Nakajima, Y. Honda, O. Kitao, H. Nakai, T. Vreven, J. A. Montgomery, J. E. Peralta, F. Ogliaro, M. Bearpark, J. J. Heyd, E. Brothers, K. N. Kudin, V. N. Staroverov, R. Kobayashi, J. Normand, K. Raghavachari, A. Rendell, J. C. Burant, S. S. Iyengar, J. Tomasi, M. Cossi, N. Rega, J. M. Millam, M. Klene, J. E. Knox, J. B. Cross, V. Bakken, C. Adamo, J. Jaramillo, R. Gomperts, R. E. Stratmann, O. Yazyev, A. J. Austin, R. Cammi, C. Pomelli, J. W. Ochterski, R. L. Martin, K. Morokuma, V. G. Zakrzewski, G. A. Voth, P. Salvador, J. J. Dannenberg, S. Dapprich, A. D. Daniels, O. Farkas, J. B. Foresman, J. V. Ortiz, J. Cioslowski, D. J. Fox, *Gaussian09, Revision A.02*, Gaussian, Inc, Wallingford CT, **2009**.

Received: June 28, 2020
Published Online: September 9, 2020

Z. Anorg. Allg. Chem. **2020** · ISSN 0044–2313

SUPPORTING INFORMATION

Title: Structure and Properties of Fumaryl Fluoride
Author(s): M. C. Bayer, C. Jessen, A. J. Kornath*
Ref. No.: z202000248

Supporting Information

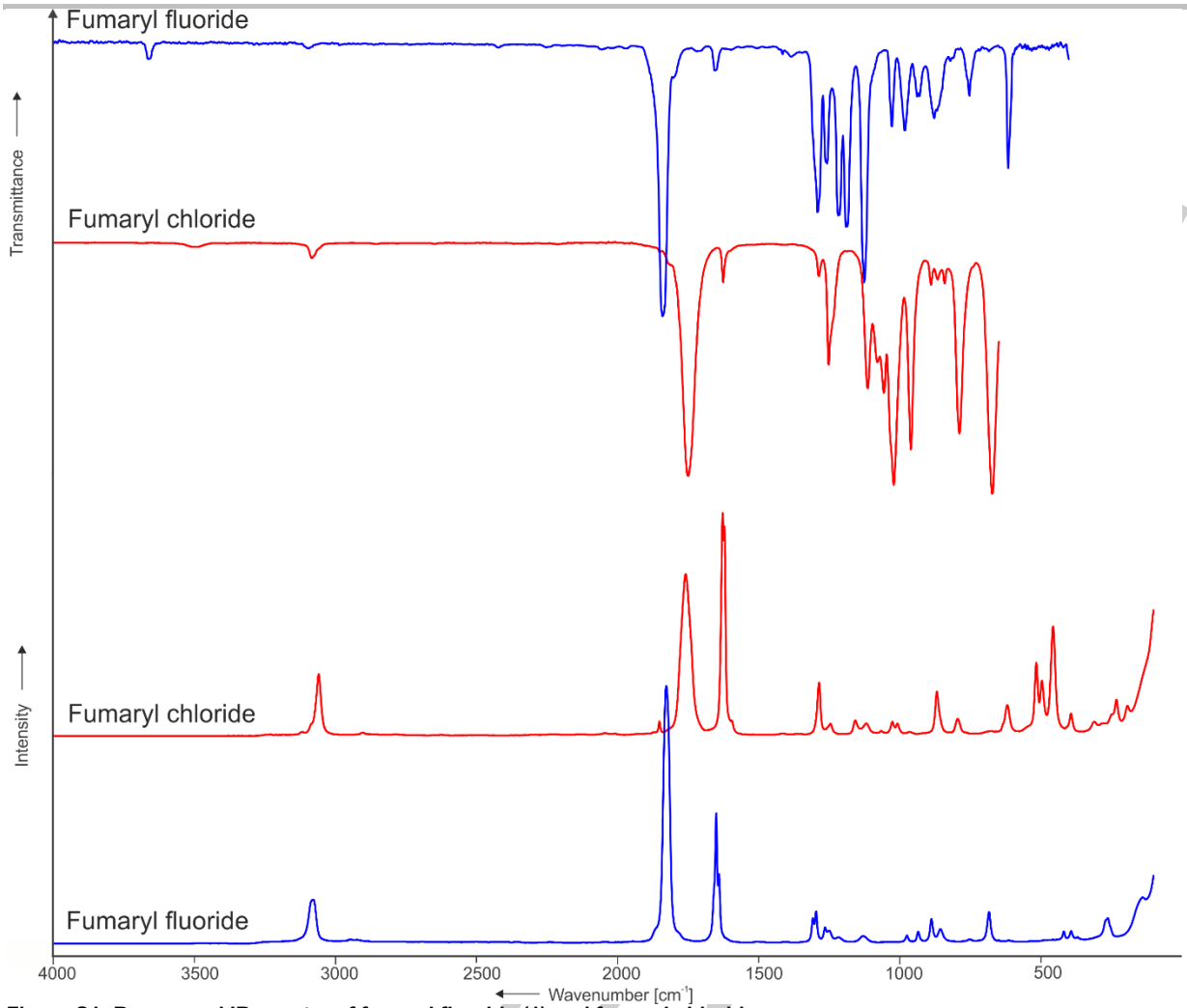

Figure S1: Raman and IR spectra of fumaryl fluoride (1) and fumaryl chloride.

Table S1: Experimental vibrational frequencies [cm^{-1}] of fumaryl chloride in comparison with literature data.[1,2]

$C_4H_2Cl_2O_2$ exp.[a]		$C_4H_2Cl_2O_2$ lit.[1,2]		*trans-trans*-$C_4H_2Cl_2O_2$ calc.[b,c]	Assignment[1]			
IR	Raman	IR	Raman	IR/Raman		*trans-trans*		*cis-trans*
3505 wv		3498					[d]	
3084 wv		3084						ν(C–H)
		3073		3198(5/0)	ν_{17}	B_u	ν_{as}(C–H)	
	3059(28)		3060	3194(0/97)	ν_1	A_g	ν_s(C–H)	
1851 vw	1851(6)						[d]	
1750 vs		1762		1826(643/0)	ν_{18}	B_u	ν_{as}(C=O)	
	1759(73)		1756	1822(0/268)	ν_2	A_g	ν_s(C=O)	
1626 vw	1628(100)	1627	1628					ν(C=C)
	1621(94)		1620	1694(0/179)	ν_3	A_g	ν(C=C)	
	1595(7)						[d]	
1287 vw	1285(24)		1284	1316(0/17)	ν_4	A_g	δ_s(C–H)	
1252 m	1246(5)	1253	1250					δ(C–H)
		1235		1263(12/0)	ν_{19}	B_u	δ_{as}(C–H)	
	1158(7)		1158	1150(0/46)	ν_5	A_g	ν_s(C–C)	
1114 m	1118(6)	1116	1116					ν(C–C)
1080 m		1081					[d]	
1057 m		1058		1068(487/0)	ν_{20}	B_u	ν_{as}(C–C)	
1022 vs	1026(6)	1027	1026				[d]	
	1008(6)						[d]	
961 vs	965(2)	964		1018(36/0)	ν_{10}	A_u	γ_{as}(C–H)	
890 vw		887					[d]	
866 vw	869(20)	867	868	927(0/5)	ν_{14}	B_g	γ_s(C–H)	
842 vw		842					[d]	
789 s	795(8)	795	795					ν(C–Cl)
673 vs		680		702(7/0)	ν_{11}	A_u	γ_{as}(OCCl)	
			626	678(255/0)	ν_{21}	B_u	ν_{as}(C–Cl)	
	619(14)	619	618					ν(C–Cl)
	517(33)						[d]	
	496(25)		496					δ(OCCl)
	457(49)	460		621(0/7)	ν_6	A_g	ν_s(C–Cl)	
			456	547(0/0)	ν_{15}	B_g	γ_s(OCCl)	
		430		503(0/28)	ν_7	A_g	δ_s(OCCl)	
	393(10)		393	449(14/0)	ν_{22}	B_u	δ_{as}(COCl)	
	311(6)	312	314					δ(CCO)
		241		428(50/0)	ν_{23}	B_u	δ_{as}(CCO)	
	233(16)		232	384(0/6)	ν_8	A_g	δ_s(CCO)	
	194(14)		194	187(0/3)	ν_9	A_g	δ_s(CCC)	
				134(0/1)	ν_{16}	B_g	γ_s(CCC)	
				131(9/0)	ν_{12}	A_u	γ_{as}(CCC)	
				117(6/0)	ν_{24}	B_u	δ_{as}(CCC)	
				31(1/0)	ν_{13}	A_u	τ(OCCl)	

[a] Abbrevations for IR intensities: vs = very strong, s = strong, m = medium, w = weak.
[b] Calculated on the B3LYP/aug-cc-pVTZ level of theory.
[c] IR intensities in km/mol; Raman intensities in Å^4/u.
[d] Very probably combination tones/ overtones.

Table S2: Experimental vibrational frequencies [cm^{-1}] of fumaryl fluoride in different states of matter in comparison with literature data[2] and calculated vibrational frequencies [cm^{-1}] of *trans-trans*-, *cis-cis*- and *cis-trans*-fumaryl fluoride.

$C_4H_2F_2O_2$ exp.[a]				$C_4H_2F_2O_2$ lit.[2]	$C_4H_2O_2F_2$ calc.[b,c]									
Raman (liquid) **(1)**	Raman (amorphous) **(2)**	Raman (crystalline) **(3)**	IR (gaseous) **(4)**	Raman				Assignment *cis-cis*			Assignment *trans-trans*			Assignment *cis-trans*		
			3664 vw					[d]								
			3097 vw		3207(3/0)	ν_{17}	B_u	ν_{as}(C–H)								
3079(17)	3080(31)	3084(23)			3203(0/96)	ν_1	A_g	ν_s(C–H)								
			1840 vs		1866(517/0)	ν_{18}	B_u	ν_{as}(C=O)								
1827(100)	1825(100)				1867(345/208)									ν_4	A'	ν(C=O)
		1819(39)			1868(0/351)				ν_2	A_g	ν_s(C=O)					
	1803(97)	1806(100)			1871(0/154)	ν_2	A_g	ν_s(C=O) [d]								
	1667(10)															
1651(51)	1655(52)		1655 vw	1650	1700(22/147)									ν_5	A'	ν(C=C)
1641(27)	1643(50)	1643(53)			1706(0/165)	ν_3	A_g	ν(C=C)								
			1385 vw		1328(43/12)									ν_6	A'	δ(CCH)
	1315(5)							[d]								
1307(10)	1306(28)	1305(32)			1331(0/9)	ν_4	A_g	δ_s(CCH) [d]								
1296(13)																
			1292 s		1305(379/0)	ν_{19}	B_u	δ_{as}(CCH) [d]								
	1288(2)															
	1273(4)				1285(92/6)									ν_7	A'	δ(CCH)
1264(6)	1259(8)	1259(8)			1126(0/12)	ν_5	A_g	ν_s(C–F)								
		1257(12)			1247(0/29)				ν_5	A_g	ν_s(C–F)					
1251(5)			1257 m		1214(277/10)									ν_8	A'	ν(C–C)
1217(3)			1219 s		1123(305/6)									ν_9	A'	ν(C–C)
			1213 s					[d]								
			1192 s					[d]								
			1186 s					[d]								
	1160(2)							[d]								
	1141(9)							[d]								
1130(3)								[d]								
			1126 vs		1122(480/0)	ν_{20}	B_u	ν_{as}(C–C)								
			1028 w		1026(44/0)	ν_{10}	A_u	γ_{as}(CCH)								
975(3)	979(6)		984 w	978	939(52/3)									ν_{10}	A'	ν(C–F)
			939 w					[d]								
935(5)			932 w	931	936(1/5)									ν_{19}	A''	γ(CCH)
	899(13)	900(15)			981(0/5)	ν_6	A_g	ν_s(C–C) [d]								
	893(8)															
888(10)	889(10)				851(43/4)									ν_{11}	A'	ν(C–F)
			879 w		888(116/0)	ν_{21}	B_u	ν_{as}(C–F) [d]								
	867(10)		870 w													
		862(9)			850(0/9)				ν_6	A_g	ν_s(C–C)					
856(6)								[d]								

Table is continued on the following page.

			822 vw		773(28/0)	ν_{11}	A_u	γ_{as}(CCOF)								
753(2)			754 w		774(26/0)									ν_{20}	A''	γ(CCOF)

		691(9)	689(0/7)			ν_7	A_g	δ_s(OCF)			
684(12)	686(11)		684(8/8)						ν_{12}	A'	δ(COF)
		617 m	618(42/0)	ν_{22}	B_u	δ_{as}(COF)					
	612(2)		617(0/0)						ν_{21}	A''	γ(CCOF)
419(5)	422(9)	420(8)	355(0/2)	ν_8	A_g	δ_s(CCF) [d]					
392(5)											
371(3)	370(4)		380(0/3)			[d]			ν_{15}	A'	δ(CCO)
	280(9)										
263(10)			260(1/2)						ν_{16}	A'	δ(CCC)
	252(5)	256(4)	270(0/4)	ν_9	A_g	δ_s(CCC)					
	178(10)		148(10/1)						ν_{22}	A''	γ(CCC)
		167(9)	250(0/2)				ν_9	A_g	δ_s(CCC)		
	154(10)		132(2/1)						ν_{23}	A''	γ(CCC)
140(18)	145(11)		129(7/0)						ν_{17}	A'	δ(CCC)
		115(44)	143(0/2)				ν_{16}	B_g	γ_s(CCC)		
	105(43)		45(0/0)						ν_{24}	A''	τ(OCF)

[a] Abbrevations for IR intensities: vs = very strong, s = strong, m = medium, w = weak.
[b] Calculated on the B3LYP/aug-cc-pVTZ level of theory.
[c] IR intensities in km/mol; Raman intensities in $Å^4/u$.
[d] Very probably combination tones/ overtones.

Table S3: Selected experimental bond lengths and angles of fumaryl fluoride in comparison with fumaryl chloride[3] and fumaraldehyde.[4]

	cis-cis-fumaryl fluoride	fumaryl chloride[3]	fumaraldehyde[4]
bond lengths [Å]			
C=C	1.314(2)	1.334(5)	1.336(5)
C–C	1.477(2)	1.488(3)	1.479(2)
C=O	1.190(2)	1.191(2)	1.207(2)
C–*X*	1.334(2) (*X* = F)	1.783(2) (*X* = Cl)	---
bond angles [°]			
O–C–C	127.3(2)	125.5(4)	123.6(5)
C–C–C	120.3(2)	125.2(6)	122.7(6)

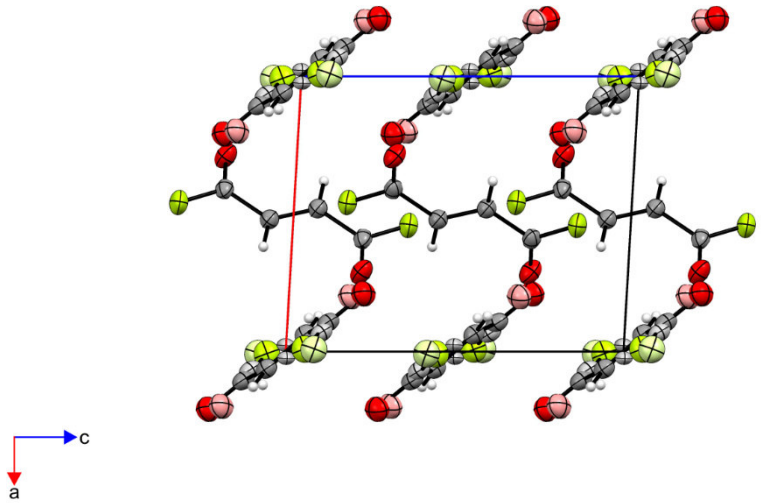

Figure S2: Illustration of the crystal packing along the *b*-axis (50% probability displacement ellipsoids).

Table S4: Selected bond lengths and angles of *trans-cis*-$C_4H_2F_2O_2 \cdot AsF_5$, *cis-trans*-$C_4H_2F_2O_2 \cdot AsF_5$ and *trans-trans*-$C_4H_2F_2O_2 \cdot 2\ AsF_5$. Symmetry operations: *ii* = –x, –y, 2–z.

bond lengths [Å]	*trans-cis*-$C_4H_2F_2O_2 \cdot AsF_5$		*cis-trans*-$C_4H_2F_2O_2 \cdot AsF_5$		*trans-trans*-$C_4H_2F_2O_2 \cdot 2\ AsF_5$
C4–C5 (C=C)	1.316(3)	C8–C9 (C=C)	1.326(3)	C12–C12*ii* (C=C)	1.334(4)
C5–C6 (C–C)	1.474(3)	C9–C10 (C–C)	1.484(3)		
C3–C4 (C–C)	1.458(3)	C7–C8 (C–C)	1.451(3)	C11–C12 (C–C)	1.467(3)
C6–O3 (C=O)	1.177(3)	C10–O5 (C=O)	1.170(3)		
C3–O2 (C=O)	1.221(2)	C7–O4 (C=O)	1.220(2)	C11–O6 (C=O)	1.215(3)
C6–F7 (C–F)	1.342(2)	C10–F9 (C–F)	1.344(2)		
C3–F6 (C–F)	1.301(2)	C7–F8 (C–F)	1.309(2)	C11–F10 (C–F)	1.304(2)
As1–O2 (As–O)	2.037(2)	As2–O4 (As–O)	2.047(1)	As3–O6 (As–O)	2.044(1)
bond angles [°]					
O3–C6–F7	120.9(2)	O5–C10–F9	121.0(2)		
O2–C3–F6	120.3(2)	O4–C7–F8	119.8(2)	O6–C11–F10	121.2(2)
O3–C6–C5	126.6(2)	O5–C10–C9	128.6(2)		
O2–C3–C4	124.4(2)	O4–C7–C8	124.4(2)	O6–C11–C12	122.5(2)
F7–C6–C5	112.5(2)	F9–C10–C9	110.3(2)		
F6–C3–C4	115.3(2)	F8–C7–C8	115.8(2)	F10–C11–C12	116.3(2)
C4–C5–C6	123.6(2)	C8–C9–C10	120.1(2)		
C5–C4–C3	119.7(2)	C9–C8–C7	120.8(2)	C12*ii*–C12–C11	120.8(3)
C3–O2–As1	132.3(2)	C7–O4–As2	130.7(1)	C11–O6–As3	130.8(1)
angle of torsion [°]					
O3–C6–C5–C4	177.6(2)	O5–C10–C9–C8	6.4(4)		
F7–C6–C5–C4	–3.7(3)	F9–C10–C9–C8	–172.6(2)		
C3–C4–C5–C6	178.6(2)	C10–C9–C8–C7	178.1(2)		
F6–C3–C4–C5	–175.8(2)	F8–C7–C8–C9	8.8(3)	F10–C11–C12–C12	4.0(4)
O2–C3–C4–C5	2.4(3)	O4–C7–C8–C9	–172.3(2)	O6–C11–C12–C12	–174.5(3)
As1–O2–C3–C4	–177.4(1)	As2–O4–C7–C8	–179.4(2)	As3–O6–C11–C12	178.5(1)
As1–O2–C3–F6	0.6(3)	As2–O4–C7–F8	–0.5(3)	As3–O6–C11–F10	0.1(3)

Table S5: Selected experimental and calculated bond lengths and angles of $C_4H_2F_2O_2$. Symmetry operations: *i* = 1–x, 1–y, –z; *ii* = –x, 1–y, 1–z.

Crystal structure				Calculated structures[a]		
	cis-cis-$C_4H_2F_2O_2$		*trans-trans*-$C_4H_2F_2O_2$		*cis-cis*-$C_4H_2F_2O_2$	*trans-trans*-$C_4H_2F_2O_2$
bond lengths [Å]						
C1–C1*i* (C=C)	1.314(2)	C3–C3*ii* (C=C)	1.322(6)	C2–C3 (C=C)	1.331	1.332
C1–C2 (C–C)	1.477(2)	C3–C4 (C–C)	1.473(4)	C1–C2 (C–C)	1.478	1.474
C2–O1 (C=O)	1.190(2)	C4–O2 (C=O)	1.177(4)	C1–O1 (C=O)	1.184	1.185
C2–F1 (C–F)	1.334(2)	C4–F2 (C–F)	1.349(3)	C1–F1 (C–F)	1.356	1.358
bond angles [°]						
O1–C2–F1	120.2(1)	O2–C4–F2	119.5(3)	O1–C1–F1	121.0	120.8
O1–C2–C1	127.3(2)	O2–C4–C3	127.2(3)	O1–C1–C2	128.5	126.4
F1–C2–C1	112.5(1)	F2–C4–C3	113.2(3)	F1–C1–C2	110.5	112.8
C1*i*–C1–C2	120.3(2)	C3*ii*–C3–C4	123.1(3)	C1–C2–C3	120.5	123.6
angle of torsion [°]						
O1–C2–C1–C1*i*	–4.6(3)	O2–C4–C3–C3*ii*	177.6(5)	O1–C1–C2–C3	0.0	180.0
F1–C2–C1–C1*i*	175.6(2)	F2–C4–C3–C3*ii*	–2.1(6)	F1–C1–C2–C3	180.0	0.0

[a] Calculated on the B3LYP/aug-cc-pVTZ level of theory.

Table S6: Crystal data and structure refinement of $C_4H_2F_2O_2$.

	$C_4H_2F_2O_2$
Molecular Formula	$C_4H_2F_2O_2$
M_r[g·mol^{-1}]	120.06
Crystal size [mm^3]	0.30 x 0.26 x 0.20
Crystal system	monoclinic
Space group	$P2_1/c$
a [Å]	6.9861(5)
b [Å]	7.8349(6)
c [Å]	8.5588(6)
α [°]	90
β [°]	93.269(6)
γ [°]	90
V [A^3]	467.71(6)
Z	4
ρ_{calc} [g·cm^{-3}]	1.705
μ [mm^{-1}]	0.184
$\lambda_{MoK\alpha}$ [Å]	0.71073
F(000)	240
T [K]	115(2)
h, k, l range	-8:8; -10:9; -10:10
Measured reflexes	3743
Unique reflexes	1027
R_{int}	0.0291
Parameters	110
R(F)/wR(F^2)[a] (all data)	0.0521/0.0840
Weighting scheme[b]	0.0346/0.098700
S (Gof)[c]	1.037
Residual density [e·Å^{-3}]	0.199/-0.179
Device	Oxford XCalibur
CCDC	1995994

Table S7: Crystal data and structure refinement of $C_4H_2F_2O_2$, 4 ($C_4H_2F_2O_2 \cdot AsF_5$), $C_4H_2F_2O_2 \cdot 2\ AsF_5$.

Molecular Formula	$C_{24}H_{12}As_6F_{42}O_{12}$
M_r[g·mol^{-1}]	1739.86
Crystal size [mm^3]	0.38 x 0.26 x 0.21
Crystal system	triclinic
Space group	$P\bar{1}$
a [Å]	8.3388(4)
b [Å]	11.6747(6)
c [Å]	13.5623(8)
α [°]	67.843(5)
β [°]	80.722(4)
γ [°]	89.530(4)
V [A^3]	1204.83(12)
Z	1
ρ_{calc} [g·cm^{-3}]	2.398
μ [mm^{-1}]	4.329
$\lambda_{MoK\alpha}$ [Å]	0.71073
F(000)	828
T [K]	110(2)
h, k, l range	–11:11; –16:15; –19:19
Measured reflexes	13214
Unique reflexes	7352
R_{int}	0.0211
Parameters	416
R(F)/wR(F^2)[a] (all data)	0.0396/0.0659
Weighting scheme[b]	0.026500/0.372100
S (Gof)[c]	1.031
Residual density [e·Å^{-3}]	0.706/–0.683
Device	Oxford XCalibur
CCDC	2002516

[1] J. M. Landry, J. E. Katon, *Spectrochimica Acta Part A: Molecular Spectroscopy* **1984**, *40*, 871.
[2] D. F. Koster, T. P. Vasileff, G. L. Carlson, *Spectrochimica Acta Part A: Molecular Spectroscopy* **1971**, *27*, 1633.
[3] K. Hagen, *Journal of Molecular Structure* **1985**, *128*, 139.
[4] G. Paulen, M. Trætteberg, N. Nigri, A. Kjekshus, B. Klewe, D. L. Powell, *Acta Chem. Scand.* **1974**, *28a*, 1155.

EurJIC
European Journal of Inorganic Chemistry

Chemistry Europe
European Chemical Societies Publishing

Front Cover:
A. J. Kornath and co-workers
Intermediates in Friedel-Crafts Acylation of Fumaryl Halides

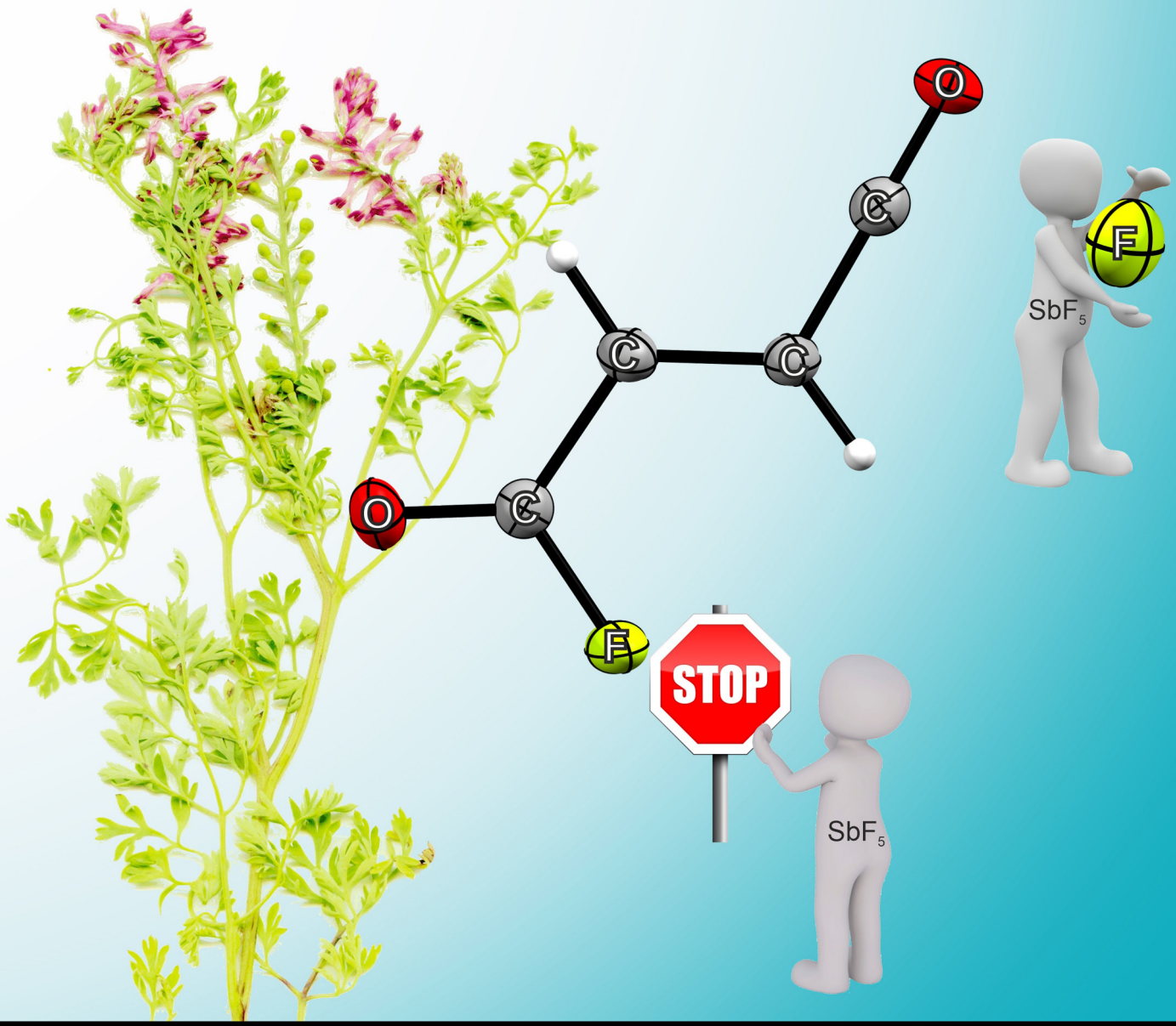

WILEY-VCH
29/2022

EurJIC
European Journal of Inorganic Chemistry

Research Article
doi.org/10.1002/ejic.202200391

Chemistry Europe
European Chemical Societies Publishing

www.eurjic.org

Intermediates in Friedel-Crafts Acylation of Fumaryl Halides

Marie C. Bayer,[a] Nikolaus Greither,[a] Christoph Jessen,[a] Alexander Nitzer,[a] and Andreas J. Kornath*[a]

Dedicated to Prof. Dr. Wolfgang Schnick on the occasion of his 65th birthday

Fumaryl chloride and fluoride were reacted with different Lewis acids to synthesize the intermediates of the Friedel-Crafts acylation. The salt of the monoacyl cation $[C_4H_2FO_2]^+[Sb_3F_{16}]^-$ was obtained from the reaction of fumaryl fluoride with SbF_5 in SO_2ClF solutions. The reaction was repeated using fumaryl chloride as starting material, which reacted under halogen exchange to obtain the salt of the monoacyl cation $[C_4H_2FO_2]^+[SbCl_2F_4]^-$. In addition, the reaction of fumaryl chloride with $SbCl_5$ in SO_2ClF was studied. The covalent donor-acceptor complex $C_4H_2Cl_2O_2 \cdot 2\ SbCl_5$ was formed, containing oxygen-bonded Lewis acids. The compounds were characterized by low-temperature vibrational spectroscopy. Single-crystal X-ray structure analyses were conducted for $[C_4H_2FO_2]^+[Sb_3F_{16}]^-$ as well as for $C_4H_2Cl_2O_2 \cdot 2\ SbCl_5$. In the solid state of $[C_4H_2FO_2]^+[Sb_3F_{16}]^-$ C···O and C···F contacts are observed and the origin of these interactions is discussed by means of ESP maps and NBO analysis. The monoacyl cation is stabilized by electrostatic attraction and electron back-donation from oxygen and fluorine ligands to the positive ring-structured π-hole at the oxocarbenium center. Besides, the formation of the diacyl cation is not observed, which is based on small distances between the positive charges involving charge-charge repulsion. The great advantage of using fumaryl halides in Friedel-Crafts acylation is featured by the possibility to synthesize ketones keeping an acyl fluoride moiety.

Introduction

Controlling chemical reactions constitutes one of the highest aims of chemistry in general. To increase product yield or eliminate side reactions, a precise knowledge of the reaction mechanism and how it can be affected is needed.[1] For industry, the Friedel-Crafts acylation represents a fundamentally important organic synthesis, as it is used to produce chemical feedstock, fine chemicals, and synthetic intermediates.[2,3] In general terms the Friedel-Crafts acylation concerns the substitution of a hydrogen atom by an acyl group catalyzed by a Lewis acid.[4,5] The first stage is the interaction between the acyl halide and the Lewis acid giving an oxonium complex followed by the formation of an acylium ion, representing the acylating agent.[6] To understand the reaction mechanism in greater detail, it is of importance to investigate these key intermediates, which are illustrated in Scheme 1. As the Friedel-Crafts acylation is usually performed with acyl chlorides,[2] we examined the reaction of fumaryl chloride with different Lewis acids to generate these intermediates. Since fluorine substituents have become a prevalent and crucial drug component,[7] we were prompted to investigate the reaction behavior of fumaryl fluoride with the Lewis acid SbF_5.

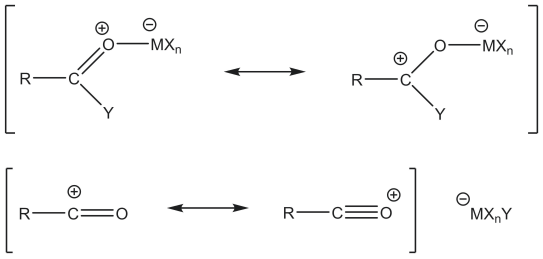

Scheme 1. Intermediates of the first step of the Friedel-Crafts acylation: Oxonium complex (top) and acylium salt (bottom).[5]

Results and Discussion

Fumaryl fluoride was reacted with SbF_5 in liquid SO_2ClF. We observe the formation of monoacylium ions according to Equation (1). It is necessary to use a very strong fluoride acceptor, such as SbF_5,[8] for the abstraction of one fluoride of $C_4H_2F_2O_2$. Attempting to synthesize the diacylium ion, twice the amount of Lewis acid was applied. However, even an eight-fold excess of SbF_5 did not result in the formation of diacyl cations.

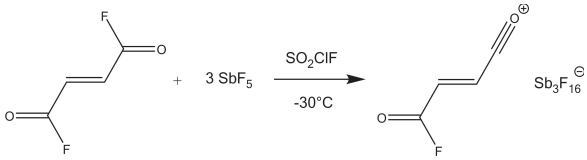

(1)

[a] M. C. Bayer, N. Greither, C. Jessen, A. Nitzer, Prof. Dr. A. J. Kornath
Department Chemie
Ludwig-Maximilians-Universität München
Butenandtstr. 5–13, (D) 81377 München, Germany
E-mail: andreas.kornath@cup.uni-muenchen.de

Supporting information for this article is available on the WWW under https://doi.org/10.1002/ejic.202200391

Research Article
doi.org/10.1002/ejic.202200391

To investigate the reaction behavior of the higher homologous element, fumaryl chloride was reacted with SbF_5 under the same conditions. Surprisingly, we detected the monoacylium ion containing fluorine, which is attributed to chlorine-fluorine exchange, as described in Equation (2).

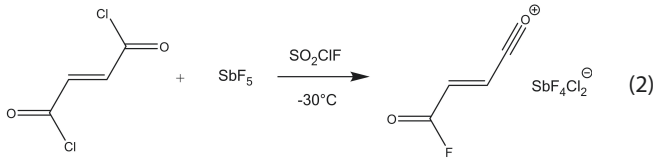

(2)

Avoiding the chlorine-fluorine exchange we chose $SbCl_5$ in liquid SO_2ClF to further analyze the Lewis basic characteristics of $C_4H_2Cl_2O_2$. This reaction resulted in a diadduct with O-coordinated $SbCl_5$ (see Equation (3)). However, neither the formation of monoacyl cations nor of diacylium ions was observed, using fumaryl chloride and the Lewis acid $SbCl_5$ as starting materials.

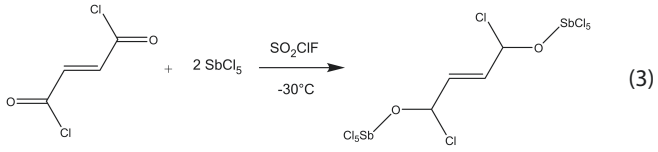

(3)

All of the reactions were performed at −30 °C. Excess SO_2ClF, which served as a solvent, was removed in a dynamic vacuum at −78 °C. The colorless salts $[C_4H_2FO_2]^+[Sb_3F_{16}]^-$ **(1)** and $[C_4H_2FO_2]^+[SbCl_2F_4]^-$ **(2)** are stable up to 20 °C. The light yellowish crystals of $C_4H_2Cl_2O_2 \cdot 2\ SbCl_5$ **(3)** decompose above 5 °C.

Crystal structure of $[C_4H_2FO_2]^+[Sb_3F_{16}]^-$

The monoacylium ion of fumaryl fluoride $[C_4H_2FO_2]^+[Sb_3F_{16}]^-$ **(1)** crystallizes in the monoclinic space group $P2_1/c$ with four formula units per unit cell. The asymmetric unit of **1** is depicted in Figure 1. Associated selected bond lengths and angles are summarized in Table 1.

As the monoacyl cation exists as *trans* conformer, we compare the bond lengths and angles to the *trans-trans* conformer of fumaryl fluoride.[9] The fluoride abstraction affects

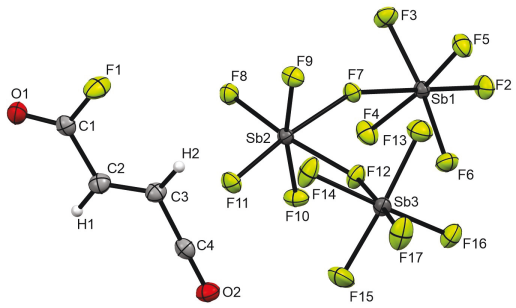

Figure 1. Asymmetric unit of $[C_4H_2FO_2]^+[Sb_3F_{16}]^-$ (displacement ellipsoids with 50% probability).

Table 1. Selected bond lengths and angles of $[C_4H_2FO_2]^+[Sb_3F_{16}]^-$ (1) with estimated standard deviations in parentheses. Symmetry operations: *i* = 2−*x*, 0.5+*y*, 0.5−*z*; *ii* = *x*, 1.5−*y*, −0.5+*z*; *iii* = 1+*x*, 1.5−*y*, −0.5+*z*; *iv* = 1+*x*, *y*, *z*.

Bond lengths [Å]			
C1–F1	1.328(3)	C2–C3	1.310(5)
C1–O1	1.169(5)	C3–C4	1.416(5)
C1–C2	1.481(5)	C4–O2	1.104(4)
Bond angles [°]			
F1–C1–O1	121.7(3)	C1–C2–C3	122.1(4)
F1–C1–C2	112.4(3)	C2–C3–C4	118.2(4)
O1–C1–C2	126.0(3)	C3–C4–O2	178.9(4)
Angles of torsion [°]			
C1–C2–C3–C4	−178.8(3)	C3–C2–C1–O1	175.9(4)
C3–C2–C1–F1	−5.2(5)		
Intermolecular contacts [Å]			
C4···F11	2.758(4)	C4···O1*i*	2.811(4)
C4···F13*ii*	2.917(4)	C4···F2*iii*	2.786(4)
C3–H2···F4*iv*	3.155(5)		

considerably the remaining C≡O bond length. Compared to the starting material,[9] the C4–O2 bond distance is with 1.104(4) Å significantly reduced and in the range between formal double (1.19 Å) and formal triple bonds (1.07 Å).[8] The C≡O bond length in **1** agrees well with the values of reported acylium ions in the literature.[10–12] The comparison of the structural parameters of the acylium ion side of $[C_4H_2FO_2]^+$ with these of fumaronitrile is appropriate due to their isoelectronicity. Hence, we examined the crystal structure of fumaronitrile $C_4H_2N_2$ which crystallizes in the monoclinic space group with two formula units per unit cell. The formula unit of $C_4H_2N_2$ is depicted in Figure S1 and the corresponding selected bond lengths and angles are summarized in Table S1 in the Supporting Information. The C4–C3 bond distance in **1** is with 1.416(5) Å notably short, in particular when compared with the respective bond length of fumaronitrile (1.436(2) Å), where the carbon atom is sp-hybridized as well. The shortening of the carbon-carbon distance is in accordance with the corresponding values observed in the methyloxocarbonium ion.[11] In addition, the C–F bond distance (1.328(2) Å) is reduced by 0.021 Å compared to *trans-trans* fumaryl fluoride.[9] The strongest impact on the bond angles in **1** is observed for C3–C4–O2, which is widened by 51.7° to 178.9(4)°, revealing the linear structure of the acyl moiety. Furthermore, the C2–C3–C4 bond angle is reduced by 4.9° to 118.2(4)°. The slightly distorted planar structure of the $[C_4H_2FO_2]^+$ cation is based on the acyl fluoride moiety being twisted out of the carbon-skeleton plane by 5°.

The terminal Sb–F bond distances in the *cis*-fluorine-bridged $[Sb_3F_{16}]^-$ anion are in the range between 1.833(2) Å and 1.853(2) Å. The bridging Sb–F bond lengths are weaker than the terminal ones with up to 2.084(2) Å. Both, the terminal and the bridging bond distances are in agreement with reported values for $[Sb_3F_{16}]^-$ anions.[13–15] The Sb–F–Sb bond angles are with 151.0(1)° and 140.5(1)° in good accordance with the literature.[13–15] In the crystal packing of **1** different types of

Research Article
doi.org/10.1002/ejic.202200391

intermolecular contacts are formed, which are demonstrated in Figure 2.

The hydrogen bond C3–H2···F4*iv* (3.155(5) Å) is classified as moderate referred to the categorization of Jeffrey.[16] Aside from that, the crystal structure of **1** exhibits interactions between the cationic C4 atom tetracoordinated by nucleophilic fluorine and oxygen atoms. The distances C4···F11 (2.758(4) Å), C4···F13*ii* (2.917(4) Å) and C4···F2*iii* (2.786(4) Å) which are in accordance with other reported C···F contacts,[11,17–19] are below the sum of the van der Waals radii of 3.17 Å,[20] respectively. In addition, an interaction between the carbonyl group of one cation and the acylium ion side of another cation is observed, which is shown in Figure 2. The C4···O1*i* contact corresponds to reported carbonyl-carbonyl (C=O···C=O) interactions known in the literature.[21,22] With a distance of 2.811(4) Å it is below the sum of the van der Waals radii of 3.22 Å.[20] As can be seen in Figure 2, the carbonyl group is arranged above the acylium moiety in an L-shaped manner with an O2–C4···O1*i* dihedral angle of 94.4(2)°. The structural motif of the L-shape is established in the literature for carbonyl-carbonyl contacts.[22]

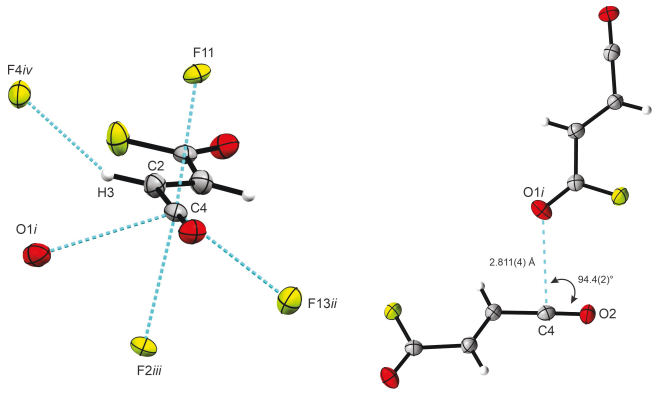

Figure 2. Left: Projection of the intermolecular contacts (drawn as dashed blue lines) in $[C_4H_2FO_2]^+[Sb_3F_{16}]^-$. Right: Illustration of the C=O···C=O interaction in $[C_4H_2FO_2]^+[Sb_3F_{16}]^-$ (displacement ellipsoids with 50% probability). Symmetry operations: *i* = 2−*x*, 0.5+*y*, 0.5−*z*; *ii* = *x*, 1.5−*y*, −0.5+*z*; *iii* = 1+*x*, 1.5−*y*, −0.5+*z*; *iv* = 1+*x*, *y*, *z*.

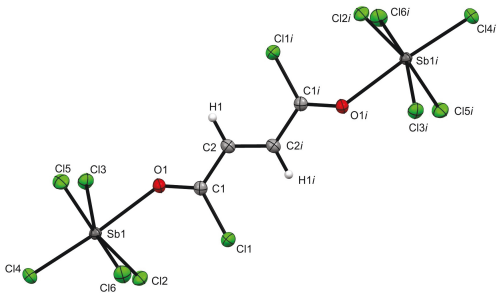

Figure 3. Formula unit of $C_4H_2Cl_2O_2 \cdot 2\ SbCl_5$ (displacement ellipsoids with 50% probability). Symmetry operation: *i* = 1−*x*, −*y*, 1−*z*.

Crystal structure of $C_4H_2Cl_2O_2 \cdot 2\ SbCl_5$

The diadduct of fumaryl chloride with $SbCl_5$ crystallizes in the orthorhombic space group *Pbca* with four formula units per unit cell. The formula unit of ($C_4H_2Cl_2O_2 \cdot 2\ SbCl_5$ **(3)**) is depicted in Figure 3 and selected structural parameters of the crystal structure of **3** are combined in Table 2.

In the solid state of the diadduct, fumaryl chloride exists as the *trans-trans* conformer. This is in accordance with reported crystal data of fumaryl chloride, revealing exclusively the thermodynamically preferred *trans-trans* conformer.[9,23,24] The donor-acceptor complex is based on the formation of Sb–O bonds. A lone pair of electrons is shared by the oxygen atom of the acyl chloride moiety with the metal of the Lewis acid. The Sb1–O1 bond length is with 2.359(2) Å longer than formal Sb–O bond distances (2.02 Å).[8] However, this bond length is in good agreement with reported values in the literature of other O-coordinated complexes like $SbCl_5 \cdot CH_3C_6H_4COCl$ (2.253(6) Å)[25] and 2 $SbCl_5 \cdot ClOCCH_2CH_2COCl$ (2.428 Å).[12] The coordination of $SbCl_5$ to the acyl chloride group leads to significant elongation of the C=O bond lengths in **3** (C1–O1 1.220(3) Å) in comparison with the starting material (1.191(2) Å).[23] Given that the C=O bond distances are increased, the C–Cl bond lengths are with 1.712(3) Å (C1–Cl1) significantly reduced compared to that in fumaryl chloride (1.783(2) Å).[23] The C=C double and C–C single bonds are not affected by the formation of the donor-acceptor complex. The value of 140.1(2)° observed for the Sb1–O1–C1 bond angle is in accordance with that determined for 2 $SbCl_5 \cdot ClOCCH_2CH_2COCl$ (143.6°).[12] The variation from the expected angle of 120° for sp^2-hybridized oxygen atom refers to intramolecular steric effects.[25] The bond angle Cl1–C1–C2 is widened by 3.3°, whereas the O1–C1–C2 is reduced by 5.5° in contrast to the educt.[23] Antimony is coordinated by six atoms forming an octahedral structure. The bond angles of the $SbCl_5O$

Table 2. Selected bond lengths and angles of $C_4H_2Cl_2O_2 \cdot 2\ SbCl_5$ **(3)** with estimated standard deviations in parentheses. Symmetry operations: *i* = 1−*x*, −*y*, 1−*z*; *ii* = 1−*x*, −0.5+*y*, 0.5−*z*, *iii* = 0.5−*x*, −0.5+*y*, *z*.

Bond lengths [Å]	
C1–Cl1	1.712(3)
C1–O1	1.220(3)
C1–C2	1.472(4)
C2–C2*i*	1.326(3)
Sb1–O1	2.359(2)
Bond angles [°]	
O1–C1–Cl1	122.0(2)
Cl1–C1–C2	117.9(2)
O1–C1–C2	120.0(2)
C1–C2–C2*i*	123.6(2)
Sb1–O1–C1	140.1(2)
Angles of torsion [°]	
C1–C2–C2*i*–C1*i*	−180.0(2)
O1–C1–C2–C2*i*	−172.5(2)
Cl1–C1–C2–C2*i*	6.9(3)
Intermolecular contacts [Å]	
C1···Cl4*iii*	3.301(3)
Cl2*i*···Cl5*ii*	3.305(1)

Research Article
doi.org/10.1002/ejic.202200391

moiety of **3** deviate up to 15° from the ideal angles indicating a distortion of the coordination polyhedra, which arises from the difference in the size of the ligands. The Sb–Cl bond lengths range between 2.314(1) Å and 2.340(1) Å, which are slightly shorter than formal Sb–Cl bond distances (2.38 Å).[8] These values comply with other reported values for $SbCl_5$ adducts.[25,26] The complexes are connected with each other via two different intermolecular contacts, which are illustrated in Figure 4. The distance C1···Cl4*iii* (3.301(3) Å) is below the sum of the van der Waals radii of 3.45 Å.[20] The halogen-halogen contact, Cl2*i*···Cl5*ii*, is with 3.305(1) Å below the sum of the van der Waals radii of 3.50 Å[20] and consonant with reported Cl···Cl interactions.[27] The attractive attribute of this contact arises in the electrostatic potential around the chlorine atom, being not completely negative but holding a small positive area. The other chlorine atom can be attracted by this region.[28]

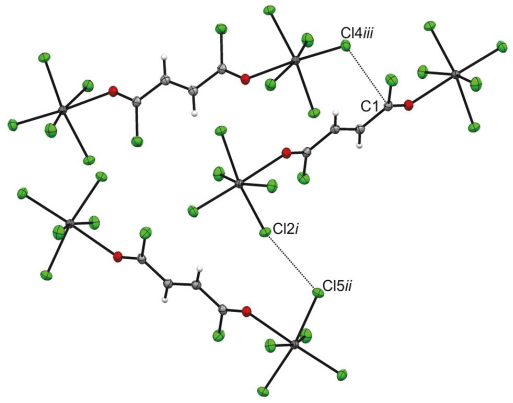

Figure 4. Projection of the intermolecular contacts in $C_4H_2Cl_2O_2 \cdot 2\ SbCl_5$ (displacement ellipsoids with 50% probability). Symmetry operations: *i* = *1*−*x*, −*y*, *1*−*z*; *ii* = *1*−*x*, −*0.5*+*y*, *0.5*−*z*, *iii* = *0.5*−*x*, −*0.5*+*y*, *z*. Intermolecular contacts are drawn as dashed lines.

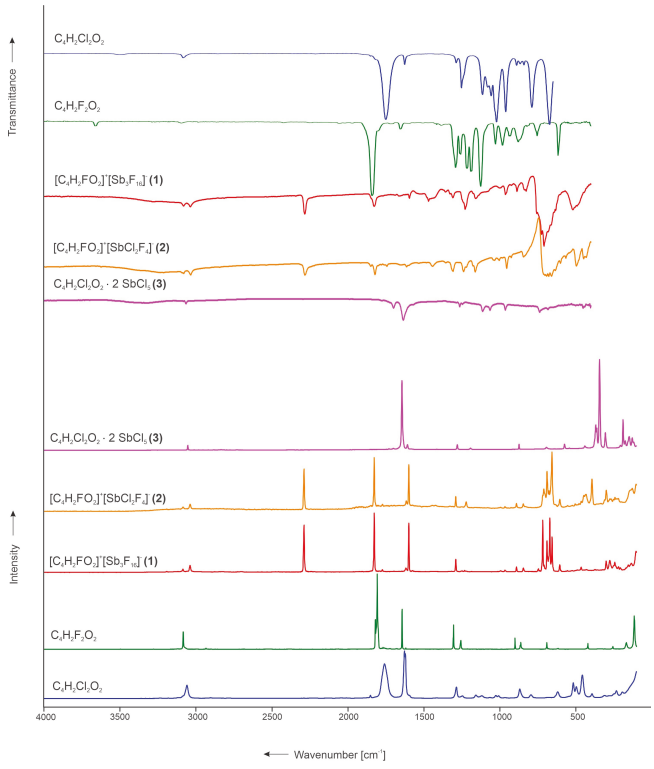

Figure 5. Low-temperature IR and Raman spectra of fumaryl chloride,[9] fumaryl fluoride,[9] $[C_4H_2FO_2]^+[Sb_3F_{16}]^-$, $[C_4H_2FO_2]^+[SbCl_2F_4]^-$ and $C_4H_2Cl_2O_2 \cdot 2\ SbCl_5$.

Vibrational spectra of $[C_4H_2FO_2]^+[Sb_3F_{16}]^-$ and $[C_4H_2FO_2]^+[SbCl_2F_4]^-$

The low-temperature vibrational spectra of $[C_4H_2FO_2]^+[Sb_3F_{16}]^-$ **(1)**, $[C_4H_2FO_2]^+[SbCl_2F_4]^-$ **(2)**, $C_4H_2Cl_2O_2 \cdot 2\ SbCl_5$ **(3)** and fumaryl chloride[9] together with crystalline fumaryl fluoride[9] are shown in Figure 5. Table 3 displays selected experimental vibrational frequencies of **1** and **2** combined with the quantum chemically calculated frequencies of the cation $[C_4H_2FO_2]^+$. The entire table (Table S2) is enclosed in the Supporting Information.

The monoacyl cation reveals a *trans* conformational structure in the crystalline form, as mentioned in the section above. Due to the abstraction of one halogen atom, the monoacylium ion is expected to have C_s point symmetry with the vibrational modes comprising the irreducible representations 15 *A′*+6 *A″*, where all modes are IR and Raman active. The vibrational frequencies were assigned by analyzing the Cartesian displacement vectors of the calculated vibrational modes of $[C_4H_2FO_2]^+$. The successful formation of the oxocarbenium ion is confirmed by the occurrence of the C≡O stretching vibration in the IR spectra at 2284 cm^{-1} **1**, **2** and in the Raman spectra at 2289 cm^{-1} **1**, **2**. The vibration of the remaining carbonyl group leads to a band in the IR spectra (1828 cm^{-1} **1**, 1821 cm^{-1} **2**) and a strong line in the Raman spectra (1826 cm^{-1} **1**, **2**), which are in good agreement with the C=O stretching vibrations of the educt[9] and confirms the appearance of monoacylium ions. The C–H stretching vibrations of the acylium ion side are red-shifted up to 61 cm^{-1} compared to the neutral compound[9] and occur in the IR spectra at 3038 cm^{-1} **1**, 3036 cm^{-1} **2**, respectively, and in the Raman spectra at 3039 cm^{-1} **1**, 3038 cm^{-1} **2**, respectively. The C–C stretching mode appearing in the Raman spectra at 995 cm^{-1} **1**, **2** is blue-shifted by 133 cm^{-1} compared to the ν_s(C–C) of fumaryl fluoride.[9] The decrease of this C–C single bond distance is in compliance with the crystal data of **1**. The C–Cl stretching vibrations in the spectra of fumaryl chloride[9] at 673 cm^{-1} (IR) and at 619 cm^{-1} (Ra), which are in agreement with the literature[24] are not detectable in the vibrational spectra of **2**. Instead, in the Raman spectrum of **2** a line arises at 1290 cm^{-1}, which is also observed in the Raman spectrum of **1**. This line is assigned to a C–F bond. We, therefore, assume a chlorine-fluorine exchange for the reaction of fumaryl chloride with the Lewis acid SbF_5, as it is described above in Equation (2). This halogen exchange between alkyl chlorides and SbF_5 giving alkyl fluorides combined with antimony chlorofluorocations is hardly reported in the literature.[29] Comparing the stretching mode of the C–F bond of **1** and **2** with the symmetric C–F stretching vibration of the neutral compound[9] it is blue-shifted by 33 cm^{-1}, which

Research Article
doi.org/10.1002/ejic.202200391

Table 3. Selected experimental vibrational frequencies [cm^{-1}] of $[C_4H_2FO_2]^+[Sb_3F_{16}]^-$ **(1)**, $[C_4H_2FO_2]^+[SbCl_2F_4]^-$ **(2)** and calculated vibrational frequencies [cm^{-1}] of $[C_4H_2FO_2]^+$.

$[C_4H_2FO_2]^+[Sb_3F_{16}]^-$ **(1)** exp.[a]		$[C_4H_2FO_2]^+[SbCl_2F_4]^-$ **(2)** exp.[a]		$[C_4H_2FO_2]^+$ calc.[b]	Assignment		
IR	Raman	IR	Raman	IR/Raman			
3082 m	3085 (6)	3080 vs	3085 (7)	3194 (20/41)	ν_1	A'	ν(C–H)
3038 m	3039 (12)	3036 vs	3038 (12)	3152 (73/52)	ν_2	A'	ν(C–H)[c]
2284 m	2289 (80)	2284 vs	2289 (72)	2327 (579/153)	ν_3	A'	ν(C≡O)[c]
1828 m	1826 (100)	1821 vs	1826 (91)	1876 (155/187)	ν_4	A'	ν(C=O)
1595 w	1599 (83)	1599 vs	1599 (79)	1612 (150/115)	ν_5	A'	ν(C=C)
1310 w	1290 (22)	1308 vs	1290 (25)	1214 (225/9)	ν_8	A'	ν(C–F)
1001 w	995 (3)	1005 s	995 (7)	1022 (44/2)	ν_9	A'	ν(C–C)[c]
962 w	966 (4)	955 vs	966 (8)	1010 (30/1)	ν_{16}	A''	γ(HCCH)
837 w	846 (8)	845 s	846 (13)	884 (38/10)	ν_{10}	A'	ν(C–C)
	605 (13)	602 s	605 (21)	676 (20/4)	ν_{11}	A'	δ(COF)

[a] Abbrevations for IR intensities: v = very, s = strong, m = medium, w = weak. IR intensities in km/mol; Raman intensities in $Å^4/u$. Experimental Raman activities are relative to a scale of 1 to 100. [b] Calculated on the B3LYP/aug-cc-pVTZ level of theory. [c] acylium ion side.

agrees well with the shortening of the C–F bond length in the crystal structure of **1**. The vibrational frequencies attributed to the $[Sb_3F_{16}]^-$ anion in **1** conform to reported data in the literature.[13,14,30] The lines and bands assigned to the chlorofluoroantimonate(v) anion $[SbCl_2F_4]^-$ in the spectra of **2** are in accordance with reported data.[31]

Vibrational spectra of $C_4H_2Cl_2O_2 \cdot 2\ SbCl_5$

The low-temperature vibrational spectra of $C_4H_2Cl_2O_2 \cdot 2\ SbCl_5$ **(3)** and fumaryl chloride[9] are shown in Figure 5. Selected experimental vibrational frequencies of **3** together with the quantum chemically calculated frequencies of the donor-acceptor complex $C_4H_2Cl_2O_2 \cdot 2\ SbCl_5$ are given in Table 4. The Supporting Information holds the entire table (Table S3).

Table 4. Selected experimental vibrational frequencies [cm^{-1}] and calculated vibrational frequencies [cm^{-1}] of $C_4H_2Cl_2O_2 \cdot 2\ SbCl_5$.

$C_4H_2Cl_2O_2 \cdot 2\ SbCl_5$ **(3)** exp.[a]		$C_4H_2Cl_2O_2 \cdot 2\ SbCl_5$ calc.[b]	Assignment		
IR	Raman	IR/Raman			
3067 w		3225(11/0)	ν_{43}	B_u	ν_{as}(C–H)
	3054 (5)	3225(0/49)	ν_1	A_g	ν_s(C–H)
	1644 (77)	1792(0/1589)	ν_2	A_g	ν_s(C=O)
1635 vs		1782(1611/0)	ν_{44}	B_u	ν_{as}(C=O)
	1607 (6)	1735(0/361)	ν_3	A_g	ν(C=C)
	1193 (2)	1213(0/72)	ν_5	A_g	ν_s(C–C)
1113 m		1135(444/0)	ν_{46}	B_u	ν_{as}(C–C)
739 s		753(159/0)	ν_{47}	B_u	ν_{as}(C–Cl)
	693 (3)	692(0/10)	ν_6	A_g	ν_s(C–Cl)
	441 (5)	437(0/9)	ν_8	A_g	ν_s(Sb–O)
442 w	368 (28)	394(0/53)	ν_9	A_g	ν_s(Sb–Cl)
413 w		393(189/0)	ν_{50}	B_u	ν_{as}(Sb–Cl)
	361 (24)	385(0/1)	ν_{10}	A_g	ν_s(Sb–Cl_2)
	344 (100)	353(0/104)	ν_{11}	A_g	ν_s(Sb–Cl_4)
	306 (19)	304(0/18)	ν_{35}	B_g	ν_s(Sb–Cl_4)

[a] Abbrevations for IR intensities: v = very, s = strong, m = medium, w = weak. IR intensities in km/mol; Raman intensities in $Å^4/u$. Experimental Raman activities are relative to a scale of 1 to 100. [b] Calculated at the M06-2X/aug-cc-pVTZ level of theory and Sb was calculated at the M06-2X/GenECP MWB46 level.

In the crystal structure of **3** fumaryl chloride reveals a *trans-trans* conformational arrangement, which was taken into account in the calculation of the local minimum structure of $C_4H_2Cl_2O_2 \cdot 2\ SbCl_5$. The simulation of the donor-acceptor complex was performed by employing the density functional M06-2X, which performs better than B3LYP in molecules, where dispersion interactions contribute.[32] A comparison of the experimental data of **3** with the calculated structural parameters and vibrational frequencies conducted by the density functionals B3LYP and M06-2X is listed in the Supporting Information (Table S4 and S5). The values obtained from the calculation at the M06-2X/aug-cc-pVTZ level of theory are overall in good agreement with the experimental parameters. For the antimony atoms the quasi-relativistic effective core potential MWB46 was applied. The diadduct $C_4H_2Cl_2O_2 \cdot 2\ SbCl_5$ is assumed to have C_{2h} point symmetry with 60 fundamental vibrations ($19\ A_g + 12\ A_u + 11\ B_g + 18\ B_u$). On account of the inversion center, the rule of mutual exclusion[33] applies to the diadduct. The assignment of the vibrational frequencies was performed by examining the Cartesian displacement vectors of the calculated vibrational modes of $C_4H_2Cl_2O_2 \cdot 2\ SbCl_5$. The coordinative Sb–O bond connecting the Lewis acid with fumaryl chloride has notable influence on the C=O stretching vibration, appearing in the IR spectrum at 1635 cm^{-1} and in the Raman spectrum at 1644 cm^{-1}. In comparison with the starting material,[24] the C=O stretching modes are red-shifted up to 127 cm^{-1}, which is in good agreement with reported vibrational frequencies of other complexes like $SbCl_5 \cdot C_6H_5COCl$.[34] The weakening of the C=O bonds, which is confirmed by the crystal data, indicates that **3** consists mostly of polarized donor-acceptor complexes.[34] The C–Cl stretching mode appearing in the Raman spectrum at 693 cm^{-1} and in the IR spectrum at 739 cm^{-1} is blue-shifted by up to 67 cm^{-1} compared to fumaryl chloride.[24] The shortening of the C–Cl bond distance is in accordance with the crystal data of **3**. The ν_s(Sb–O), observed in the Raman spectrum at 441 cm^{-1}, is red-shifted in comparison with formal Sb–O vibrational frequencies.[33] The detection of the weak Sb–O bond is in compliance with the crystal structure. The Sb–Cl stretching vibrations arise in the range between

Research Article
doi.org/10.1002/ejic.202200391

368 cm^{-1} and 306 cm^{-1}, which are in agreement with reported vibrational frequencies of other oxonium adducts of $SbCl_5$.[35]

Quantum chemical calculations

The structure of $[C_4H_2FO_2]^+$ was calculated at the B3LYP/aug-cc-pVTZ level of theory. A comparison of the single-crystal X-ray structure of **1** and the calculated structure of $[C_4H_2FO_2]^+$ along with bond lengths and angles is displayed in Figure 6.

The values obtained from the calculation are overall in good agreement with the experimental parameters. However, the C2–C3 bond length is overestimated whereas the C3–C4 is even underestimated by the calculation. The discrepancy in these values arises presumably from the intermolecular contacts in the crystal structure of **1**, which are not taken into account in the calculation. To examine the properties of these interactions, the electrostatic potential (ESP) map in combination with natural population analysis (NPA) charges of the $[C_4H_2FO_2]^+$ cation were calculated. Figure 7 illustrates the C···O and C···F contacts along with the ESP map. The ESP map in company with the NPA charges of $[C_4H_2FO_2]^+$ is shown in Figure 9. In the ESP map of the monoacyl cation, the negative charge density is concentrated at the oxygen atom O1 of the acyl fluoride group, as indicated by the red surface. The region around the sp-hybridized carbon atom suffers from a depletion of electron density and provides a positive electrostatic potential, which is observed in the ESP map. This is in accordance with the high positive NPA charge of the C4 atom of the monoacyl cation. Such a region of density depletion and positive electrostatic potential are designated in the literature as π-hole,[36,37] illustrated in the ESP map as the dark blue area around the C4 atom. The magnitude of the π-hole, quantified by the $V_{S,max}$ parameter, amounts to 150.7 kcal mol^{-1}. Approaching this positive π-hole is accordingly self-evident for nucleophiles,[36] such as the $[Sb_3F_{16}]^-$ anion and the negatively polarized O1 atom of the acyl fluoride moiety. The interaction of the latter with the π-hole generates the C4···O1*i* contact with a distance of 87 % of the sum of the van der Waals radii.[20] Three carbon-fluorine contacts are additionally built, originating from the π-hole to the $[Sb_3F_{16}]^-$. The C4···F distances range from 87 % to 92 % of the sum of the van der Waals radii.[20] Hence, the positive charge on the C4 atom is stabilized by electrostatic attraction.[38,39] In addition, orbital interactions reinforce the attractive interaction[39] between the acylium moiety and the nucleophiles. There are reported examples of sp^2-hybridized carbenium ions stabilized by fluorine bridging along the axis of the unoccupied p_z orbital.[17–19] However, in the monoacyl cation the corresponding carbon atom is supposed to be sp-hybridized. To confirm the assumption of the sp-hybridization of the C4 atom, natural bond orbital calculations of $[C_4H_2FO_2]^+$ were performed. In addition, a deeper understanding of the intermolecular interactions concerning the C4 atom is expected from the calculations. The bonding and antibonding orbitals with the participation of the C4 atom are illustrated in Figure 8. To confirm the sp-hybridization, the corresponding p-orbitals are examined. One σ-bond between C4 and C3 is formed, comprising 41.1 % p-character of C4. Another σ-bond between C4 and O2 contains 58.5 % p-character of C4. There are two π-bonds formed between C4 and O2, consisting each of 99.8 % p-character of C4, respectively. Therefore we conclude that the C4 atom is sp-hybridized and both p-orbitals are occupied and participate in the π-bonds to the O2 atom. In Table S6 in the Supporting Information, selected NBOs, regarding the acylium moiety, are summarized in combination with calculated values for electron occupancy, s-and p-character, and energy. The π-hole can be considered as positive electrostatic potential on unpopulated π* orbitals, which are thereby able to interact with electron donors.[40] Typically the regions of positive electrostatic potential are located perpendicular to the molecular framework.[38] In our case, the carbon atom is sp-hybridized leading to a π-hole formed in a ring structure around the carbon atom, representing a peculiarity of the acylium group. Concerning the C4–O2 bond in terms of bonding and antibonding orbitals, to gain a deeper understanding of the orbitals involved in the noncovalent interactions. Due to the π_z*(C4–O2) orbital being orientated towards the electron

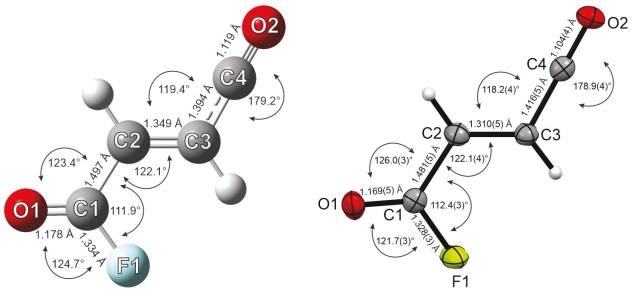

Figure 6. Calculated (left) and experimental (right) structures of $[C_4H_2FO_2]^+$ including bond lengths and angles.

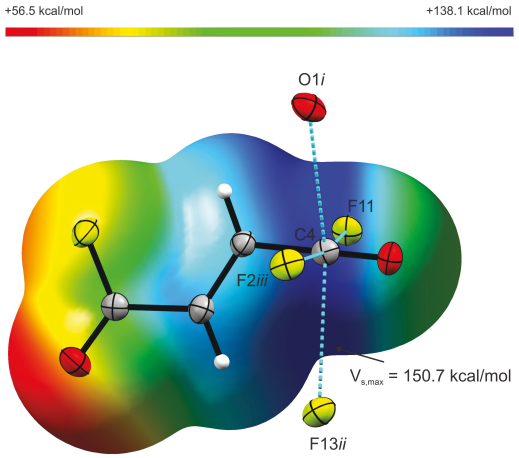

Figure 7. Intermolecular interactions in the crystal structure of **1** (displacement ellipsoids with 50 % probability). C···O and C···F contacts are drawn as dashed blue lines. The calculated ESP surface mapped onto an electron density isosurface value of 0.0004 $bohr^{-3}$ with the color scale range from 56.5 kcal mol^{-1} to 138.1 kcal mol^{-1}. Symmetry operations: *i* = 2−*x*, 0.5+*y*, 0.5−*z*; *ii* = *x*, 1.5−*y*, −0.5+*z*; *iii* = 1+*x*, 1.5−*y*, −0.5+*z*.

Research Article
doi.org/10.1002/ejic.202200391

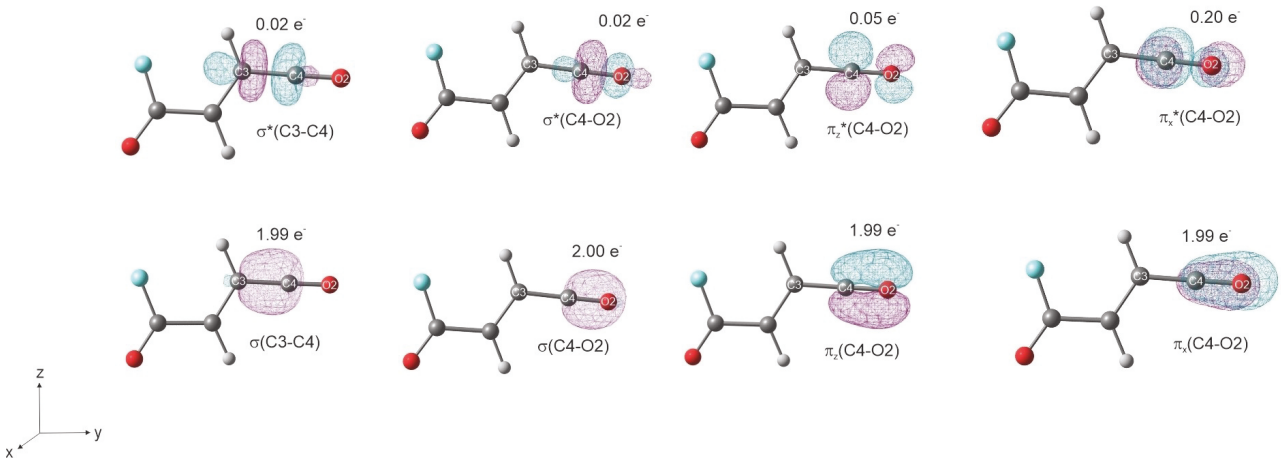

Figure 8. Selected NBOs for the C3–C4 and C4–O2 bonds with associated occupancies of $[C_4H_2FO_2]^+$.

donors O1*i* and F13*ii*, their lone pairs can delocalize into the antibonding orbital. The π_x*(C4–O2) is populated by the lone pairs of F11 and F2*iii*, because it is arranged towards these ligands. To summarize, we can say that the highly electron-deficient oxocarbenium center, which is associated with a π-hole providing a ring structure, is stabilized by electrostatic attraction[38,39] and electron back-donation[18,41] from one oxygen and three fluorine ligands (lp→π*(C4–O2)). The stabilization effect is confirmed by the high stability of the acylium salts **1** and **2** up to 20 °C.

Aside from that, we were interested in analyzing the electron distribution and charge-related properties of the diacyl cation $[C_4H_2O_2]^{2+}$, which cannot be formed even with the employment of large excess of SbF_5. Hence, calculations of the ESP map including NPA charges were performed. Figure 9 shows a comparison of the ESP maps along with the NPA charges of $[C_4H_2FO_2]^+$ and of $[C_4H_2O_2]^{2+}$. In the same way, as it is observed in the ESP map of the monoacyl cation, the regions around the sp-hybridized carbon atoms hold a positive electrostatic potential in the ESP map of $[C_4H_2O_2]^{2+}$. This is consonant with the high positive NPA charges of the C1 and C4 atoms of the diacyl cation. The ESP map of the diacyl cation shows a negative electrostatic potential located at the oxygen atoms. Compared to the O2 atom of $[C_4H_2FO_2]^+$ the negative NPA charges of O1 and O2 of the diacyl cation are decreased. In the ESP map of $[C_4H_2O_2]^{2+}$ the region along the C=C double bond holds a slightly positive charge density but negative NPA charges. The charge distribution providing only a small distance between the positive charges of C1 and C4 leads to repulsive effects. This represents the explanation for the inability to prepare the diacyl cation. In the literature this observation is known, as it is possible to prepare diacylium ions from diacyl fluorides FOC–$(CH_2)_n$–COF only for $n \geq 3$.[42-44] Certainly, the diprotonation of fumaryl fluoride is observed,[45] owning two positive charges as well, with the same distance between the charged centers. Compared to the diacyl cation the positive charges in the diprotonated species are distributed to a greater extent over the protonated acyl fluoride group, as it is illustrated in the calculated ESP map of the diprotonated fumaryl fluoride.[45] The diacyl cation, however, is characterized by a remarkable charge-charge repulsion, without the possibility of delocalization, as it is depicted in the ESP map in Figure 9. The same observation has been made with succinyl fluoride and succinic acid.[43,44,46] Charge-charge repulsive effects prevent the formation of the diacyl cation of succinyl fluoride and the delocalization of the positive charges enables the formation of the diprotonated succinic acid.[43,44,46]

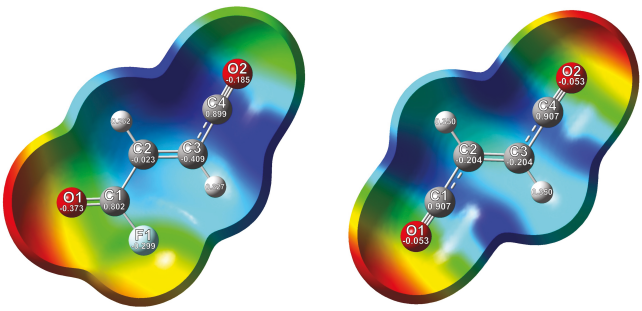

Figure 9. Left: Calculated ESP surface mapped onto an electron density isosurface value of 0.0004 bohr^{-3} with the color scale range from 56.5 kcal mol^{-1} (red) to 138.1 kcal mol^{-1} (blue) of $[C_4H_2FO_2]^+$. Right: Calculated ESP surface mapped onto an electron density isosurface value of 0.0004 bohr^{-3} with the color scale range from 169.4 kcal mol^{-1} (red) to 251.0 kcal mol^{-1} (blue) of $[C_4H_2O_2]^{2+}$. The NPA charges are given in a. u.

Conclusions

The key intermediates of the first step of the Friedel-Crafts acylation were synthesized by reacting fumaryl halides with different Lewis acids. The reaction of fumaryl fluoride with the Lewis acid SbF_5 in SO_2ClF solutions results in the formation of the monoacyl cation $[C_4H_2FO_2]^+$. Surprisingly, the monoacyl cation containing fluorine concerning the salt $[C_4H_2FO_2]^+[SbCl_2F_4]^-$ was obtained for the reaction of fumaryl chloride

with SbF_5 in SO_2ClF due to chlorine-fluorine exchange. Furthermore, the reaction of fumaryl chloride with $SbCl_5$ in SO_2ClF was examined. The covalent donor-acceptor complex $C_4H_2Cl_2O_2 \cdot 2\ SbCl_5$ was formed, containing the oxygen-bonded Lewis acids. The compounds were isolated and characterized by low-temperature vibrational spectroscopy. Single-crystal X-ray structure analyses were undertaken for $[C_4H_2FO_2]^+[Sb_3F_{16}]^-$ and for $C_4H_2Cl_2O_2 \cdot 2\ SbCl_5$. To interpret the experimental results, quantum chemical calculations were performed for $[C_4H_2FO_2]^+$ on the B3LYP/aug-cc-pVTZ and for $C_4H_2Cl_2O_2 \cdot 2\ SbCl_5$ on the M06-2X/aug-cc-pVTZ level of theory. In the crystal structure of $[C_4H_2FO_2]^+[Sb_3F_{16}]^-$ one C···O and three C···F contacts are observed and the origin of these interactions is investigated with the help of ESP maps, NPA charges, and NBO analysis. A ring-shaped π-hole is formed around the oxocarbenium center, due to the sp-hybridization of the carbon atom. The positive charge is stabilized by electrostatic attraction and electron back-donation from the ligands (lp→π*(C≡O)). In addition, calculations of ESP maps including NPA charges for the diacyl cation $[C_4H_2O_2]^{2+}$ were executed. Small distances between the positive charges involving charge-charge repulsion elucidate why the formation of the diacyl cation cannot be observed. The observation that fumaryl chloride, as well as fumaryl fluoride, would not give diacylium ions can be considered as benefit for the Friedel-Crafts synthesis of ketones proving an acyl fluoride group because fluorine substituents are a common and essential drug component.

Experimental Section

Caution! Any contact with the components must be avoided. Be aware that the hydrolysis of SbF_5 and the reported salts might release HF, burning skin, and cause irreparable injury. Adequate safety precautions must be undertaken when using and handling these materials.

Apparatus and materials: All reactions were conducted by using standard Schlenk techniques with an electropolished stainless-steel vacuum line. Transparent FEP/PFA-reactors combined with stainless-steel valves were employed for the syntheses. The vacuum line and the reactors were dried with fluorine, before use. Excess fluorine was removed in a dynamic vacuum and absorbed by Sodalime. Antimony pentafluoride was managed in a Duran glass high vacuum line exerting Young valves. Low-temperature Raman spectroscopic measurements were performed in a glass cell under vacuum cooled down to −196 °C on a Bruker MultiRAMII FT-Raman spectrometer with Nd:YAG laser excitation (λ = 1064 nm). For the IR measurements, the respective sample was put on a CsBr single-crystal plate in a cooled cell. A Bruker Vertex-80 V-FT-IR spectrometer was employed for recording the low-temperature IR spectra. The low-temperature single-crystal X-ray diffractions of **1** and **3** were performed on an Oxford XCalibur3 diffractometer equipped with a Spellman generator (50 kV, 40 mA) and a Kappa CCD-detector, operating with MoKα radiation (λ = 0.71073 Å). Data collection and reduction were executed using the program CrysAlisPro 1.171.38.46 (Rigaku OD, 2015).[47] The crystal structures were solved using SHELXT[48] and SHELXL-2018/3[49] of the WINGX software package.[50] The structures were checked by employing the software PLATON.[51] The absorption correction was carried out with the help of the SCALE3 ABSPACK multiscan method.[52] Selected data and parameters of the reported single-crystal structures **1**, **3**, and fumaronitrile are listed in Table S7 (Supporting Information). Quantum chemical calculations were performed on the B3LYP/aug-cc-pVTZ, M06-2X/aug-cc-pVTZ levels of theory and for Sb the basis set GenECP was applied using the software package Gaussian 09[53], and Gaussian16.[54] GaussView 6.0 was employed for the visualization and illustration of the ESP calculations.[55]

Syntheses of $[C_4H_2FO_2]^+[Sb_3F_{16}]^-$ (1) and $[C_4H_2FO_2]^+[SbCl_2F_4]^-$ (2): For **1**, the starting material, fumaryl fluoride, was prepared as previously reported, without further purification.[9] Antimony pentafluoride (540 mg, 2.5 mmol) was condensed at −196 °C into an FEP reactor vessel. Afterwards, for **1** fumaryl fluoride (100 mg, 0.8 mmol) and for **2** fumaryl chloride (230 mg, 1.5 mmol) were added under nitrogen atmosphere. Subsequently, 2 mL of SO_2ClF were condensed into the reactor vessel at −196 °C, respectively. The reaction mixture was warmed up to −30 °C and homogenized until the respective salts were completely dissolved. For crystallization of **1**, the reactor was left in an ethanol bath at −70 °C until the salts were recrystallized. For the vibrational measurements, the solvent SO_2ClF was removed in a dynamic vacuum at −78 °C. The compounds were obtained as colorless crystalline solids, stable up to 20 °C.

Synthesis of $C_4H_2Cl_2O_2 \cdot 2\ SbCl_5$ (3): Antimony pentachloride (598 mg, 2.0 mmol) and fumaryl chloride (153 mg, 1.0 mmol) were filled under a nitrogen atmosphere into an FEP reactor vessel. Accordingly, 2 mL of SO_2ClF were condensed into the reactor vessel at −196 °C. The reaction mixture was warmed up to −30 °C and homogenized until the compound was thoroughly dissolved. For crystallization, the reactor was left in an ethanol bath at -40 °C until the complex was recrystallized. For the vibrational measurements, the solvent SO_2ClF was removed in a dynamic vacuum at −78 °C. The compound was obtained as light yellowish crystals, which decompose above 5 °C.

Deposition Numbers 2155394 (for **1**), 2155395 (for **3**), and 2155396 (for fumaronitrile) contain the supplementary crystallographic data for this paper. These data are provided free of charge by the joint Cambridge Crystallographic Data Centre and Fachinformationszentrum Karlsruhe Access Structures service www.ccdc.cam.ac.uk/structures.

Acknowledgments

We gratefully acknowledge the financial support of the Department of Chemistry of the Ludwig-Maximilians-Universität München, the Deutsche Forschungsgemeinschaft (DFG) and the F-Select GmbH. Open Access funding is enabled and organized by Projekt DEAL. Open Access funding enabled and organized by Projekt DEAL.

Conflict of Interest

The authors declare no conflict of interest.

Data Availability Statement

The data that support the findings of this study are available in the supplementary material of this article.

Keywords: π-hole · acyl cations · $SbCl_5$ donor-acceptor complex · electrostatic potential maps · natural bond orbital analysis · Friedel-Crafts acylation intermediates · noncovalent interactions

[1] E. Kraka, D. Cremer, *Acc. Chem. Res.* **2010**, *43*, 59.
[2] E. K. Raja, D. J. DeSchepper, S. O. N. Lill, D. A. Klumpp, *J. Org. Chem.* **2012**, *77*, 5788.
[3] H. G. Frank, in *Industrial Aromatic Chemistry*, Springer, Berlin, **1988**.
[4] G. A. Olah, in *Friedel-Crafts and Related Reactions*, Wiley, New York, **1963**.
[5] J. K. Groves, *Chem. Soc. Rev.* **1972**, *1*, 73.
[6] a) Jie Jack Li, *Name Reactions. A Collection of Detailed Reaction Mechanisms*, Springer, Berlin, Heidelberg, **2006**; b) P. H. Gore, *Chem. Rev.* **1955**, *55*, 229.
[7] K. Müller, C. Faeh, F. Diederich, *Science* **2007**, *317*, 1881.
[8] A. F. Holleman, E. Wiberg, N. Wiberg, G. Fischer, in *Anorganische Chemie*, De Gruyter, Berlin, Boston, **2017**.
[9] M. C. Bayer, C. Jessen, A. J. Kornath, *Z. Anorg. Allg. Chem.* **2021**, *647*, 258.
[10] I. Bernhardi, T. Drews, K. Seppelt, *Angew. Chem. Int. Ed.* **1999**, *38*, 2232.
[11] F. P. Boer, *J. Am. Chem. Soc.* **1968**, *90*, 6706.
[12] J. M. Le Carpentier, R. Weiss, *Acta Crystallogr.* **1972**, *B28*, 1442.
[13] M. Gerken, D. A. Dixon, G. J. Schrobilgen, *Inorg. Chem.* **2002**, *41*, 259.
[14] R. Faggiani, D. K. Kennepohl, C. J. L. Lock, G. J. Schrobilgen, *Inorg. Chem.* **1986**, *25*, 563.
[15] A. J. Edwards, G. R. Jones, R. J. C. Sills, *Chem. Commun.* **1968**, 1527.
[16] G. A. Jeffrey, in *An introduction to hydrogen bonding, Topics in physical chemistry*, Oxford University Press, New York, **1997**.
[17] S. Beck, M. Feller, L. Spies, K. J. Dietrich, C. Jessen, K. Stierstorfer, A. J. Kornath, *ChemistryOpen* **2021**, *10*, 8.
[18] K. O. Christe, X. Zhang, R. Bau, J. Hegge, G. A. Olah, G. K. S. Prakash, J. A. Sheehy, *J. Am. Chem. Soc.* **2000**, *122*, 481.
[19] N. R. Götz, in *Ludwig-Maximilians-Universität, Diss.*, Universitätsbibliothek der Ludwig-Maximilians-Universität, München, **2011**.
[20] A. Bondi, *J. Phys. Chem.* **1964**, *68*, 441.
[21] W. Bolton, *Nature* **1964**, *201*, 987.
[22] B. Sahariah, B. K. Sarma, *Chem. Sci.* **2019**, *10*, 909.
[23] K. Hagen, *J. Mol. Struct.* **1985**, *128*, 139.
[24] J. M. Landry, J. E. Katon, *Spectrochim. Acta Part A* **1984**, *40*, 871.
[25] B. Chevrier, J. M. Le Carpentier, R. Weiss, *J. Am. Chem. Soc.* **1972**, *94*, 5718.
[26] L. Brun, C.-I. Brändén, *Acta Crystallogr.* **1966**, *20*, 749.
[27] V. R. Hathwar, T. N. Guru Row, *J. Phys. Chem. A* **2010**, *114*, 13434.
[28] S. Scheiner, *J. Phys. Chem. A* **2011**, *115*, 11202.
[29] J. Bacon, P. A. W. Dean, R. J. Gillespie, *Can. J. Chem.* **1971**, *49*, 1276.
[30] G. S. H. Chen, J. Passmore, *J. Chem. Soc. Dalton Trans.* **1979**, *8*, 1251.
[31] M. F. A. Dove, J. C. P. Sanders, *J. Chem. Soc. Dalton Trans.* **1992**, *23*, 3311.
[32] M. Walker, A. J. A. Harvey, A. Sen, C. E. H. Dessent, *J. Phys. Chem. A* **2013**, *117*, 12590.
[33] J. Weidlein, U. Müller, K. Dehnicke, in *Schwingungsspektroskopie*, Thieme, Stuttgart, **1988**.
[34] G. A. Olah, S. J. Kuhn, W. S. Tolgyesi, E. B. Baker, *J. Am. Chem. Soc.* **1962**, *84*, 14, 2733.
[35] M. Burgard, J. P. Brunette, M. J. F. Leroy, *Inorg. Chem.* **1976**, *15*, 1225.
[36] W. Zierkiewicz, M. Michalczyk, S. Scheiner, *Molecules* **2021**, *26*, 1740.
[37] H. Wang, W. Wang, W. J. Jin, *Chem. Rev.* **2016**, *116*, 5072.
[38] J. S. Murray, P. Lane, T. Clark, K. E. Riley, P. Politzer, *J. Mol. Model.* **2012**, *18*, 541.
[39] O. Loveday, J. Echeverría, *Nat. Commun.* **2021**, *12*, 5030.
[40] A. Bauzá, T. J. Mooibroek, A. Frontera, *ChemPhysChem* **2015**, *16*, 2496.
[41] T. Laube, *Chem. Rev.* **1998**, *98*, 1277.
[42] a) B. Chevrier, R. Weiss, *Angew. Chem. Int. Ed.* **1974**, *13*, 1; b) D. A. Klumpp, *Chem. Eur. J.* **2008**, *14*, 2004.
[43] J. W. Larsen, P. A. Bouis, *J. Am. Chem. Soc.* **1975**, *97*, 6094.
[44] G. A. Olah, M. B. Comisarow, *J. Am. Chem. Soc.* **1966**, *88*, 3313.
[45] M. C. Bayer, C. Kremser, C. Jessen, A. Nitzer, A. J. Kornath, *Chem. Eur. J.* **2022**, *28*, e202104422.
[46] G. A. Olah, A. M. White, *J. Am. Chem. Soc.* **1967**, *89*, 4752.
[47] Rigaku Oxford Diffraction, CrysAlisPro Software System, *Version 1.171.38.46*, Rigaku Corporation, Oxford, UK, **2015**.
[48] G. M. Sheldrick, *Acta Crystallogr.* **2015**, *A71*, 3.
[49] G. M. Sheldrick, *Acta Crystallogr.* **2015**, *C71*, 3.
[50] L. J. Farrugia, *J. Appl. Crystallogr.* **1999**, *32*, 837.
[51] A. L. Spek, *J. Appl. Crystallogr.* **2003**, *36*, 7.
[52] SCALE3 ABSPACK, *An Oxford Diffraction Program*, Oxford Diffraction Ltd, UK, **2005**.
[53] M. J. Frisch, G. W. Trucks, H. B. Schlegel, G. E. Scuseria, M. A. Robb, J. R. Cheeseman, G. Scalmani, V. Barone, B. Mennucci, G. A. Petersson, H. Nakatsuji, M. Caricato, X. Li, H. P. Hratchian, A. F. Izmaylov, J. Bloino, G. Zheng, J. L. Sonnenberg, M. Hada, M. Ehara, K. Toyota, R. Fukuda, J. Hasegawa, M. Ishida, T. Nakajima, Y. Honda, O. Kitao, H. Nakai, T. Vreven, J. A. Montgomery, Jr., J. E. Peralta, F. Ogliaro, M. Bearpark, J. J. Heyd, E. Brothers, K. N. Kudin, V. N. Staroverov, R. Kobayashi, J. Normand, K. Raghavachari, A. Rendell, J. C. Burant, S. S. Iyengar, J. Tomasi, M. Cossi, N. Rega, J. M. Millam, M. Klene, J. E. Knox, J. B. Cross, V. Bakken, C. Adamo, J. Jaramillo, R. Gomperts, R. E. Stratmann, O. Yazyev, A. J. Austin, R. Cammi, C. Pomelli, J. W. Ochterski, R. L. Martin, K. Morokuma, V. G. Zakrzewski, G. A. Voth, P. Salvador, J. J. Dannenberg, S. Dapprich, A. D. Daniels, O. Farkas, J. B. Foresman, J. V. Ortiz, J. Cioslowski, D. J. Fox, *Gaussian 09, Revision A.02*, Gaussian, Inc., Wallingford CT, **2009**.
[54] M. J. Frisch, G. W. Trucks, H. B. Schlegel, G. E. Scuseria, M. A. Robb, J. R. Cheeseman, G. Scalmani, V. Barone, G. A. Petersson, H. Nakatsuji, X. Li, M. Caricato, A. V. Marenich, J. Bloino, B. G. Janesko, R. Gomperts, B. Mennucci, H. P. Hratchian, J. V. Ortiz, A. F. Izmaylov, J. L. Sonnenberg, D. Williams-Young, F. Ding, F. Lipparini, F. Egidi, J. Goings, B. Peng, A. Petrone, T. Henderson, D. Ranasinghe, V. G. Zakrzewski, J. Gao, N. Rega, G. Zheng, W. Liang, M. Hada, M. Ehara, K. Toyota, R. Fukuda, J. Hasegawa, M. Ishida, T. Nakajima, Y. Honda, O. Kitao, H. Nakai, T. Vreven, K. Throssell, J. A. Montgomery, Jr., J. E. Peralta, F. Ogliaro, M. J. Bearpark, J. J. Heyd, E. N. Brothers, K. N. Kudin, V. N. Staroverov, T. A. Keith, R. Kobayashi, J. Normand, K. Raghavachari, A. P. Rendell, J. C. Burant, S. S. Iyengar, J. Tomasi, M. Cossi, J. M. Millam, M. Klene, C. Adamo, R. Cammi, J. W. Ochterski, R. L. Martin, K. Morokuma, O. Farkas, J. B. Foresman, D. J. Fox, *Gaussian 16, Revision A.03*, Gaussian, Inc., Wallingford CT, **2016**.
[55] R. Dennington, T. A. Keith, J. M. Millam, *GaussView, Version 6.0*, Semichem Inc., Shawnee Mission, **2016**.

Manuscript received: June 20, 2022
Revised manuscript received: July 1, 2022
Accepted manuscript online: July 4, 2022

RESEARCH ARTICLE

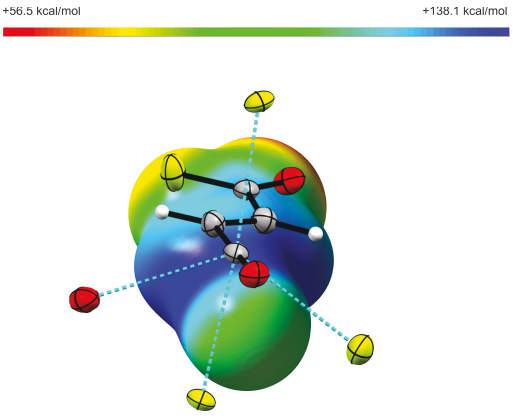

*M. C. Bayer, N. Greither, C. Jessen, A. Nitzer, Prof. Dr. A. J. Kornath**

The reaction of fumaryl halides with Lewis acids results in monoacyl cations and oxonium complexes. One C···O and three C···F contacts are formed for $[C_4H_2FO_2]^+[Sb_3F_{16}]^-$. The monoacylium ion is stabilized by electron back-donation from its ligands to the positive ring-structured π-hole at the oxocarbenium center.

European Journal of Inorganic Chemistry

Supporting Information

Intermediates in Friedel-Crafts Acylation of Fumaryl Halides

Marie C. Bayer, Nikolaus Greither, Christoph Jessen, Alexander Nitzer, and Andreas J. Kornath*

Figure S1: Formula unit of $C_4H_2N_2$ (displacement ellipsoids with 50% probability). Symmetry operation: *i = 1–x, 1–y, 1–z*.

Table S1: Selected bond lengths and angles of $C_4H_2N_2$ with estimated standard deviations in parentheses. Symmetry operations: *i = 1–x, 1–y, 1–z; ii = 2–x, 1–y, 1–z.*

Table S2: Experimental vibrational frequencies [cm^{-1}] of $[C_4H_2FO_2]^+[Sb_3F_{16}]^-$, $[C_4H_2FO_2]^+[SbCl_2F_4]^-$ and calculated vibrational frequencies [cm^{-1}] of $[C_4H_2FO_2]^+$.

Table S3: Experimental vibrational frequencies [cm^{-1}] of C4H2Cl2O2 · 2 SbCl5 and calculated vibrational frequencies [cm^{-1}] of C4H2Cl2O2 · 2 SbCl5.

Table S4: Selected bond lengths and angles of $C_4H_2Cl_2O_2 \cdot 2\ SbCl_5$ calculated at different density functionals in comparison with the experimental structural parameters of $C_4H_2Cl_2O_2 \cdot 2\ SbCl_5$. The estimated standard deviation is marked in parentheses.

Table S5: Selected vibrational frequencies [cm^{-1}] of $C_4H_2Cl_2O_2 \cdot 2\ SbCl_5$ calculated at different density functionals in comparison with the experimental vibrational frequencies [cm^{-1}] of $C_4H_2Cl_2O_2 \cdot 2\ SbCl_5$.

Table S6: Selected NBOs of $[C_4H_2FO_2]^+$ (BD = 2-center bond; BD* = 2-center antibond) combined with calculated values for occupancy, energy and s- and p-character.[a]

Table S7: Crystal data and structure refinement of $[C_4H_2FO_2]^+[Sb_3F_{16}]^-$, $C_4H_2Cl_2O_2 \cdot 2\ SbCl_5$

Table S8: Cartesian coordinates of calculated minimum structures of $[C_4H_2FO_2]^+$ at the B3LYP/aug-cc-pVTZ level of theory.

Table S9: Cartesian coordinates of calculated minimum structures of $[C_4H_2O_2]^{2+}$ at the B3LYP/aug-cc-pVTZ level of theory.

Table S10: Cartesian coordinates of calculated minimum structures of $C_4H_2Cl_2O_2 \cdot 2\ SbCl_5$ at the B3LYP/aug-cc-pVTZ level of theory and Sb was calculated at the B3LYP/GenECP MWB46 level.

Table S11: Cartesian coordinates of calculated minimum structures of $C_4H_2Cl_2O_2 \cdot 2\ SbCl_5$ at the M06-2X/aug-cc-pVTZ level of theory and Sb was calculated at the M06-2X/GenECP MWB46 level.

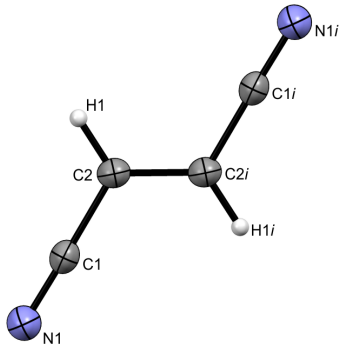

Figure S1: Formula unit of $C_4H_2N_2$ (displacement ellipsoids with 50% probability). Symmetry operation: *i = 1–x, 1–y, 1–z*.

Table S1: Selected bond lengths and angles of $C_4H_2N_2$ with estimated standard deviations in parentheses. Symmetry operations: *i = 1–x, 1–y, 1–z; ii = 2–x, 1–y, 1–z.*

Bond lengths [Å]	
N1–C1	1.147(2)
C2–C1	1.436(2)
C2–C2*i*	1.328(2)
Bond angles [°]	
C1–C2–C2*i*	121.3(1)
N1–C1–C2	178.9(1)
Angles of torsion [°]	
C2*i*–C2–C1–N1	178(7)
C1–C2–C2*i*–C1*i*	180.0(1)
Intermolecular contacts [Å]	
C2···C2*ii*	3.383(2)

Table S2: Experimental vibrational frequencies [cm^{-1}] of $[C_4H_2FO_2]^+[Sb_3F_{16}]^-$, $[C_4H_2FO_2]^+[SbCl_2F_4]^-$ and calculated vibrational frequencies [cm^{-1}] of $[C_4H_2FO_2]^+$.

$[C_4H_2FO_2]^+[Sb_3F_{16}]^-$ exp.[a]		$[C_4H_2FO_2]^+[SbCl_2F_4]^-$ exp.[a]		$[C_4H_2FO_2]^+$ calc.[b]	Assignment		
IR	Raman	IR	Raman	IR/Raman			
3082 m	3085 (6)	3080 vs	3085 (7)	3194 (20/41)	ν_1	*A'*	ν(C–H)
3038 m	3039 (12)	3036 vs	3038 (12)	3152 (73/52)	ν_2	*A'*	ν(C–H)[d]
2284 m	2289 (80)	2284 vs	2289 (72)	2327 (579/153)	ν_3	*A'*	ν(C≡O)[d]
		1850 vs					[c]
1828 m	1826 (100)	1821 vs	1826 (91)	1876 (155/187)	ν_4	*A'*	ν(C=O)
		1780 vs					[c]
1769 w	1773 (4)	1759 vs	1772 (12)				[c]
		1743 vs					[c]
1661 w		1657 vs					[c]
	1618 (7)	1614 vs	1616 (18)				[c]
1595 w	1599 (83)	1599 vs	1599 (79)	1612 (150/115)	ν_5	*A'*	ν(C=C)
	1575 (3)		1575 (11)				[c]
1470 m							[c]
		1443 vs	1445 (10)	1304 (11/23)	ν_6	*A'*	δ(CCH)
			1424 (10)				[c]
1358 w		1356 s		1257 (15/2)	ν_7	*A'*	δ(CCH)[d]
1327 w							[c]
1310 w	1290 (22)	1308 vs	1290 (25)	1214 (225/9)	ν_8	*A'*	ν(C–F)
	1249 (3)						[c]
1229 m	1231 (3)	1238 vs					[c]
		1221 vs	1222(16)				[c]
		1176 vs					[c]
1159 w		1161 vs					[c]
		1034 s					[c]
1001 w	995 (3)	1005 s	995 (7)	1022 (44/2)	ν_9	*A'*	ν(C–C)[d]
962 w	966 (4)	955 vs	966 (8)	1010 (30/1)	ν_{16}	*A''*	γ(HCCH)
924 w		926 s					[c]
887 w	890 (9)		891 (14)				[c]
837 w	846 (8)	845 s	846 (13)	884 (38/10)	ν_{10}	*A'*	ν(C–C)
827 w							[c]
758 m	745 (6)			867 (15/2)	ν_{17}	*A''*	γ(HCCH)
633 m		635 vs		688 (32/0)	ν_{18}	*A''*	γ(CCOF)
	605 (13)	602 s	605 (21)	676 (20/4)	ν_{11}	*A'*	δ(COF)
	555 (3)		555 (10)	573 (4/1)	ν_{12}	*A'*	δ(CCO)[d]
519 m				519 (0/0)	ν_{19}	*A''*	γ(CCO)[d]
	465 (9)		465 (17)	456 (13/2)	ν_{13}	*A'*	δ(CCO)
	430 (5)	430 s	433 (29)				[c]
	373 (5)						[c]
	301 (19)		300 (36)	251 (3/3)	ν_{14}	*A'*	δ(CCC)
	188 (5)			126 (12/0)	ν_{20}	*A''*	γ(CCC)
	171 (7)			125 (10/1)	ν_{15}	*A'*	δ(CCC)
	154 (12)						[c]
	136 (15)						[c]
	104 (36)		103 (46)	65 (1/1)	ν_{21}	*A''*	γ(CCC)
Vibrations of anions							
	737 (3)						$[Sb_3F_{16}]^-$
725 vs	717 (88)		717 (27)				$[Sb_3F_{16}]^-$; $[SbCl_2F_4]^-$
710 vs	709 (12)	702 vs	711 (38)				$[Sb_3F_{16}]^-$; $[SbCl_2F_4]^-$
683 s	689 (53)	692 vs	689 (67)				$[Sb_3F_{16}]^-$; $[SbCl_2F_4]^-$
663 s	671 (92)	679 vs	677 (35)				$[Sb_3F_{16}]^-$; $[SbCl_2F_4]^-$
642 m	657 (60)	660 vs	657 (100)				$[Sb_3F_{16}]^-$; $[SbCl_2F_4]^-$
			633(11)				$[SbCl_2F_4]^-$
		565 s					$[SbCl_2F_4]^-$
			523 (10)				$[SbCl_2F_4]^-$
			504 (13)				$[SbCl_2F_4]^-$
492 m		496 vs	493 (11)				$[Sb_3F_{16}]^-$; $[SbCl_2F_4]^-$
			479 (13)				$[SbCl_2F_4]^-$
		449 s	447 (27)				$[SbCl_2F_4]^-$
			393 (54)				$[SbCl_2F_4]^-$
			335 (14)				$[SbCl_2F_4]^-$
			310 (20)				$[SbCl_2F_4]^-$
	277 (20)		277 (21)				$[Sb_3F_{16}]^-$; $[SbCl_2F_4]^-$
			269 (21)				$[SbCl_2F_4]^-$
			252 (20)				$[SbCl_2F_4]^-$
	244 (17)		242 (24)				$[Sb_3F_{16}]^-$; $[SbCl_2F_4]^-$
			228 (21)				$[SbCl_2F_4]^-$

Table is continued on the following page.

	219 (10)		220 (22)				$[Sb_3F_{16}]^-$; $[SbCl_2F_4]^-$
	207 (8)						$[Sb_3F_{16}]^-$
			129 (39)				$[SbCl_2F_4]^-$

[a] Abbrevations for IR intensities: v = very, s = strong, m = medium, w = weak. IR intensities in km/mol; Raman intensities in Å⁴/u. Experimental Raman activities are relative to a scale of 1 to 100.
[b] Calculated at the B3LYP/aug-cc-pVTZ level of theory.
[c] Very probably combination tones/ overtones.
[d] acylium ion side.

Table S3: Experimental vibrational frequencies [cm^{-1}] of $C_4H_2Cl_2O_2 \cdot 2\ SbCl_5$ and calculated vibrational frequencies [cm^{-1}] of $C_4H_2Cl_2O_2 \cdot 2\ SbCl_5$.

$C_4H_2Cl_2O_2 \cdot 2\ SbCl_5$ exp.[a]		$C_4H_2Cl_2O_2 \cdot 2\ SbCl_5$ calc.[b]	Assignment		
IR	Raman	IR/Raman			
3067 w		3225(11/0)	ν_{43}	B_u	ν_{as}(C–H)
	3054 (5)	3225(0/49)	ν_1	A_g	ν_s(C–H)
1699 m					[c]
	1644 (77)	1792(0/1589)	ν_2	A_g	ν_s(C=O)
1635 vs		1782(1611/0)	ν_{44}	B_u	ν_{as}(C=O)
	1607 (6)	1735(0/361)	ν_3	A_g	ν(C=C)
1570 w					[c]
	1279 (6)	1315(0/47)	ν_4	A_g	δ(CCH)
1263 w		1264(7/0)	ν_{45}	B_u	δ(CCH)
1246 w					[c]
	1193 (2)	1213(0/72)	ν_5	A_g	ν_s(C–C)
1113 m		1135(444/0)	ν_{46}	B_u	ν_{as}(C–C)
1065 m		1025(30/0)	ν_{20}	A_u	γ(HCCH)
964 m					[c]
	874 (7)	935(0/7)	ν_{32}	B_g	γ(HCCH)
739 s		753(159/0)	ν_{47}	B_u	ν_{as}(C–Cl)
683 m		714(6/0)	ν_{21}	A_u	γ(CCOCl)
	693 (3)	692(0/10)	ν_6	A_g	ν_s(C–Cl)
	575 (7)	570(0/28)	ν_7	A_g	δ(CCC)
	542 (2)				[c]
		565(0/0)	ν_{33}	B_g	γ(CCOCl)
500 w		515(19/0)	ν_{48}	B_u	δ(COCl)
453 m		453(24/0)	ν_{49}	B_u	δ(CCCl)
442 w	441 (5)	437(0/9)	ν_8	A_g	ν_s(Sb–O)
	368 (28)	394(0/53)	ν_9	A_g	ν_s(Sb–Cl)
413 w		393(189/0)	ν_{50}	B_u	ν_{as}(Sb–Cl)
		387(184/0)	ν_{22}	A_u	ν_{as}(Sb–Cl_2)
		386(0/0)	ν_{34}	B_g	ν_s(Sb–Cl_2)
		386(164/0)	ν_{51}	B_u	ν_{as}(Sb–Cl_2)
	361 (24)	385(0/1)	ν_{10}	A_g	ν_s(Sb–Cl_2)
		354(7/0)	ν_{52}	B_u	ν_{as}(Sb–Cl_4)
	344 (100)	353(0/104)	ν_{11}	A_g	ν_s(Sb–Cl_4)
	306 (19)	304(0/18)	ν_{35}	B_g	ν_s(Sb–Cl_4)
		304(0/0)	ν_{23}	A_u	ν_{as}(Sb–Cl_4)
		211(21/0)	ν_{24}	A_u	γ(CCOSb)
	206 (5)	208(0/1)	ν_{12}	A_g	δ(CCCl)
		198(0/0)	ν_{36}	B_g	γ(CCOSb)
		187(2/0)	ν_{53}	B_u	δ(SbCl_2)
	189 (34)	186(0/6)	ν_{13}	A_g	δ(SbCl_2)
		183(11/0)	ν_{54}	B_u	ν_{as}(Sb–O)
	174 (10)	174(0/1)	ν_{14}	A_g	δ(OSbCl)
		172(18/0)	ν_{55}	B_u	δ(SbCl_2)
		171(18/0)	ν_{25}	A_u	γ(COSbCl)
	148 (15)	168(0/2)	ν_{37}	B_g	γ(CCOSb)
	129 (14)	158(0/1)	ν_{15}	A_g	δ(SbCl_4)
		158(88/0)	ν_{56}	B_u	δ(SbCl_4)
		135(1/0)	ν_{57}	B_u	δ(SbCl_3)
	119 (9)	134(0/5)	ν_{16}	A_g	δ(SbCl_3)
		131(0/1)	ν_{38}	B_g	γ(HCCH)
		130(0/0)	ν_{26}	A_u	γ(CClOSb)
		109(0/5)	ν_{39}	B_g	γ(HCCH)
		104(0/0)	ν_{27}	A_u	γ(ClCOSbCl)
		103(0/2)	ν_{17}	A_g	δ(OSbCl)
		90(0/0)	ν_{40}	B_g	γ(SbCl_4)
		88(0/0)	ν_{28}	A_u	γ(SbCl_4)
		79(28/0)	ν_{58}	B_u	δ(ClSbO)
		72(28/0)	ν_{59}	B_u	δ(ClSbO)

Table is continued on the following page.

		50(0/0)	ν_{29}	A_u	τ(COCl)
		49(0/0)	ν_{18}	A_g	δ(ClSbO)
		45(0/2)	ν_{41}	B_g	γ(CCCC)
		35(0/1)	ν_{19}	A_g	δ(COSb)
		21(1/0)	ν_{60}	B_u	δ(COSb)
		18(0/1)	ν_{42}	B_g	γ(CCCC)

	18(0/0)	ν_{30}	A_u	γ($SbCl_5$)
	9(1/0)	ν_{31}	A_u	γ(CCCC)

[a] Abbrevations for IR intensities: v = very, s = strong, m = medium, w = weak. IR intensities in km/mol; Raman intensities in $Å^4/u$. Experimental Raman activities are relative to a scale of 1 to 100.
[b] Calculated at the M06-2X/aug-cc-pVTZ level of theory and Sb was calculated at the M06-2X/GenECP MWB46 level.
[c] Very probably combination tones/ overtones.

Table S4: Selected bond lengths and angles of $C_4H_2Cl_2O_2 \cdot 2\ SbCl_5$ calculated at different density functionals in comparison with the experimental structural parameters of $C_4H_2Cl_2O_2 \cdot 2\ SbCl_5$. The estimated standard deviation is marked in parentheses.

	$C_4H_2Cl_2O_2 \cdot 2\ SbCl_5$ B3LYP[a]	$C_4H_2Cl_2O_2 \cdot 2\ SbCl_5$ M06-2X[b]	Crystal structure of $C_4H_2Cl_2O_2 \cdot 2\ SbCl_5$	
Bond length [Å]				
C1–Cl6	1.769	1.726	C1–Cl1	1.712(3)
C1–O1	1.198	1.201	C1–O1	1.220(3)
C1–C2	1.477	1.481	C1–C2	1.472(4)
C2–C3	1.332	1.326	C2–C2*i*	1.326(3)
Sb1–O1	2.789	2.490	Sb1–O1	2.359(2)
Bond angle [°]				
O1–C1–Cl6	121.3	122.2	O1–C1–Cl1	122.0(2)
Cl6–C1–C2	117.0	117.8	Cl1–C1–C2	117.9(2)
O1–C1–C2	121.7	120.0	O1–C1–C2	120.0(2)
C1–C2–C3	125.1	124.0	C1–C2–C2*i*	123.6(2)
Sb1–O1–C1	149.9	143.0	Sb1–O1–C1	140.1(2)
Angle of torsion [°]				
C1–C2–C3–C4	–180.0	–180.0	C1–C2–C2*i*–C1*i*	–180.0(2)
O1–C1–C2–C3	–180.0	180.0	O1–C1–C2–C2*i*	–172.5(2)
Cl1–C1–C2–C3	0.0	–0.0	Cl1–C1–C2–C2*i*	6.9(3)

[a] Calculated at the B3LYP/aug-cc-pVTZ level of theory and Sb was calculated at the B3LYP/GenECP MWB46 level.
[b] Calculated at the M06-2X/aug-cc-pVTZ level of theory and Sb was calculated at the M06-2X/GenECP MWB46 level.

Table S5: Selected vibrational frequencies [cm^{-1}] of $C_4H_2Cl_2O_2 \cdot 2\ SbCl_5$ calculated at different density functionals in comparison with the experimental vibrational frequencies [cm^{-1}] of $C_4H_2Cl_2O_2 \cdot 2\ SbCl_5$.

$C_4H_2Cl_2O_2 \cdot 2\ SbCl_5$ exp.[a]		$C_4H_2Cl_2O_2 \cdot 2\ SbCl_5$ B3LYP[b]	$C_4H_2Cl_2O_2 \cdot 2\ SbCl_5$ M06-2X[c]	
IR	Raman	IR/Raman	IR/Raman	Assignment
3067 w		3200(7/0)	3225(11/0)	ν_{as}(C–H)
	3054 (5)	3197(0/53)	3225(0/49)	ν_{s}(C–H)
	1644 (77)	1764(0/1661)	1792(0/1589)	ν_{s}(C=O)
1635 vs		1762(1319/0)	1782(1611/0)	ν_{as}(C=O)
	1607 (6)	1692(0/557)	1735(0/361)	ν(C=C)
	1279 (6)	1317(0/63)	1315(0/47)	δ(CCH)
1263 w		1269(7/0)	1264(7/0)	δ(CCH)
	1193 (2)	1166(0/80)	1213(0/72)	ν_{s}(C–C)
1113 m		1089(407/0)	1135(444/0)	ν_{as}(C–C)
1065 m		1018(28/0)	1025(30/0)	γ(HCCH)
	874 (7)	930(0/6)	935(0/7)	γ(HCCH)
739 s		706(177/0)	753(159/0)	ν_{as}(C–Cl)
683 m		705(5/0)	714(6/0)	γ(CCOCl)
	693 (3)	645(0/23)	692(0/10)	ν_{s}(C–Cl)
	575 (7)	537(0/34)	570(0/28)	δ(CCC)
500 w		476(11/0)	515(19/0)	δ(COCl)
453 m		441(28/0)	453(24/0)	δ(CCCl)
442 w	441 (5)	404(0/6)	437(0/9)	ν_{s}(Sb–O)
	368 (28)	371(0/57)	394(0/53)	ν_{s}(Sb–Cl)
413 w		370(160/0)	393(189/0)	ν_{as}(Sb–Cl)

[a] Abbrevations for IR intensities: v = very, s = strong, m = medium, w = weak. IR intensities in km/mol; Raman intensities in $Å^4/u$. Experimental Raman activities are relative to a scale of 1 to 100.

[b] Calculated at the B3LYP/aug-cc-pVTZ level of theory and Sb was calculated at the B3LYP/GenECP MWB46 level.

[c] Calculated at the M06-2X/aug-cc-pVTZ level of theory and Sb was calculated at the M06-2X/GenECP MWB46 level.

Table S6: Selected NBOs of $[C_4H_2FO_2]^+$ (BD = 2-center bond; BD* = 2-center antibond) combined with calculated values for occupancy, energy and s- and p-character.[a]

Bond	Occupancy	Energy	s-, p- character
BD(1) C3–C4	1.99 e^-	–1.06770	C3 s(27.77%), p 2.59 (71.91%) C4 s(58.87%), p 0.70 (41.09%)
BD(1) C4–O2	2.00 e^-	–1.56489	C4 s(41.41%), p 1.41 (58.50%) O2 s(43.35%), p 1.29 (55.76%)
BD(2) C4–O2	1.99 e^-	–0.75133	C4 s(0.01%), p 1.00 (99.84%) O2 s(0.00%), p 1.00 (99.42%)
BD(3) C4–O2	1.99 e^-	–0.75029	C4 s(0.00%), p 1.00 (99.84%) O2 s(0.00%), p 1.00 (99.43%)
BD*(1) C3–C4	0.02 e^-	0.21843	C3 s(27.77%), p 2.59 (71.91%) C4 s(58.87%), p 0.70 (41.09%)
BD*(1) C4–O2	0.01 e^-	0.48975	C4 s(41.41%), p 1.41 (58.50%) O2 s(43.35%), p 1.29 (55.76%)
BD*(2) C4–O2	0.05 e^-	–0.26394	C4 s(0.01%), p 1.00 (99.84%) O2 s(0.00%), p 1.00 (99.42%)
BD*(3) C4–O2	0.20 e^-	–0.26962	C4 s(0.00%), p 1.00 (99.84%) O2 s(0.00%), p 1.00 (99.43%)

[a] calculated on the B3LYP/aug-cc-pVTZ level of theory.

Table S7: Crystal data and structure refinement of $[C_4H_2FO_2]^+[Sb_3F_{16}]^-$, $C_4H_2Cl_2O_2 \cdot 2\ SbCl_5$ and $C_4H_2N_2$.

	$[C_4H_2FO_2]^+[Sb_3F_{16}]^-$	$C_4H_2Cl_2O_2 \cdot 2\ SbCl_5$	$C_4H_2N_2$
Molecular Formula	$C_4H_2F_{17}O_2Sb_3$	$C_4H_2Cl_{12}O_2Sb_2$	$C_4H_2N_2$
M_r[g·mol^{-1}]	770.31	750.96	78.08
Crystal size [mm^3]	0.245 x 0.116 x 0.104	0.241 x 0.203 x 0.129	0.237 x 0.179 x 0.065
Crystal system	monoclinic	orthorhombic	monoclinic
Space group	$P2_1/c$	$Pbca$	$P2_1/c$
a [Å]	8.3960(6)	11.6766(4)	3.7955(11)
b [Å]	12.5909(9)	12.6353(4)	5.5220(10)
c [Å]	15.2119(12)	13.2307(5)	9.718(2)
α [°]	90	90	90
β [°]	104.578(8)	90	97.39(2)
γ [°]	90	90	90
V [A^3]	1556.3(2)	1952.02(12)	201.99(8)
Z	4	4	2
ρ_{calc} [g·cm^{-3}]	3.288	2.555	1.284
μ [mm^{-1}]	5.358	4.403	0.086
$\lambda_{MoK\alpha}$ [Å]	0.71073	0.71073	0.71073
F(000)	1392	1392	80
T [K]	105(2)	103(2)	106(2)
h, k, l range	–10:12; –18:15; –22:22	–13:17; –17:18; –18:18	–3:4; –6:6; –12:11
Measured reflexes	17099	19959	1372
Unique reflexes	5243	3302	414
R_{int}	0.0392	0.0446	0.0312
Parameters	243	91	32
R(F)/wR(F^2)[a)] (all data)	0.0427/0.0548	0.0405/0.0587	0.0491/0.0813
Weighting scheme[b)]	0.017000	0.022200/0.083300	0.029800/0.042000
S (Gof)[c)]	1.048	1.095	1.061
Residual density [e·Å^{-3}]	0.971/–0.795	1.004/–0.738	0.158/–0.119
Device	Oxford XCalibur	Oxford XCalibur	Oxford XCalibur
CCDC	2155394	2155395	2155396

[a)] $R_1 = \Sigma||F_o|-|F_c||/\Sigma|F_o|$;
[b)] $wR_2 = [\Sigma[w(F_o^2-F_c^2)^2]/\Sigma[w(F_o)^2]]^{1/2}$; $w = [\sigma_c^2(F_o^2)+(xP)^2+yP]^{-1}$; $P = (F_o^2+2F_c^2)/3$
[c)] GoF = $\{\Sigma[w(F_o^2-F_c^2)^2]/(n-p)\}^{1/2}$ (n = number of reflexions; p = total number of parameters).

Table S8: Cartesian coordinates of calculated minimum structures of $[C_4H_2FO_2]^+$ at the B3LYP/aug-cc-pVTZ level of theory.

Atom	x	y	z
C	0.000113216	0.000109498	0.000000000
H	-0.000046609	-0.000050227	0.000000000
C	-0.000038511	-0.000074973	0.000000000
H	-0.000000681	0.000011798	0.000000000
C	0.000046483	-0.000028884	0.000000000
C	0.000037649	-0.000013800	0.000000000
O	-0.000085302	0.000007197	0.000000000
O	0.000009130	0.000047417	0.000000000
F	-0.000035375	-0.000008026	0.000000000

Table S9: Cartesian coordinates of calculated minimum structures of $[C_4H_2O_2]^{2+}$ at the B3LYP/aug-cc-pVTZ level of theory.

Atom	x	y	z
C	0.000110242	0.000041626	0.000000000
H	-0.000030054	-0.000050726	0.000000000
C	-0.000110242	-0.000041626	0.000000000
H	0.000030054	0.000050726	0.000000000
C	-0.000090023	0.000022151	0.000000000
C	0.000090023	-0.000022151	0.000000000
O	0.000132478	0.000015846	0.000000000
O	-0.000132478	-0.000015846	0.000000000

Table S10: Cartesian coordinates of calculated minimum structures of $C_4H_2Cl_2O_2 \cdot 2\ SbCl_5$ at the B3LYP/aug-cc-pVTZ level of theory and Sb was calculated at the B3LYP/GenECP MWB46 level.

Atom	x	y	z
O	-0.000000037	-0.000001780	0.000000001
C	0.000000384	-0.000001248	-0.000000001
C	-0.000000217	-0.000000378	0.000000000
H	-0.000000830	-0.000000439	-0.000000000
O	0.000000020	0.000001788	0.000000000
C	-0.000000364	0.000001237	0.000000001
C	0.000000210	0.000000375	0.000000000
H	0.000000833	0.000000441	-0.000000000
Cl	0.000001308	-0.000001076	-0.000000000
Cl	-0.000001309	0.000001080	0.000000000
Sb	-0.000000045	-0.000003561	-0.000000001
Sb	0.000000047	0.000003560	-0.000000002
Cl	-0.000000938	0.000003322	-0.000000026
Cl	0.000000092	0.000004980	0.000000001
Cl	0.000001080	0.000003263	-0.000000010
Cl	0.000001080	0.000003263	0.000000010
Cl	-0.000000937	0.000003321	0.000000026
Cl	0.000000938	-0.000003322	-0.000000026
Cl	-0.000000092	-0.000004980	0.000000001
Cl	-0.000001080	-0.000003263	-0.000000010
Cl	-0.000001080	-0.000003264	0.000000010
Cl	0.000000937	-0.000003322	0.000000026

Table S11: Cartesian coordinates of calculated minimum structures of $C_4H_2Cl_2O_2 \cdot 2\ SbCl_5$ at the M06-2X/aug-cc-pVTZ level of theory and Sb was calculated at the M06-2X/GenECP MWB46 level.

Atom	x	y	z
O	0.000001129	-0.000004431	0.000000018
C	-0.000001367	-0.000003475	-0.000000020
C	0.000000736	-0.000001052	-0.000000018
H	0.000002163	-0.000000949	-0.000000020
O	0.000000822	0.000005135	0.000000083
C	-0.000000988	0.000002489	-0.000000005
C	0.000000111	0.000000771	0.000000040
H	-0.000002339	0.000001115	0.000000009
Cl	-0.000003344	-0.000002954	-0.000000007
Cl	0.000003494	0.000003354	-0.000000077
Sb	0.000000026	-0.000008713	-0.000000021
Sb	-0.000000381	0.000008710	0.000000002
Cl	0.000002440	0.000008070	-0.000000016
Cl	-0.000000010	0.000012432	0.000000050
Cl	-0.000002828	0.000008183	-0.000000032
Cl	-0.000002781	0.000008176	0.000000037
Cl	0.000002512	0.000008063	0.000000031
Cl	-0.000002483	-0.000008000	-0.000000024
Cl	-0.000000004	-0.000012423	-0.000000003
Cl	0.000002816	-0.000008211	0.000000030
Cl	0.000002777	-0.000008247	-0.000000009
Cl	-0.000002499	-0.000008045	-0.000000049

Journal of Inorganic and General Chemistry

ZAAC

Zeitschrift für anorganische und allgemeine Chemie

2020

646/7

Front Cover: Preparation and Characterization of Protonated Fumaric Acid

Marie C. Bayer, Christoph Jessen, and Andreas J. Kornath

WILEY-VCH

www.zaac.wiley-vch.de

Journal of Inorganic and General Chemistry
ZAAC
Zeitschrift für anorganische und allgemeine Chemie
DOI: 10.1002/zaac.202000091
ARTICLE

Preparation and Characterization of Protonated Fumaric Acid

Marie C. Bayer,[a] Christoph Jessen,[a] and Andreas J. Kornath*[a]

Dedicated to Dr. Klaus Römer on the Occasion of his 80th Birthday

Abstract. Fumaric acid was reacted with the binary superacidic systems HF/SbF_5 and HF/AsF_5. The *O,O′*-diprotonated $[C_4H_6O_4]^{2+}([MF_6]^-)_2$ (M = As, Sb) and the *O*-monoprotonated $[C_4H_5O_4]^+[MF_6]^-$ (M = As, Sb) species are formed depending on the stoichiometric ratio of the Lewis acid to fumaric acid. The colorless salts were characterized by low-temperature vibrational spectroscopy. In case of the hexafluoridoantimonates single-crystal X-ray structure analyses were carried out. The $[C_4H_6O_4]^{2+}([SbF_6]^-)_2$ crystallizes in the monoclinic space group *C*2/*c* with four formula units per unit cell and $[C_4H_5O_4]^+[SbF_6]^-$ crystallizes in the triclinic space group $P\bar{1}$ with one formula unit per unit cell. The protonation of fumaric acid does not cause a notable change of the C=C bond length. The experimental data are discussed together with quantum chemical calculations of the cations $[C_4H_6O_4 \cdot 4\ HF]^{2+}$ and $[C_4H_6O_4 \cdot 2\ H_2CO \cdot 2\ HF]^{2+}$.

Introduction

Fumaric acid (*trans*-1,2-ethylenedicarboxylic acid) was isolated by *Braconnot* in 1810 from mushrooms.[1] It is used nowadays as food acidulant E297 (pK_{a1} = 3.02 and pK_{a2} = 4.38).[2,3] The strength of commonly used acids is not sufficient for a protonation of fumaric acid. Therefore, *Larsen* et al. investigated fumaric acid in superacidic media. The authors reported an *O,O′*-diprotonation in the superacidic solution FSO_3H/SbF_5 observed by NMR spectroscopy.[4] Furthermore, a study of *Amat* et al. showed that fumaric acid is *O*-monoprotonated in oleum and concentrated sulfuric acid.[5] However, structural parameters as well as vibrational spectroscopic studies are still unkown.[4,5] This prompted us to isolate and structurally characterize salts containing the $[C_4H_6O_4]^{2+}$ and the $[C_4H_5O_4]^+$ cation.

Results and Discussion

Fumaric acid was reacted with the binary superacidic solutions HF/MF_5 (M = As, Sb). To form the $[C_4H_6O_4]^{2+}$ cation an excess of the Lewis acids (AsF_5 or SbF_5) is required [Equation (1)]. The preparation of the salt containing the *O*-monoprotonated cation was carried out according to Equation (2). It is necessary to ensure that an equimolar amount of the Lewis acids with respect to the starting material is used.

Anhydrous hydrogen fluoride (*a*HF) acts as solvent as well as a reagent. The reactions were carried out at a temperature of –20 °C. After the removal of the excess of *a*HF in a dynamic vacuum at –78 °C, the colorless salts $[C_4H_6O_4]^{2+}([SbF_6]^-)_2$ (**1**), $[C_4H_6O_4]^{2+}([AsF_6]^-)_2$ (**2**), $[C_4H_5O_4]^+[SbF_6]^-$ (**3**), and $[C_4H_5O_4]^+[AsF_6]^-$ (**4**) were obtained, which are stable up to 25 °C. Under these reaction conditions no addition of HF to the carbon double bond occurs.

The corresponding deuterated salts $[C_4H_2D_4O_4]^{2+}([SbF_6]^-)_2$ (**5**) and $[C_4H_2D_4O_4]^{2+}([AsF_6]^-)_2$ (**6**) were prepared by varying the superacidic system from HF/MF_5 to DF/MF_5 (M = As, Sb). Since deuterium fluoride is used in large excess, the hydroxy hydrogens are thoroughly replaced by deuterium, leading to a degree of deuteration of approximately 96 %.

Vibrational Spectra of $[C_4H_6O_4]^{2+}([MF_6]^-)_2$ (M = As, Sb)

The low-temperature vibrational spectra of $[C_4H_6O_4]^{2+}([SbF_6]^-)_2$ (**1**), $[C_4H_6O_4]^{2+}([AsF_6]^-)_2$ (**2**) and fumaric acid are shown in Figure 1. The vibrational spectra of the D-isotopomeric salts $[C_4H_2D_4O_4]^{2+}([SbF_6]^-)_2$ (**5**) and $[C_4H_2D_4O_4]^{2+}([AsF_6]^-)_2$ (**6**) as well as deuterated fumaric acid are illustrated in Figure S1 (Supporting Information). In Table 1 selected experimental vibrational frequencies of (**1**) and (**2**) as well as the calculated frequencies of the cation $[C_4H_6O_4 \cdot 4\ HF]^{2+}$ are summarized. The complete table (Table S1) and a table of the vibrational frequencies of fumaric acid (Table S2) are listed in the Supporting Information. The experimental vibrational frequencies of (**5**) and (**6**) together with the calculated frequencies of the cation $[C_4H_2D_4O_4 \cdot 4\ HF]^{2+}$ are given in Table S3 (Supporting Information). According to quantum chemical calculations, which are discussed later, the cation $[C_4H_6O_4]^{2+}$ displays a C_2 symmetry. 36 fundamental vibrations are expected, of which 19 modes are active in the Raman spectra and 17 modes are active in the IR spectra. The assignment of the vibrational modes was carried out by analyzing the Cartesian displacement vectors of the calculated vibrational modes of $[C_4H_6O_4 \cdot 4\ HF]^{2+}$ and by a comparison with the vibrations of fumaric acid.[6,7]

* Prof. Dr A. J. Kornath
E-Mail: andreas.kornath@cup.uni-muenchen.de
[a] Department Chemie
Ludwig-Maximilians-Universität München
Butenandstr. 5–13(D)
81377 Munich, Germany
Supporting information for this article is available on the WWW under **http://dx.doi.org/10.1002/zaac.202000091** or from the author.

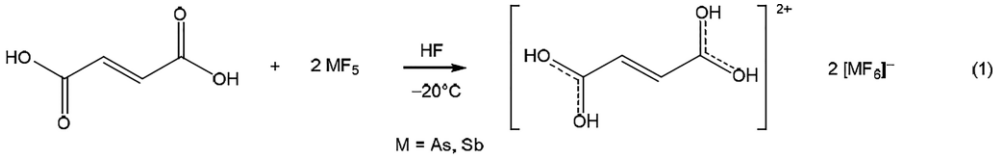

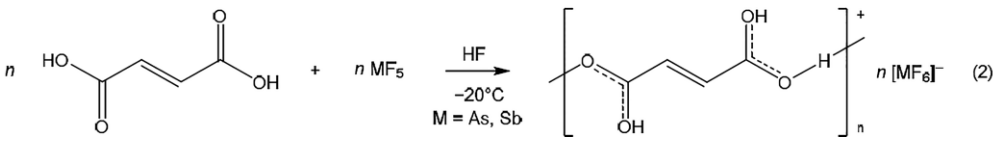

The symmetric C–H stretching mode is detected in the Raman spectra at 3092 cm^{-1} (**1**) and at 3087 cm^{-1} (**2**), respectively. It is blue-shifted by 23 cm^{-1} (**1**) and 18 cm^{-1} (**2**), respectively, compared to that of fumaric acid. Based on the measurement method, moisture condensed on the IR plate. Therefore no meaningful IR bands for the O–H vibrations are observable. In the IR spectra of (**5**) and (**6**) broad bands in the range of 2334 cm^{-1} to 2280 cm^{-1} are observed, as well as in the Raman spectra of (**5**) and (**6**) in the range of 2295 cm^{-1} to 2186 cm^{-1}. In agreement with the theoretical calculations the bands and lines arise from O–D stretching vibrations. The broadening of the IR bands and Raman lines relies on hydrogen bonds in the solid state. The C=C stretching mode occurs at 1686 cm^{-1} (**1**) and at 1684 cm^{-1} (**2**), respectively, and it is blue-shifted by 81 cm^{-1} (**1**) and 79 cm^{-1} (**2**), respectively, compared to fumaric acid. The blue-shift of the C=C stretching mode is due to the positive charge of the ion, resulting from the protonation. The C–O stretching mode is observed at 1637 cm^{-1} (**1**) and 1643 cm^{-1} (**2**), respectively, in the Raman spectra as well as at 1610 cm^{-1} (**1**) and 1612 cm^{-1} (**2**), respectively, in the IR spectra. The C–O stretching vibrations are shifted to lower wavenumbers in comparison to those of the starting material. The shift is a result of the protonation which causes a weakening of the C–O bond.

For the anions $[SbF_6]^-$ and $[AsF_6]^-$ more vibrations are detected than expected for an ideal octahedral symmetry. This indicates a distortion of the octahedral arrangement, which is confirmed by the single-crystal X-ray structural analysis.

Crystal Structure of $[C_4H_6O_4]^{2+}([SbF_6]^-)_2$

The $[C_4H_6O_4]^{2+}([SbF_6]^-)_2$ (**1**) crystallizes in the monoclinic space group *C*2/*c* with four formula units per unit cell. Figure 2 shows the formula unit of (**1**). Selected structural parameters of (**1**) and fumaric acid[8] are listed in Table 2.

The C–O bond lengths are with 1.273(5) Å (C2–O1) and 1.261(5) Å (C2–O2) not significantly different and are in the range between formal C–O single (1.43 Å) and C=O double bonds (1.19 Å).[9] In comparison with fumaric acid,[8] no significant difference of the lengths of the C–OH bonds is observed. The diprotonation causes a significant elongation of the C=O bond lengths of fumaric acid (1.228(4) Å),[8] whereas the C–C and C=C bonds are not significantly affected. The bond angles of fumaric acid are not changed remarkably by

Table 1. Selected experimental vibrational frequencies [cm^{-1}] of $[C_4H_6O_4]^{2+}([MF_6]^-)_2$ (M = As, Sb) and calculated vibrational frequencies [cm^{-1}] of $[C_4H_6O_4 \cdot 4\ HF]^{2+}$.

$[C_4H_6O_4]^{2+}([SbF_6]^-)_2$ (**1**) exp.[a]		$[C_4H_6O_4]^{2+}([AsF_6]^-)_2$ (**2**) exp.[a]		$[C_4H_6O_4 \cdot 4\ HF]^{2+}$ calcd.[b) c)]	Assignment		
IR	Raman	IR	Raman	IR/Raman			
	3092(31)		3087(24)	3040(0/68)	ν_2	A	ν_s(C–H)
	1686(89)		1684(100)	1672(0/185)	ν_4	A	ν(C=C)
	1637(37)		1643(32)	1605(0/126)	ν_5	A	ν(C–O)
1610 m		1612 s		1617(620/0)	ν_{23}	B	ν(C–O)
	1528(13)		1531(12)	1489(0/26)	ν_6	A	ν(C–O)
	1325(11)		1326(19)	1293(0/13)	ν_7	A	δ(CCH)
1279 s		1279 s		1264(229/0)	ν_{25}	B	δ(CCH)
	1281(7)		1272(7)	1264(0/5)	ν_8	A	δ(COH)
1252 m		1250 s		1237(287/0)	ν_{26}	B	δ(COH)
	1233(82)		1223(67)	1220(0/48)	ν_9	A	δ(COH)
1229 s		1217 s		1216(232/0)	ν_{27}	B	δ(COH)
949 s		962 s		950(67/0)	ν_{10}	A	γ(CCH)
	989(24)		985(31)	950(0/8)	ν_{11}	A	ν(C–C)
941 s	952(8)	937 s	956(2)	901(51/0)	ν_{28}	B	ν(C–C)
802 s		797 s		822(256/0)	ν_{13}	A	γ(COH)

a) Abbrevations for IR intensities: vs. = very strong, s = strong, m = medium, w = weak. b) Calculated on the ωB97XD/aug-cc-pVTZ level of theory; scaling factor 0.945. c) IR intensities in km · mol^{-1}; Raman intensities in $Å^4 \cdot u^{-1}$.

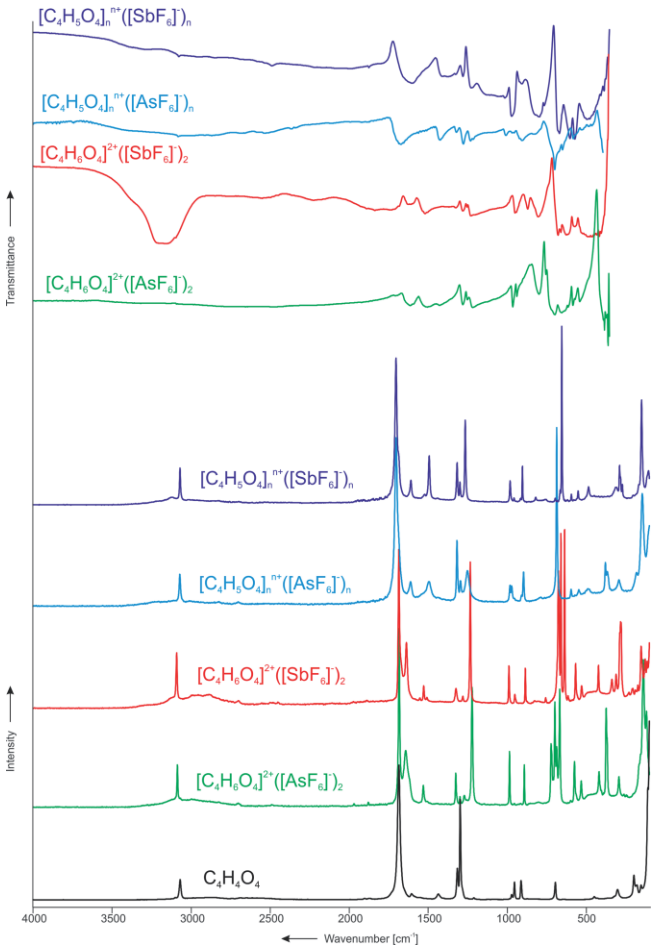

Figure 1. Low-temperature Raman and IR spectra of $[C_4H_6O_4]^{2+}([SbF_6]^-)_2$ (**1**), $[C_4H_6O_4]^{2+}([AsF_6]^-)_2$ (**2**), $[C_4H_5O_4]^+[SbF_6]^-$ (**3**), $[C_4H_5O_4]^+[AsF_6]^-$ (**4**), and the Raman spectrum of $C_4H_4O_4$.

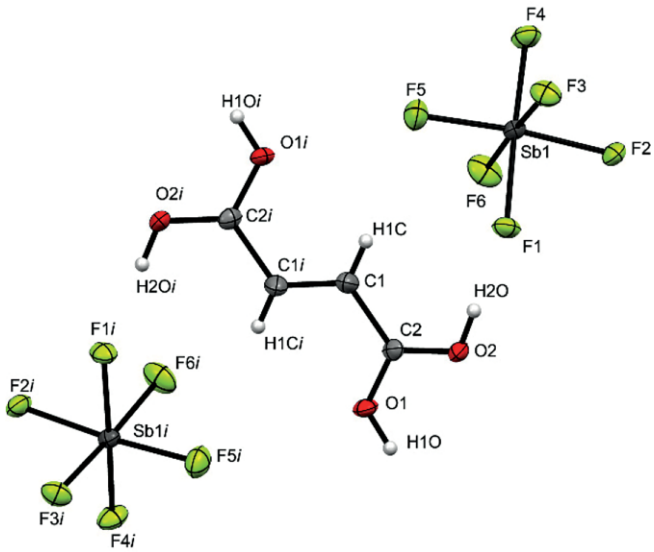

Figure 2. Formula unit of $[C_4H_6O_4]^{2+}([SbF_6]^-)_2$ (displacement ellipsoids with 50 % probability). Symmetry operations: i = 1 –*x*, y, 0.5–z.

the diprotonation. Only the carboxy groups are twisted against one another by 17 ° out of the carbon skeleton plane.

The Sb–F bond lengths in the $[SbF_6]^-$ anion are in the range between 1.913(2) Å and 1.861(2) Å. These values are typical for an $[SbF_6]^-$ anion, indicating a distorted octahedral structure.[10,11] In the crystal packing hydrogen bonds cause an elongation of the Sb1–F1 and Sb1–F2 bonds.

In the solid state of (**1**), the cations and anions are linked by hydrogen bonds with O–H···F donor-acceptor distances in the range of 2.584(4) Å to 2.584(3) Å, which can be categorized as moderate hydrogen bonds in accordance with the classification of *Jeffrey*.[12] The moderate hydrogen bonds O1–H1O···F2*i* and O2-H2O···F1 connect the cations and anions,

Table 2. Selected bond lengths and angles of $C_4H_4O_4$, $[C_4H_6O_4]^{2+}([SbF_6]^-)_2$, and $[C_4H_5O_4]^+[SbF_6]^-$.

	$C_4H_4O_4$ [8]	$[C_4H_6O_4]^{2+}([SbF_6]^-)_2$	$[C_4H_5O_4]^+[SbF_6]^-$
Bond length (Å)			
C1–C1*i* (C=C)	1.315(7)	1.299(9)	1.311(8)
C1–C2 (C–C)	1.490(5)	1.463(6)	1.479(5)
C2–O2 (C=O)	1.228(4)	1.261(5)	1.235(5)
C2–O1 (C–O)	1.289(5)	1.273(5)	1.298(5)
Bond angle [°]			
O1–C2–O2	124.4(7)	120.0(4)	121.3(4)
O1–C2–C1	116.0(6)	117.4(4)	115.3(3)
O2–C2–C1	119.5(6)	122.7(3)	123.5(4)
C1*i*–C1–C2	122.5(8)	121.8(5)	121.7(5)
Angle of torsion [°]			
O1–C2–C1–C1*i*		16.9(6)	7.1(8)
O2–C2–C1–C1*i*		–162.3(4)	–172.8(6)
C2–C1–C1*i*–C2*i*		178.2(4)	180.0
Donor–acceptor distance [Å]			
O1–H1O···F2*i*		2.584(4)	
O2–H2O···F1		2.584(3)	
O2–H3···O2*iii*			2.425(6)
O1-H2···F2			2.628(4)

forming chains along the *c* axis (Figure S2, Supporting Information).

Vibrational spectra of $[C_4H_5O_4]^+[MF_6]^-$ (M = As, Sb)

The low-temperature vibrational spectra of $[C_4H_6O_4]^{2+}([SbF_6]^-)_2$ (**1**), $[C_4H_5O_4]^+[SbF_6]^-$ (**3**), $[C_4H_5O_4]^+[AsF_6]^-$ (**4**) and fumaric acid are shown in Figure 1. Selected experimental vibrational frequencies of (**3**) and (**4**) and the calculated frequencies of the cation $[C_4H_6O_4 \cdot 2\ H_2CO \cdot 2\ HF]^{2+}$ are summarized in Table 3. The complete table (Table S4) as well as a table of the vibrational frequencies of fumaric acid (Table S2) are summarized in the Supporting Information. According to the quantum chemical calculations, C_1 symmetry is predicted for the cation $[C_4H_5O_4]^+$ with 33 fundamental vibrations. In the solid state the cations are connected via hydrogen bonds leading to the formation of chains, which is discussed later, but it should be noted that this leads to a higher symmetry (C_2) of the cation. The assignment of the vibrational frequencies is based on the analysis of the Cartesian displacement vectors of the calculated vibrational modes of $[C_4H_6O_4 \cdot 2H_2CO \cdot 2HF]^{2+}$ (see the theoretical section below) and on the comparison with the spectra of fumaric acid.[6,7]

The C–H stretching modes of the monoprotonated species observed in the Raman (3070 cm^{-1} for (**3**), 3072 cm^{-1} for (**4**)) and in the IR spectra (3078 cm^{-1} for (**3**), 3082 cm^{-1} for (**4**)), are comparable with those of fumaric acid and are not affected by the protonation. The C=C stretching vibrations of the monoprotonated fumaric acid are observed in the Raman spectra (1704 cm^{-1} for (**3**), 1703 cm^{-1} for (**4**)). These ν(C=C) vibrations are shifted to higher wavenumbers in comparison with those of the diprotonated species and of the starting material. The C=O stretching mode is detected in the Raman spectra at 1609 cm^{-1} for (**3**) and 1611 cm^{-1} for (**4**), respectively. It is red-shifted compared to fumaric acid (1685 cm^{-1}) and the diprotonated species (1637 cm^{-1} for (**1**)). Similarly, the C–O stretching mode displays a large red-shift. Both red-shifts are attributed to the formation of O–H···O bonds. The C–C stretching mode occurs in the Raman spectra (982 cm^{-1} for (**3**), (**4**)) at nearly the same position as for the diprotonated species (989 cm^{-1} (**1**)).

For the anions $[SbF_6]^-$ and $[AsF_6]^-$ more vibrations are observed (see Supporting Information) than expected for an ideal octahedral symmetry, leading to the assumption of distorted octahedral structures. This is confirmed by the results of the single-crystal X-ray structural analysis.

Crystal Structure of $[C_4H_5O_4]^+[SbF_6]^-$

$[C_4H_5O_4]^+[SbF_6]^-$ (**3**) crystallizes in the triclinic space group $P\bar{1}$ with one formula unit per unit cell. Selected structural parameters of (**3**) are given in Table 2. The formula unit of (**3**) is depicted in Figure 3.

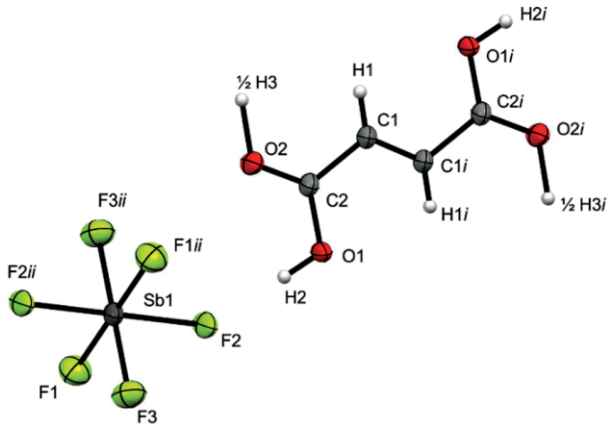

Figure 3. Formula unit of $[C_4H_5O_4]^+[SbF_6]^-$ (displacement ellipsoids with 50 % probability). Symmetry operations: i = –*x*, 2 –*y*, 2 –*z*; ii = 1 –*x*, 1 –*y*, 1 –*z*.

Surprisingly, the carbon-oxygen skeleton of the monoprotonated fumaric acid does not possess significant differences

Table 3. Selected experimental vibrational frequencies [cm^{-1}] of $[C_4H_5O_4]^+[MF_6]^-$ (M = As, Sb) and calculated vibrational frequencies [cm^{-1}] of $[C_4H_6O_4 \cdot 2\ H_2CO \cdot 2\ HF]^{2+}$.

$[C_4H_5O_4]^+[SbF_6]^-$ (**3**) exp.[a]		$[C_4H_5O_4]^+[AsF_6]^-$ (**4**) exp.[a]		$[C_4H_6O_4 \cdot 2H_2CO \cdot 2HF]^{2+}$ calcd.[b) c)]	Assignment		
IR	Raman	IR	Raman	IR/Raman			
3078 w		3082 s		3050(33/0)	ν_{21}	B	ν_{as}(C–H)
	3070(21)		3072(18)	3049(0/80)	ν_2	A	ν_s(C–H)
	1704(82)		1703(94)	1687(0/253)	ν_4	A	ν(C=C)
	1609(14)		1611(14)	1595(0/89)	ν_5	A	ν_s(C=O)
	1494(27)		1495(14)	1491(1/45)	ν_6	A	ν_s(C=O)
	1299(13)		1296(14)	1290(0/25)	ν_8	A	δ(CCH)
1277 m		1275 s		1247(122/0)	ν_{26}	B	δ(CCH)
	1317(24)		1318(37)	1372(1/23)	ν_7	A	δ(COH)
1323 m		1319 m		1365(2776/0)	ν_{25}	B	δ(COH)
	1265(48)		1251(20)	1228(0/47)	ν_9	A	δ(COH)
1225 m		1230 s		1225(779/0)	ν_{27}	B	δ(COH)
1013 s		1007 s		956(40/0)	ν_{11}	A	γ(CCH)
	982(13)		982(12)	946(0/11)	ν_{12}	A	ν(C–C)
905 m		903 s		895(257/0)	ν_{30}	B	ν(C–C)
818 s		822 s		847(222/0)	ν_{13}	A	γ(COH)

a) Abbrevations for IR intensities: vs. = very strong, s = strong, m = medium, w = weak. b) Calculated on the ωB97XD/aug-cc-pVTZ level of theory; scaling factor 0.945. c) IR intensities in km · mol^{-1}; Raman intensities in $Å^4 \cdot u^{-1}$.

to that of fumaric acid (except for the O2–C2–C1 angle). The reasons for this similarity are hydrogen bonds. In the crystal packing of (**3**) the cations are connected via strong hydrogen bonds[12] O–H···O forming chains (Figure 4). The strong hydrogen bond O2–H3···O2*iii* (2.425(6) Å) is formed by two oxygen atoms sharing one proton. Formally only half of a proton is connected to the O2 oxygen atom. Therefore, the formally monoprotonated fumaric acid is better described as a double hemi-protonated fumaric acid. A hemi-protonation has a smaller influence on the C=O bond than a monoprotonation of a carboxy group would have. It should be noted that the crystal packing of fumaric acid itself contains also hydrogen bonds. These hydrogen bonds affect the C=O and C–OH bonds of fumaric acid. Consequently, this leads to the similarity of the carbon-oxygen skeleton of both species.

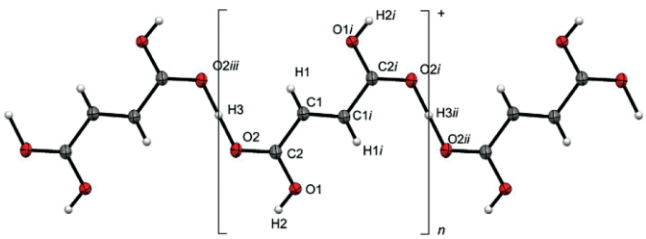

Figure 4. Cation chains in $[C_4H_5O_4]^+[SbF_6]^-$ based on the double hemi-protonation (displacement ellipsoids with 50 % probability). Symmetry operations: i = –*x*, 2 –*y*, 2 –*z*; ii = x, 1+y, z; iii = –*x*, 1 –*y*, 2 –*z*.

In the $[SbF_6]^-$ anion the Sb–F bond lengths are in the range between 1.857(3) Å and 1.895(2) Å, which are in the typical region for $[SbF_6]^-$ anions. Two hydrogen bonds in the crystal packing lead to the Sb1–F2 and Sb1–F2*ii* bond elongation and distortion of the ideal octahedral symmetry.[10,11]

In the solid state, the $[C_4H_5O_4]^+$ chains are linked by the moderate hydrogen bond,[12] O1–H2···F2 (2.628(4) Å) forming layers (Figure S3, Supporting Information).

Quantum Chemical Calculations

The quantum chemical calculations of the free cations $[C_4H_6O_4]^{2+}$ and $[C_4H_5O_4]^+$ were carried out using the B3LYP/ aug-cc-pVTZ level of theory. Since hydrogen bonds are involved in the solid state, further calculations were performed. To simulate hydrogen bonds in (**1**) HF molecules were added to the free cation.[16] To simulate the structure of (**3**), one fumaric acid molecule is supplemented by two hydrogen fluoride molecules and two protonated formaldehyde molecules (Figure S4, Supporting Information). The adducts $[C_4H_6O_4 \cdot 4\ HF]^{2+}$ and $[C_4H_6O_4 \cdot 2\ H_2CO \cdot 2\ HF]^{2+}$ were calculated by applying the ωB97XD/ aug-cc-pVTZ level of theory.[17–19] A comparison of the calculated and the experimental cationic structures of $[C_4H_6O_4]^{2+}$ and $[C_4H_5O_4]^+$ is shown in Figure 5. For clarification, the added hydrogen fluoride molecules as well as the formaldehyde molecules are omitted in the case of the calculated structures.

The structural parameters of the adducts are in good agreement with the experimental values (Tables S5 and S6, Supporting Information) and the experimental vibrational frequencies are better represented by the solvated cations (Table S7, Supporting Information).

The C–C and C–O bond lengths of some selected protonated and deprotonated salts containing fumaric acid are summarized in Table 4. Surprisingly, independent of the fumaric acid's charge, no significant difference in the C=C doule bonds is observable. Only the C–C bond length of the dianion is slightly longer than that of the dication. Apart from that, no significant

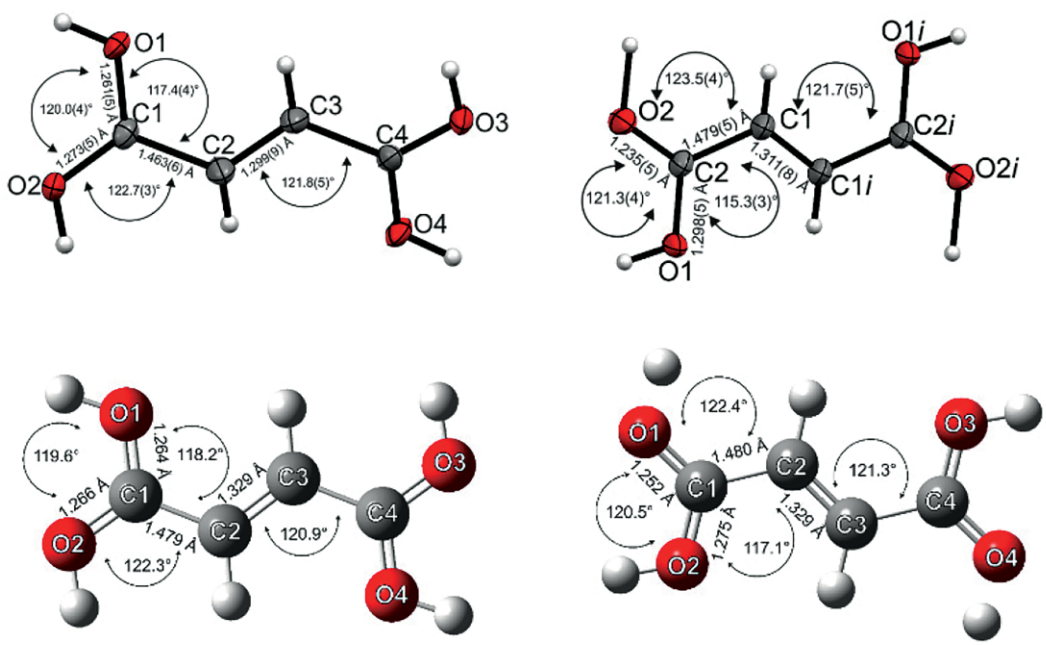

Figure 5. Experimental and calculated cationic structures of $[C_4H_6O_4]^{2+}$ (left) and $[C_4H_5O_4]^+$ (right). The HF molecules as well as the formaldehyde molecules are omitted in the calculated stuctures for clarification.

Table 4. Selected bond lengths of different protonated and deprotonated fumaric acid derivatives.

Chrage of the fumarate backbone	Compound	C=C distance [Å]	C–C distance [Å]	C=O distance [Å]	C–O distance [Å]
–2	$(NH_4)_2C_4H_2O_4$ [14]	1.314(1)	1.496(1)	1.253(1)	1.266(1)
–1	$NaC_4H_3O_4$ [15]	1.327(9)	1.488(8)	1.274(10)	1.287(9)
			1.489(9)	1.227(11)	1.332(8)
0	$C_4H_4O_4$ [8]	1.315(7)	1.490(5)	1.228(4)	1.289(5)
+1	$C_4H_5F_6O_4Sb$	1.311(8)	1.479(5)	1.235(5)	1.298(5)
+2	$C_4H_6F_{12}O_4Sb_2$	1.299(9)	1.463(6)	1.261(5)	1.273(5)

change of the C–C bond lengths is observed. Hydrogen bonds have greater influence on the C–O bonds than the level of protonation or deprotonation. Therefore, varying C–O bond lengths are detected. The carbon-oxygen skeleton of the fumaric acid derivatives remains unchanged regardless of protonation or deprotonation.

Conclusion

Fumaric acid was investigated in the superacidic solutions HF/SbF_5 and HF/AsF_5. The salts of the diprotonated fumaric acid $[C_4H_6O_4]^{2+}([MF_6]^-)_2$ (M = As, Sb) and the monoprotonated fumaric acid $[C_4H_5O_4]^+[MF_6]^-$ (M = As, Sb) were isolated for the first time. The salts were characterized by IR and Raman spectroscopy. Furthermore, single-crystal X-ray structural analyses of $[C_4H_6O_4]^{2+}([SbF_6]^-)_2$ and $[C_4H_5O_4]^+[SbF_6]^-$ are reported. Quantum chemical calculations at the B3LYP/aug-cc-pVTZ and ωB97XD/aug-cc-pVTZ level of theory were considered for the assignment of the vibrational spectra. The C-O and C–C bond lengths do not differ significantly from dianion to dication of fumaric acid. The carbon-oxygen skeleton remains unchanged regardless of protonation or deprotonation.

Experimental Section

Caution! Any contact with the components must be avoided. The hydrolysis of AsF_5, SbF_5, and the reported salts might release HF, burning skin and causing irreparable damage. Adequate safety precautions must be undertaken when handling these materials.

Apparatus and Materials: All experiments were conducted on an electropolished stainless-steel vacuum line. For the syntheses, transparent FEP-reactors with PFA-adapters were employed. To dry the stainless-steel vacuum line and the reaction vessels fluorine was used. Excess fluorine was removed in dynamic vacuum and absorbed by Sodalime. Antimony pentafluoride was handled in a Duran glass high vacuum line using Young valves. Low-temperature Raman spectroscopic measurements were executed on a Bruker® MultiRAMII FT-Raman spectrometer equipped with a Nd:YAG laser (λ = 1064 nm). The interpretation of the spectra was carried out with the aid of the software Advanced Chemistry Development, Inc.® (ACD/Labs 2015). Low-temperature IR spectra were recorded on a Bruker® Vertex-80V-FT-IR spectrometer. The spectra were evaluated using the same software as for the Raman spectra. The low-temperature single-crystal X-ray diffraction was performed on an Oxford XCalibur3 diffractometer equipped with a Spellman generator (50 kV, 40 mA) and a Kappa CCD-detector, operating with $Mo_{K\alpha}$ radiation (λ = 0.7107 Å) at 120 K. Data collection was performed using the CrysAlisCCD software[20] and for the reduction of the data set CrysAlisRED[21] was utilized. For the solution and refinement of the structure the programs SHELXS-97[22] and SHELXL-97[23] integrated in the WinGX software package[24] were employed. The structures were checked with the help of the software PLATON.[25] The absorption correction was carried out using the SCALE3 ABSPACK multiscan method.[26] Crystal data and structure refinement for the reported single-crystal structures are given in Table S8 (Supporting Information). Quantum chemical calculations were carried out using the software package Gaussian09.[27] The theoretical calculations of the naked cations were performed at the B3LYP/aug-cc-pVTZ level of theory. Considering the hydrogen bonds in the solid state, the theoretical calculations of the solvated cations were carried out on the ωB97XD/aug-cc-pVTZ level of theory.

Syntheses of $[C_4H_2X_4O_4]^{2+}([MF_6]^-)_2$ (X = H, D; M = As, Sb): Initially, the Lewis acid AsF_5 or SbF_5 (1.5 mmol) was condensed in a FEP reactor vessel at –196 °C together with anhydrous hydrogen fluoride (*a*HF) or deuterium fluoride (*a*DF) (2 mL). To form the superacidic system, both components were warmed up in static vacuum to –20 °C and homogenized. At –196 °C the superacidic mixture was refrozen. Afterwards, fumaric acid (0.5 mmol) was added to the frozen mixture under nitrogen atmosphere. The reaction mixture was warmed in static vacuum up to –20 °C at which the reaction occurs. In dynamic vacuum excess solvent was removed within 14 h at –78 °C. Colorless crystalline solids were formed in all of these experiments.

Syntheses of $[C_4H_2X_3O_4]^+[MF_6]^-$ (X = H, D; M = As, Sb): The Lewis acid AsF_5 or SbF_5 (1.0 mmol) was condensed in a FEP reactor vessel followed by *a*HF or *a*DF (2 mL) at –196 °C. The mixture was warmed up to –20 °C and mixed to ensure the formation of the superacid. Accordingly, the mixture was refrozen at –196 °C. $C_4H_4O_4$ (1.0 mmol) was added to the frozen mixture under inert gas atmosphere. The reaction mixture was then warmed up to –20 °C and mixed until a colorless solution was received. Excess solvent was removed at –78 °C in dynamic vacuum. Colorless crystalline solids were obtained in all of the experiments.

Supporting Information (see footnote on the first page of this article): The supporting information contains the low-temperature IR and Raman spectra of $[C_4H_2D_4O_4]^{2+}([SbF_6]^-)_2$ (**5**), $[C_4H_2D_4O_4]^{2+}([AsF_6]^-)_2$ (**6**) and deuterated fumaric acid (Figure S1); Experimental vibrational frequencies [cm^{-1}] of $[C_4H_6O_4]^{2+}([MF_6]^-)_2$ (M = As, Sb) and calculated vibrational frequencies [cm^{-1}] of $[C_4H_6O_4 \cdot 4\ HF]^{2+}$ (Table S1); Experimental vibrational frequencies [cm^{-1}] of fumaric acid in comparison with literature data[6,7] (Table S2); Experimental vibrational frequencies [cm^{-1}] of $[C_4H_2D_4O_4]^{2+}([MF_6]^-)_2$ (M = As, Sb) and calculated vibrational frequencies [cm^{-1}] of $[C_4H_2D_4O_4 \cdot 4\ HF]^{2+}$ (Table S3); Detail of the crystal structure of $[C_4H_6O_4]^{2+}([SbF_6]^-)_2$. (Displacement ellipsoids with 50% probability) (Figure S2); Experimental vibrational frequencies [cm^{-1}] of $[C_4H_5O_4]^+[MF_6]^-$ (M = As, Sb) and calculated vibrational frequencies [cm^{-1}] of $[C_4H_6O_4 \cdot 2\ H_2CO \cdot 2\ HF]^{2+}$ (Table S4); Layers formed by hygrogen bonds in $[C_4H_5O_4]^+[SbF_6]^-$. (Displacement ellipsoids with 50% prob-

ability) (Figure S3); Quantum chemical calculated structure of simulated double hemi-protonated fumaric acid under consideration of hydrogen bonds in the solid state $[C_4H_6O_4 \cdot 2\ H_2CO \cdot 2\ HF]^{2+}$ (Figure S4); Selected experimental obtained and calculated bond lengths and angles of the $[C_4H_6O_4]^{2+}$ cation. Symmetry operations: i = C_2-Rotation (Table S5); Selected experimentally obtained and calculated bond lengths and bond angles of the naked and the solvated cation $[C_4H_5O_4]^+$. Symmetry operations: i = C_2-Rotation (Table S6); Selected experimental vibrational frequencies [cm^{-1}] of $[C_4H_5O_4]^+[MF_6]^-$ (M = As, Sb) and calculated vibrational frequencies [cm^{-1}] of $[C_4H_5O_4]^+$ and $[C_4H_6O_4 \cdot 2\ H_2CO \cdot 2\ HF]^{2+}$ (Table S7); and crystal data and structure refinement of $[C_4H_6O_4]^{2+}([SbF_6]^-)_2$ and $[C_4H_5O_4]^+[SbF_6]^-$ (Table S8).

Acknowledgements

We gratefully acknowledge the financial support of the Deutsche Forschungsgemeinschaft (DFG), the Ludwig-Maximilians-Universität (LMU), and the F-Select GmbH.

Keywords: Fumaric acid; Quantum chemical calculations; Superacidic systems, Vibrational spectroscopy; X-ray structure analyses

References

[1] W. Karrer, *Konstitution und Vorkommen der organischen Pflanzenstoffe*. *Exclusive Alkaloide*, Birkhäuser Basel, Basel, s. l., **1958**.
[2] H.-D. Belitz, W. Grosch, P. Schieberle, *Lehrbuch der Lebensmittelchemie*. *Mit 634 Tabellen*, Springer, Berlin, Heidelberg, **2008**.
[3] David R. Lide, CRC Handbook of Chemistry and Physics, Internet version, CRC Press, Boca Raton, FL, **2005**.
[4] J. W. Larsen, P. A. Bouis, *J. Org. Chem.* **1973**, *38*, 1415.
[5] A. M. Amat, G. Asensio, M. J. Castello, M. A. Miranda, A. Simon-Fuentes, *Tetrahedron* **1987**, *43*, 905.
[6] https://sdbs·db.aist.go.jp (National Institute of Advanced Industrial Science and Technology, 21.05.2019).
[7] Y. Du, H. X. Fang, Q. Zhang, H. L. Zhang, Z. Hong, *Spectrochim. Acta Part A Mol. Biomolecular. Spectrosc.* **2016**, *153*, 580.
[8] A. L. Bednowitz, B. Post, *Acta Crystallogr.* **1966**, *21*, 566.
[9] E. Wiberg, N. Wiberg, A. F. Holleman, *Anorganische Chemie*, 103. Aufl., De Gruyter, Berlin, Boston, **2017**.
[10] R. Minkwitz, C. Hirsch, T. Berends, *Eur. J. Inorg. Chem.* **1999**, *1999*, 2249.
[11] R. Minkwitz, S. Schneider, *Angew. Chem.***1999**, *111*, 229.
[12] G. A. Jeffrey, *An Introduction to Hydrogen Bonding*, *Topics in Physical Chemistry*, Oxford University Press, New York, **1997**.
[13] M. P. Gupta, B. N. Sahu, *Acta Crystallogr., Sect. B Struct. Crystallogr. Cryst. Chem.* **1970**, *26*, 1969.
[14] H. Hosomi, Y. Ito, S. Ohba, *Acta Crystallogr., Sect. C Cryst. Struct. Commun.* **1998**, *54*, 142.
[15] M. P. Gupta, R. G. Sahu, *Acta Crystallogr., Sect. B Struct. Crystallogr. Cryst. Chem.* **1970**, *26*, 1964.
[16] T. Soltner, N. R. Goetz, A. Kornath, *Eur. J. Inorg. Chem.* **2011**, *2011*, 3076.
[17] K. S. Thanthiriwatte, E. G. Hohenstein, L. A. Burns, C. D. Sherrill, *J. Chem. Theory Computation* **2011**, *7*, 88.
[18] M. D. Struble, C. Kelly, M. A. Siegler, T. Lectka, *Angew. Chem. Int. Ed.* **2014**, *53*, 8924.
[19] L. A. Burns, A. Vázquez-Mayagoitia, B. G. Sumpter, C. D. Sherrill, *J. Chem. Phys.* **2011**, *134*, 84107.
[20] CrysAlisCCD, Version 1.171.35.11 (release 16–05–2011 CrysAlis 171.NET), Oxford Diffraction Ltd, UK, **2011**.
[21] CrysAlisRED, Version 1.171.35.11 (release 16–05–2011 CrysAlis 171.NET), Oxford Diffraction Ltd, UK, **2011**.
[22] G. M. Sheldrick, *SHELXS-97*, Program for Crystal Structure Solution, University of Göttingen, Germany, **1997**.
[23] G. M. Sheldrick, *SHELXL-97*, Program for Crystal Structure Solution, University of Göttingen, Germany, **1997**.
[24] L. J. Farrugia, *J. Appl. Crystallogr.* **1999**, *32*, 837.
[25] A. L. Speck, *PLATON*, A Multipurpose Crystallographic Tool, Utrecht University, Utrecht, Netherlands, **1999**.
[26] SCALE3 ABSPACK, An Oxford Diffraction Program, Oxford Diffraction Ltd, UK, **2005**.
[27] M. J. Frisch, G. W. Trucks, H. B. Schlegel, G. E. Scuseria, M. A. Robb, J. R. Cheeseman, G. Scalmani, V. Barone, B. Mennucci, G. A. Petersson, H. Nakatsuji, M. Caricato, X. Li, H. P. Hratchian, A. F. Izmaylov, J. Bloino, G. Zheng, J. L. Sonnenberg, M. Hada, M. Ehara, K. Toyota, R. Fukuda, J. Hasegawa, M. Ishida, T. Nakajima, Y. Honda, O. Kitao, H. Nakai, T. Vreven, J. A. Montgomery, J. E. Peralta, F. Ogliaro, M. Bearpark, J. J. Heyd, E. Brothers, K. N. Kudin, V. N. Staroverov, R. Kobayashi, J. Normand, K. Raghavachari, A. Rendell, J. C. Burant, S. S. Iyengar, J. Tomasi, M. Cossi, N. Rega, J. M. Millam, M. Klene, J. E. Knox, J. B. Cross, V. Bakken, C. Adamo, J. Jaramillo, R. Gomperts, R. E. Stratmann, O. Yazyev, A. J. Austin, R. Cammi, C. Pomelli, J. W. Ochterski, R. L. Martin, K. Morokuma, V. G. Zakrzewski, G. A. Voth, P. Salvador, J. J. Dannenberg, S. Dapprich, A. D. Daniels, O. Farkas, J. B. Foresman, J. V. Ortiz, J. Cioslowski, D. J. Fox, *Gaussian09, Revision A.02*, Gaussian, Inc, Wallingford CT, **2009**.

Received: February 24, 2020

Z. Anorg. Allg. Chem. **2020** · ISSN 0044–2313

SUPPORTING INFORMATION

Title: Preparation and Characterization of Protonated Fumaric Acid
Author(s): M. C. Bayer, C. Jessen, A. J. Kornath*
Ref. No.: z202000091

Supporting Information

Figure S1: Low-temperature IR and Raman spectra of $[C_4H_2D_4O_4]^{2+}([SbF_6]^-)_2$ **(5)**, $[C_4H_2D_4O_4]^{2+}([AsF_6]^-)_2$ **(6)** and deuterated fumaric acid.

Table S1: Experimental vibrational frequencies [cm^{-1}] of $[C_4H_6O_4]^{2+}([MF_6]^-)_2$ (M = As, Sb) and calculated vibrational frequencies [cm^{-1}] of $[C_4H_6O_4 \cdot 4\ HF]^{2+}$.

Table S2: Experimental vibrational frequencies [cm^{-1}] of fumaric acid in comparison with literature data[6,7].

Table S3: Experimental vibrational frequencies [cm^{-1}] of $[C_4H_2D_4O_4]^{2+}([MF_6]^-)_2$ (M = As, Sb) and calculated vibrational frequencies [cm^{-1}] of $[C_4H_2D_4O_4 \cdot 4\ HF]^{2+}$.

Figure S2: Detail of the crystal structure of $[C_4H_6O_4]^{2+}([SbF_6]^-)_2$. (Displacement ellipsoids with 50% probability).

Table S4: Experimental vibrational frequencies [cm^{-1}] of $[C_4H_5O_4]^+[MF_6]^-$ (M = As, Sb) and calculated vibrational frequencies [cm^{-1}] of $[C_4H_6O_4 \cdot 2\ H_2CO \cdot 2\ HF]^{2+}$.

Figure S3: Layers formed by hygrogen bonds in $[C_4H_5O_4]^+[SbF_6]^-$. (Displacement ellipsoids with 50% probability).

Figure S4: Quantum chemical calculated structure of simulated double hemi-protonated fumaric acid under consideration of hydrogen bonds in the solid state $[C_4H_6O_4 \cdot 2\ H_2CO \cdot 2\ HF]^{2+}$.

Table S5: Selected experimental obtained and calculated bond lengths and angles of the $[C_4H_6O_4]^{2+}$ cation. Symmetry operations: i = C_2-Rotation.

Table S6: Selected experimentally obtained and calculated bond distances and bond angles of the naked and the solvated cation $[C_4H_5O_4]^+$. Symmetry operations: i = C_2-Rotation.

Table S7: Selected experimental vibrational frequencies [cm^{-1}] of $[C_4H_5O_4]^+[MF_6]^-$ (M = As, Sb) and calculated vibrational frequencies [cm^{-1}] of $[C_4H_5O_4]^+$ and $[C_4H_6O_4 \cdot 2\ H_2CO \cdot 2\ HF]^{2+}$.

Table S8: Crystal data and structure refinement of $[C_4H_6O_4]^{2+}([SbF_6]^-)_2$ and $[C_4H_5O_4]^+[SbF_6]^-$.

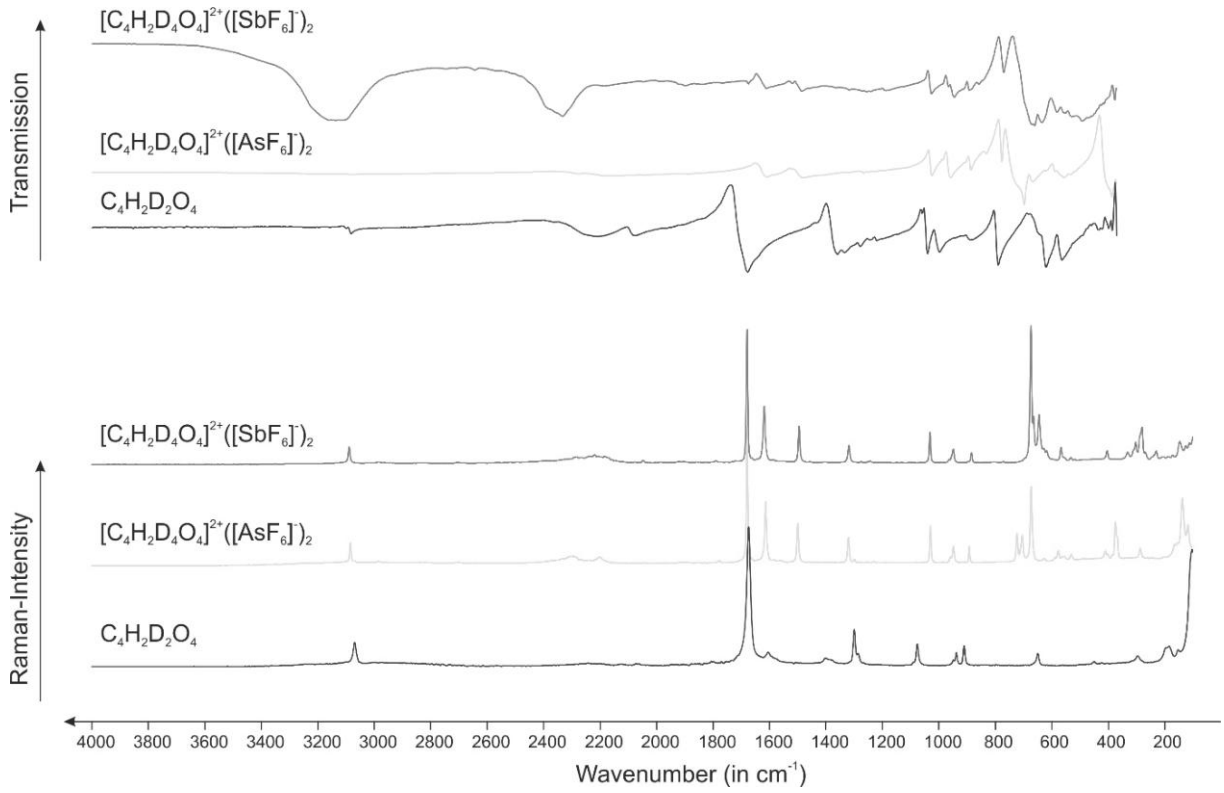

Figure S1: Low-temperature IR and Raman spectra of $[C_4H_2D_4O_4]^{2+}([SbF_6]^-)_2$ (5), $[C_4H_2D_4O_4]^{2+}([AsF_6]^-)_2$ (6) and deuterated fumaric acid.

Table S1: Experimental vibrational frequencies [cm^{-1}] of $[C_4H_6O_4]^{2+}([MF_6]^-)_2$ (M = As, Sb) and calculated vibrational frequencies [cm^{-1}] of $[C_4H_6O_4 \cdot 4\ HF]^{2+}$.

$[C_4H_6O_4]^{2+}([SbF_6]^-)_2$ **(1)** exp.[a]		$[C_4H_6O_4]^{2+}([AsF_6]^-)_2$ **(2)** exp.[a]		$[C_4H_6O_4 \cdot 4\ HF]^{2+}$ calc.[b,c]	Assignment		
IR	Raman	IR	Raman	IR/Raman			
				3123(0/236)	ν_1	A	ν_s(O-H)
				3115(2958/0)	ν_{20}	B	ν_{as}(O-H)
3157 vs							[d]
3099 vs				3041(14/0)	ν_{21}	B	ν_{as}(C-H)
	3092(31)		3087(24)	3040(0/68)	ν_2	A	ν_s(C-H)
				2989(0/273)	ν_3	A	ν_s(O-H)
				2976(4577/0)	ν_{22}	B	ν_{as}(O-H)
	1686(89)		1684(100)	1672(0/185)	ν_4	A	ν(C=C)
1682 m							[d]
1610 m		1612 s		1617(620/0)	ν_{23}	B	ν(C-O)
	1637(37)		1643(32)	1605(0/126)	ν_5	A	ν(C-O)
	1552(6)						[d]
	1528(13)		1531(12)	1489(0/26)	ν_6	A	ν(C-O)
1518 s		1502 s		1488(932/0)	ν_{24}	B	ν(C-O)
	1508(6)						[d]
		1423 s					[d]
	1325(11)		1326(19)	1293(0/13)	ν_7	A	δ(CCH)
1321 m							[d]
			1299(6)				[d]
	1281(7)		1272(7)	1264(0/5)	ν_8	A	δ(COH)
1279 s		1279 s		1264(229/0)	ν_{25}	B	δ(CCH)
1252 m		1250 s		1237(287/0)	ν_{26}	B	δ(COH)
	1233(82)		1223(67)	1220(0/48)	ν_9	A	δ(COH)
1229 s		1217 s		1216(232/0)	ν_{27}	B	δ(COH)
949 s		962 s		950(67/0)	ν_{10}	A	γ(CCH)
	989(24)		985(31)	950(0/8)	ν_{11}	A	ν(C-C)
941 s	952(8)	937 s	956(2)	901(51/0)	ν_{28}	B	ν(C-C)
	886(22)		893(24)	893(0/5)	ν_{29}	B	γ(CCCH)
				888(3/1)	ν_{30}	B	γ(COH)
868 m				888(107/0)	ν_{12}	A	γ(COH)
802 s		797 s		822(256/0)	ν_{13}	A	γ(COH)
				822(0/0)	ν_{31}	B	γ(COH)
	757(6)	752 m		748(12/0)	ν_{14}	A	γ(CCOO)
				681(0/8)	ν_{15}	A	δ(COO)
		650 s					[d]
613 vs	614(7)	611 s		613(7/0)	ν_{32}	B	δ(COO)
	568(25)	581 s	576(26)	587(0/0)	ν_{33}	B	γ(CCOO)
	530(13)	538 s	532(15)	554(5/0)	ν_{34}	B	δ(CCC)
415 vs	423(24)		419(20)				[d]
		380 vs					[d]
		357 vs		359(0/0)	ν_{16}	A	δ(CCO)
				316(0/2)	ν_{17}	A	δ(CCC)
	206(11)						[d]
	190(10)						[d]
	183(10)						[d]
	174(13)						[d]
	153(35)						[d]
			140(83)				[d]
	128(28)						[d]
	115(26)						[d]
			119(54)				[d]
				90(0/0)	ν_{35}	B	Frameworkvib.
				84(13/0)	ν_{18}	A	Frameworkvib.
				44(0/1)	ν_{36}	B	Frameworkvib.
				13(0/0)	ν_{19}	A	τ(C(OH)$_2$)
Vibrations of anions MF_6^- (M = As, Sb)							
			722(36)				$[AsF_6]^-$
Table is continued on the following page							
			710(16)				$[AsF_6]^-$

		696 vs	699(59)	$[AsF_6]^-$
675 vs	677(77)		686(34)	$[AsF_6]^-$; $[SbF_6]^-$
658 vs	660(98)		668(66)	$[AsF_6]^-$; $[SbF_6]^-$
621 vs	637(100)		599(4)	$[AsF_6]^-$; $[SbF_6]^-$
569 vs		567 s		$[AsF_6]^-$; $[SbF_6]^-$
			405(10)	$[AsF_6]^-$
	338(16)	370 vs	374(56)	$[AsF_6]^-$; $[SbF_6]^-$
	312(19)			$[SbF_6]^-$
	283(49)		293(17)	$[AsF_6]^-$; $[SbF_6]^-$
	280(48)			$[SbF_6]^-$

[a] Abbrevations for IR intensities: vs = very strong, s = strong, m = medium, w = weak.
[b] Calculated on the ωB97XD/aug-cc-pVTZ level of theory. Scaling factor 0.945.
[c] IR intensities in km/mol; Raman intensities in $Å^4$/u.
[d] Very probably combination tones/ overtones.

Table S2: Experimental vibrational frequencies [cm^{-1}] of fumaric acid in comparison with literature data.[1,2]

$C_4H_4O_4$ exp.[a]		$C_4H_4O_4$ calc.[b,c]	$C_4H_4O_4$ lit.[1,2]		Assignment		
IR	Raman	IR/Raman	IR[1]	Raman[2]			
		3543(4/223)	3412		ν_1	A	ν_s(OH)
		3543(191/5)	3400		ν_{17}	B	ν_{as}(OH)
3078 s		3039(2/0)	3084		ν_{18}	B	ν_{as}(CH)
	3069(15)	3033(0/91)			ν_2	A	ν_s(CH)
			2876				[d]
			2694				[d]
			2583				[d]
			2638				[d]
1745 s							[d]
	1685(100)	1692(0/325)		1685	ν_3	A	ν_s(C=O)
1666 vs		1686(771/0)	1676		ν_{19}	B	ν_{as}(C=O)
	1605(5)	1597(0/81)		1605	ν_4	A	ν(C=C)
			1512				[d]
	1437(4)	1303(0/11)		1435	ν_5	A	δ(COH)
1406 vs			1431				[d]
	1315(23)			1315			[d]
1315 vs		1284(141/0)	1317		ν_{20}	B	δ(COH)
	1298(74)	1249(0/21)		1299	ν_6	A	δ(CCH)
1269 vs			1278				[d]
1225 vs			1234				[d]
1209 vs		1207(20/0)	1216		ν_{21}	B	δ(CCH)
		1135(0/35)			ν_7	A	ν_s(C-O)
1009 vs		1091(556/0)	1010		ν_{22}	B	ν_{as}(C-O)
997 vs	972(4)	978(43/0)	972	971	ν_8	A	γ(CCH)
951 vs	955(13)			954			[d]
	913(14)	891(0/5)		913	ν_{23}	B	γ(CCH)
		861(0/9)			ν_9	A	ν_s(C-C)
			919				[d]
889 vs		856(14/0)	907		ν_{24}	B	ν_{as}(C-C)
			792				[d]
777 vs		755(51/0)	784		ν_{10}	A	γ(CCOO)
717 vs							[d]
	695(13)	627(0/2)		694	ν_{25}	B	γ(CCOO)
		617(0/7)			ν_{11}	A	δ(COO)
640 vs			646				[d]
573 vs		569(81/0)	582		ν_{26}	B	δ(COO)
		551(193/0)			ν_{12}	A	γ(COH)
	449(2)	527(0/2)			ν_{27}	B	γ(COH)
440 vs		512(37/0)	456		ν_{28}	B	δ(CCO)
417 vs							[d]
	303(8)						[d]
399 s							[d]
388 s		385(0/2)			ν_{13}	A	δ(CCO)
374 vs							[d]
359 s							[d]
	199(18)	249(0/2)			ν_{14}	A	δ(CCC)
	180(11)	134(0/0)			ν_{15}	A	Frameworkvi.
	153(11)	128(4/0)			ν_{29}	B	Frameworkvi.
		123(0/1)			ν_{30}	B	Frameworkvi.
		42(4/0)			ν_{16}	A	τ($C(OH)_2$)

[a] Abbrevations for IR intensities: vs = very strong, s = strong, m = medium, w = weak.
[b] Calculated on the ωB97XD/aug-cc-pVTZ level of theory. Scaling factor 0.945.
[c] IR intensities in km/mol; Raman intensities in $Å^4/u$.
[d] Very probably combination tones/ overtones.

Table S3: Experimental vibrational frequencies [cm^{-1}] of $[C_4H_2D_4O_4]^{2+}([MF_6]^-)_2$ (M = As, Sb) and calculated vibrational frequencies [cm^{-1}] of $[C_4H_2D_4O_4 \cdot 4\ HF]^{2+}$.

$[C_4H_2D_4O_4]^{2+}([SbF_6]^-)_2$ **(5)** exp.[a]		$[C_4H_2D_4O_4]^{2+}([AsF_6]^-)_2$ **(6)** exp.[a]		$[C_4H_2D_4O_4 \cdot 4\ HF]^{2+}$ calc.[b,c]	Assignment		
IR	Raman	IR	Raman	IR/Raman			
3136 vs		3088 s		3041(37/0)	ν_{20}	B	ν_{as}(C-H)
	3089(12)		3085(17)	3040(0/77)	ν_1	A	ν_s(C-H)
	2283(5)		2295(7)	2284(0/100)	ν_2	A	ν_s(O-D)
2334 vs		2280 s		2278(1512/0)	ν_{21}	B	ν_{as}(O-D)
	2186(6)		2203(6)	2184(0/123)	ν_3	A	ν_s(O-D)
				2173(2431/0)	ν_{22}	B	ν_{as}(O-D)
	1679(97)		1679(100)	1668(0/201)	ν_4	A	ν(C=C)
1674 m							[d]
1610 m		1610 s		1603(687/0)	ν_{23}	B	ν(C-O)
	1618(41)		1613(46)	1588(0/104)	ν_5	A	ν(C-O)
1520 m		1520 s					[d]
	1495(27)		1499(30)	1453(0/61)	ν_6	A	ν(C-O)
1485 s		1481 s		1439(828/0)	ν_{24}	B	ν(C-O)
	1318(14)		1320(20)	1288(0/27)	ν_7	A	δ(CCH)
1257 s		1267 s		1242(10/0)	ν_{25}	B	δ(CCH)
1188 s							[d]
	1032(23)		1030(28)	1011(0/10)	ν_8	A	δ(COD)
1026 s		1024 s		1010(143/0)	ν_{26}	B	δ(COD)
966 m		959 s		949(52/0)	ν_9	A	$\delta(CCH)_{oop}$
	949(11)		949(14)	931(0/4)	ν_{10}	A	δ(COD)
945 s				924(191/0)	ν_{27}	B	δ(COD)
	884(9)		892(14)	910(0/10)	ν_{11}	A	ν(C-C)
				892(0/5)	ν_{28}	B	$\delta(CCH)_{oop}$
891 s		885 s		855(94/0)	ν_{29}	B	ν(C-C)
		831 m					[d]
858 m							[d]
770 m		777 m		766(46/0)	ν_{12}	A	γ(CCOO)
		698 vs					[d]
				678(0/0)	ν_{30}	B	$\delta(COD)_{oop}$
669 vs		667 s		635(18/0)	ν_{13}	A	$\delta(COD)_{oop}$
	629(12)		628(5)	632(0/7)	ν_{14}	A	δ(COO)
				596(0/0)	ν_{31}	B	$\delta(COD)_{oop}$
581 vs		588 s		596(136/0)	ν_{15}	A	$\delta(COD)_{oop}$
552 vs		557 s		574(17/0)	ν_{32}	B	δ(COO)
				560(0/0)	ν_{33}	B	γ(CCOO)
				542(6/0)	ν_{34}	B	δ(CCO)
	404(10)		401(8)				[d]
	303(16)			309(0/2)	ν_{16}	A	δ(CCC)
				89(0/0)	ν_{35}	B	δ(CCC)
				83(10/0)	ν_{17}	A	Frameworkvi.
				44(0/1)	ν_{36}	B	Frameworkvi.
				32(5/0)	ν_{18}	A	Frameworkvi.
				13(0/0)	ν_{19}	A	$\tau(C(OH)_2)$
Vibrations of anions MF_6^- (M = As, Sb)							
660 vs	674(100)	619 s	723(23)				$[AsF_6]^-$; $[SbF_6]^-$
635 vs	665(34)	536 s	705(22)				$[AsF_6]^-$; $[SbF_6]^-$
528 vs	645(36)	388 vs	674(57)				$[AsF_6]^-$; $[SbF_6]^-$
492 vs	568(12)		577(11)				$[AsF_6]^-$; $[SbF_6]^-$
471 vs	533(5)		531(8)				$[AsF_6]^-$; $[SbF_6]^-$
424 s	332(9)		411(10)				$[AsF_6]^-$; $[SbF_6]^-$
415 s	280(26)		386(8)				$[AsF_6]^-$; $[SbF_6]^-$
376 s	230(10)		375(31)				$[AsF_6]^-$; $[SbF_6]^-$
	173(7)		286(13)				$[AsF_6]^-$; $[SbF_6]^-$
	147(16)		165(16)				$[AsF_6]^-$; $[SbF_6]^-$
	125(13)		154(17)				$[AsF_6]^-$; $[SbF_6]^-$
	113(15)		138(49)				$[AsF_6]^-$; $[SbF_6]^-$
			118(29)				$[AsF_6]^-$

Table is continued on the following page.

[a] Abbrevations for IR intensities: vs = very strong, s = strong, m = medium, w = weak.

[b] Calculated on the ωB97XD/aug-cc-pVTZ level of theory. Scaling factor 0.945.
[c] IR intensities in km/mol; Raman intensities in $Å^4$/u.
[d] Very probably combination tones/ overtones.

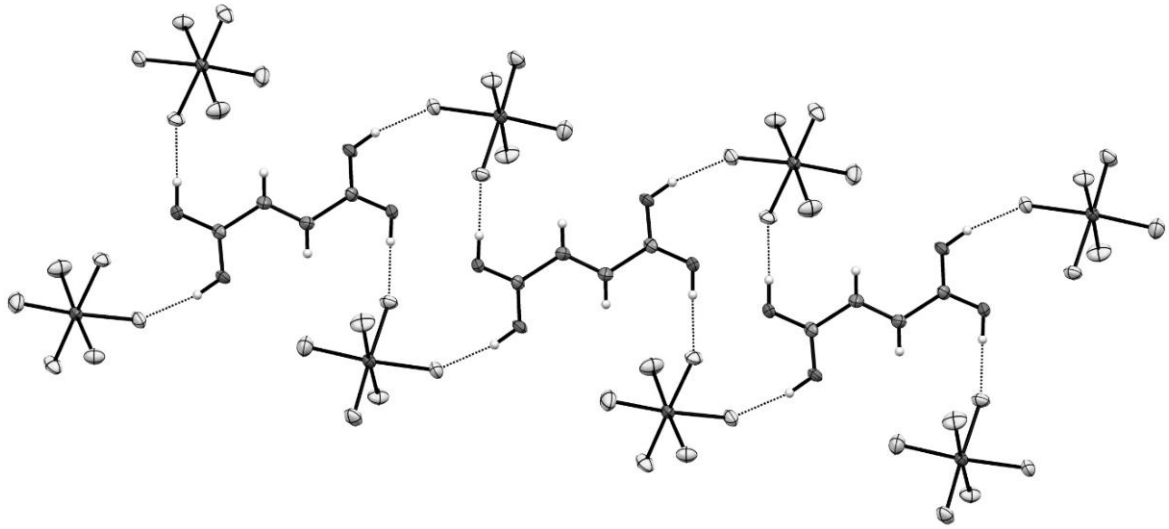

Figure S2: Detail of the crystal structure of $[C_4H_6O_4]^{2+}([SbF_6]^-)_2$. (Displacement ellipsoids with 50% probability).

Table S4: Experimental vibrational frequencies [cm^{-1}] of $[C_4H_5O_4]^+[MF_6]^-$ (M = As, Sb) and calculated vibrational frequencies [cm^{-1}] of $[C_4H_6O_4 \cdot 2\ H_2CO \cdot 2\ HF]^{2+}$.

$[C_4H_5O_4]^+[SbF_6]^-$ **(3)** exp.		$[C_4H_5O_4]^+[AsF_6]^-$ **(4)** exp.		$[C_4H_6O_4 \cdot 2\ H_2CO \cdot 2\ HF]^{2+}$ calc.	Assignment		
IR	Raman	IR	Raman	IR/Raman			
				3148(0/324)	ν_1	A	ν_s(O-H)
				3135(3410/0)	ν_{20}	B	ν_{as}(O-H)
3078 w		3082 s		3050(33/0)	ν_{21}	B	ν_{as}(C-H)
	3070(21)		3072(18)	3049(0/80)	ν_2	A	ν_s(C-H)
2488 w							[d]
				1870(14/124)	ν_3	A	ν_s(O-H)
				1862(4707/0)	ν_{22}	B	ν_{as}(O-H)
1875 w							[d]
	1704(82)		1703(94)	1687(0/253)	ν_4	A	ν(C=C)
		1670 s		1613(1840/0)	ν_{23}	B	ν_{as}(C=O)
1599 m							[d]
	1609(14)		1611(14)	1595(0/89)	ν_5	A	ν_s(C=O)
	1522(6)						[d]
	1494(27)		1495(14)	1491(1/45)	ν_6	A	ν_s(C=O)
1408 m		1421 s		1449(1994/0)	ν_{24}	B	ν_{as}(C=O)
1377 m							[d]
	1317(24)		1318(37)	1372(1/23)	ν_7	A	δ(COH)
1323 m		1319 m		1365(2776/0)	ν_{25}	B	δ(COH)
	1299(13)		1296(14)	1290(0/25)	ν_8	A	δ(CCH)
1277 m		1275 s		1247(122/0)	ν_{26}	B	δ(CCH)
	1265(48)		1251(20)	1228(0/47)	ν_9	A	δ(COH)
1225 m		1230 s		1225(779/0)	ν_{27}	B	δ(COH)
		1213 s					[d]
1124 s				1180(154/0)	ν_{10}	A	γ(COH)
				1179(3/0)	ν_{28}	B	γ(COH)
1013 s		1007 s		956(40/0)	ν_{11}	A	γ(CCH)
	982(13)		982(12)	946(0/11)	ν_{12}	A	ν(C-C)
			972(12)				[d]
970 s		966 m					[d]
	957(4)	955 m	955(5)				[d]
	914(4)		909(6)				[d]
	903(22)		898(19)	898(1/6)	ν_{29}	B	γ(CCCH)
905 m		903 s		895(257/0)	ν_{30}	B	ν(C-C)
818 s		822 s		847(222/0)	ν_{13}	A	γ(COH)
	820(4)			843(0/1)	ν_{31}	B	γ(COH)
795 vs							[d]
762 s	761(3)			754(0/0)	ν_{14}	A	γ(CCOO)
	665(9)			666(0/15)	ν_{15}	A	δ(COO)
598 vs	595(6)		596(10)	598(251/0)	ν_{32}	B	δ(COO)
				595(54/0)	ν_{33}	B	γ(CCOO)
				557(3/0)	ν_{34}	B	δ(CCO)
	486(10)		489(10)	434(0/2)	ν_{16}	A	δ(CCO)
	313(10)			308(0/2)	ν_{17}	A	δ(CCC)
	272(12)						[d]
			182(19)				[d]
	168(12)						[d]
	150(59)		146(63)	174(57/0)	ν_{18}	A	Frameworkvi.
	107(19)			104(0/5)	ν_{35}	B	Frameworkvi.
				42(0/0)	ν_{36}	B	Frameworkvi.
				7(1/0)	ν_{19}	A	τ($C(OH)_2$)
Vibrations of anions MF_6^- (M = As, Sb)							
	696(4)	696 vs	686(100)				$[AsF_6]^-$, $[SbF_6]^-$
667 vs	655(100)	646 s					$[AsF_6]^-$, $[SbF_6]^-$
569 vs	551(8)	579 s	547(9)				$[AsF_6]^-$, $[SbF_6]^-$
490 vs		521 m					$[AsF_6]^-$, $[SbF_6]^-$
403 s		482 m	379(25)				$[AsF_6]^-$, $[SbF_6]^-$
384 m		461 m	367(20)				$[AsF_6]^-$, $[SbF_6]^-$

Table is continued on the following page.

	298(22)	390 vs	293(15)				$[AsF_6]^-$, $[SbF_6]^-$

284(16)	378 s	$[AsF_6]^-$, $[SbF_6]^-$

[a] Abbrevations for IR intensities: vs = very strong, s = strong, m = medium, w = weak.
[b] Calculated on the ωB97XD/aug-cc-pVTZ level of theory. Scaling factor 0.945.
[c] IR intensities in km/mol; Raman intensities in $Å^4$/u.
[d] Very probably combination tones/ overtones.

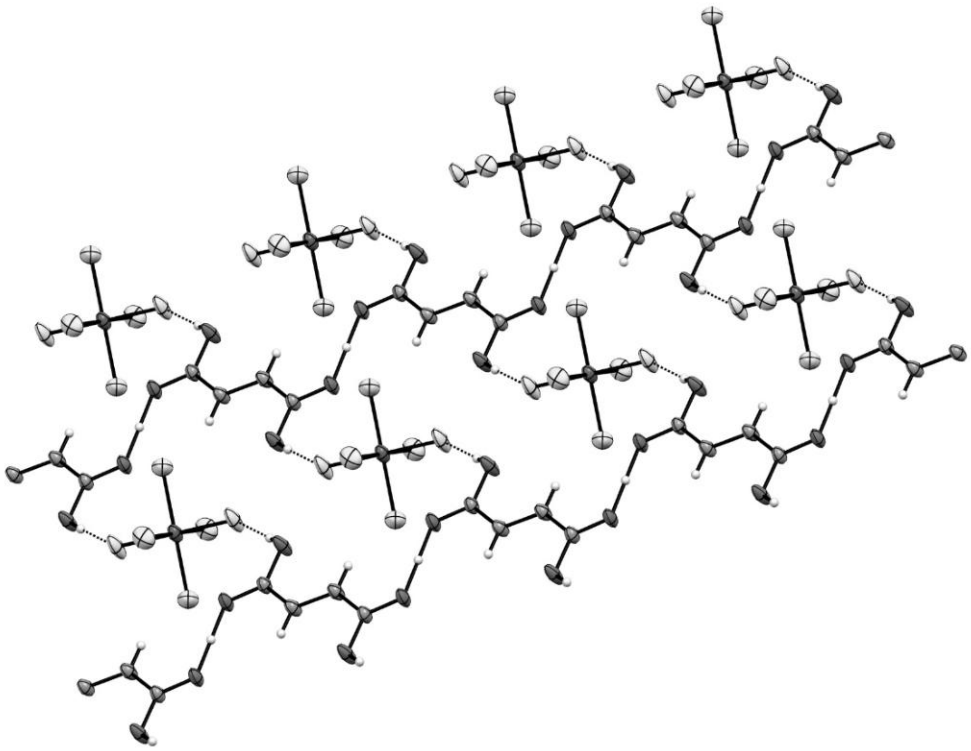

Figure S3: Layers formed by hygrogen bonds in $[C_4H_5O_4]^+[SbF_6]^-$ (displacement ellipsoids with 50% probability).

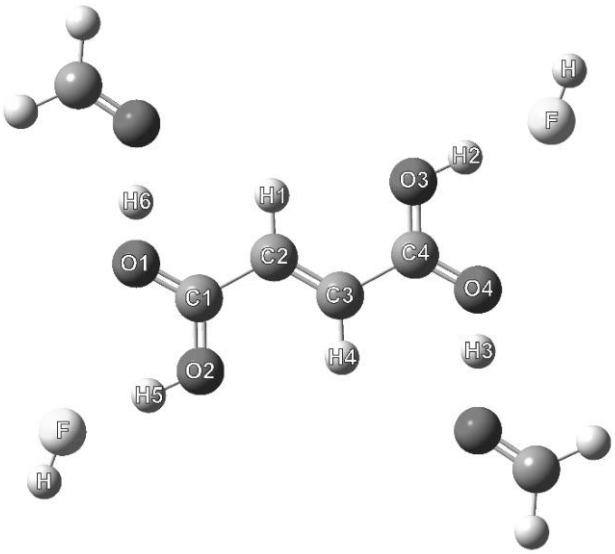

Figure S4: Quantum chemical calculated structure of simulated double hemi-protonated fumaric acid under consideration of hydrogen bonds in the solid state $[C_4H_6O_4 \cdot 2\ H_2CO \cdot 2\ HF]^{2+}$.

Table S5: Selected experimental obtained and calculated bond lengths and angles of the $[C_4H_6O_4]^{2+}$ cation. Symmetry operations: i = C_2-Rotation.

	Free cation[a] $[C_4H_6O_4]^{2+}$	Solvated cation[b] $[C_4H_6O_4 \cdot 4\ HF]^{2+}$		Crystal structure $[C_4H_6O_4]^{2+}([SbF_6]^-)_2$
Bond lengths [Å]				
O2-C1	1.276	1.266	O2-C2	1.273(5)
O1-C1	1.278	1.264	O1-C2	1.261(5)
C1-C2	1.475	1.479	C1-C2	1.463(6)
C2-C3	1.337	1.329	C1-C1*i*	1.299(9)
C3-C4	1.475	1.479		
O3-C4	1.276	1.266		
O4-C4	1.278	1.264		
Bond angles [°]				
O1-C1-O2	126.7	119.6	O1-C2-O2	120.0(4)
O1-C1-C2	118.4	118.2	O1-C2-C1	117.4(4)
O2-C1-C2	115.0	122.3	O2-C2-C1	122.7(3)
C1-C2-C3	121.7	120.9	C1*i*-C1-C2	121.8(5)
O3-C4-O4	126.7	119.6		
O3-C4-C3	115.0	122.3		
O4-C4-C3	118.4	118.2		
C2-C3-C4	121.7	120.9		
Torsion angle [°]				
O2-C1-C2-C3	–180.0	–180.0	O2-C2-C1-C1*i*	–162.3(4)
O1-C1-C2-C3	0.0	0.0	O1-C2-C1-C1*i*	16.9(6)
C1-C2-C3-C4	180.0	180.0	C2-C1-C1*i*-C2*i*	178.2(4)

[a] Calculated on the B3LYP/aug-cc-pVTZ level of theory.

[b] Calculated on the ωB97XD/aug-cc-pVTZ level of theory.

Table S6: Selected experimentally obtained and calculated bond distances and bond angles of the naked and the solvated cation $[C_4H_5O_4]^+$. Symmetry operations: i = C_2-Rotation.

	Free cation[a] $[C_4H_5O_4]^+$	Solvated cation[b] $[C_4H_6O_4 \cdot 2\,H_2CO \cdot 2HF]^{2+}$		Crystal structure $[C_4H_5O_4]^+[SbF_6]^-$
Bond lengths [Å]				
O3-C4	1.293	1.275		
C4-O4	1.293	1.252		
C4-C3	1.434	1.480		
C3-C2	1.343	1.329	C1-C1*i*	1.311(8)
C2-C1	1.496	1.480	C2-C1	1.479(5)
C1-O1	1.199	1.252	C2-O2	1.235(5)
C1-O2	1.338	1.275	C2-O1	1.298(5)
Bond angles [°]				
O3-C4-O4	123.5	120.5		
O3-C4-C3	119.9	117.1		
O4-C4-C3	116.6	122.4		
C4-C3-C2	121.7	121.3		
C1-C2-C3	123.8	121.3	C2-C1-C1*i*	121.7(5)
C2-C1-O1	121.1	122.4	O2-C2-C1	123.5(4)
C2-C1-O2	112.6	117.1	C1-C2-O1	115.3(3)
O1-C1-O2	126.4	120.5	O1-C2-O2	121.3(4)
Torsion angles [°]				
O1-C1-C2-C3	–180.0	178.8	O2-C2-C1-C1*i*	–172.8(6)
C1-C2-C3-C4	180.0	180.0	C2-C1-C1*i*-C2*i*	180.0
O2-C1-C2-C3	0.0	–1.3	O1-C2-C1-C1*i*	7.1(8)

[a] Calculated on the B3LYP/aug-cc-pVTZ level of theory.

[b] Calculated on the ωB97XD/aug-cc-pVTZ level of theory.

Table S7. Selected experimental vibrational frequencies [cm^{-1}] of $[C_4H_5O_4]^+[MF_6]^-$ (M = As, Sb) and calculated vibrational frequencies [cm^{-1}] of $[C_4H_5O_4]^+$ and $[C_4H_6O_4 \cdot 2\,H_2CO \cdot 2\,HF]^{2+}$.

$[C_4H_5O_4]^+[SbF_6]^-$ **(3)** exp.[a]		$[C_4H_5O_4]^+$ calc.[b,d]	$[C_4H_6O_4 \cdot 2\,H_2CO \cdot 2\,HF]^{2+}$ calc.[c,d]	Assignment		
IR	Raman	IR/Raman	IR/Raman			
		3513(104/157)	3148(0/324)	ν_1	A	ν_s(O-H)
		3506(555/116)	3135(3410/0)	ν_{20}	B	ν_{as}(O-H)
3078 w		3039(22/25)	3050(33/0)	ν_{21}	B	ν_{as}(C-H)
	3070(21)	3027(3/55)	3049(0/80)	ν_2	A	ν_s(C-H)
		3490(111/48)	1870(14/124)	ν_3	A	ν_s(O-H)
			1862(4707/0)	ν_{22}	B	ν_{as}(O-H)
	1704(82)	1577(321/167)	1687(0/253)	ν_4	A	ν(C=C)
		1698(236/214)	1613(1840/0)	ν_{23}	B	ν_{as}(C=O)
	1609(14)	1482(258/23)	1595(0/89)	ν_5	A	ν_s(C=O)
	1494(27)	1457(271/4)	1491(1/45)	ν_6	A	ν_s(C=O)
		1297(92/14)	1449(1994/0)	ν_{24}	B	ν_{as}(C=O)

[a] Abbrevations for IR intensities: vs = very strong, s = strong, m = medium, w = weak.
[b] Calculated on the B3LYP/aug-cc-pVTZ level of theory. Scaling factor 0.945.
[c] Calculated on the ωB97XD/aug-cc-pVTZ level of theory. Scaling factor 0.945.
[d] IR intensities in km/mol; Raman intensities in $Å^4/u$.

Table S8: Crystal data and structure refinement of $[C_4H_6O_4]^{2+}([SbF_6]^-)_2$ and $[C_4H_5O_4]^+[SbF_6]^-$.

	$[C_4H_6O_4]^{2+}([SbF_6]^-)_2$	$[C_4H_5O_4]^+[SbF_6]^-$
Molecular Fomula	$C_4H_6F_{12}O_4Sb_2$	$C_4H_5F_6O_4Sb$
M_r[g·mol^{-1}]	589.59	352.83
Crystal size [mm^3]	0.45 x 0.30 x 0.08	0.33 x 0.19 x 0.13
Crystal system	monoclinic	triclinic
Space group	*C*2/*c*	$P\bar{1}$
a [Å]	10.1389(5)	5.8479(8)
b [Å]	8.0260(4)	6.5959(8)
c [Å]	16.4701(8)	6.7570(6)
α [°]	90	90.484(8)
β [°]	100.498(4)	97.054(9)
γ [°]	90	114.504(12)
V [A^3]	1317.82(11)	234.85(5)
Z	4	1
ρ_{calc} [g·cm^{-3}]	2.972	2.495
μ [mm^{-1}]	4.261	3.027
$\lambda_{MoK\alpha}$ [Å]	0.71073	0.71073
F(000)	1088	166
T [K]	153(2)	160(2)
h, k, l range	-11:12; -5:9; -18:20	-7:8; -9:8; -9:9
Measured reflexes	2329	2064
Unique reflexes	1292	1257
R_{int}	0.0234	0.0381
Parameters	110	78
R(F)/wR(F^2)[a] (all data)	0.0284/0.0626	0.0376/0.0737
Weighting scheme[b]	0.0325	0.0159
S (Gof)[c]	1.032	1.091
Residual density [e·Å^{-3}]	0.901/-1.152	0.819/-1.245
Device	Oxford XCalibur	Oxford XCalibur
CCDC	1941237	1941238

[1] *https://sdbs.db.aist.go.jp (National Institute of Advanced Industrial Science and Technology,date of access)*.
[2] Y. Du, H. X. Fang, Q. Zhang, H. L. Zhang, Z. Hong, *Spectrochimica acta. Part A, Molecular and biomolecular spectroscopy* **2016**, *153*, 580.

EurJIC
European Journal of Inorganic Chemistry

Research Article
doi.org/10.1002/ejic.202200501

Chemistry Europe
European Chemical Societies Publishing

www.eurjic.org

Stabilizing the C—N Double Bond Character in Fumaramide with the Aid of Superacids

Marie C. Bayer,[a] Nikolaus Greither,[a] Valentin Bockmair,[a] Alexander Nitzer,[a] and Andreas J. Kornath*[a]

Fumaramide was reacted with the superacidic systems XF/SbF_5 and XF/BF_3 (X = H, D) leading to the formation of the O-diprotonated species. Using an equimolar amount of the Lewis acids relating to fumaramide, a mixture of the diprotonated salt and the diadduct with O-coordinated HF was obtained. The salts $[C_4H_2X_6N_2O_2]^{2+}[(BF_4)^-]_2$ and $[C_4H_2X_6N_2O_2]^{2+}[(SbF_6)^-]_2$ (X = H, D) were characterized by low-temperature vibrational spectroscopy. Single-crystal X-ray structure analyses were carried out for the compounds $[C_4H_8N_2O_2]^{2+}[(BF_4)^-]_2$, $C_4H_6N_2O_2\cdots 2HF$, and fumaramide. To discuss the experimental results, quantum chemical calculations were executed at the B3LYP/aug-cc-pVTZ level of theory. To investigate the impact of the protonation on the resonance +M effect and the electron distribution concerning the conjugated system ESP maps, NPA charges, and NBO analyses were consulted. Due to the protonation, the nitrogen lone pair contributes completely to the formation of the C=N π-bond, stabilizing the C=N double bond character. Since no monoprotonation of fumaramide is observed, amide hydrolysis is possible simultaneously on both amide groups.

Introduction

The amide bond represents one of the most fundamental functional groups in chemistry and biology.[1] With its remarkable geometrical and energetic features, the amide bond is essential for its structural role as the key facet in the structure of proteins.[2,3] One characteristic of amides is described by the high resonance stabilization, as illustrated by the example of fumaramide in Scheme 1, which is based on the strong influence of the +M effect.[4] As a consequence of amidic resonance, the majority of amides reveal a planar structure.[5-8] The donation from the lone pair on the nitrogen atom into the carbonyl π* orbital results in a 40 % double bond character on the C=N bond,[3,4,6,8,9] and a large C=N rotation barrier of around 63–84 kJ mol^{-1}.[3] Hence, the carbon and the nitrogen atoms reveal sp^2 hybridization.[10] The $n_N \rightarrow \pi^*_{C=O}$ conjugation and the concomitant planarity regulate most of the chemical and physical properties of amides.[1,11]

Amide hydrolysis is an essential process in biochemistry occurring via acid catalysis.[12,13] The initial step of amide hydrolysis is the protonation of the amide moiety.[12] The investigation of the protonated amide intermediate helps to gain further information about the reaction mechanism. With two amide groups, fumaramide provides four possible protonation sites serving as interesting starting material for investigations in strongly acidic media. Herein, we present our studies on fumaramide in different binary superacidic systems regarding the protonation site and its impact on amidic resonance.

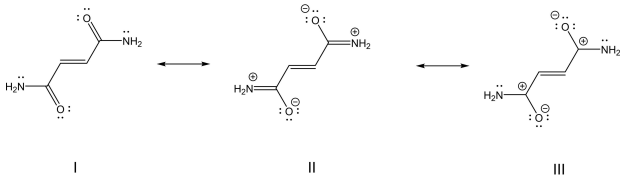

Scheme 1. Resonance structures of fumaramide.

Results and Discussion

Fumaramide was reacted in the superacidic solutions HF/SbF_5 and HF/BF_3 according to Scheme 2. The O-diprotonated species $[C_4H_8N_2O_2]^{2+}$ was obtained by using an excess of the Lewis acids (SbF_5 or BF_3).

The reactions were performed at a temperature of −30 °C, using anhydrous hydrogen fluoride as solvent as well as a reagent. Subsequently, the excess solvent was removed at −78 °C in a dynamic vacuum. The salts $[C_4H_8N_2O_2]^{2+}[(BF_4)^-]_2$ (1) and $[C_4H_8N_2O_2]^{2+}[(SbF_6)^-]_2$ (2) were obtained as colorless crystals

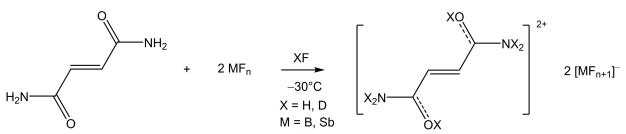

Scheme 2. Reaction of fumaramide in HF/SbF_5 and in HF/BF_3.

[a] M. C. Bayer, N. Greither, V. Bockmair, A. Nitzer, Prof. Dr. A. J. Kornath
Department Chemie
Ludwig-Maximilians-Universität München
Butenandtstr. 5–13(D), 81377 München, Deutschland
E-mail: andreas.kornath@cup.uni-muenchen.de

Supporting information for this article is available on the WWW under https://doi.org/10.1002/ejic.202200501

Research Article
doi.org/10.1002/ejic.202200501

and are stable at room temperature. The respective deuterated compounds $[C_4D_6H_2N_2O_2]^{2+}[(SbF_6)^-]_2$ (3) and $[C_4D_6H_2N_2O_2]^{2+}[(BF_4)^-]_2$ (4) were synthesized by modifying the superacid systems to DF/BF_3 and DF/SbF_5, respectively. Deuterium fluoride provokes an H/D-exchange of all acidic protons, which are in the case of fumaramide also the protons of the amino groups. Bearing in mind that fumaramide holds four possible basic centers, including the amino groups, an eight-to-one ratio of the stronger Lewis acid SbF_5[14] was used to prepare a tri- or tetraprotonated cation. However, even an excess of SbF_5 produces the diprotonated species.

For completeness, an equimolar amount of the Lewis acids in reference to fumaramide was applied to form the monoprotonated salt. Surprisingly, a mixture of the diadduct with O-coordinated HF, $C_4H_6N_2O_2 \cdots 2HF$ (5), and the diprotonated species **1** was obtained. In this work, no monoprotonated species were observed.

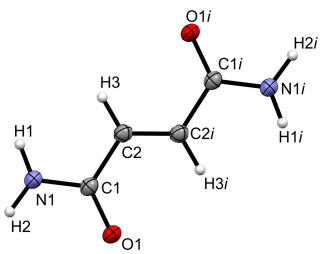

Figure 1. Formula unit of $C_4H_6N_2O_2$ (displacement ellipsoids with 50% probability). Symmetry operation: *i = 1−x, 1−y, 1−z.*

Crystal structure of $C_4H_6N_2O_2$

Since the structural parameters of fumaramide have not been reported yet, we were motivated to investigate the crystal structure. In order to analyze the influence of protonation on the bond lengths and angles, it is important to know the crystal data of the reactant. $C_4H_6N_2O_2$ crystallizes in the monoclinic space group $P2_1/n$ with two formula units per unit cell. The formula unit of fumaramide is shown in Figure 1 and Table 1 summarizes selected structural parameters. The neutral compound exists as the *cis-cis* conformer.

The crystal structure of acetamide[15] is consulted to better compare the crystallographic data of fumaramide. The C1–O1 bond distances of 1.245(2) Å are in agreement with the value 1.247(1) Å found in acetamide[15] and are slightly longer than formal C=O double bonds (1.19 Å).[16] The C1–N1 bond lengths are with 1.328(2) Å considerably reduced compared to formal C–N single bonds (1.47 Å).[16] They are in accordance with the C–N distance in acetamide (1.335(1) Å).[15] The elongation of the C=O bond and the simultaneous shortening of the C–N bond demonstrates the importance of the resonance structure II in fumaramide (Scheme 1). With a bond distance of 1.322(2) Å the C2–C2*i* does not differ from the value for formal C=C double bonds (1.33 Å).[16] The C1–C2 bond length of 1.487(2) Å is slightly shortened compared with formal C–C single bonds (1.54 Å).[16] The angles found in the molecule deviate up to 4.5° from the ideal bond angle of 120° for sp^2 hybridized carbon atoms. The molecule of fumaramide is found to be almost planar. The variation of the NH_2 groups from the median plane through the molecule amounts to 2.6°.

Table 1. Selected bond lengths and angles of $C_4H_6N_2O_2$ (symmetry operations: *i = 1−x, 1−y, 1−z; ii = 2−x, −y, 1−z; iii = −0.5 +x, 0.5−y, −0.5 +z*), $C_4H_6N_2O_2 \cdots 2HF$ (5) (symmetry operations: *i = −x, 1−y, 1−z; ii = −1 +x, y, 1 +z; iii = x, 1.5−y, 0.5 +z*), and $[C_4H_8N_2O_2]^{2+}[(BF_4)^-]_2$ (1) (symmetry operations: *i = −x, −y, 1−z; ii = −1 +x, y, z; iii = 1−x, 1−y, 1−z; iv = −x, 1−y, 1−z; v = −1.5 +x, 0.5−y, −0.5 +z*) with estimated standard deviation marked in parentheses.

	$C_4H_6N_2O_2$	$C_4H_6N_2O_2 \cdots 2HF$ (5)		$[C_4H_8N_2O_2]^{2+}[(BF_4)^-]_2$ (1)
Bond length [Å]				
C2–C2*i*	1.322(2)	1.323(2)		1.324(2)
C1–C2	1.487(2)	1.485(2)		1.468(2)
C1–O1	1.245(2)	1.259(2)		1.301(1)
C1–N1	1.328(2)	1.314(2)		1.288(2)
Bond angle [°]				
O1–C1–N1	122.5(1)	122.8(1)		123.8(1)
O1–C1–C2	122.0(1)	120.0(1)		116.4(1)
N1–C1–C2	115.5(1)	117.2(1)		119.8(1)
C1–C2–C2*i*	122.3(1)	121.0(1)		121.3(1)
Angle of Torsion [°]				
O1–C1–C2–C2*i*	1.3(2)	5.0(2)		1.9(2)
N1–C1–C2–C2*i*	−177.4(1)	−174.5(1)		−178.1(1)
C1–C2–C2*i*–C1*i*	−180.0(1)	−180.0(1)		−180.0(1)
Donor-acceptor distance [Å]				
N1–H1···O1*iii*	2.862(2)		O1–H4···F1	2.735(1)
N1–H2···O1*ii*	2.946(2)		O1–H4···F2*ii*	3.125(1)
F1–H1···O1		2.414(1)	O1–H4···F2*iii*	3.032(1)
N1*i*–H3*i*···F1*ii*		2.806(1)	C2–H3···F3*v*	3.125(2)
N1*i*–H2*i*···O1*iii*		2.992(2)	N1–H2···F2*iii*	2.976(1)
			N1–H2···F1*iv*	2.965(1)
			N1–H1···F3*v*	2.830(1)

Research Article
doi.org/10.1002/ejic.202200501

In the crystal packing of $C_4H_6N_2O_2$, the molecules are connected via two hydrogen bonds which are illustrated in Figure S1 and described in the Supporting Information.

Crystal structure of $C_4H_6N_2O_2$···2HF

$C_4H_6N_2O_2$···2HF (5) crystallizes in the monoclinic space group $P2_1/c$ with two formula units per unit cell. Figure 2 shows the formula unit of the diadduct of fumaramide with HF and Table 1 holds selected structural parameters.

The formation of the diadduct of fumaramide with HF leads to a further elongation of the C1–O1 distances of 1.259(2) Å when compared with the starting material. The C1–N1 single bond lengths of 1.314(2) Å are shortened in comparison to fumaramide. In the crystal structure of **5**, fumaramide molecules are linked through two different hydrogen bonds with hydrogen fluoride molecules, as illustrated in Figure S3 and described in the Supporting Information.

Crystal structure of $[C_4H_8N_2O_2]^{2+}[(BF_4)^-]_2$

The diprotonated fumaramide $[C_4H_8N_2O_2]^{2+}[(BF_4)^-]_2$ (1) crystallizes in the monoclinic space group $P2_1/n$ with two formula units per unit cell. Figure 3 shows the formula unit of **1** and corresponding selected bond lengths and angles combined in Table 1.

The diprotonation of fumaramide has a major influence on the C=O bond lengths. In comparison to fumaramide, the C1–O1 bond distances (1.301(1) Å) are significantly elongated by 0.056 Å and slightly shorter than formal C–O single bonds (1.43 Å).[16] The C1–N1 bond lengths of 1.288(2) Å are significantly shorter in contrast to the starting material and are in the range of formal C=N double bonds (1.22 Å).[16] Also, the C1–C2 bond distances of 1.468(2) Å are significantly decreased due to the protonation, compared to the reactant. In comparison with protonated acetamide, the C–O (1.292(3) Å), C–N (1.285(4) Å) and C–C (1.470(4) Å) bond distances are in the same range, respectively.[17] The C2–C2*i* double bonds are not significantly

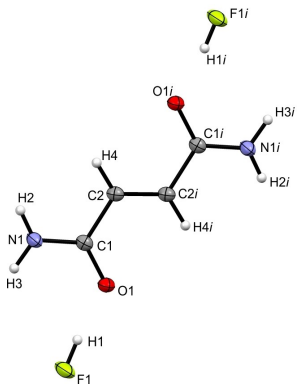

Figure 2. Formula unit of $C_4H_6N_2O_2$···2HF (displacement ellipsoids with 50% probability). Symmetry operation: *i* = −*x*, 1−*y*, 1−*z*.

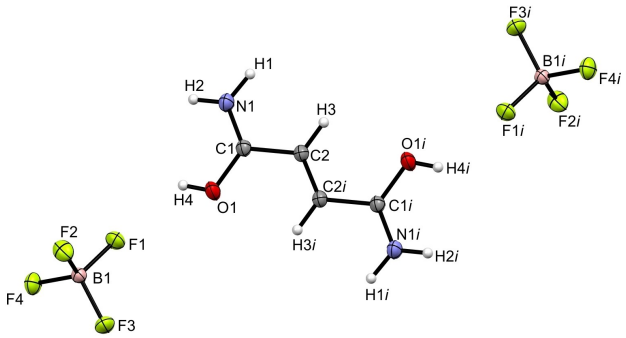

Figure 3. Formula unit of $[C_4H_8N_2O_2]^{2+}[(BF_4)^-]_2$ (displacement ellipsoids with 50% probability). Symmetry operation: *i* = −*x*, −*y*, 1−*z*.

affected by the protonation. As regards bond angles, the greatest impact is observed for the O1–C1–C2 bond angle, which is reduced by 5.6° to 116.4(1)°. The N1–C1–C2 bond angle, on the other hand, is widened by 4.3° to 119.8(1)°, in contrast to fumaramide. The torsion angles in the dication approach the ideal planar values, which means that the OH and the NH_2 moieties are twisted out of the carbon plane by merely 1.9°.

The B–F bond lengths of the $[BF_4]^-$ anion are in the range between 1.378(2) Å and 1.403(2) Å. The data are in good accordance with reported B–F bond distances of $[BF_4]^-$ anions.[18] The bond angles in the anion deviate marginally from the ideal tetrahedral bond angle.

In the crystalline state of **1**, the cations and anions are linked via several hydrogen bonds and intermolecular contacts, which are illustrated in Figure S5 and described in the Supporting Information.

Vibrational spectra

The low-temperature vibrational spectra of $[C_4H_8N_2O_2]^{2+}[(BF_4)^-]_2$ (1), $[C_4H_8N_2O_2]^{2+}[(SbF_6)^-]_2$ (2), $[C_4D_6H_2N_2O_2]^{2+}[(SbF_6)^-]_2$ (3), together with fumaramide are displayed in Figure 4. The Raman and corresponding IR spectra of **3** in combination with $[C_4D_6H_2N_2O_2]^{2+}[(BF_4)^-]_2$ (4) and fumaramide are given in Figure S8 in the Supporting Information. Selected experimental vibrational frequencies of **1** and **2** combined with the quantum chemically calculated frequencies of the N-coordinated HF complex of the cation $[C_4H_8N_2O_2$···$2HF]^{2+}$ are summarized in Table 2. All observed frequencies of **1** and **2** are listed in Table S2 and the experimental frequencies of **3** and **4** are summarized in Table S3 in the Supporting Information. To improve the accordance of the calculated frequencies with the experimental ones, two HF molecules were added to the gas phase structure of the cation coordinating the amino group to simulate hydrogen bonds in the solid state.[19] Since the vibrational spectra of fumaramide have not been thoroughly reported yet,[20] we determined the vibrational frequencies of our reactant. To assign the vibrational frequencies of the diprotonated species, the comparison with the neutral com-

Research Article
doi.org/10.1002/ejic.202200501

Chemistry Europe
European Chemical Societies Publishing

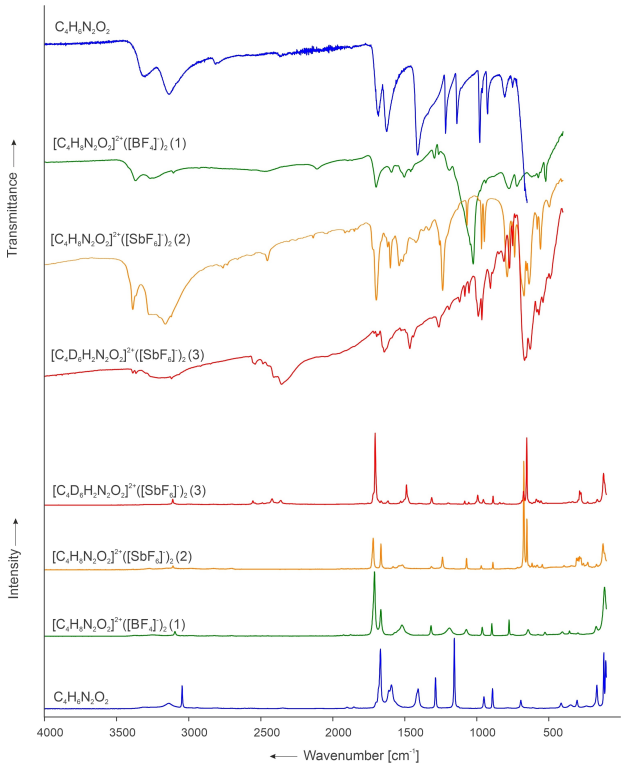

Figure 4. Low-temperature Raman and IR spectra of fumaramide, $[C_4H_8N_2O_2]^{2+}[(BF_4)^-]_2$ (1), $[C_4H_8N_2O_2]^{2+}[(SbF_6)^-]_2$ (2) and $[C_4D_6H_2N_2O_2]^{2+}[(SbF_6)^-]_2$ (3).

pound is fundamental. The *cis-cis* conformer of fumaramide, which exists in the solid state, is expected to have C_{2h} symmetry with 36 fundamental vibrations (13 A_g + 5 B_g + 6 A_u + 12 B_u). The rule of mutual exclusion is applicable,[21] concerning the inversion center of the molecule. The vibrational spectra of fumaramide were assigned by analyzing the Cartesian displacement vectors of the calculated vibrational modes of $C_4H_6N_2O_2$, as well as by comparing them to literature data for the IR spectrum.[20] The observed and assigned frequencies are listed in Table S4 in the Supporting Information. The diprotonated cations reveal *cis-cis* conformers in the crystalline state, as reported in the section above. The *cis-cis*-$[C_4H_8N_2O_2]^{2+}$ is expected to have C_{2h} symmetry with 42 fundamental vibrations (15 A_g + 6 B_g + 7 A_u + 14 B_u). On account of the inversion center of the cation, the rule of mutual exclusion applies.[21] The vibrational frequencies were assigned by analyzing the Cartesian displacement vectors of the calculated vibrational modes of $[C_4H_8N_2O_2]^{2+}$, as well as by comparing them to experimental data of fumaramide. The first evidence for a successful protonation is the O–H stretching vibration, which is observed in the IR spectra at 3369 cm^{-1} **1** and at 3367 cm^{-1} **2**. The symmetric O–H stretching modes are not detectable in the Raman spectra, owing to the poor polarizability of the vibration. In the Raman spectra, the O–D stretching vibrations are observable at 2540 cm^{-1} **3** and at 2546 cm^{-1} **4**. The antisymmetric O–D stretching modes are detected at 2538 cm^{-1} **3** and at 2540 cm^{-1} **4** in the IR spectra. The red-shifts of the ν(O–D) are in agreement with the Teller-Redlich rule for a H/D isotopic effect.[21] The antisymmetric NH_2 stretching vibrations, observed in the IR spectra at 3265 cm^{-1} **1**, 3275 cm^{-1} **2**, and at 3161 cm^{-1} **2** are red-shifted up to 141 cm^{-1} compared to the neutral compound. In the IR spectra of **3** and **4**, the antisymmetric ND_2 stretching modes are detected at 2484 cm^{-1} **3**, 2486 cm^{-1} **4**, and at 2409 cm^{-1} **3**, 2395 cm^{-1} **4**. The observed red-shifts of the ν(N–D) conform to the Teller-Redlich rule.[21] In the Raman spectrum of **1** the symmetric NH_2 stretching vibrations, detectable at 3376 cm^{-1} and 3255 cm^{-1}, are blue-shifted by 67 cm^{-1} and 117 cm^{-1}, respectively, in comparison to the starting material. The equivalent NH_2 stretching modes of **2** are observed at 3327 cm^{-1} and 3273 cm^{-1} and are blue-shifted by

Table 2. Selected experimental vibrational frequencies [cm^{-1}] of $[C_4H_8N_2O_2]^{2+}[(BF_4)^-]_2$ (1), $[C_4H_8N_2O_2]^{2+}[(SbF_6)^-]_2$ (2) and calculated vibrational frequencies [cm^{-1}] of the N-coordinated HF complex of the cation $[C_4H_8N_2O_2\cdots 2HF]^{2+}$.

$[C_4H_8N_2O_2]^{2+}[(BF_4)^-]_2$ (1) exp.[a]		$[C_4H_8N_2O_2]^{2+}[(SbF_6)^-]_2$ (2) exp.[a]		N-coordinated HF complex of the cation $[C_4H_8N_2O_2\cdots 2HF]^{2+}$ calc.[b]	Assignment[c]		
IR	Raman	IR	Raman	IR/Raman			
3369 w		3367 vs		3693 (550/0)	ν_{29}	B_u	ν_{as}(O–H)
	3376 (2)		3327 (1)	3557 (0/153)	ν_2	A_g	ν_s(NH_2)
3265 w		3275 vs		3556 (438/0)	ν_{30}	B_u	ν_{as}(NH_2)
	3255 (2)		3273 (1)	3359 (0/243)	ν_3	A_g	ν_s(NH_2)
		3161 vs		3355 (1616/0)	ν_{31}	B_u	ν_{as}(NH_2)
3105 w		3121 vs		3200 (27/0)	ν_{32}	B_u	ν_{as}(C–H)
	3095 (7)		3109 (4)	3195 (0/70)	ν_4	A_g	ν_s(C–H)
	1709 (100)		1719 (29)	1741 (0/292)	ν_5	A_g	ν_s(C=N)
1697 m		1697 vs		1726 (647/0)	ν_{33}	B_u	ν_{as}(C=N)
	1666 (42)		1665 (24)	1699 (0/214)	ν_6	A_g	ν(C=C)
1591 w		1599 s		1621 (175/0)	ν_{34}	B_u	ν_{as}(C–O)
			1541 (4)	1601 (0/19)	ν_7	A_g	ν_s(C–O)
1043 vs		1067 w		1104 (1/0)	ν_{38}	B_u	ρ_{as}(NH_2)
	1072 (11)		1071 (11)	1104 (0/28)	ν_{11}	A_g	ρ_s(NH_2)
	962 (14)		969 (4)	972 (0/10)	ν_{12}	A_g	ν_s(C–C)
937 w		947 m		939 (31/0)	ν_{39}	B_u	ν_{as}(C–C)
777 m		789 s		807 (204/0)	ν_{17}	A_u	ω_{as}(NH_2)

[a] Abbrevations for IR intensities: v = very, s = strong, m = medium, w = weak. IR intensities in km/mol; Raman intensities in $Å^4/u$. Experimental Raman activities are relative to a scale of 1 to 100. [b] Calculated on the B3LYP/aug-cc-pVTZ level of theory. [c] ρ = rocking, ω = wagging.

Research Article
doi.org/10.1002/ejic.202200501

18 cm^{-1} and 135 cm^{-1}, respectively, compared to fumaramide. The antisymmetric C–H stretching vibrations in the IR spectra of **1** (3105 cm^{-1}) and **2** (3121 cm^{-1}) are red-shifted, whereas the symmetric ones observed in the Raman spectra of **1** (3095 cm^{-1}) and **2** (3109 cm^{-1}) are blue-shifted in contrast to the reactant. The protonation of the oxygen atom has a great impact on the C–N bond. The respective C–N stretching vibration is substantially blue-shifted by 287 cm^{-1} in the IR spectra (1697 cm^{-1} **1**, **2**) and by up to 311 cm^{-1} in the Raman spectra (1709 cm^{-1} **1**, 1719 cm^{-1} **2**). This blue-shift indicates a strengthening of the C–N bond due to the protonation, which is also observed in the crystal data of **1**. The C=C stretching mode appears in the Raman spectra at 1666 cm^{-1} **1** and at 1665 cm^{-1} **2**. By comparing to the starting material, the ν(C=C) is blue-shifted by up to 56 cm^{-1}. As a result of the diprotonation, the C=O bonds are weakened and appear in the IR spectra at 1591 cm^{-1} **1** and at 1599 cm^{-1} **2**, and in the Raman spectrum at 1541 cm^{-1} **2**. These vibrations are red-shifted by up to 128 cm^{-1} compared to fumaramide. The weakening of the C=O bond is confirmed by the crystal structure of **1**. A blue-shift of the C–C stretching vibration of up to 78 cm^{-1} compared to the neutral compound is observed in the IR spectra at 937 cm^{-1} **1**, 947 cm^{-1} **2**, and in the Raman spectra at 962 cm^{-1} **1**, 969 cm^{-1} **2**. The crystal structure of **1** supports the strengthening of the C–C single bond because of the protonation. For the $[SbF_6]^-$ anion with ideal O_h three Raman lines and two IR bands are anticipated. Indeed a higher number of vibrations is observed in the spectra of **2** and **3**, implying a distortion of the octahedral structure of the anion. The anion $[BF_4]^-$ is assigned to the point group T_d and provides four vibrational modes, which are all Raman active and two of which are IR active.[22] The occurrence of more than these expected vibrations is attributed to a lowering of the symmetry of the ion by solid-state effects. This is verified by the crystal structure of **1**.

Quantum chemical calculations

The quantum chemical calculations were performed at the B3LYP/aug-cc-pVTZ level of theory. The comparison of the experimental data with the calculated frequencies and structural parameters of the free cation $[C_4H_8N_2O_2]^{2+}$ reveals a discrepancy (Tables S5 and S6). These differences are caused by several hydrogen bonds present in the crystal structure of **1**. To improve the calculation, different hydrogen bonds are simulated by adding HF molecules to the gas phase structure of the free cation.[19] The comparison of the different calculated bond lengths and angles with the experimental structural parameters revealed that the N-coordinated HF complex of the cation $[C_4H_8N_2O_2\cdots 2HF]^{2+}$ agrees best with the experimental data (Tables S5 and S6). A comparison of the calculated structure of the cation with N-coordinated HF molecules $[C_4H_8N_2O_2\cdots 2HF]^{2+}$ with the single-crystal X-ray structure of **1** along with bond lengths and angles is illustrated in Figure S9. All of the experimentally obtained bond lengths and angles of the dication are in good agreement with the calculated structure, except for the bond distances N1–C1 and C2–C3, which are slightly overestimated in the calculation, in contrast to the experimental data. This is attributable to further hydrogen bonds and intermolecular interactions in the solid state of **1**, which are not regarded in the calculation.

To investigate the diprotonated species and the reactant in terms of the conjugated system, electrostatic potential (ESP) maps in conjunction with natural population analysis (NPA) charges were calculated. Figure 5 illustrates the ESP maps combined with NPA charges of fumaramide and $[C_4H_8N_2O_2]^{2+}$. In the following, we focus on the ESP map of the free cation $[C_4H_8N_2O_2]^{2+}$ since it provides more details concerning the

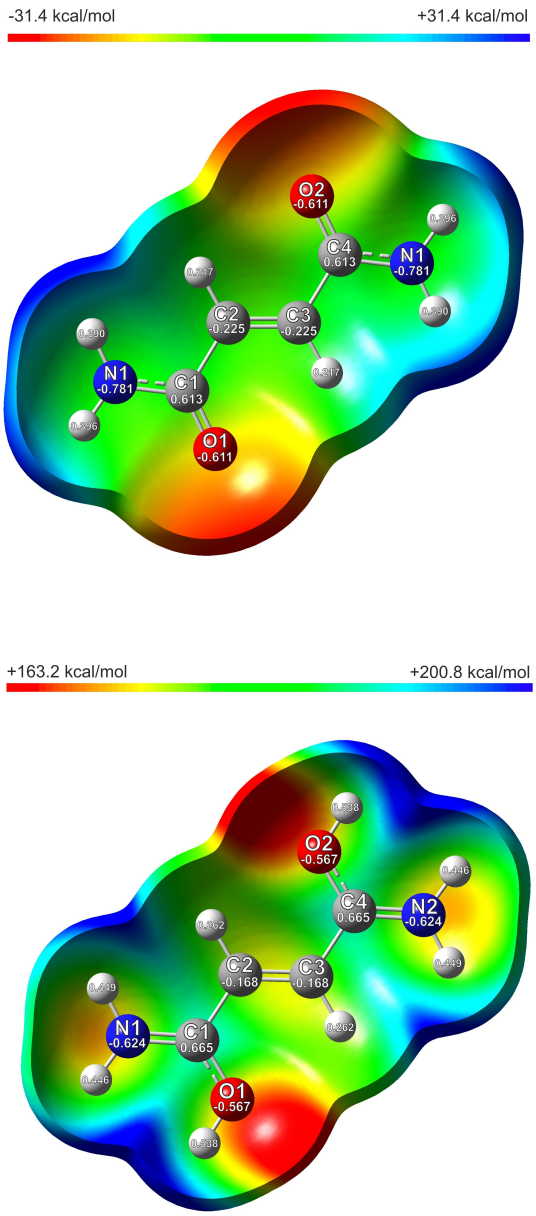

Figure 5. Top: Calculated ESP surface mapped onto an electron density isosurface value of 0.0004 $bohr^{-3}$ with the color scale ranging from −31.4 kcal mol^{-1} to +31.4 kcal mol^{-1} of $C_4H_6N_2O_2$. Bottom: Calculated ESP surface mapped onto an electron density isosurface value of 0.0004 $bohr^{-3}$ with the color scale ranging from +163.2 kcal mol^{-1} to +200.8 kcal mol^{-1} of $[C_4H_8N_2O_2]^{2+}$.

Research Article
doi.org/10.1002/ejic.202200501

conjugated system than the ESP map of the N-coordinated HF complex of the cation $[C_4H_8N_2O_2\cdots 2HF]^{2+}$, which is illustrated in Figure S10 in the Supporting Information. The ESP map of fumaramide shows the negative charge density is located in the region around the oxygen atoms displayed by the red surface. The positive electrostatic potential is concentrated in the amino groups. According to the resonance form II in Scheme 1 this charge distribution indicates that the π-electrons are shifted from nitrogen toward oxygen. Both, the σ- as well as the π-electrons are affected by the NPA charge differences between nitrogen and oxygen. The σ-electrons are polarized in the reversed way to the π-electrons.[3] The NPA charges of the nitrogen atoms possess even a higher negative value than the oxygen atoms. The ESP map of the neutral compound shows a neutral electrostatic potential along with the carbon skeleton. The diprotonation of fumaramide entails a realignment of the electrostatic potential distribution, as illustrated in the ESP map of the free cation $[C_4H_8N_2O_2]^{2+}$ in Figure 5 (bottom). The charge density on the amino groups shifted from positive to neutral, whereas the negative charge density, is still concentrated on the carbonyl oxygen atom. A neutral electrostatic potential is also found in the carbon skeleton. The negative NPA charges of the N1 and N2 atoms, as well as of the O1 and O2 atoms decline. It can be assumed that on account of the protonation the electron density of the conjugated system shifts from the oxygen to the nitrogen atoms thereby strengthening the C=N and weakening the C–O bond. The positive electrostatic potential is concentrated in the region between the amino group and the protonated oxygen, displaying the delocalization of the positive charge along the amide moiety. Another positive electrostatic potential is located between the amino group and the CH moiety. Both positive regions indicate exactly where the four-center hydrogen bonds and the bifurcated hydrogen bonds are formed, which is illustrated in Figure 6. The formation of plenty of hydrogen bonds is favored because the diprotonated fumaramide is highly polar, as illustrated in the ESP map.

To go into further detail, regarding the impact of the diprotonation on the resonance effect and the hybridization, we performed natural bond orbital calculations of $[C_4H_8N_2O_2]^{2+}$ and compared it with fumaramide. The NBO analysis of the neutral compound confirmed that the nitrogen, as well as the carbon atom of the amide moiety, are sp^2-hybridized. The nitrogen atom possesses one lone pair, occupied with 1.74 e^-, which is available for contributing to planar amidic bond resonance ($n_N \rightarrow \pi^*_{C=O}$ conjugation),[5,23] which is illustrated in Figure 7. According to the NBO calculations, the oxygen atom reveals sp-hybridization. The conjugation in fumaramide changes significantly due to the diprotonation. The nitrogen and the carbon atoms are still sp^2-hybridized. However, the nitrogen lone pair is not located at the nitrogen anymore. It contributes completely to the formation of the C=N π-bond, as shown in Figure 7. The diprotonation supports the +M effect and thereby favoring the resonance form II (Scheme 1). Simultaneously the resonance form I gets irrelevant for the diprotonated species. The assumption arises that in the diprotonated species the double bond character increases from 40 %[6] to 100 % and the resonance effect becomes obsolete. On account of the protonation, the C=N double bond character is stabilized. A rehybridization is observed from sp to sp^2 for the oxygen atom.

We were interested to find out if an additional N-protonation on the amide moiety is theoretically possible. An inspiring example in which an N,O-diprotonation was observed, is represented by urea.[24] Urea can be described as one amide group combined with one amino moiety. The O-monoprotonation is followed by the N,O-diprotonation. However, the additional N-protonation of urea takes place in the amino group and leads to the formation of $-NH_3^+$. Interestingly, the nitrogen atom of the amide moiety remains unprotonated and no triprotonation is found for urea.[24]

Since the nitrogen atoms of the diprotonated fumaramide have no lone pairs at their disposal, a further protonation on the nitrogen atoms leading to tri- and fourfold-protonated species seems to be impossible. Although O-protonation is preferred over N-protonation in simple amides, such as fumaramide, there is evidence for N-protonation appearing to be favored for instance in strained molecular systems.[13] As O-protonated cations become planar, N-protonation provokes disruption of the amide bond resonance.[11,13] We assume that a

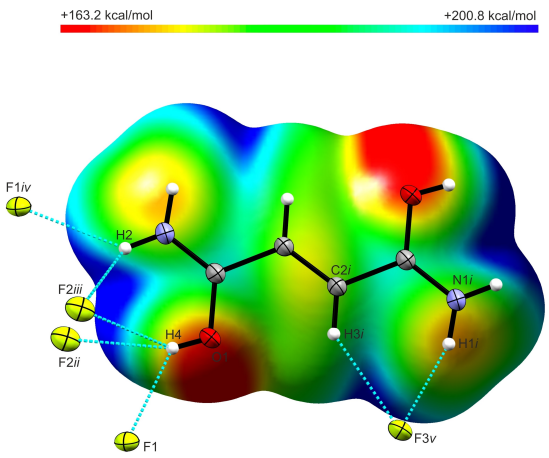

Figure 6. Selected hydrogen bonds in the crystal structure of 1 (displacement ellipsoids with 50 % probability). The hydrogen bonds are drawn as dashed blue lines. The calculated ESP surface mapped onto an electron density isosurface value of 0.0004 $bohr^{-3}$ with the color scale ranging from +163.2 kcal mol^{-1} to +200.8 kcal mol^{-1}. Symmetry operations: *i* = −*x*, −*y*, 1−*z*; *ii* = −1 +*x*, *y*, *z*; *iii* = 1−*x*, 1−*y*, 1−*z*; *iv* = −*x*, 1−*y*, 1−*z*; *v* = 1.5−*x*, −0.5 +*y*, 1.5−*z*.

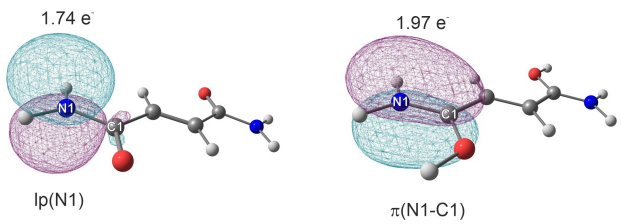

Figure 7. Selected NBOs for the nitrogen lone pair of fumaramide (left) and for the CN bond of $[C_4H_8N_2O_2]^{2+}$ (right) with corresponding occupancies.

Research Article
doi.org/10.1002/ejic.202200501

further N-protonation leads to a distortion of the planarity of the molecular system which comes along with a loss of symmetry and is therefore not observed.

Conclusion

Fumaramide was examined in the superacidic systems XF/SbF_5 and XF/BF_3 (X = H, D). The salts of the O-diprotonated fumaramide were isolated and characterized by low-temperature vibrational spectroscopy. Using an equimolar amount of the Lewis acids in relation to fumaramide, a mixture of the diprotonated salt and the diadduct with O-coordinated HF was obtained. Single-crystal X-ray structure analyses were performed for $[C_4H_8N_2O_2]^{2+}[(BF_4)^-]_2$, $C_4H_6N_2O_2\cdots 2HF$, as well as for the neutral compound fumaramide. To interpret the experimental results, quantum chemical calculations were executed at the B3LYP/aug-cc-pVTZ level of theory. To investigate the impact of the protonation on the resonance +M effect and the electron distribution concerning the conjugated system ESP maps, NPA charges, and NBO analyses were consulted. On account of the protonation the electron density of the conjugated system shifts from the oxygen atoms to the nitrogen atoms thereby strengthening the C=N and weakening the C–O bond, which is confirmed by crystal data and vibrational frequencies. Owing to the protonation the C=N double bond character is stabilized. Since no monoprotonation of fumaramide is observed, amide hydrolysis is possible simultaneously on both amide groups. Fumaramide is especially suitable for biochemical hydrolysis reactions of both amide moieties.

Experimental Section

Caution! Contact with the components must be avoided. The hydrolysis of SbF_5, BF_3, and the reported salts might release HF, burn skin, and cause irreparable damage. Adequate safety precautions must be undertaken when using and handling these materials.

Apparatus and materials: The reactions were conducted by using standard Schlenk techniques with an electropolished stainless-steel vacuum line. Transparent FEP/PFA-reactors in combination with stainless-steel valves were employed for the reactions in superacidic media. The vacuum line, as well as the reactors, were dried with fluorine, before use. Excess fluorine was removed in a dynamic vacuum and absorbed by Sodalime. Antimony pentafluoride was managed in a Duran glass high vacuum line by using Young valves. Low-temperature Raman spectroscopic measurements were performed in a glass cell under vacuum cooled down to −196 °C on a Bruker MultiRAMII FT-Raman spectrometer with Nd:YAG laser excitation (λ = 1064 nm). For the IR measurements, the respective sample was put on a CsBr single-crystal plate in a cooled cell. A Bruker Vertex-80 V-FT-IR spectrometer was used for recording the low-temperature IR spectra. The low-temperature single-crystal X-ray diffractions of $C_4H_6N_2O_2$, **1**, and **5** were conducted on an Oxford XCalibur3 diffractometer equipped with a Spellman generator (50 kV, 40 mA) and a Kappa CCD-detector, which operates with MoK_α radiation (λ = 0.71073 Å). Data collection and reduction were performed using the program CrysAlisPro 1.171.38.46 (Rigaku OD, 2015).[25] The crystal structures were solved using SHELXT[26] and SHELXL-2018/3[27] of the WINGX software package.[28] The structures were checked by applying the software PLATON.[29] The absorption correction was performed with the help of the SCALE3 ABSPACK multiscan method.[30] Selected data and parameters of the reported single-crystal structures $C_4H_6N_2O_2$, **1**, and **5** are summarized in Table S8 (Supporting Information). Quantum chemical calculations were carried out on the B3LYP/aug-cc-pVTZ level of theory using the software package Gaussian 09[31] and Gaussian 16.[32] GaussView 6.0 was used for the visualization and illustration of the ESP calculations.[33]

Syntheses of $[C_4H_8N_2O_2]^{2+}[(BF_4)^-]_2$ (1) and $[C_4D_6H_2N_2O_2]^{2+}([BF_4]^-)_2$ (4): At first, boron trifluoride (203 mg, 3.00 mmol) was condensed into an FEP reactor vessel at −196 °C. Approximately 2 mL of anhydrous hydrogen fluoride (*a*HF) (**1**) or deuterium fluoride (*a*DF) (**4**), respectively, were condensed into the FEP reactor vessel at −196 °C. The superacid was warmed up to −10 °C, homogenized, and accordingly refreezed at −196 °C. Under a nitrogen atmosphere fumaramide (114 mg, 1.00 mmol) was added to the frozen mixture. The reaction mixture was warmed up to −30 °C and mixed until the solution was clear. In dynamic vacuum excess HF or DF, respectively, was removed at −78 °C. The compounds were obtained as colorless crystalline solids being stable up to 20 °C. The rector was left in an ethanol bath at −40 °C for crystallization of **1**.

Syntheses of $[C_4H_8N_2O_2]^{2+}([SbF_6]^-)_2$ (2) and $[C_4D_6H_2N_2O_2]^{2+}([SbF_6]^-)_2$ (3): Antimony pentafluoride (370 mg, 1.71 mmol) was condensed into an FEP reactor vessel at −196 °C. In addition, approximately 2 mL of anhydrous hydrogen fluoride (*a*HF) (**2**) or deuterium fluoride (*a*DF) (**3**), respectively, were condensed into the FEP reactor vessel at −196 °C. The mixture was warmed up to −10 °C, homogenzied and afterwards refreezed at −196 °C. Fumaramide (65 mg, 0.57 mmol) was added under a nitrogen atmosphere to the frozen mixture. The reaction mixture was warmed up to −30 °C and homogenized until the formed salt was dissolved thoroughly. Excess HF or DF, respectively, was removed in a dynamic vacuum at −78 °C. The compounds were obtained as colorless crystalline solids, which are stable up to 20 °C.

Syntheses of $C_4H_6N_2O_2\cdots 2HF$ (5): At the beginning, boron trifluoride (68 mg, 1.00 mmol) was condensed into an FEP reactor vessel at −196 °C. Approximately 2 mL of anhydrous hydrogen fluoride (*a*HF) were condensed into the FEP reactor vessel at −196 °C. To form the superacid, the mixture was warmed up to −10 °C, homogenized, and accordingly refreezed at −196 °C. Under a nitrogen atmosphere fumaramide (114 mg, 1.00 mmol) was added to the frozen mixture. The reaction mixture was warmed up to −30 °C and mixed until a clear solution was obtained. In dynamic vacuum excess HF was removed at −78 °C. The compound was obtained as a colorless crystalline solid. The rector was left in an ethanol bath at −70 °C for crystallization of **5**.

Deposition Numbers 2178675 (for **1**), 2178678 (for **5**), and 2178670 (for fumaramide) contain the supplementary crystallographic data for this paper. These data are provided free of charge by the joint Cambridge Crystallographic Data Centre and Fachinformationszentrum Karlsruhe Access Structures service www.ccdc.cam.ac.uk/structures.

Acknowledgments

We acknowledge gratefully the financial support of the Department of Chemistry of the Ludwig-Maximilians-Universität München, the Deutsche Forschungsgemeinschaft (DFG) and the F-Select GmbH. Open Access funding enabled and organized by Projekt DEAL.

Research Article
doi.org/10.1002/ejic.202200501

Conflict of Interest

The authors declare no conflict of interest.

Data Availability Statement

The data that support the findings of this study are available in the supplementary material of this article.

Keywords: C=N double bond character · Electrostatic potential maps · Fumaramide · Natural bond analysis · Superacids

[1] A. Greenberg, C. M. Breneman, J. F. Liebman, *The Amide Linkage: Structural Significance in Chemistry, Biochemistry, and Materials Science*, Wiley, New York, NY, **200**.
[2] J. I. Mujika, J. M. Matxain, L. A. Eriksson, X. Lopez, *Chem. Eur. J.* **2006**, *12*, 7215.
[3] C. R. Kemnitz, M. J. Loewen, *J. Am. Chem. Soc.* **2007**, *129*, 2521.
[4] T. Schirmeister, C. Schmuck, P. R. Wich, *Beyer/Walter Organische Chemie*, Hirzel Verlag, Stuttgart, **2016**.
[5] G. Meng, J. Zhang, M. Szostak, *Chem. Rev.* **2021**, *121*, 12746.
[6] L. Pauling, *The Nature of the Chemical Bond*, Cornell University Press, New York, **1940**.
[7] a) L. Pauling, R. B. Corey, H. R. Branson, *Proc. Natl. Acad. Sci. USA* **1951**, *37*, 205; b) D. Eisenberg, *Proc. Natl. Acad. Sci. USA* **2003**, *100*, 11207.
[8] A. S. Edison, *Nat. Struct. Biol.* **2001**, *8*, 201.
[9] K. P. C. Vollhardt, N. E. Schore, *Organische Chemie*, Wiley-VCH, Weinheim, **2020**.
[10] H. Hart, L. E. Craine, D. J. Hart, C. M. Hadad, *Organische Chemie*, Wiley-VCH, Weinheim, **2007**.
[11] R. Szostak, J. Aubé, M. Szostak, *Chem. Commun.* **2015**, *51*, 6395.
[12] D. Zahn, *J. Phys. Chem. B* **2003**, *107*, 12303.
[13] S. J. Cho, C. Cui, J. Y. Lee, J. K. Park, S. B. Suh, J. Park, B. H. Kim, K. S. Kim, *J. Org. Chem.* **1997**, *62*, 4068.
[14] G. A. Olah, G. K. Prakash, J. Sommer, *Science* **1979**, *206*, 13.
[15] G. A. Jeffrey, J. R. Ruble, R. K. McMullan, D. J. DeFrees, J. S. Binkley, J. A. Pople, *Acta Crystallogr.* **1980**, *B36*, 2292.
[16] A. F. Holleman, E. Wiberg, N. Wiberg, G. Fischer, *Anorganische Chemie*, De Gruyter, Berlin, Boston, **2017**.
[17] J. Axhausen, C. Ritter, K. Lux, A. Kornath, *Z. Anorg. Allg. Chem.* **2013**, *639*, 65.
[18] a) M. Finze, E. Bernhardt, H. Willner, C. W. Lehmann, F. Aubke, *Inorg. Chem.* **2005**, *44*, 4206; b) D. Leitz, M. C. Bayer, Y. Morgenstern, F. Zischka, A. J. Kornath, *Chem. Eur. J.* **2018**, *24*, 15825.
[19] T. Soltner, N. R. Goetz, A. Kornath, *Eur. J. Inorg. Chem.* **2011**, 3076.
[20] M. S. G. Flett, *Spectrochim. Acta* **1962**, *18*, 1537.
[21] J. Weidlein, U. Müller, K. Dehnicke, *Schwingungsspektroskopie*, Thieme, Stuttgart, New York, **1988**.
[22] M. Azeem, M. Brownstein, R. J. Gillespie, *Can. J. Chem.* **1969**, *47*, 4159.
[23] K. Govindan, W.-Y. Lin, *Org. Lett.* **2021**, *23*, 1600.
[24] J. Axhausen, *Ludwig-Maximilians-Universität*, *Diss.*, Universitätsbibliothek der Ludwig-Maximilians-Universität, München, **2013**.
[25] Rigaku Oxford Diffraction, CrysAlisPro Software System, *Version 1.171.38.46*, Rigaku Corporation, Oxford, UK, **2015**.
[26] G. M. Sheldrick, *Acta Crystallogr.* **2015**, *A71*, 3.
[27] G. M. Sheldrick, *Acta Crystallogr.* **2015**, *C71*, 3.
[28] L. J. Farrugia, *J. Appl. Crystallogr.* **1999**, *32*, 837.
[29] A. L. Spek, *J. Appl. Crystallogr.* **2003**, *36*, 7.
[30] SCALE3 ABSPACK, *An Oxford Diffraction Program*, Oxford Diffraction Ltd, UK, **2005**.
[31] M. J. Frisch, G. W. Trucks, H. B. Schlegel, G. E. Scuseria, M. A. Robb, J. R. Cheeseman, G. Scalmani, V. Barone, B. Mennucci, G. A. Petersson, H. Nakatsuji, M. Caricato, X. Li, H. P. Hratchian, A. F. Izmaylov, J. Bloino, G. Zheng, J. L. Sonnenberg, M. Hada, M. Ehara, K. Toyota, R. Fukuda, J. Hasegawa, M. Ishida, T. Nakajima, Y. Honda, O. Kitao, H. Nakai, T. Vreven, J. A. Montgomery, Jr., J. E. Peralta, F. Ogliaro, M. Bearpark, J. J. Heyd, E. Brothers, K. N. Kudin, V. N. Staroverov, R. Kobayashi, J. Normand, K. Raghavachari, A. Rendell, J. C. Burant, S. S. Iyengar, J. Tomasi, M. Cossi, N. Rega, J. M. Millam, M. Klene, J. E. Knox, J. B. Cross, V. Bakken, C. Adamo, J. Jaramillo, R. Gomperts, R. E. Stratmann, O. Yazyev, A. J. Austin, R. Cammi, C. Pomelli, J. W. Ochterski, R. L. Martin, K. Morokuma, V. G. Zakrzewski, G. A. Voth, P. Salvador, J. J. Dannenberg, S. Dapprich, A. D. Daniels, O. Farkas, J. B. Foresman, J. V. Ortiz, J. Cioslowski, D. J. Fox, *Gaussian 09*, *Revision A.02*, Gaussian, Inc., Wallingford CT, **2009**.
[32] M. J. Frisch, G. W. Trucks, H. B. Schlegel, G. E. Scuseria, M. A. Robb, J. R. Cheeseman, G. Scalmani, V. Barone, G. A. Petersson, H. Nakatsuji, X. Li, M. Caricato, A. V. Marenich, J. Bloino, B. G. Janesko, R. Gomperts, B. Mennucci, H. P. Hratchian, J. V. Ortiz, A. F. Izmaylov, J. L. Sonnenberg, D. Williams-Young, F. Ding, F. Lipparini, F. Egidi, J. Goings, B. Peng, A. Petrone, T. Henderson, D. Ranasinghe, V. G. Zakrzewski, J. Gao, N. Rega, G. Zheng, W. Liang, M. Hada, M. Ehara, K. Toyota, R. Fukuda, J. Hasegawa, M. Ishida, T. Nakajima, Y. Honda, O. Kitao, H. Nakai, T. Vreven, K. Throssell, J. A. Montgomery, Jr., J. E. Peralta, F. Ogliaro, M. J. Bearpark, J. J. Heyd, E. N. Brothers, K. N. Kudin, V. N. Staroverov, T. A. Keith, R. Kobayashi, J. Normand, K. Raghavachari, A. P. Rendell, J. C. Burant, S. S. Iyengar, J. Tomasi, M. Cossi, J. M. Millam, M. Klene, C. Adamo, R. Cammi, J. W. Ochterski, R. L. Martin, K. Morokuma, O. Farkas, J. B. Foresman, D. J. Fox, *Gaussian 16*, *Revision A.03*, Gaussian, Inc., Wallingford CT, **2016**.
[33] R. Dennington, T. A. Keith, J. M. Millam, *GaussView, Version 6.0*, Semichem Inc., Shawnee Mission, **2016**.

Manuscript received: August 5, 2022
Revised manuscript received: August 31, 2022
Accepted manuscript online: September 2, 2022

European Journal of Inorganic Chemistry

Supporting Information

Stabilizing the C–N Double Bond Character in Fumaramide with the Aid of Superacids

Marie C. Bayer, Nikolaus Greither, Valentin Bockmair, Alexander Nitzer, and Andreas J. Kornath*

Supporting Information

Figure S1: Projection of the hydrogen bonds in C4H6N2O2 (displacement ellipsoids 50% probability). Symmetry operations: *i = 1–x, 1–y, 1–z; ii = 2–x, –y, 1–z; iii = –0.5+x, 0.5–y, –0.5+z; iv = 0.5–x, 0.5+y, 0.5–z; v = –1+x, 1+y, z; vi = 1.5–x, 0.5+y, 1.5–z; vii = 0.5+x, 0.5–y, 0.5+z.* Hydrogen bonds are drawn as dashed lines.

Figure S2: Detail of the crystal structure of C4H6N2O2 (displacement ellipsoids with 50% probability). Hydrogen bonds are drawn as dashed lines. Symmetry operations: *i = 1–x, 1–y, 1–z; ii = 2–x, –y, 1–z; iii = –1+x, 1+y, z; iv = 1.5–x, 0.5+y, 1.5–z.*

Figure S3: Projection of fumaramide in C4H6N2O2 · 2HF and the hydrogen bonds formed in the crystal structure (displacement ellipsoids with 50% probability). Symmetry operations: *i = –x, 1–y, 1–z; ii = –1+x, y, 1+z; iii = x, 1.5–y, 0.5+z; iv = –x, 0.5+y, 0.5–z; v = 1–x, 1–y, –z; vi = –x, –0.5+y, 0.5–z; vii = x, 0.5–y, 0.5+z.* Hydrogen bonds are drawn as dashed blue lines.

Figure S4: Detail of the crystal structure of C4H6N2O2 · 2HF (displacement ellipsoids with 50% probability). Hydrogen bonds are drawn as dashed lines.

Figure S5: Projection of the hydrogen bonds and intermolecular contacts in $[C4H8N2O2]^{2+}[(BF4)^{-}]_2$ (displacement ellipsoids 50% probability). Symmetry operations: *i = –x, –y, 1–z; ii = –1+x, y, z; iii = 1–x, 1–y, 1–z; iv = –x, 1–y, 1–z; v = –1.5+x, 0.5–y, –0.5+z; vi = –0.5+x, 0.5–y, –0.5+z; vii = 1–x, –y, 1–z; viii = –1+x, –1+y, z; ix = x, –1+y, z; x = 1.5–x, –0.5+y, 1.5–z; xi = 0.5–x, –0.5+y, 1.5–z.* All contacts are drawn as dashed blue lines.

Figure S6: Selected hydrogen bonds in $[C4H8N2O2]^{2+}[(BF4)^{-}]_2$ (displacement ellipsoids 50% probability). Symmetry operations: *i = –x, –y, 1–z; ii = –1+x, y, z; iii = 1–x, 1–y, 1–z; iv = –x, 1–y, 1–z; v = 1.5–x, –0.5+y, 1.5–z.* All contacts are drawn as dashed blue lines.

Figure S7: Detail of the crystal structure of $[C4H8N2O2]^{2+}[(BF4)^{-}]_2$ (displacement ellipsoids with 50% probability). Hydrogen bonds are drawn as dashed lines.

Table S1: Selected intermolecular contacts of $[C4H8N2O2]^{2+}[(BF4)^{-}]_2$ with estimated standard deviation marked in parentheses. Symmetry operations: *i = –1+x, y, z; ii = –x, 1–y, 1–z; iii = –0.5+x, 0.5–y, –0.5+z.*

Figure S8: Low-temperature Raman and IR spectra of fumaramide, $[C4D6H2N2O2]^{2+}[(BF4)^{-}]_2$ and $[C4D6H2N2O2]^{2+}[(SbF6)^{-}]_2$.

Table S2: Experimental vibrational frequencies [cm^{-1}] of $[C4H8N2O2]^{2+}[(BF4)^{-}]_2$, $[C4H8N2O2]^{2+}[(SbF6)^{-}]_2$ and calculated vibrational frequencies [cm^{-1}] of the N-coordinated HF complex of the cation $[C_4H_8N_2O_2 \cdot 2\ HF]^{2+}$.

Table S3: Experimental vibrational frequencies [cm^{-1}] of $[C4D6H2N2O2]^{2+}[(BF4)^{-}]_2$, $[C4D6H2N2O2]^{2+}[(SbF6)^{-}]_2$ and calculated vibrational frequencies [cm^{-1}] of the N-coordinated HF complex of the cation $[C_4D_6H_2N_2O_2 \cdot 2\ HF]^{2+}$.

Table S4: Experimental vibrational frequencies [cm^{-1}] and calculated vibrational frequencies [cm^{-1}] of C4H6N2O2.

Table S5: Calculated bond lengths and angles of the free cation $[C4H8N2O2]^{2+}$, the N-coordinated HF complex of the cation $[C4H8N2O2 \cdot {}^{2HF}]2+$, and the O-coordinated HF complex of the cation $[{}^{C4H8N2O2} \cdot 2HF]2+$ in comparison with the experimental structural parameters of $[C4H8N2O2]2+{}^{[}{}_{(BF4)}–]2$. The estimated standard deviation is marked in parentheses. Symmetry *operation: i = –x, –y,* **1–z.**

Table S6: Selected experimental vibrational frequencies [cm^{-1}] of $[C4H8N2O2]^{2+}[(BF4)^{-}]_2$ and calculated vibrational frequencies [cm-1] of the free cation $[C4H8N2O2]^{2+}$, the N-coordinated HF complex of the cation $[C4H8N2O2 \cdot {}^{2HF}]2+$ and the O-coordinated HF complex of the cation $[C4H8N2O2 \cdot {}^{2HF}]^{2+}$.

Figure S10: Calculated ESP surface of the N-coordinated HF complex of the cation $[C4H8N2O2 \cdot 2HF]^{2+}$ mapped onto an electron density isosurface value of 0.0004 $bohr^{-3}$ with the color scale ranging from +131.8 kcal mol^{-1} to +188.3 kcal mol^{-1}.

Table S7: Selected NBOs of $[C4H8N2O2]^{2+}$ and of C4H6N2O2 (BD = 2-center bond; BD* = 2-center antibond; LP = 1-center valence lone pair) combined with calculated values for occupancy, energy and s- and p-character.[a]

Table S8: Crystal data and structure refinement of C4H6N2O2, $[C4H8N2O2]^{2+}[(BF4)^{-}]_2$ and C4H6N2O2 · 2HF.

Table S9: Cartesian coordinates of calculated minimum structures of C4H6N2O2 at the B3LYP/aug-cc-pVTZ level of theory.

Table S10: Cartesian coordinates of calculated minimum structures of $[C4H8N2O2]^{2+}$ at the B3LYP/aug-cc-pVTZ level of theory.

Table S11: Cartesian coordinates of calculated minimum structures of the O-coordinated HF complex of the cation $[C4H8N2O2 \cdot 2HF]^{2+}$ at the B3LYP/aug-cc-pVTZ level of theory.

Table S12: Cartesian coordinates of calculated minimum structures of the N-coordinated HF complex of the cation $[C4H8N2O2 \cdot 2HF]^{2+}$ at the B3LYP/aug-cc-pVTZ level of theory.

Table S13: Cartesian coordinates of calculated minimum structures of the N-coordinated HF complex of the cation $[C4D6H2N2O2 \cdot 2HF]^{2+}$ at the B3LYP/aug-cc-pVTZ level of theory.

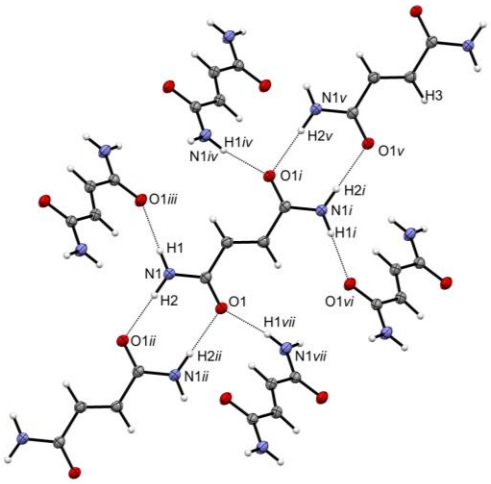

Figure S1: Projection of the hydrogen bonds in $C_4H_6N_2O_2$ (displacement ellipsoids 50% probability). Symmetry operations: *i = 1–x, 1–y, 1–z; ii = 2–x, –y, 1–z; iii = –0.5+x, 0.5–y, –0.5+z; iv = 0.5–x, 0.5+y, 0.5–z; v = –1+x, 1+y, z; vi = 1.5–x, 0.5+y, 1.5–z; vii = 0.5+x, 0.5–y, 0.5+z.* Hydrogen bonds are drawn as dashed lines.

In the crystal packing of $C_4H_6N_2O_2$, the molecules are connected via two hydrogen bonds (N1–H1···O1*iii* and N1–H2···O1*ii*), which are categorized as moderate referred to the classification of Jeffrey.[1] The hydrogen bonds N1–H2···O1*ii* form an alveolar chain structure, which is illustrated in Figure S1. These chains are linked by the hydrogen bonds N1–H1···O1*iii* building a layered structure, as it is shown in Figure S2.

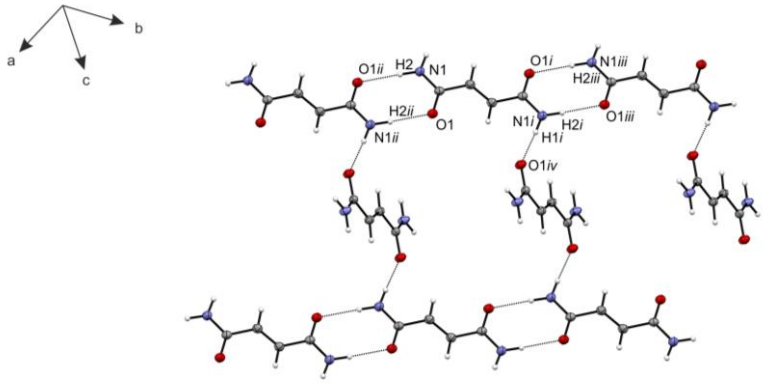

Figure S2: Detail of the crystal structure of $C_4H_6N_2O_2$ (displacement ellipsoids with 50% probability). Hydrogen bonds are drawn as dashed lines. Symmetry operations: *i = 1–x, 1–y, 1–z; ii = 2–x, –y, 1–z; iii = –1+x, 1+y, z; iv = 1.5–x, 0.5+y, 1.5–z.*

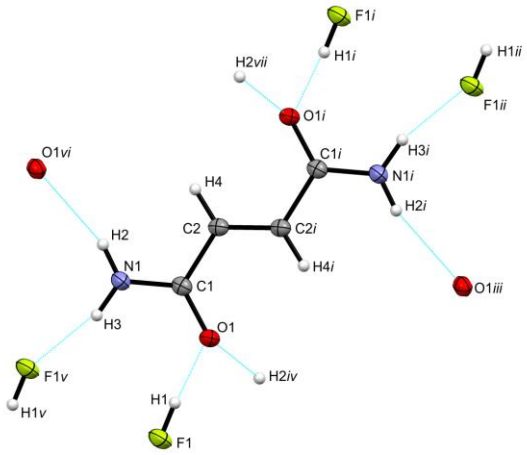

Figure S3: Projection of fumaramide in $C_4H_6N_2O_2 \cdot 2HF$ and the hydrogen bonds formed in the crystal structure (displacement ellipsoids with 50% probability). Symmetry operations: *i* = *–x, 1–y, 1–z; ii* = *–1+x, y, 1+z; iii* = *x, 1.5–y, 0.5+z; iv* = *–x, 0.5+y, 0.5–z; v* = *1–x, 1–y, –z; vi* = *–x, –0.5+y, 0.5–z; vii* = *x, 0.5–y, 0.5+z*. Hydrogen bonds are drawn as dashed blue lines.

With a donor-acceptor distance of 2.414(1) Å the hydrogen bond F1–H1···O1 is categorized as strong as defined in the classification of Jeffrey.[1] The formation of this strong hydrogen bond explains the elongation of the C1–O1 bond distance. As a result, the resonance structure II in fumaramide (Scheme 1) gains an even higher weighting. According to Jeffrey,[1] the second hydrogen bond N1*i*–H3*i*···F1*ii* is classified as moderate. The molecules of fumaramide and hydrogen fluoride are connected by these two hydrogen bonds forming alveolar chains, as depicted in Figure S4. The chains are attached by another hydrogen bond N1*i*–H2*i*···O1*iii* building a network. This hydrogen bond, formed between two formamide molecules, is classified as moderate after Jeffrey.[1]

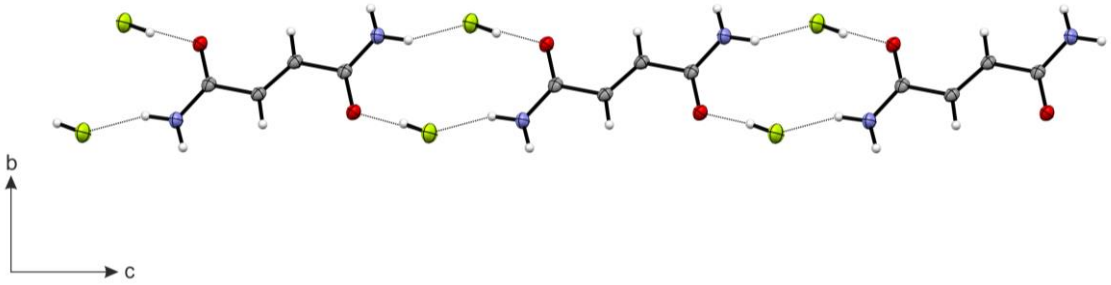

Figure S4: Detail of the crystal structure of $C_4H_6N_2O_2 \cdot 2HF$ (displacement ellipsoids with 50% probability). Hydrogen bonds are drawn as dashed lines.

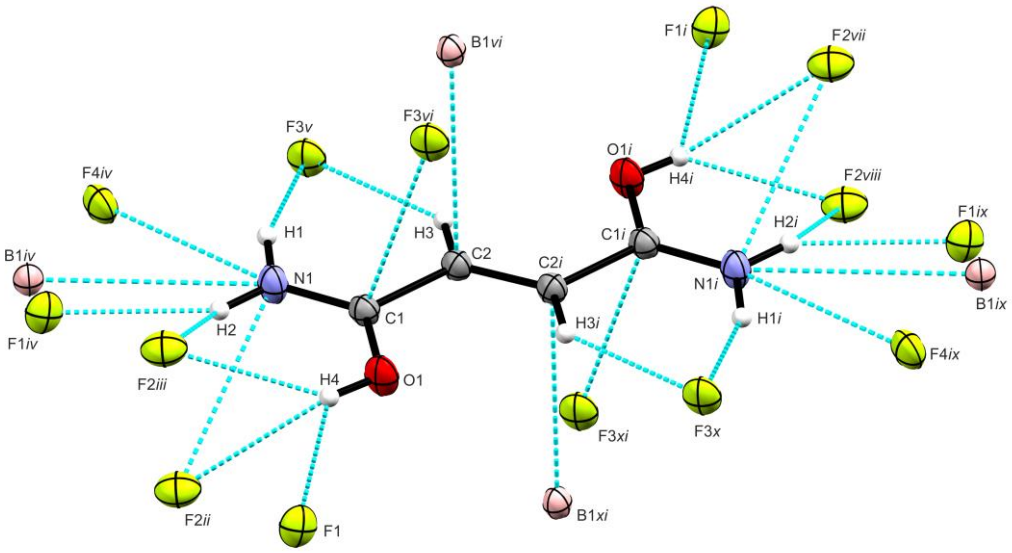

Figure S5: Projection of the hydrogen bonds and intermolecular contacts in $[C_4H_8N_2O_2]^{2+}[(BF_4)^-]_2$ (displacement ellipsoids 50% probability). Symmetry operations: *i = –x, –y, 1–z; ii = –1+x, y, z; iii = 1–x, 1–y, 1–z; iv = –x, 1–y, 1–z; v = –1.5+x, 0.5–y, –0.5+z; vi = –0.5+x, 0.5–y, –0.5+z; vii = 1–x, –y, 1–z; viii = –1+x, –1+y, z; ix = x, –1+y, z; x = 1.5–x, –0.5+y, 1.5–z; xi = 0.5–x, –0.5+y, 1.5–z.* All contacts are drawn as dashed blue lines.

In addition to the classical hydrogen bonds C2–H3···F3*v* and N1–H1···F3*v*, both categorized as moderate,[1] where the hydrogen bond donor interacts with one acceptor, three- and four-center hydrogen bonds are detected. These are interactions between one donor and two or three hydrogen bond acceptors, respectively, concerning the number of atoms bonding to the respective hydrogen atom.[2,3] An illustration of the three- and four-center hydrogen bonds is given in Figure S6. In the crystal structure of **1**, the amino nitrogen N1 forms a three-center hydrogen bond with F2*iii* and F1*iv* of two different $[BF_4]^-$ anions. The hydrogen atom H2 is located in a plane, generated by the donor atom N1 and the acceptor atoms F2*iii* and F1*iv*, as described in the literature.[3,4] The electron density is evenly shared by the H2 atom and the two acceptor fluorine atoms.[4] Since three-center hydrogen bonds are common in organic crystal structures,[5] four-center hydrogen bonds are comparatively unusual.[3] In the crystalline state of **1**, such a four-center hydrogen bond is formed between the oxygen atom O1 and three fluorine atoms F1, F2*ii*, and F2*iii*, each belonging to another $[BF_4]^-$ molecule, as illustrated in Figure S6. The donor-acceptor distances ranging from 2.735(1) Å (O1–H4···F1) to 3.125(1) Å (O1–H4···F2*ii*), are in accordance with reported distances of four-center hydrogen bonds.[6] A two-dimensional layered structure is formed via O1–H4···F1 and N1–H1···F3*v* along the *bc*-plane, which is depicted in Figure S7. In addition, bifurcated hydrogen bonds, involving two proton donors and one acceptor,[2] are observed in the crystal structure of **1**. As depicted in Figure S6, the bifurcated H-bonds are formed from the acceptor fluorine atom F3*v* to the amino group on one side and the olefinic carbon on the other side (C2*i*–H3*i*···F3*v*···H1*i*–N1*i*). In addition, the F2*iii* forms a bifurcated hydrogen bond to the hydroxy group on the one hand and the amino group on the other hand (N1–H2···F2*iii*···H4–O1). As a remarkable consequence, this F2*iii* atom is simultaneously involved in a three-center, a four-center, and a bifurcated hydrogen bond. Apart from the hydrogen bonds, further contacts are observed in the solid state of **1**. Selected intermolecular distances are summarized in Table S1.

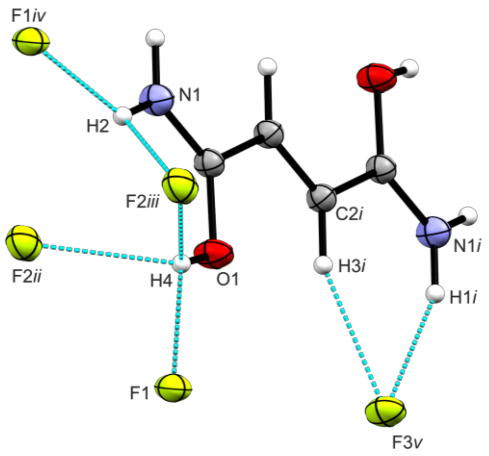

Figure S6: Selected hydrogen bonds in $[C_4H_8N_2O_2]^{2+}[(BF_4)^-]_2$ (displacement ellipsoids 50% probability). Symmetry operations: *i = –x, –y, 1–z; ii = –1+x, y, z; iii = 1–x, 1–y, 1–z; iv = –x, 1–y, 1–z; v = 1.5–x, –0.5+y, 1.5–z.* All contacts are drawn as dashed blue lines.

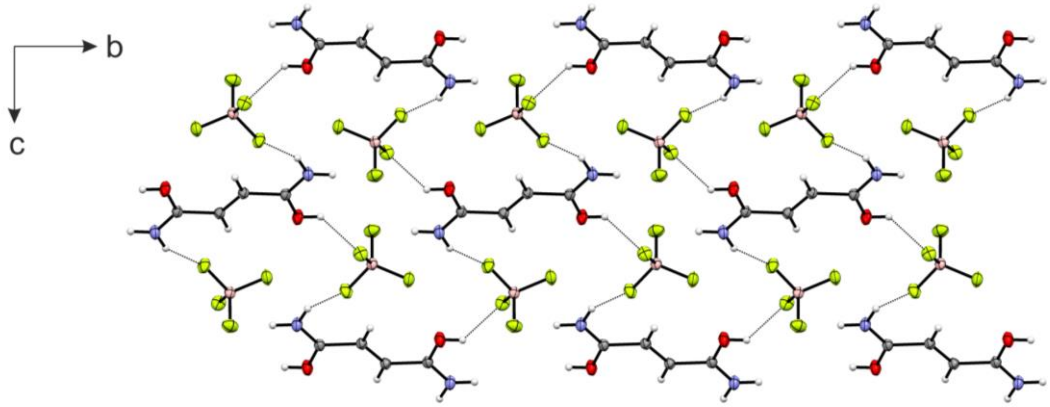

Figure S7: Detail of the crystal structure of $[C_4H_8N_2O_2]^{2+}[(BF_4)^-]_2$ (displacement ellipsoids with 50% probability). Hydrogen bonds are drawn as dashed lines.

Table S1: Selected intermolecular contacts of $[C_4H_8N_2O_2]^{2+}[(BF_4)^-]_2$ with estimated standard deviation marked in parentheses. Symmetry operations: *i = –1+x, y, z; ii = –x, 1–y, 1–z; iii = –0.5+x, 0.5–y, –0.5+z.*

Intermolecular contact [Å]			
N1···F2*i*	2.951(1)	C2···B1*iii*	3.375(2)
N1···F4*ii*	2.938(1)	C1···F3*iii*	3.055(1)
N1···B1*ii*	3.408(2)		

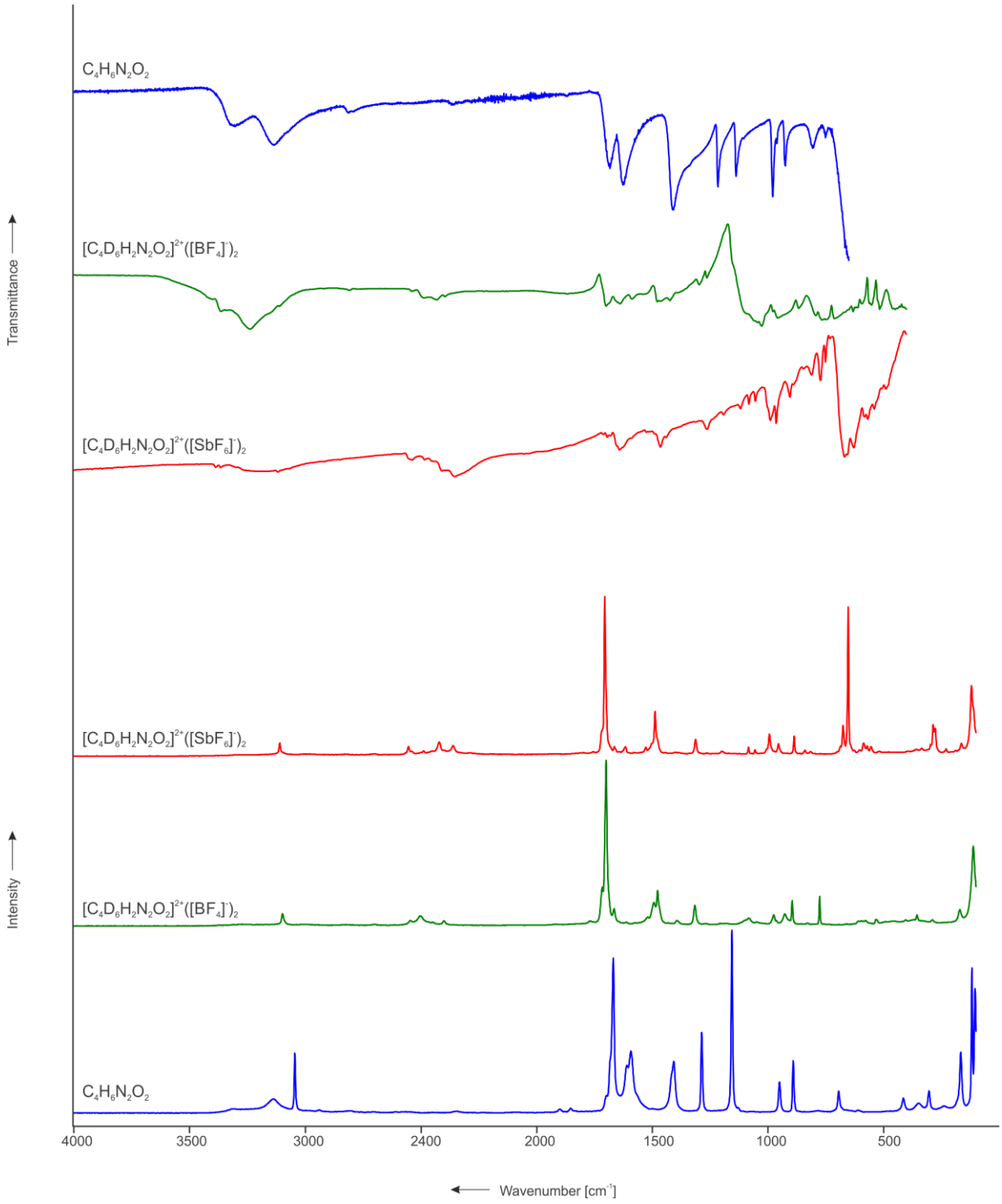

Figure S8: Low-temperature Raman and IR spectra of fumaramide, $[C_4D_6H_2N_2O_2]^{2+}[(BF_4)^-]_2$ and $[C_4D_6H_2N_2O_2]^{2+}[(SbF_6)^-]_2$.

Table S2: Experimental vibrational frequencies [cm^{-1}] of $[C_4H_8N_2O_2]^{2+}[(BF_4)^-]_2$, $[C_4H_8N_2O_2]^{2+}[(SbF_6)^-]_2$ and calculated vibrational frequencies [cm^{-1}] of the N-coordinated HF complex of the cation $[C_4H_8N_2O_2 \cdot 2HF]^{2+}$.

$[C_4H_8N_2O_2]^{2+}[(BF_4)^-]_2$ exp.[a]		$[C_4H_8N_2O_2]^{2+}[(SbF_6)^-]_2$ exp.[a]		N-coordinated HF complex of the cation $[C_4H_8N_2O_2 \cdot 2HF]^{2+}$. calc.[b]	Assignment[d]		
IR	Raman	IR	Raman	IR/Raman			
				3695 (0/185)	ν_1	A_g	ν_s(O–H)
		3387 vs					[c]
3369 w		3367 vs		3693 (550/0)	ν_{29}	B_u	ν_{as}(O–H)
	3376 (2)		3327 (1)	3557 (0/153)	ν_2	A_g	ν_s(NH_2)
3265 w		3275 vs		3556 (438/0)	ν_{30}	B_u	ν_{as}(NH_2)
		3202 vs					[c]
	3255 (2)		3273 (1)	3359 (0/243)	ν_3	A_g	ν_s(NH_2)
		3161 vs		3355 (1616/0)	ν_{31}	B_u	ν_{as}(NH_2)
3105 w		3121 vs		3200 (27/0)	ν_{32}	B_u	ν_{as}(C–H)
		2453 m					[c]
	3095 (7)		3109 (4)	3195 (0/70)	ν_4	A_g	ν_s(C–H)
	1709 (100)		1719 (29)	1741 (0/292)	ν_5	A_g	ν_s(C=N)
		1718 m					[c]
1697 m		1697 vs		1726 (647/0)	ν_{33}	B_u	ν_{as}(C=N)
		1618 m					[c]
	1666 (42)		1665 (24)	1699 (0/214)	ν_6	A_g	ν(C=C)
1591 w		1599 s		1621 (175/0)	ν_{34}	B_u	ν_{as}(C–O)
			1581 (3)				[c]
			1541 (4)	1601 (0/19)	ν_7	A_g	ν_s(C–O)
		1539 m					[c]
	1521 (17)		1518 (4)	1528 (0/120)	ν_8	A_g	δ_s(HNCOH)
1502 w		1512 m		1520 (264/0)	ν_{35}	B_u	δ_{as}(HNCOH)
1458 w							[c]
1448 w		1421 m					[c]
		1371 w					[c]
		1333 w					[c]
	1318 (17)		1316 (3)	1351 (0/41)	ν_9	A_g	δ_s(HCCH)
1294 w							[c]
1263 vw		1257 m		1305 (9/0)	ν_{36}	B_u	δ_{as}(HCCH)
1190 w	1190 (13)			1186 (0/72)	ν_{10}	A_g	δ_s(COH)
		1236 s	1238 (12)	1177 (374/0)	ν_{37}	B_u	δ_{as}(COH)
1043 vs		1067 w		1104 (1/0)	ν_{38}	B_u	ρ_{as}(NH_2)
	1072 (11)		1071 (11)	1104 (0/28)	ν_{11}	A_g	ρ_s(NH_2)
1024 vs				1021 (52/0)	ν_{16}	A_u	γ_{as}(HCCH)
		966 m					[c]
	962 (14)		969 (4)	972 (0/10)	ν_{12}	A_g	ν_s(C–C)
	896 (20)		888 (7)	943 (0/7)	ν_{23}	B_g	γ_s(HCCH)
937 w		947 m		939 (31/0)	ν_{39}	B_u	ν_{as}(C–C)
777 m		789 s		807 (204/0)	ν_{17}	A_u	ω_{as}(NH_2)
				804 (0/0)	ν_{24}	B_g	ω_s(NH_2)
		754 w		771 (33/0)	ν_{18}	A_u	γ_{as}(CCNO)
	748 (3)			731 (0/1)	ν_{25}	B_g	τ_s(NH_2)
719 m		737 m		690 (193/0)	ν_{19}	A_u	τ_{as}(NH_2)
	644 (10)			650 (0/12)	ν_{13}	A_g	δ_s(CNO)
	576 (3)		579 (4)	577 (0/1)	ν_{26}	B_g	γ_s(CCNO)
557 w		557 m		572 (23/0)	ν_{40}	B_u	δ_{as}(CCO)
		498 w		559 (10/0)	ν_{41}	B_u	δ_{as}(CCN)
				520 (0/2)	ν_{27}	B_g	γ_s(H_2NCOH)
				517 (162/0)	ν_{20}	A_u	γ_{as}(H_2NCOH)
	357 (9)		345 (4)	403 (0/4)	ν_{14}	A_g	δ_s(CCN)
	298 (5)		296 (11)	276 (0/2)	ν_{15}	A_g	δ_s(CCC)
	172 (15)		170 (5)	160 (0/1)	ν_{28}	B_g	γ_s(HCCH)
				151 (4/0)	ν_{21}	A_u	γ_{as}(CCCC)
	114 (76)		114 (15)	126 (2/0)	ν_{42}	B_u	δ_{as}(CCC)
				83 (14/0)	ν_{22}	A_u	τ_{as}(CON)
Vibrations of anions $[BF_4]^-$ and $[SbF_6]^-$							
	776 (26)		716 (2)				$[BF_4]^-$; $[SbF_6]^-$
		671 vs	674 (100)				$[SbF_6]^-$
		654 s	653 (47)				$[SbF_6]^-$
617 w		636 s	617 (6)				$[BF_4]^-$; $[SbF_6]^-$
600 w			601 (4)				$[BF_4]^-$; $[SbF_6]^-$
573 w		581 w	584 (4)				$[BF_4]^-$; $[SbF_6]^-$
521 w	526 (6)		546 (5)				$[BF_4]^-$; $[SbF_6]^-$
405 vw	406 (7)						$[BF_4]^-$
			394 (4)				$[SbF_6]^-$
			307 (11)				$[SbF_6]^-$
			286 (12)				$[SbF_6]^-$
			280 (11)				$[SbF_6]^-$

Table is continued on the following page.

	278 (11)	$[SbF_6]^-$
	260 (6)	$[SbF_6]^-$
	230 (7)	$[SbF_6]^-$
	124 (24)	$[SbF_6]^-$

[a] Abbrevations for IR intensities: v = very, s = strong, m = medium, w = weak. IR intensities in km/mol; Raman intensities in $Å^4/u$. Experimental Raman activities are relative to a scale of 1 to 100.

[b] Calculated on the B3LYP/aug-cc-pVTZ level of theory.

[c] Very probably combination tones/ overtones.

[d] ρ = rocking, τ = twisting, ω = wagging

Table S3: Experimental vibrational frequencies [cm^{-1}] of $[C_4D_6H_2N_2O_2]^{2+}[(BF_4)^-]_2$, $[C_4D_6H_2N_2O_2]^{2+}[(SbF_6)^-]_2$ and calculated vibrational frequencies [cm^{-1}] of the N-coordinated HF complex of the cation $[C_4D_6H_2N_2O_2 \cdot 2HF]^{2+}$.

$[C_4D_6H_2N_2O_2]^{2+}[(BF_4)^-]_2$ exp.[a]		$[C_4D_6H_2N_2O_2]^{2+}[(SbF_6)^-]_2$ exp.[a]		N-coordinated HF complex of the cation $[C_4D_6H_2N_2O_2 \cdot 2HF]^{2+}$ calc.[b]	Assignment[d]		
IR	Raman	IR	Raman	IR/Raman			
3400 s		3387 vs					[c]
3364 vs		3365 vs					[c]
3238 vs		3205 vs					[c]
3111 s		3119 vs		3200 (44/0)	ν_{29}	B_u	ν_{as}(C–H)
	3099 (7)		3111 (8)	3196 (0/80)	ν_1	A_g	ν_s(C–H)
			2554 (6)				[c]
	2546 (3)		2540 (3)	2693 (0/86)	ν_2	A_g	ν_s(O–D)
2540 s		2538 vs		2691 (325/0)	ν_{30}	B_u	ν_{as}(O–D)
	2504 (6)		2489 (3)	2628 (0/59)	ν_3	A_g	ν_s(ND_2)
2486 s		2484 vs		2628 (276/0)	ν_{31}	B_u	ν_{as}(ND_2)
2430 s							[c]
	2451 (2)		2421 (9)	2447 (0/93)	ν_4	A_g	ν_s(ND_2)
2395 s	2401 (3)	2409 vs		2444 (896/0)	ν_{32}	B_u	ν_{as}(ND_2)
		2355 vs	2361 (7)				[c]
	1768 (3)		1757 (3)				[c]
	1716 (24)	1711 s					[c]
1699 s	1700 (100)	1693 s	1706 (100)	1723 (0/498)	ν_5	A_g	ν_s(C=N)
		1682 s					[c]
1639 s		1641 vs		1664 (572/0)	ν_{33}	B_u	ν_{as}(C=N)
	1665 (10)		1664 (6)	1630 (0/14)	ν_6	A_g	ν(C=C)
1587 s	1612 (2)		1616 (6)				[c]
1537 s		1526 s					[c]
	1520 (5)		1528 (6)				[c]
	1493 (14)						[c]
1477 s	1477 (21)		1488 (28)	1483 (0/174)	ν_7	A_g	ν_s(C–O)
1462 s		1464 s		1460 (394/0)	ν_{34}	B_u	ν_{as}(C–O)
1423 s		1441 s					[c]
	1394 (3)						[c]
1296 m	1316 (13)		1313 (10)	1354 (0/40)	ν_8	A_g	δ_s(HCCH)
1263 m		1263 s		1322 (6/0)	ν_{35}	B_u	δ_{as}(HCCH)
		1192 m	1200 (3)				[c]
		1119 m					[c]
	1083 (5)	1082 m	1084 (6)	1216 (0/12)	ν_9	A_g	σ_s(ND_2)
1043 vs		1053 m		1212 (18/0)	ν_{36}	B_u	σ_{as}(ND_2)
1026 vs				1021 (44/0)	ν_{16}	A_u	γ_{as}(HCCH)
	1049 (3)		1056 (4)	994 (0/27)	ν_{10}	A_g	δ_s(COD)
978 vs		989 s		988 (147/0)	ν_{37}	B_u	δ_{as}(COD)
	975 (7)		994 (14)	941 (0/29)	ν_{11}	A_g	ν_s(C–C)
	927 (7)		954 (8)	941 (0/7)	ν_{23}	B_g	γ_s(HCCH)
957 vs		964 s		883 (29/0)	ν_{38}	B_u	ν_{as}(C–C)
		905 m					[c]
866 vs				850 (24/0)	ν_{39}	B_u	δ_{as}(DNCOD)
	896 (15)	889 w	887 (12)	842 (0/3)	ν_{12}	A_g	δ_s(DNCOD)
		847 w	840 (4)				[c]
	828 (2)	810 w	816 (3)				[c]
793 vs							[c]
766 vs		773 w		768 (36/0)	ν_{17}	A_u	γ_{as}(CCNO)
748 vs		750 w					[c]
	609 (3)		603 (4)	667 (0/1)	ν_{24}	B_g	γ_s(CCNO)
631 vs		629 vs		604 (101/0)	ν_{18}	A_u	ω_{as}(ND_2)
	596 (3)		587 (8)	602 (0/1)	ν_{25}	B_g	ω_s(ND_2)
	579 (3)		572 (6)	571 (0/8)	ν_{13}	A_g	δ_s(CNO)
594 s		582 m		552 (23/0)	ν_{40}	B_u	δ_{as}(CCO)
561 s		569 s		522 (92/0)	ν_{19}	A_u	τ_{as}(ND_2)
552 s		540 m		487 (6/0)	ν_{41}	B_u	δ_{as}(CCN)
	533 (4)		520 (3)	470 (0/0)	ν_{26}	B_g	τ_s(ND_2)
	406 (4)		395 (3)	379 (0/1)	ν_{27}	B_g	γ_s(D_2NCOD)
517 vs		507 w		377 (70/0)	ν_{20}	A_u	γ_{as}(D_2NCOD)
	356 (7)		359 (4)	338 (0/1)	ν_{14}	A_g	δ_s(CCN)
	289 (4)		297 (7)	268 (0/2)	ν_{15}	A_g	δ_s(CCC)
	172 (10)		164 (8)	156 (0/1)	ν_{28}	B_g	γ_s(HCCH)
				142 (4/0)	ν_{21}	A_u	γ_{as}(CCCC)
				123 (2/0)	ν_{42}	B_u	δ_{as}(CCC)
				78 (11/0)	ν_{22}	A_u	τ_{as}(CON)
Vibrations of anions $[BF_4]^-$ and $[SbF_6]^-$							
	777 (18)		686 (6)				$[BF_4]^-$; $[SbF_6]^-$

Table is continued on the following page.

712 vs		667 vs	676 (19)	$[BF_4]^-$; $[SbF_6]^-$
621 s		656 vs	654 (93)	$[BF_4]^-$; $[SbF_6]^-$
611 s			630 (4)	$[BF_4]^-$; $[SbF_6]^-$
			626 (4)	$[SbF_6]^-$
			554 (6)	$[SbF_6]^-$
461 vs	462 (3)	490 w		$[BF_4]^-$; $[SbF_6]^-$
449 vs			336 (5)	$[BF_4]^-$; $[SbF_6]^-$
442 vs			286 (20)	$[BF_4]^-$; $[SbF_6]^-$
428 s			278 (17)	$[BF_4]^-$; $[SbF_6]^-$
			230 (4)	$[SbF_6]^-$
	113 (48)		120 (44)	$[BF_4]^-$; $[SbF_6]^-$

[a] Abbrevations for IR intensities: v = very, s = strong, m = medium, w = weak. IR intensities in km/mol; Raman intensities in $Å^4/u$. Experimental Raman activities are relative to a scale of 1 to 100.

[b] Calculated on the B3LYP/aug-cc-pVTZ level of theory.

[c] Very probably combination tones/ overtones.

[d] σ = scissoring, τ = twisting, ω = wagging

Table S4: Experimental vibrational frequencies [cm^{-1}] and calculated vibrational frequencies [cm^{-1}] of $C_4H_6N_2O_2$.

$C_4H_6N_2O_2$ exp.[a]		$C_4H_6N_2O_2$ calc.[b]	Assignment[d]		
IR	Raman	IR/Raman			
		3721 (92/0)	ν_{25}	B_u	$\nu_{as}(NH_2)$
	3309 (2)	3721 (0/115)	ν_1	A_g	$\nu_s(NH_2)$
	3138 (8)	3589 (0/359)	ν_2	A_g	$\nu_s(NH_2)$
3302 w		3589 (121/0)	ν_{26}	B_u	$\nu_{as}(NH_2)$
3135 w		3165 (4/0)	ν_{27}	B_u	ν_{as}(C–H)
	3046 (33)	3161 (0/83)	ν_3	A_g	ν_s(C–H)
	1669 (85)	1759 (0/29)	ν_4	A_g	ν_s(C=O)
1682 m		1734(619/0)	ν_{28}	B_u	ν_{as}(C=O)
	1610 (26)	1702 (0/294)	ν_5	A_g	ν(C=C)
	1593 (34)	1623 (0/15)	ν_6	A_g	$\sigma_s(NH_2)$
1626 m		1620 (240/0)	ν_{29}	B_u	$\sigma_{as}(NH_2)$
1410 s		1378 (514/0)	ν_{30}	B_u	ν_{as}(C–N)
	1408 (28)	1365 (0/4)	ν_7	A_g	ν_s(C–N)
	1286 (44)	1296 (0/57)	ν_8	A_g	δ_s(HCCH)
1216 m		1221 (57/0)	ν_{31}	B_u	δ_{as}(HCCH)
	1156 (100)	1097 (0/29)	ν_9	A_g	$\rho_s(NH_2)$
1137 m		1076 (11/0)	ν_{32}	B_u	$\rho_{as}(NH_2)$
979 s		1012 (40/0)	ν_{14}	A_u	γ_{as}(HCCH)
961 w	951 (17)	928 (0/5)	ν_{20}	B_g	γ_s(HCCH)
	891 (29)	917 (0/9)	ν_{10}	A_g	ν_s(C–C)
924 m		899 (4/0)	ν_{33}	B_u	ν_{as}(C–C)
806 w		784 (12/0)	ν_{15}	A_u	γ_{as}(CCNO)
751 w		684 (0/0)	ν_{21}	B_g	γ_s(CCNO)
	694 (12)	656 (0/7)	ν_{11}	A_g	δ_s(CNO)
	613 (2)	596 (37/0)	ν_{34}	B_u	δ_{as}(CCO)
		582 (18/0)	ν_{16}	A_u	$\tau_{as}(NH_2)$
		533 (0/0)	ν_{22}	B_g	$\tau_s(NH_2)$
	415 (8)	517 (15/0)	ν_{35}	B_u	δ_{as}(CCN)
	349 (5)	357 (0/2)	ν_{12}	A_g	δ_s(CCN)
	305 (12)	274 (0/3)	ν_{13}	A_g	δ_s(CCC)
		234 (362/0)	ν_{17}	A_u	$\omega_{as}(NH_2)$
	238 (4)	230 (0/0)	ν_{23}	B_g	$\omega_s(NH_2)$
	167 (33)	146 (1/0)	ν_{18}	A_u	γ_{as}(CCCC)
	119 (79)	141 (0/1)	ν_{24}	B_g	γ_s(HCCH)
	105 (68)	124 (19/0)	ν_{36}	B_u	δ_{as}(CCC)
		52 (28/0)	ν_{19}	A_u	τ_{as}(CON)

[a] Abbrevations for IR intensities: v = very, s = strong, m = medium, w = weak. IR intensities in km/mol; Raman intensities in Å^4/u. Experimental Raman activities are relative to a scale of 1 to 100.

[b] Calculated on the B3LYP/aug-cc-pVTZ level of theory.

[c] Very probably combination tones/ overtones.

[d] σ = scissoring, ρ = rocking, τ = twisting, ω = wagging

Table S5: Calculated bond lengths and angles of the free cation $[C_4H_8N_2O_2]^{2+}$, the N-coordinated HF complex of the cation $[C_4H_8N_2O_2 \cdot 2HF]^{2+}$, and the O-coordinated HF complex of the cation $[C_4H_8N_2O_2 \cdot 2HF]^{2+}$ in comparison with the experimental structural parameters of $[C_4H_8N_2O_2]^{2+}[(BF_4)^-]_2$. The estimated standard deviation is marked in parentheses. Symmetry operation: *i* = *–x, –y, 1–z*.

	Free cation[a] $[C_4H_8N_2O_2]^{2+}$	N-coordinated HF complex of the cation[a] $[C_4H_8N_2O_2 \cdot 2HF]^{2+}$	O-coordinated HF complex of the cation[a] $[C_4H_8N_2O_2 \cdot 2HF]^{2+}$	Crystal structure of $[C_4H_8N_2O_2]^{2+}[(BF_4)^-]_2$	
Bond length [Å]					
C1–O1	1.296	1.300	1.291	C1–O1 (C=O)	1.301(1)
C1–N1	1.303	1.300	1.305	C1–N1 (C–N)	1.288(2)
C1–C2	1.473	1.471	1.472	C1–C2 (C–C)	1.468(2)
C2–C3	1.336	1.336	1.335	C2–C2*i* (C=C)	1.324(2)
C3–C4	1.473	1.471	1.472		
C4–O2	1.296	1.300	1.291		
C4–N2	1.303	1.300	1.305		
Bond angle [°]					
O1–C1–N1	123.8	124.0	123.2	O1–C1–N1	123.8(1)
O1–C1–C2	116.2	116.2	116.9	O1–C1–C2	116.4(1)
N1–C1–C2	120.0	119.8	119.9	N1–C1–C2	119.8(1)
C1–C2–C3	121.7	121.6	121.6	C1–C2–C2*i*	121.3(1)
O2–C4–N2	123.8	124.0	123.2		
O2–C4–C3	116.2	116.2	116.9		
N2–C4–C3	120.0	119.8	119.9		
C2–C3–C4	121.7	121.6	121.6		
Angle of torsion [°]					
O1–C1–C2–C3	0.0	0.0	0.0	O1–C1–C2–C2*i*	1.9(2)
N1–C1–C2–C3	180.0	180.0	–180.0	N1–C1–C2–C2*i*	–178.1(1)
C1–C2–C3–C4	180.0	–180.0	–180.0	C1–C2–C2*i*–C1*i*	–180.0(1)
O2–C4–C3–C2	0.0	0.0	0.0		
N2–C4–C3–C2	180.0	–180.0	180.0		

[a] Calculated at the B3LYP/aug-cc-pVTZ level of theory.

Table S6: Selected experimental vibrational frequencies [cm^{-1}] of $[C_4H_8N_2O_2]^{2+}[(BF_4)^-]_2$ and calculated vibrational frequencies [cm^{-1}] of the free cation $[C_4H_8N_2O_2]^{2+}$, the N-coordinated HF complex of the cation $[C_4H_8N_2O_2 \cdot 2HF]^{2+}$ and the O-coordinated HF complex of the cation $[C_4H_8N_2O_2 \cdot 2HF]^{2+}$.

$[C_4H_8N_2O_2]^{2+}[(BF_4)^-]_2$ exp.[a]		Free cation $[C_4H_8N_2O_2]^{2+}$ calc.[b]	N-coordinated HF complex of the cation[a] $[C_4H_8N_2O_2 \cdot 2HF]^{2+}$ calc.[b]	O-coordinated HF complex of the cation[a] $[C_4H_8N_2O_2 \cdot 2HF]^{2+}$ calc.[b]	Assignment[c]
IR	Raman	IR/Raman	IR/Raman	IR/Raman	
3369 w		3674 (626/0)	3693 (550/0)	3405 (1879/1)	ν_{as}(O–H)
	3376 (2)	3594 (0/80)	3557 (0/153)	3609 (0/80)	ν_s(NH_2)
3265 w		3594 (296/0)	3556 (438/0)	3609 (391/0)	ν_{as}(NH_2)
	3255 (2)	3492 (0/205)	3359 (0/243)	3498 (0/327)	ν_s(NH_2)
3105 w		3195 (25/0)	3200 (27/0)	3197 (20/0)	ν_{as}(C–H)
	3095 (7)	3190 (0/68)	3195 (0/70)	3192 (0/68)	ν_s(C–H)
	1709 (100)	1735 (0/305)	1741 (0/292)	1735 (0/35)	ν_s(C=N)
1697 m		1716 (732/0)	1726 (647/0)	1711 (701/0)	ν_{as}(C=N)
	1666 (42)	1691 (0/179)	1699 (0/214)	1690 (0/153)	ν(C=C)
1591 w		1609 (97/0)	1621 (175/0)	1605 (85/0)	ν_{as}(C–O)
	1521 (17)	1526 (0/119)	1528 (0/120)	1551 (0/74)	δ_s(HNCOH)
1502 w		1522 (312/0)	1520 (264/0)	1552 (416/0)	δ_{as}(HNCOH)
	1318 (17)	1354 (0/32)	1351 (0/41)	1354 (0/16)	δ_s(HCCH)
1263 vw		1300 (9/0)	1305 (9/0)	1294 (0/0)	δ_{as}(HCCH)
1190 w	1190 (13)	1182 (0/66)	1186 (0/72)	1283 (0/106)	δ_s(COH)
1043 vs		1075 (2/0)	1104 (1/0)	1090 (5/0)	ρ_{as}(NH_2)
	1072 (11)	1076 (0/27)	1104 (0/28)	1091 (0/35)	ρ_s(NH_2)
1024 vs		1005 (54/0)	1021 (52/0)	1007 (51/0)	γ_{as}(HCCH)
	962 (14)	967 (0/10)	972 (0/10)	970 (0/11)	ν_s(C–C)
	896 (20)	932 (0/7)	943 (0/7)	934 (0/7)	γ_s(HCCH)
937 w		934 (30/0)	939 (31/0)	941 (25/0)	ν_{as}(C–C)
777 m		710 (357/0)	807 (204/0)	705 (161/0)	ω_{as}(NH_2)
	748 (3)	688 (0/1)	731 (0/1)	662 (0/0)	τ_s(NH_2)
719 m		656 (14/0)	690 (193/0)	634 (100/0)	τ_{as}(NH_2)
	644 (10)	644 (0/10)	650 (0/12)	666 (0/9)	δ_s(CNO)
	576 (3)	566 (0/1)	577 (0/1)	567 (0/0)	γ_s(CCNO)
557 w		574 (29/0)	572 (23/0)	595 (5/0)	δ_{as}(CCO)
	357 (9)	373 (0/3)	403 (0/4)	377 (0/3)	δ_s(CCN)
	298 (5)	275 (0/2)	276 (0/2)	309 (0/2)	δ_s(CCC)
	172 (15)	147 (0/1)	160 (0/1)	159 (0/1)	γ_s(HCCH)
	114 (76)	138 (10/0)	126 (2/0)	142 (21/0)	δ_{as}(CCC)

[a] Abbrevations for IR intensities: v = very, s = strong, m = medium, w = weak. IR intensities in km/mol; Raman intensities in Å^4/u. Experimental Raman activities are relative to a scale of 1 to 100.
[b] Calculated on the B3LYP/aug-cc-pVTZ level of theory.
[c] ρ = rocking, ω = wagging, τ = twisting

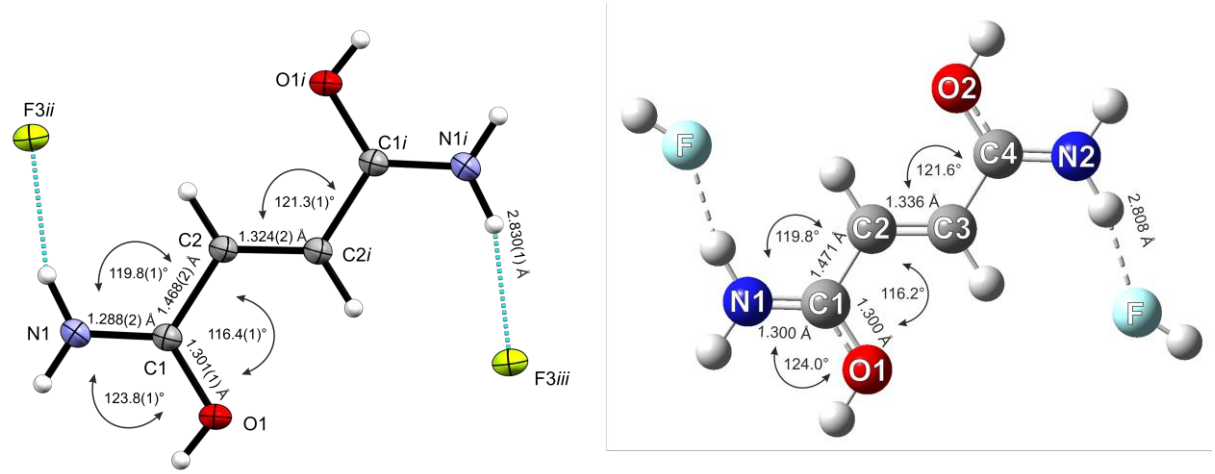

Figure S9: Calculated structure of the cation with N-coordinated HF molecules $[C_4H_8N_2O_2 \cdot 2HF]^{2+}$ (right) compared with the experimental structure of 1 together with the N1–H1···F3*ii* hydrogen bond (left) including bond lengths and angles. Symmetry operations: *i = –x, –y, 1–z; ii = –1.5+x, 0.5–y, –0.5+z; iii = 1.5–x, –0.5+y, 1.5–z.*

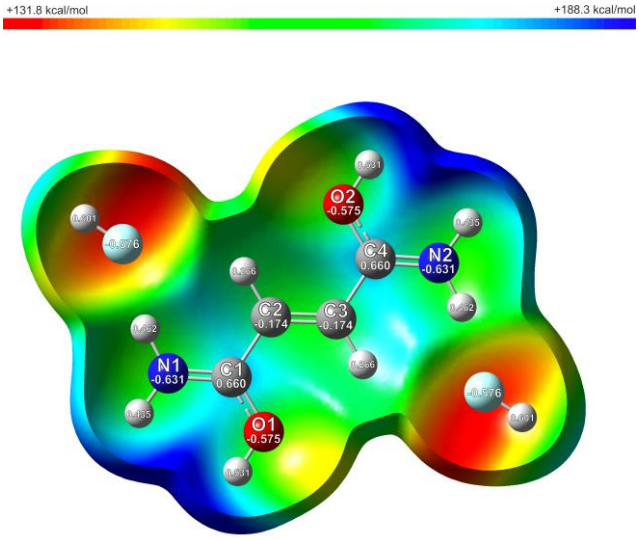

Figure S10: Calculated ESP surface of the N-coordinated HF complex of the cation $[C_4H_8N_2O_2 \cdot 2HF]^{2+}$ mapped onto an electron density isosurface value of 0.0004 bohr^{-3} with the color scale ranging from +131.8 kcal mol^{-1} to +188.3 kcal mol^{-1}.

Table S7: Selected NBOs of $[C_4H_8N_2O_2]^{2+}$ and of $C_4H_6N_2O_2$ (BD = 2-center bond; BD* = 2-center antibond; LP = 1-center valence lone pair) combined with calculated values for occupancy, energy and s- and p-character.[a]

	Bond	Occupancy	Energy	s-, p- character
$[C_4H_8N_2O_2]^{2+}$	BD(2) C1–N1	1.97 e$^-$	–0.72856	C1 s(0.00%), p 1.00 (99.71%) N1 s(0.00%), p 1.00 (99.86%)
	BD*(2) C1–N1	0.33 e$^-$	–0.39201	C1 s(0.00%), p 1.00 (99.71%) N1 s(0.00%), p 1.00 (99.86%)
$C_4H_6N_2O_2$	BD(1) C1–O1	1.99 e$^-$	–1.05798	C1 s(34.05%), p 1.93 (65.88%) O1 s(39.10%), p 1.54 (60.24%)
	BD(2) C1–O1	1.98 e$^-$	–0.37363	C1 s(0.00%), p 1.00 (99.75%) O1 s(0.00%), p 1.00 (99.63%)
	LP(1) N1	1.74 e$^-$	–0.28173	s(0.00%), p 1.00 (99.92%)
	LP(1) O1	1.98 e$^-$	–0.70567	s(60.83%), p 0.64 (39.06%)
	LP(2) O1	1.86 e$^-$	–0.25711	s(0.01%), p 1.00 (99.74%)
	BD*(1) C1–O1	0.01 e$^-$	0.60271	C1 s(34.05%), p 1.93 (65.88%) O1 s(39.10%), p 1.54 (60.24%)
	BD*(2) C1–O1	0.30 e$^-$	0.00283	C1 s(0.00%), p 1.00 (99.75%) O1 s(0.00%), p 1.00 (99.63%)

[a] calculated on the B3LYP/aug-cc-pVTZ level of theory.

Table S8: Crystal data and structure refinement of $C_4H_6N_2O_2$, $[C_4H_8N_2O_2]^{2+}[(BF_4)^-]_2$ and $C_4H_6N_2O_2 \cdot 2HF$.

	$C_4H_6N_2O_2$	$[C_4H_8N_2O_2]^{2+}[(BF_4)^-]_2$	$C_4H_6N_2O_2 \cdot 2HF$
Molecular Formula	$C_4H_6N_2O_2$	$C_4H_8B_2F_8N_2O_2$	$C_4H_8F_2N_2O_2$
M_r[g·mol^{-1}]	114.11	289.74	154.12
Crystal size [mm^3]	0.261 x 0.130 x 0.107	0.376 x 0.218 x 0.198	0.291 x 0.086 x 0.079
Crystal system	monoclinic	monoclinic	monoclinic
Space group	$P2_1/n$	$P2_1/n$	$P2_1/c$
a [Å]	3.7466(5)	4.9361(3)	3.6399(2)
b [Å]	7.0459(11)	9.8047(6)	9.4069(5)
c [Å]	9.6140(9)	10.5049(7)	9.4220(4)
α [°]	90	90	90
β [°]	100.123(11)	99.188(7)	90.296(5)
γ [°]	90	90	90
V [A^3]	249.84(6)	501.88(6)	322.61(3)
Z	2	2	2
ρ_{calc} [g·cm^{-3}]	1.517	1.917	1.587
μ [mm^{-1}]	0.123	0.231	0.160
$\lambda_{MoK\alpha}$ [Å]	0.71073	0.71073	0.71073
F(000)	120	288	160
T [K]	115(2)	104(2)	100(2)
h, k, l range	–5:4; –9:6; –12:13	–6:7; –12:14; –15:15	–4:4; –12:12; –12:11
Measured reflexes	1159	4936	2446
Unique reflexes	668	1664	714
R_{int}	0.0232	0.0285	0.0320
Parameters	49	98	62
R(F)/wR(F^2)[a)] (all data)	0.0625/0.0993	0.0560/0.0870	0.0398/0.0743
Weighting scheme[b)]	0.036900/0.074800	0.033300/0.082700	0.028200/0.064300
S (Gof)[c)]	1.028	1.049	1.070
Residual density [e·Å^{-3}]	0.258/–0.181	0.434/–0.233	0.233/–0.146
Device	Oxford XCalibur	Oxford XCalibur	Oxford XCalibur
CCDC	2178670	2178675	2178678

[a)] $R_1 = \Sigma||F_o|-|F_c||/\Sigma|F_o|$;
[b)] $wR_2 = [\Sigma[w(F_o^2-F_c^2)^2]/\Sigma[w(F_o)^2]]^{1/2}$; $w = [\sigma_c^2(F_o^2)+(xP)^2+yP]^{-1}$; $P = (F_o^2+2F_c^2)/3$
[c)] GoF = $\{\Sigma[w(F_o^2-F_c^2)^2]/(n-p)\}^{1/2}$ (n = number of reflexions; p = total number of parameters).

Table S9: Cartesian coordinates of calculated minimum structures of $C_4H_6N_2O_2$ at the B3LYP/aug-cc-pVTZ level of theory.

Atom	x	y	z
C	–0.000252786	–0.000020957	0.000070530
C	0.000121258	–0.000035782	0.000017583
H	–0.000007583	0.000024771	0.000010366
C	–0.000024441	0.000038182	–0.000019518
H	0.000012382	–0.000024619	–0.000010488
C	–0.000062339	0.000013562	–0.000063482
O	0.000090410	0.000092213	–0.000033599
O	0.000033365	–0.000089226	0.000030705
N	0.000052096	–0.000059692	–0.000112144
H	0.000004665	0.000011353	0.000052133
H	0.000014100	–0.000027390	0.000023144
N	0.000020683	0.000061274	0.000110435
H	–0.000011188	0.000027358	–0.000023258
H	0.000009378	–0.000011047	–0.000052408

Table S10: Cartesian coordinates of calculated minimum structures of $[C_4H_8N_2O_2]^{2+}$ at the B3LYP/aug-cc-pVTZ level of theory.

Atom	x	y	z
C	–0.000087932	–0.000007432	–0.000004666
C	0.000045864	–0.000221513	–0.000022714
H	–0.000001762	0.000048788	0.000005362
C	–0.000045864	0.000221513	0.000022715
H	0.000001763	–0.000048787	–0.000005375
C	0.000087930	0.000007428	0.000004704
O	0.000039536	0.000111317	0.000014154
O	–0.000039536	–0.000111316	–0.000014160
N	0.000146024	–0.000133583	–0.000008510
H	–0.000041870	0.000013602	–0.000000321
H	–0.000028419	0.000055015	0.000004894
N	–0.000146024	0.000133583	0.000008509
H	0.000028420	–0.000055015	–0.000004896
H	0.000041870	–0.000013601	0.000000313
H	0.000044503	0.000017428	0.000003889
H	–0.000044503	–0.000017427	–0.000003900

Table S11: Cartesian coordinates of calculated minimum structures of the O-coordinated HF complex of the cation $[C_4H_8N_2O_2 \cdot 2HF]^{2+}$ at the B3LYP/aug-cc-pVTZ level of theory.

Atom	x	y	z
F	0.000001364	–0.000014559	0.000003573
O	0.000003330	–0.000007802	–0.000005498
N	0.000004773	0.000001882	–0.000003131
C	–0.000001846	–0.000002238	0.000010532
C	0.000001961	0.000000131	–0.000004060
H	–0.000004341	–0.000000126	–0.000000790
H	0.000000610	0.000001934	0.000000870
H	0.000000262	–0.000000699	–0.000002264
H	–0.000003418	0.000017849	–0.000001289
O	–0.000010771	–0.000002500	–0.000000656
N	–0.000006282	0.000001801	0.000001830
C	0.000008340	–0.000002280	0.000001412
C	–0.000001698	–0.000001124	–0.000000984
H	0.000003823	0.000001127	–0.000000118
H	0.000000255	–0.000001716	–0.000001669
H	–0.000001485	0.000000316	0.000002282
H	0.000006999	0.000009081	0.000002586
F	–0.000003322	–0.000008376	–0.000000796
H	–0.000001414	0.000003988	–0.000002259
H	0.000002862	0.000003310	0.000000430

Table S12: Cartesian coordinates of calculated minimum structures of the N-coordinated HF complex of the cation $[C_4H_8N_2O_2 \cdot 2HF]^{2+}$ at the B3LYP/aug-cc-pVTZ level of theory.

Atom	x	y	z
O	–0.000006099	–0.000013173	0.000006754
N	0.000006787	0.000005411	0.000008244
C	0.000000234	0.000004033	–0.000022659
C	–0.000000717	–0.000000099	0.000007963
H	–0.000001499	–0.000003874	–0.000001240
H	–0.000005262	–0.000007176	–0.000000052
H	–0.000000470	0.000000034	0.000000555
H	0.000007180	0.000010337	0.000000340
O	0.000006909	0.000014542	0.000003913
N	–0.000009775	–0.000005284	–0.000000987
C	0.000001770	–0.000004551	–0.000015985
C	0.000000178	–0.000000861	0.000006462
H	0.000002576	0.000001641	0.000002282
H	0.000004799	0.000007837	0.000002264
H	0.000000240	0.000000100	0.000000346
H	–0.000007653	–0.000010106	0.000001316
F	–0.000001596	–0.000002765	–0.000000504
F	–0.000002854	0.000009328	0.000000554
H	0.000002369	–0.000000386	0.000000523
H	0.000002882	–0.000004989	–0.000000089

Table S13: Cartesian coordinates of calculated minimum structures of the N-coordinated HF complex of the cation $[C_4D_6H_2N_2O_2 \cdot 2HF]^{2+}$ at the B3LYP/aug-cc-pVTZ level of theory.

Atom	x	y	z
O	–0.000005633	0.000013130	–0.000006836
N	0.000006602	–0.000005324	–0.000008357
C	–0.000000757	–0.000003518	0.000022835
C	–0.000000109	0.000000055	–0.000007971
D	–0.000001433	0.000003718	0.000001253
D	–0.000005141	0.000007188	0.000000071
H	–0.000000612	–0.000000215	–0.000000540
D	0.000007034	–0.000010341	–0.000000325
O	0.000007038	–0.000014727	–0.000003876
N	–0.000010313	0.000005260	0.000001063
C	0.000002155	0.000004153	0.000015908
C	0.000000440	0.000001041	–0.000006543
D	0.000002732	–0.000001417	–0.000002284
D	0.000004837	–0.000007923	–0.000002294
H	0.000000098	–0.000000147	–0.000000295
D	–0.000007729	0.000010275	–0.000001319
F	–0.000001385	0.000002888	0.000000504
F	–0.000002576	–0.000009154	–0.000000562
H	0.000002146	0.000000258	–0.000000524
H	0.000002606	0.000004801	0.000000092

[1] G. A. Jeffrey, *An introduction to hydrogen bonding, Topics in physical chemistry*, Oxford University Press, New York, **1997**.

[2] K. Nieszporek, P. Podkościelny, J. Nieszporek, *Phys. Chem. Chem. Phys.* **2016**, *18*, 5957.

[3] G. A. Jeffrey, W. Saenger, *Hydrogen Bonding in Biological Structures*, Springer-Verlag, Berlin, Heidelberg, **1991**.

[4] I. Rozas, I. Alkorta, J. Elguero, *J. Phys. Chem. A* **1998**, *102*, 9925.

[5] R. Taylor, O. Kennard, W. Versichel, *J. Am. Chem. Soc.* **1984**, *106*, 244.

[6] G. S. Padiyar, T. P. Seshadri, *Nucleosides and Nucleotides* **1996**, *15*, 857.

Chemistry A European Journal

Chemistry Europe
European Chemical Societies Publishing

Cover Feature:
A. J. Kornath et al.
Strengthening of the C–F Bond in Fumaryl Fluoride with Superacids

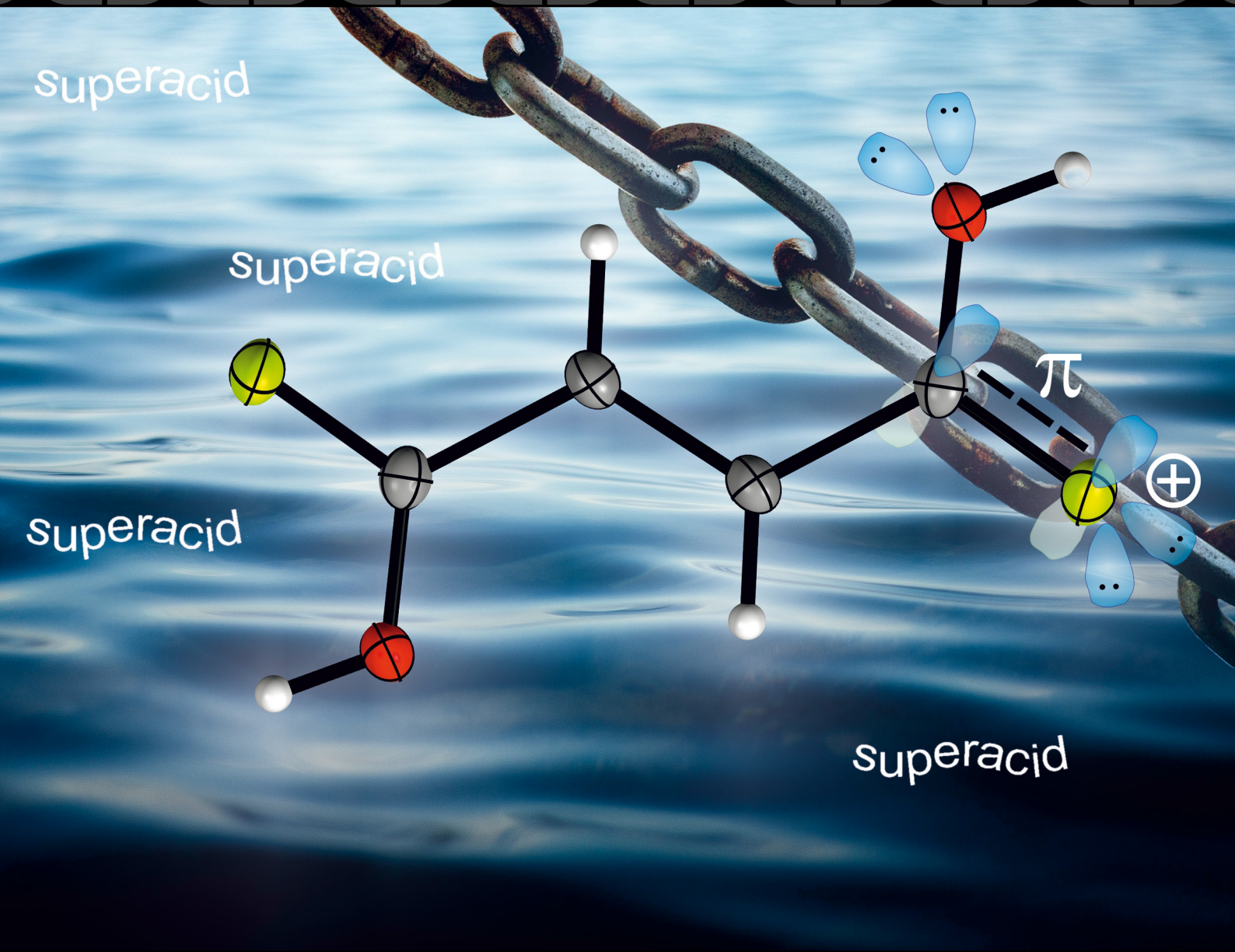

15/2022
WILEY-VCH

Chemistry–A European Journal
Research Article
doi.org/10.1002/chem.202104422
Chemistry Europe
European Chemical Societies Publishing
www.chemeurj.org

VIP Strengthening of the C–F Bond in Fumaryl Fluoride with Superacids

Marie C. Bayer,[a] Christoph Kremser,[a] Christoph Jessen,[a] Alexander Nitzer,[a] and Andreas J. Kornath*[a]

Abstract: The reaction of fumaryl fluoride with the superacidic solutions XF/MF_5 (X=H, D; M=As, Sb) results in the formation of the monoprotonated and diprotonated species, dependent on the stoichiometric ratio of the Lewis acid to fumaryl fluoride. The salts $[C_4H_3F_2O_2]^+[MF_6]^-$ (M=As, Sb) and $[C_4H_2X_2F_2O_2]^{2+}([MF_6]^-)_2$ (X=H, D; M=As, Sb) are the first examples with a protonated acyl fluoride moiety. They were characterized by low-temperature vibrational spectroscopy. Low-temperature NMR spectroscopy and single-crystal X-ray structure analyses were carried out for $[C_4H_3F_2O_2]^+[SbF_6]^-$ as well as for $[C_4H_4F_2O_2]^{2+}([MF_6]^-)_2$ (M=As, Sb). The experimental results are discussed together with quantum chemical calculations of the cations $[C_4H_4F_2O_2\cdot 2HF]^{2+}$ and $[C_4H_3F_2O_2\cdot HF]^+$ at the B3LYP/aug-cc-pVTZ level of theory. In addition, electrostatic potential (ESP) maps combined with natural population analysis (NPA) charges were calculated in order to investigate the electron distribution and the charge-related properties of the diprotonated species. The C–F bond lengths in the protonated dication are considerably reduced on account of the +R effect.

Introduction

The prosperity of fluoroorganic compounds in every area of the chemical industry is conspicuous.[1] The exceptional stability of the carbon-fluorine bond is the most apparent property of organofluorine compounds.[2] This stability, which is predicated by the electrostatic attraction between $F^{\delta-}$ and $C^{\delta+}$, distinguishes acyl fluorides from acyl halides in general.[1,3] Acyl fluorides are key intermediates, serving as synthetic fragments, such as RCO and F sources, with an extensive range of applications in organic chemistry.[3,4] A series of acyl fluorides were treated with various Lewis acids resulting in the formation of acyl cations (oxocarbenium ions).[5,6] In addition, the complex formation of acyl fluorides with Lewis acid fluorides in SO_2ClF was previously reported.[6,7] Recently, the oxygen-coordinated adducts of fumaryl fluoride, containing two acyl fluoride moieties, were characterized.[8] Fumaric acid,[9,10] as well as several carboxylic acids,[11,12] were previously investigated in superacidic systems. In contrast, the acyl fluoride moiety has not been examined in superacids so far. This prompted us to investigate fumaryl fluoride in different binary superacid systems regarding its basicity.

Results and Discussion

The superacid systems HF/MF_5 (M=As, Sb) led to the formation of the monoprotonated and diprotonated fumaryl fluoride. An excess of the Lewis acids (AsF_5 or SbF_5) is necessary to synthesize the dication $[C_4H_4F_2O_2]^{2+}$ according to Equation (1).

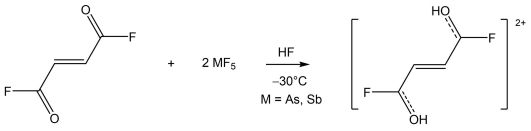

(1)

An equimolar amount of the Lewis acids in reference to fumaryl fluoride is required to form the salt containing the monoprotonated cation [Eq. (2)].

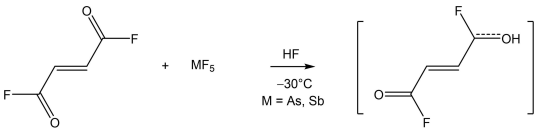

(2)

The reactions were carried out at a temperature of −30 °C. Excess of anhydrous hydrogen fluoride, which was used as both solvent and reagent, was removed at −78 °C in a dynamic vacuum. The salts $[C_4H_4F_2O_2]^{2+}([AsF_6]^-)_2$ (**1**) and $[C_4H_4F_2O_2]^{2+}([SbF_6]^-)_2$ (**2**) were obtained as colorless crystalline solids, which are stable up to 15 °C. The colorless crystals of $[C_4H_3F_2O_2]^+[AsF_6]^-$ (**3**) and $[C_4H_3F_2O_2]^+[SbF_6]^-$ (**4**) decompose above −10 °C. The corresponding deuterated species $[C_4H_2D_2F_2O_2]^{2+}([AsF_6]^-)_2$ (**5**) and $[C_4H_2D_2F_2O_2]^{2+}([SbF_6]^-)_2$ (**6**) were prepared by modifying the superacid systems to DF/MF_5 (M=As, Sb).

To test whether the protonation is possible under milder conditions, the superacidic solutions HF/MF_4 (M=Ge, S) and HF/

[a] M. C. Bayer, C. Kremser, C. Jessen, A. Nitzer, Prof. Dr. A. J. Kornath
Department Chemie
Ludwig-Maximilians-Universität München
Butenandtstrasse 5–13, (D) 81377 Munich (Germany)
E-mail: andreas.kornath@cup.uni-muenchen.de

Supporting information for this article is available on the WWW under https://doi.org/10.1002/chem.202104422

BF_3, which are lower in acidity than fluoroantimonic acid,[13] were used. However, no reaction was observable.

Crystal structure of $[C_4H_4F_2O_2]^{2+}([AsF_6]^-)_2$

$[C_4H_4F_2O_2]^{2+}([AsF_6]^-)_2$ (**1**) crystallizes in the orthorhombic space group *Pbcn* with four formula units per unit cell. Figure S1 in the Supporting Information shows the formula unit of **1** and Table S1 summarizes selected structural parameters. The cation in the crystal structure of **1**, which is shown in Figure 1, exists as the *cis-cis* conformer. Selected bond lengths and angles of *cis-cis*-fumaryl fluoride[8] compared with **1** are summarized in Table 1. The diprotonation of fumaryl fluoride has a great influence on the C=O bond lengths. The C1–O1 bonds are with 1.223(2) Å significantly elongated compared to fumaryl fluoride,[8] and are in the range between formal C–O single (1.43 Å) and C=O double bonds (1.19 Å).[14] In contrast, the C1–F1 bonds are with 1.281(2) Å shorter than formal C–F single bonds (1.36 Å).[14] In comparison with the reactant[8] the C1–F1 bonds are significantly shortened. The C=C bond is also affected by the diprotonation. By contrast with fumaryl fluoride,[8] the C2–C2*i* is with 1.330(3) Å significantly elongated and agrees well with formal C=C bond lengths (1.33 Å).[14] The C1–C2 single bonds are not significantly affected by the diprotonation. The most pronounced effect of the diprotonation on the bond angles is for the O–C–C and F–C–C angles. The O1–C1–C2 angle is reduced by 3.9° to 123.4(2)°, whereas the F1–C1–C2 bond angle is widened to 116.4(2)°. The protonated acyl fluoride groups are twisted against one another by 10° out of the carbon-skeleton plane, resulting in a slightly distorted planar structure.

The As–F bond lengths in the $[AsF_6]^-$ anion are in the range between 1.702(1) and 1.717(1) Å. These values are in accordance with reported As–F bond lengths of hexafluoroarsenate anions.[15] The As1–F2 bond (1.800(1) Å) is involved in hydrogen bonding in the crystal packing and is therefore elongated in comparison with the other As–F bonds. Besides, the bond angles deviate up to 5° from the ideal octahedron angles, indicating a distorted structure of the anion. In the crystal packing of **1**, the cation is connected with the anions by different types of interatomic contacts. A cutout of these contacts is given in Figure 1, and the detailed illustration is shown in Figure S2.

The hydrogen bonds O1–H1···F2 with donor-acceptor distances of 2.429(2) Å are categorized as strong hydrogen bonds according to the classification of Jeffrey.[16] Additionally, two interatomic contacts between C1 and F3*iv* (2.868(2) Å) and between C1 and F4*iii* (2.614(2) Å) are observed. Both interatomic C–F distances are below the sum of the van der Waals radii (3.17 Å).[17] A zigzag chain structure is formed through the O1–H1···F2 hydrogen bonds and the C1···F4*iii* contacts along the *c*-axis, as it is shown in Figure S3.

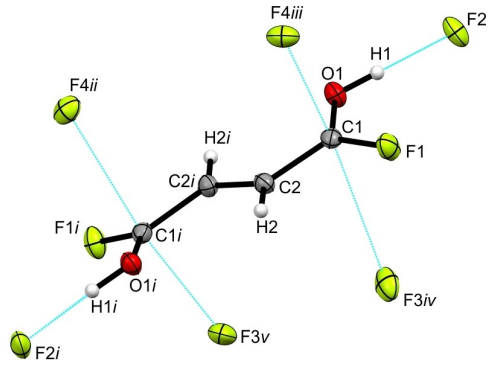

Figure 1. Projection of the cation in $[C_4H_4F_2O_2]^{2+}([AsF_6]^-)_2$ and its interatomic contacts (displacement ellipsoids with 50% probability). Symmetry operations: *i* = 1−*x*, *y*, 0.5−*z*; *ii* = *x*, 1−*y*, −0.5+*z*; *iii* = 1−*x*, 1−*y*, 1−*z*; *iv* = 1−*x*, −*y*, 1−*z*; *v* = *x*, −*y*, −0.5+*z*. Interatomic contacts are drawn as dashed blue lines.

Table 1. Comparison of selected bond lengths and angles of *cis,cis-* and *trans,trans*-fumaryl fluoride,[8] $[C_4H_4F_2O_2]^{2+}([AsF_6]^-)_2$ (**1**) (symmetry operation: *i* = 1−*x*, *y*, 0.5−*z*), $[C_4H_4F_2O_2]^{2+}([SbF_6]^-)_2$ (**2**) (symmetry operation: *i* = 2−*x*, −*y*, 1−*z*.) and $[C_4H_3F_2O_2]^+[SbF_6]^-$ (**4**) with estimated standard deviation in parentheses.

	cis-cis-$C_4H_2F_2O_2$[8]	*trans-trans*-$C_4H_2F_2O_2$[8]		1	2	4
Bond length [Å]						
C=C	1.314(2)	1.322(6)	C2–C2*i*	1.330(3)	1.336(5)	
			C2–C3			1.334(7)
C–C	1.477(2)	1.473(4)	C1–C2	1.465(2)	1.461(4)	1.476(8)
			C3–C4			1.454(7)
C=O	1.190(2)	1.177(4)	C1–O1	1.223(2)	1.223(4)	1.187(6)
			C4–O2			1.239(6)
C–F	1.334(2)	1.349(3)	C1–F1	1.281(2)	1.287(4)	1.332(6)
			C4–F2			1.285(6)
Bond angle [°]						
O–C–F	120.2(1)	119.5(3)	O1–C1–F1	120.2(2)	120.6(3)	120.7(5)
			O2–C4–F2			118.6(4)
O–C–C	127.3(2)	127.2(3)	O1–C1–C2	123.4(2)	121.1(3)	126.4(5)
			O2–C4–C3			122.5(5)
F–C–C	112.5(1)	113.2(3)	F1–C1–C2	116.4(2)	118.2(3)	112.9(4)
			F2–C4–C3			118.9(4)
C–C–C	120.3(2)	123.1(3)	C1–C2–C2*i*	119.1(2)	120.1(3)	
			C1–C2–C3			122.1(5)
			C4–C3–C2			118.6(5)

Crystal structure of $[C_4H_4F_2O_2]^{2+}([SbF_6]^-)_2$

$[C_4H_4F_2O_2]^{2+}([SbF_6]^-)_2$ (**2**) crystallizes in the monoclinic space group $P2_1/c$ with two formula units per unit cell. Figure S4 shows the formula unit of **2** and selected structural parameters are listed in Table S2. The crystal structure of **1** and **2** differ in terms of their cationic conformational structure. As the cation of **1** is a *cis-cis* conformer, the cation in the crystal structure of **2**, depicted in Figure 2, exists as the *trans-trans* conformer.

Selected bond lengths and angles of *cis-cis*- and *trans-trans*-fumaryl fluoride,[8] **1** and **2** are listed in Table 1. By analogy with **1**, the diprotonation of fumaryl fluoride causes a significant elongation of the C1–O1 bond (1.223(4) Å), whereas the C1–F1 bond is significantly shortened (1.287(4) Å), compared to the starting material.[8] No significant difference in the lengths of the double C=C and single C–C bonds is observable in comparison to the neutral *trans-trans*-compound.[8] The bond lengths of the cations in the crystal structure of **1** and **2** are consistent with one another. The bond angle O1–C1–C2 is significantly reduced to 121.1(3)° compared to **1** and *trans-trans*-fumaryl fluoride.[8] Though, the bond angle F1–C1–C2 is significantly widened to 118.2(3)° in contrast to **1** and the neutral compound.[8] The protonated acyl fluoride groups are twisted against one another by 6° out of the carbon-skeleton plane, leading to a slightly distorted planar structure.

The Sb–F bond lengths of the $[SbF_6]^-$ anion range between 1.858(2) and 1.934(2) Å, revealing a distorted octahedral structure. The values are in accordance with literature data for $[SbF_6]^-$ anions.[18,19]

In the solid state of **2** three different interatomic contacts connect the cations and the anions, illustrated in detail in Figure S5. Figure 2 shows a cutout of the interatomic contacts. The O1–H1···F2 hydrogen bond (2.426(3) Å), categorized as strong,[16] agrees well with the corresponding hydrogen bond in the crystal structure of **1**. On the other hand, the C2–H2···F5*iii* hydrogen bond with a donor-acceptor distance of 3.072(4) Å is classified as moderate.[16] Additionally, one interatomic contact between C1 and F3*ii* (2.578(4) Å) is detected, which is below the sum of the van der Waals radii of 3.17 Å.[17]

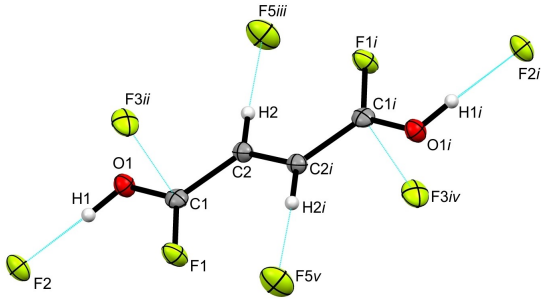

Figure 2. Visualization of the cation in $[C_4H_4F_2O_2]^{2+}([SbF_6]^-)_2$ with its interatomic contacts (displacement ellipsoids with 50% probability). Symmetry operations: *i* = 2−*x*, −*y*, 1−*z*; *ii* = 2−*x*, 1−*y*, 1−*z*; *iii* = 1+x, −1+*y*, *z*; *iv* = *x*, −1+*y*, *z*; *v* = 1−*x*, 1−*y*, 1−*z*. Interatomic contacts are shown as dashed blue lines.

Crystal structure of $[C_4H_3F_2O_2]^+[SbF_6]^-$

$[C_4H_3F_2O_2]^+[SbF_6]^-$ (**4**) crystallizes in the monoclinic space group *Cc* with four formula units per unit cell. Figure S6 shows the asymmetric unit of **4** and selected structural parameters are summarized in Table S3. In compliance with the crystal structure of **2**, the cation of **4**, which is illustrated in Figure 3, exists as the *trans-trans* conformer.

In order to better compare the structural data of the monoprotonated cation, selected bond lengths and angles of *cis-cis*- and *trans-trans*-fumaryl fluoride,[8] as well as **1**, **2** and **4** are summarized in Table 1. The C=O bond lengths of the monoprotonated cation differ considerably from each other. Since the unprotonated C1–O1 bond (1.187(6) Å) remains unaffected and conforms to the *trans-trans*-fumaryl fluoride,[8] the protonated C4–O2 bond is with 1.239(6) Å significantly elongated and accords with the diprotonated species of **2**. The C–F bonds in **4** vary in bond distances as well. The C1–F1 bond length (1.332(6) Å) of the unprotonated carbonyl fluoride group remains unchanged and corresponds to *trans-trans*-fumaryl fluoride.[8] However, the C4–F2 bond distance is with 1.285(6) Å significantly shortened compared to the reactant,[8] but in good agreement with the diprotonated cation of **2**. The C=C double bond and the C–C single bonds are in accordance with the starting material,[8] as well as with **2**. The O2–C4–C3 angle is reduced to 122.5(5)° due to the protonation, whereas the unprotonated O1–C1–C2 bond angle remains constant and agrees well with the *trans-trans* conformer.[8] Since the F2–C4–C3 bond angle is significantly widened to 118.9(4)° based on the monoprotonation, which conforms to **2**, the F1–C1–C2 bond angle is unaltered and in accordance with the reactant.[8] A slightly distorted planar structure of the monocation results from the acyl groups being twisted against each other by around 8° out of the carbon-skeleton plane.

In the $[SbF_6]^-$ anion the Sb–F bond distances range between 1.863(3) and 1.873(3) Å, and are in the typical range of Sb–F bond lengths.[18,20] The Sb1–F3 bond (1.936(3) Å) is elongated in comparison to reported Sb–F bond distances, owing to the fact that it is involved in hydrogen bonding in the crystal structure of **4**. A distorted octahedral structure of the $[SbF_6]^-$ is implied by the bond angles, which deviate by up to about 5° from the ideal octahedron angles.

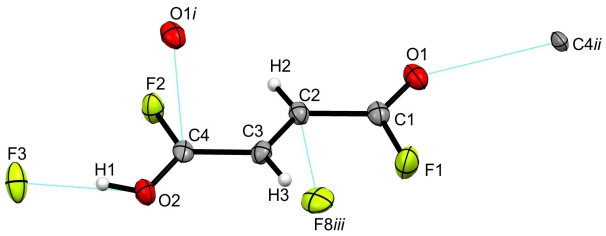

Figure 3. Illustration of the cation in $[C_4H_3F_2O_2]^+[SbF_6]^-$ and its interatomic contacts (displacement ellipsoids with 50% probability). Symmetry operations: *i* = 0.5+*x*, 1.5−*y*, −0.5+*z*; *ii* = −0.5+*x*, 1.5−*y*, 0.5+*z*; *iii* = −1+*x*, 1−*y*, 0.5+*z*. Interatomic contacts are shown as dashed blue lines.

The ions are linked together by three different types of interatomic contacts in the crystal structure of **4**, which are visualized elaborately in Figure S7. Figure 3 depicts a detail of the interatomic contacts. Referred to the categorization of Jeffrey[16] the hydrogen bond O2–H1···F3 (2.470(5) Å), connecting the cations with the anions, is designated as strong. Additionally the interatomic contact between C2 and F8*iii* (2.839(7) Å) connects the cations with the anions, which is below the sum of the van der Waals radii (3.17 Å).[17] A cation-cation contact is observed between C4 and O1*i* forming a zigzag chain along the *c*-axis, which is illustrated in Figure S8. This C4···O1*i* distance of 2.809(6) Å is below the sum of the van der Waals radii (3.22 Å).[17]

Vibrational spectra of $[C_4H_4F_2O_2]^{2+}([MF_6]^-)_2$ (M=As, Sb)

Figure 4 shows the low-temperature vibrational spectra of $[C_4H_4F_2O_2]^{2+}([AsF_6]^-)_2$ (**1**), $[C_4H_4F_2O_2]^{2+}([SbF_6]^-)_2$ (**2**) and crystalline fumaryl fluoride.[8] The vibrational spectra of the deuterium isotopomeric salts $[C_4H_2D_2F_2O_2]^{2+}([AsF_6]^-)_2$ (**5**) and $[C_4H_2D_2F_2O_2]^{2+}([SbF_6]^-)_2$ (**6**) are illustrated in Figure S9 (Supporting Information). Selected experimental vibrational frequencies

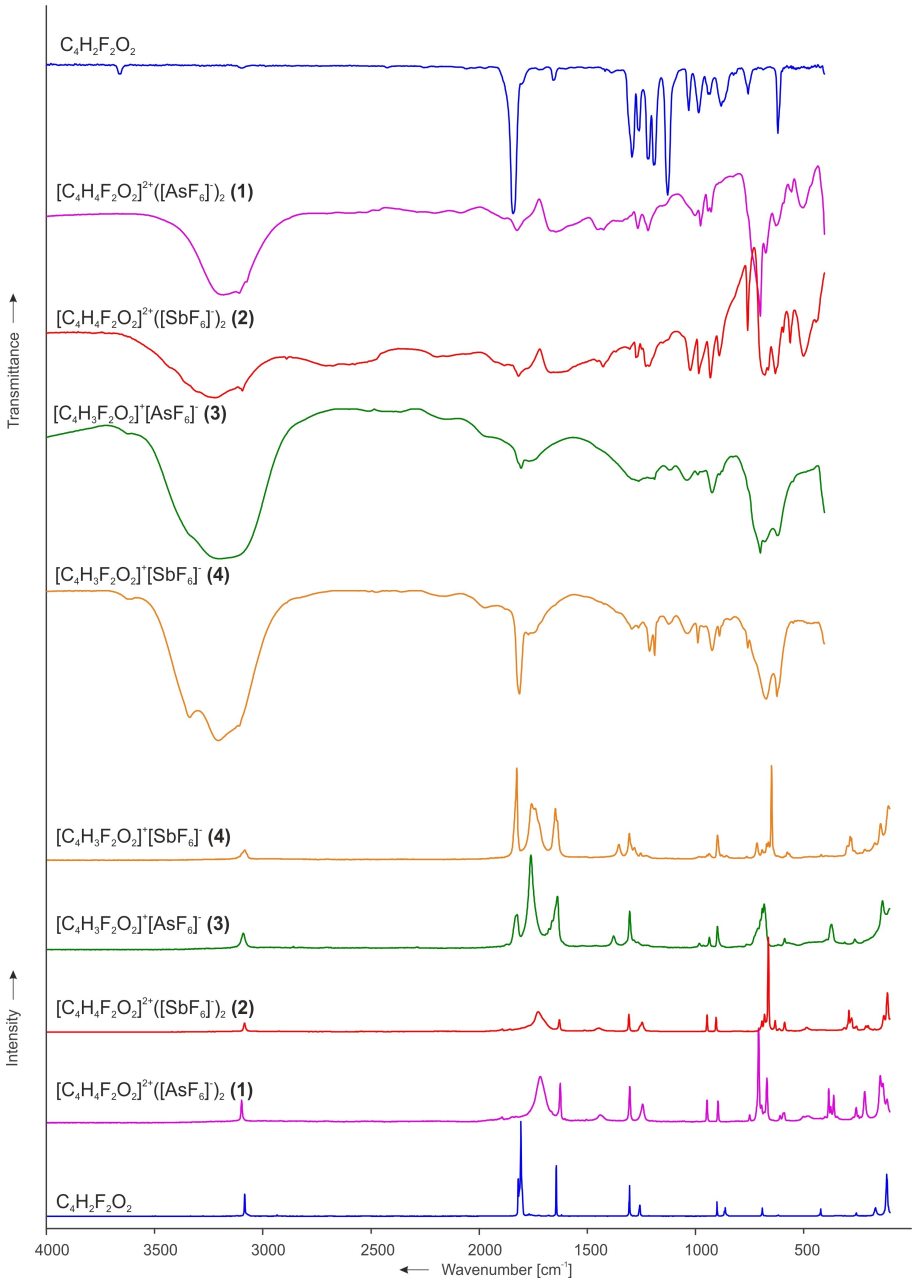

Figure 4. Low-temperature Raman and IR spectra of crystalline fumaryl fluoride,[8] $[C_4H_4F_2O_2]^{2+}([AsF_6]^-)_2$ (**1**), $[C_4H_4F_2O_2]^{2+}([SbF_6]^-)_2$ (**2**), $[C_4H_3F_2O_2]^+[AsF_6]^-$ (**3**) and $[C_4H_3F_2O_2]^+[SbF_6]^-$ (**4**).

of **1** and **2** as well as the quantum chemically calculated frequencies of the cation $[C_4H_4F_2O_2 \cdot 2HF]^{2+}$ are summarized in Table 2. The complete data are given in Table S4. The experimental vibrational frequencies of **5** and **6** accompanied by the calculated frequencies of the cation $[C_4H_2D_2F_2O_2 \cdot 2HF]^{2+}$ are given in Table S5.

As crystalline fumaryl fluoride consists mainly of the *cis-cis* conformers,[8] we assume the same conformational arrangement for the $[C_4H_4F_2O_2]^{2+}$ cation, which is confirmed by the single-crystal X-ray structural analysis of **1**. Therefore the following calculated vibrational frequencies refer to the *cis,cis* conformer of the $[C_4H_4F_2O_2]^{2+}$ cation, displaying C_{2h} symmetry with 30 fundamental vibrations ($11A_g + 4B_g + 5A_u + 10B_u$). The rule of mutual exclusion applies by reason of the inversion center.[21] The assignment of the vibrational modes was performed by analyzing the Cartesian displacement vectors of the calculated vibrational modes of $[C_4H_4F_2O_2 \cdot 2HF]^{2+}$ and by comparing to literature data of fumaryl fluoride.[8,22] To improve consistency of the calculated frequencies with the experimental ones, two HF molecules were attached to the gas phase structure of the cation simulating hydrogen bonds in the solid state.[23]

The antisymmetric O–H stretching vibration, indicating the successful protonation, is detected in the IR spectra at 3182 (**1**) and 3217 cm^{-1} (**2**). However, the corresponding calculated value for the O–H stretching mode is underestimated. The two added HF molecules, simulating hydrogen bonds in the crystal structure, result in the calculation of lower values for the O–H stretching vibration.[23] We assume the hydrogen bonds being weaker than supposed in the calculation. Owing to the poor polarizability of the O–H bond, corresponding Raman lines are not observable. By contrast, the O–D stretching vibrations are identifiable in the Raman spectra at 2307 (**5**) and 2293 cm^{-1} (**6**). In the IR spectra the antisymmetric O–D stretching modes are observed at 2359 (**5**) and 2318 cm^{-1} (**6**). These H/D red-shifts are consistent with the Teller-Redlich rule for a H/D isotopic effect.[21] The C–H stretching vibrations of **1** are slightly blue-shifted by 14 cm^{-1} (3098 cm^{-1} (Ra)) and by 12 cm^{-1} (3109 cm^{-1} (IR)) by comparison with the starting material.[8] Though, the C–H stretching modes of **2** remain unshifted. As a result of the twofold protonation the C=O bonds are weakened occurring in the Raman spectra at 1717 (**1**) and at 1726 cm^{-1} (**2**), and in the IR spectra at 1641 (**1**) and at 1666 cm^{-1} (**2**). Compared to fumaryl fluoride,[8] those vibrations are red-shifted by up to 165 cm^{-1}. The weakening of the C=O bonds is also observed in the crystal structure of **1** and **2**. The C=C stretching mode appears in the Raman spectra at 1625 (**1**) and at 1629 cm^{-1} (**2**), and by comparing to the neutral compound,[8] it is slightly red-shifted by 18 (**1**) and by 14 cm^{-1} (**2**). This indicates a slight elongation of the C=C double bond that is verified by the crystal structure of **1**. In the Raman spectra, the symmetric C–F stretching vibration is observed at 1441 (**1**) and at 1445 cm^{-1} (**2**). In contrast to fumaryl fluoride,[8] it is blue-shifted by 182 (**1**) and by 186 cm^{-1} (**2**), displaying a strengthening of the C–F bond as a result of the protonation, which is also observed in the crystal structure of **1** and **2**. Three Raman lines and two IR bands are expected for the anions $[AsF_6]^-$ and $[SbF_6]^-$ with ideal O_h symmetry. However, more vibrations are observed in the spectra of **1**, **2**, and **5**, **6**, signifying a distorted octahedral structure of the anions, confirmed by single-crystal X-ray structural analysis of **1** and **2**.

Vibrational spectra of $[C_4H_3F_2O_2]^+[MF_6]^-$ (M=As, Sb)

The low-temperature vibrational spectra of $[C_4H_3F_2O_2]^+[AsF_6]^-$ (**3**) and $[C_4H_3F_2O_2]^+[SbF_6]^-$ (**4**) in comparison with the diprotonated salts and crystalline fumaryl fluoride[8] are depicted in Figure 4. Table 3 combines selected experimental vibrational frequencies of **3**, **4** and the quantum chemically calculated frequencies of the cation $[C_4H_3F_2O_2 \cdot HF]^+$. The complete data can be found in Table S6.

The monoprotonated cations reveal a *trans-trans* conformational structure in the solid state, as described in the section above. The following calculated vibrational frequencies accordingly correspond to the *trans-trans* conformer of the $[C_4H_3F_2O_2]^+$ cation, having C_s symmetry with 27 fundamental vibrations ($19A' + 8A''$). The vibrational frequencies were assigned by examining the Cartesian displacement vectors of the calculated

Table 2. Selected experimental vibrational frequencies [cm^{-1}] of $[C_4H_4F_2O_2]^{2+}([MF_6]^-)_2$ (M=As, Sb) and calculated vibrational frequencies [cm^{-1}] of $[C_4H_4F_2O_2 \cdot 2HF]^{2+}$.

$[C_4H_4F_2O_2]^{2+}([AsF_6]^-)_2$ exp.[a]		$[C_4H_4F_2O_2]^{2+}([SbF_6]^-)_2$ exp.[a]		$[C_4H_4F_2O_2 \cdot 2HF]^{2+}$ calcd.[b]	Assignment		
IR	Raman	IR	Raman	IR/Raman			
3109 vs		3094 vs		3190 (60/0)	ν_{21}	B_u	ν_{as}(C–H)
	3098 (24)		3085 (9)	3188 (0/79)	ν_1	A_g	ν_s(C–H)
3182 vs		3217 vs		2490 (7585/0)	ν_{22}	B_u	ν_{as}(O–H)
	1717 (49)		1726 (21)	1713 (0/8)	ν_3	A_g	ν_s(C=O)
	1625 (42)		1629 (13)	1685 (0/384)	ν_4	A_g	ν(C=C)
1641 m		1666 vs		1681 (816/0)	ν_{23}	B_u	ν_{as}(C=O)
1450 m		1452 s		1485 (717/0)	ν_{24}	B_u	ν_{as}(C–F)
	1441 (8)		1445 (4)	1454 (0/4)	ν_5	A_g	ν_s(C–F)
	1244 (20)	1246 s	1246 (10)	1280 (0/38)	ν_7	A_g	δ_s(COH)
	946 (24)		946 (18)	995 (0/6)	ν_8	A_g	ν_s(C–C)
926 w		930 vs		933 (127/0)	ν_{27}	B_u	ν_{as}(C–C)
	693 (19)		692 (12)	712 (0/11)	ν_9	A_g	δ_s(COF)

[a] Abbrevations for IR intensities: v = very, s = strong, m = medium, w = weak. IR intensities in km/mol; Raman intensities in $Å^4/u$. Experimental Raman activities are relative to a scale of 1 to 100. [b] Calculated at the B3LYP/aug-cc-pVTZ level of theory.

Table 3. Selected experimental vibrational frequencies [cm^{-1}] of $[C_4H_3F_2O_2]^+[MF_6]^-$ (M=As, Sb) and calculated vibrational frequencies [cm^{-1}] of $[C_4H_3F_2O_2\cdot HF]^+$.

$[C_4H_3F_2O_2]^+[AsF_6]^-$ exp.[a] IR	Raman	$[C_4H_3F_2O_2]^+[SbF_6]^-$ exp.[a] IR	Raman	$[C_4H_3F_2O_2\cdot HF]^+$ calcd.[b] IR/Raman	Assignment		
		3109 vs		3212 (26/29)	ν_1	A'	ν(C–H)[c]
	3090 (17)		3084 (11)	3199 (6/54)	ν_2	A'	ν(C–H)
3196 vs		3203 vs		3061 (2649/166)	ν_3	A'	ν(O–H)[c]
1803 m	1823 (37)	1813 s	1825 (97)	1872 (180/260)	ν_4	A'	ν(C=O)
	1637 (56)		1647 (54)	1675 (636/227)	ν_5	A'	ν(C=C)
1770 m	1761 (100)	1770 w	1757 (60)	1621 (181/2)	ν_6	A'	ν(C=O)[c]
	1378 (14)		1354 (17)	1489 (195/12)	ν_7	A'	ν(C–F)[c]
	1304 (41)		1305 (28)	1316 (7/29)	ν_8	A'	δ(CCH)
1290 m	1284 (10)	1292 w	1281 (13)	1280 (22/1)	ν_9	A'	δ(CCH)
1261 m	1265 (8)	1261 w	1252 (8)	1259 (205/24)	ν_{10}	A'	δ(COH)[c]
1205 m		1209 m	1227 (5)	1213 (433/9)	ν_{11}	A'	ν(C–F)
987 w	981 (7)	987 w	982 (4)	956 (27/12)	ν_{12}	A'	ν(C–C)[c]
922 m	935 (13)	920 m	936 (7)	916 (122/0)	ν_{22}	A''	γ(COH)[c]
885 w	899 (24)	887 w	898 (26)	882 (34/13)	ν_{13}	A'	ν(C–C)

[a] Abbrevations for IR intensities: v = very, s = strong, m = medium, w = weak. IR intensities in km/mol; Raman intensities in $Å^4/u$. Experimental Raman activities are relative to a scale of 1 to 100. [b] Calculated at the B3LYP/aug-cc-pVTZ level of theory. [c] Protonated acyl fluoride moiety.

vibrational modes of $[C_4H_3F_2O_2\cdot HF]^+$ as well as by comparing to literature data of fumaryl fluoride.[8,22] The successful monoprotonation of fumaryl fluoride is shown, inter alia, in the O–H stretching vibration noted in the IR spectra at 3196 (**3**) and 3203 cm^{-1} (**4**). Admittedly the related calculated frequency for the ν(O–H) mode is underestimated, caused by the added HF molecule. The C–H stretching vibration of the monoprotonated cation is observed in the Raman spectra at 3090 cm^{-1} **3**, which is slightly blue-shifted by 6 cm^{-1}, and at 3084 cm^{-1} **4**, which remains unaltered compared to the neutral compound.[8] Further evidence for the monoprotonation is the C=O stretching vibration. The vibration of the unprotonated C=O bond in the Raman spectra of **3** and **4** remains unshifted and agrees with that of the starting material.[8] The stretching mode of the protonated C=O bond is red-shifted in the Raman spectra by 58 cm^{-1} (1761 cm^{-1}, **3**) and by 62 cm^{-1} (1757 cm^{-1}, **4**), respectively, as well as in the IR spectra by 70 cm^{-1} (1770 cm^{-1} **3**, **4**) in comparison with the starting material.[8] The weakening of the protonated C=O bond is in agreement with the crystal structure of **4**. The C=C stretching mode appearing in the Raman spectra at 1637 (**3**) and 1647 cm^{-1} (**4**), respectively, is comparable with that of the reactant[8] and is hardly affected by the monoprotonation, which is in agreement with the crystal structure of **4**. In the Raman spectra, the C–F stretching vibration of the protonated carbonyl fluoride group is observed at 1378[1] (**3**) and at 1354 cm^{-1} (**4**), respectively. In contrast to the *trans-trans* conformer of the neutral compound,[8] it is blue-shifted by 121 (**3**) and by 97 cm^{-1} (**4**), respectively. The strengthening of this C–F bond length is in accordance with the observed shortening of the C4–F2 bond distance in the crystal structure of **4**. The C–F stretching vibration of the unprotonated group is also shifted to higher wavenumbers, appearing in the IR spectra at 1205 (**3**) and at 1209 cm^{-1} (**4**), respectively. For the octahedral anions $[MF_6]^-$ (M=As, Sb) five vibrational modes are estimated. Indeed more lines and bands are noticed in the spectra of **3** and **4**, thus implying a lowered symmetry of the structure of the anions, which agrees well with the crystal structure of **4**.

NMR spectroscopy

^1H, ^{13}C and ^{19}F NMR spectra of fumaryl fluoride dissolved in $CDCl_3$ were recorded at 26 °C. A complete analysis of these spectra, including the ^{13}C satellites, result in the NMR parameters that are shown in Table S7. Anhydrous hydrogen fluoride solutions of $C_4H_2F_2O_2$, as well as of the salts **1**, **2** and **4** were measured at −40 °C. Selected observed chemical shifts and spin-spin coupling constants of **1**, **2** and **4** together with $C_4H_2F_2O_2$ in the different solvents are summarized in Table S8. Figure S10 illustrates the stacked ^1H NMR spectra of $C_4H_2F_2O_2$ dissolved in $CDCl_3$ and in *a*HF, respectively, and **1**, **2**, **4** in *a*HF. All of the experimental NMR spectra are depicted in Figures S11–S27.

The NMR parameters of fumaryl fluoride in $CDCl_3$ are consistent with those published in the literature.[24] Depending on the solvent used the signals occur at different resonant frequencies. Fumaryl fluoride contains each two chemically equivalent protons and fluorine nuclei. Hence the ^1H and ^{19}F spectra of the four-spin system is of the type AA′XX′.[24] Figure 5 shows the molecular structure of fumaryl fluoride together with the spin–spin coupling constants. The higher electronegativity

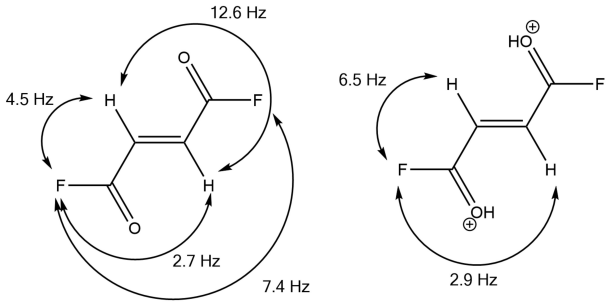

Figure 5. Molecular structure of fumaryl fluoride showing the $^1H,^1H$, $^1H,^{19}F$ and $^{19}F,^{19}F$ *J* couplings (left). Cationic structure of $[C_4H_4F_2O_2]^{2+}$ displaying the $^1H,^{19}F$ *J* couplings (right).

of the fluorine substituents results in a decreased $^{1}H,^{1}H$ J coupling of $^{3}J_{HH}=12.6$ Hz, compared to that of fumaric acid ($^{3}J_{HH}=15.7$ Hz).[25] The sp^2 hybridization of the olefinic carbon atoms is confirmed by the $^{1}H,^{13}C$ J coupling of $^{1}J_{CH}=175.5$ Hz, which is increased compared to that of ethylene ($^{1}J_{CH}=156$ Hz)[26] due to the fluorine substituents.[27]

The ^{1}H NMR spectra of **1**, **2** and **4** in *a*HF show each a signal at approximately 10 ppm, which is attributed to the C(OH)F moiety and confirms the successful protonation. A doublet of doublets at around 7.2 ppm is observed for the olefinic protons with a proton-fluorine coupling constant $^{3}J_{HF}=6.5$ Hz, which is increased compared to that of the neutral compound $^{3}J_{HF}=4.5$ Hz. This indicates that, owing to the protonation, the electron withdrawing property of fluorine is reduced and the resonance-electron-donating ability is simultaneously increased.[28] This observation is discussed in the section below in further detail. There is high correspondance between the NMR spectra of **1**, **2** and **4**. In *a*HF solution no difference between the monoprotonated and diprotonated fumaryl fluoride is observable due to rapid proton exchange with the superacidic solvent.[9,11]

Quantum chemical calculations

All quantum chemical calculations were carried out at the B3LYP/aug-cc-pVTZ level of theory with the Gaussian program package. By comparing the calculated frequencies and structural parameters of the free cation $[C_4H_4F_2O_2]^{2+}$ with the experimental data, large differences are shown (Tables S9 and S10). This is based on the hydrogen bonds confirmed by the crystal structure of **1** and **2**. To simulate the hydrogen bonds, HF molecules were added to the gas phase structure of the free cation, as it is established in the literature.[23] The structural parameters of the HF complex of the cation $[C_4H_4F_2O_2\cdot 2\,HF]^{2+}$ agree well with the experimental data of **1** (Table S9) and the experimental vibrational frequencies of **1** are better described by the $[C_4H_4F_2O_2\cdot 2\,HF]^{2+}$ cation (Table S10). A comparison of the calculated structure of the $[C_4H_4F_2O_2\cdot 2\,HF]^{2+}$ cation with the experimental cationic structure of **1** is shown in Figure 6. The added HF molecules are omitted in the calculated structure for clarification. All experimentally obtained bond lengths and angles of the dication are in good agreement with the calculated structure. An exception is the C1–O1 bond distance, which is slightly overestimated in the calculation, compared to the experimental value. Presumably this is based on intermolecular interactions existing in the solid state, which are not taken into account comparably in the calculations.

In the same fashion as for the dicationic species an HF complex[23] was calculated for the monoprotonated cation $[C_4H_3F_2O_2\cdot HF]^{+}$ to simulate the hydrogen bonds in the solid state. The calculated structural parameters agree well with the experimental data of **4** (Table S11, Supporting Information Information). In Figure 7, the calculated structure of $[C_4H_3F_2O_2\cdot HF]^{+}$, in which the added HF molecule is omitted for clarification, and the monocation of the single-crystal X-ray structure are illustrated. Overall, the calculated and experimentally obtained parameters of the monocation are in good compliance. Though the C3–C4 bond distance is underestimated in the calculated structure of $[C_4H_3F_2O_2\cdot HF]^{+}$, compared to the crystal structure of **4**.

As the protonation results in an elongation of the C=O bond lengths in contrast to fumaryl fluoride, the C–F bond distances are reduced, which is predicted by the quantum chemical calculations and confirmed by the vibrational spectra, as well as by the single-crystal X-ray structure analyses. This peculiarity of the protonated acyl fluoride moiety prompted us to further investigate the electron distribution and the charge-related properties of the dication in comparison with the reactant. Thus, electrostatic potential (ESP) maps combined with natural population analysis (NPA) charges were calculated. In Figure 8, the ESP maps together with the NPA charges of *cis-cis*-fumaryl fluoride and $[C_4H_4F_2O_2\cdot 2\,HF]^{2+}$ are illustrated. The ESP map of the neutral compound shows a positive electrostatic potential along the carbon skeleton. The negative electrostatic potential is found on the oxygen and fluorine atoms, which also reveal the highest negative NPA charges. The C–F bond of the acyl fluoride group is polarized, increasing the

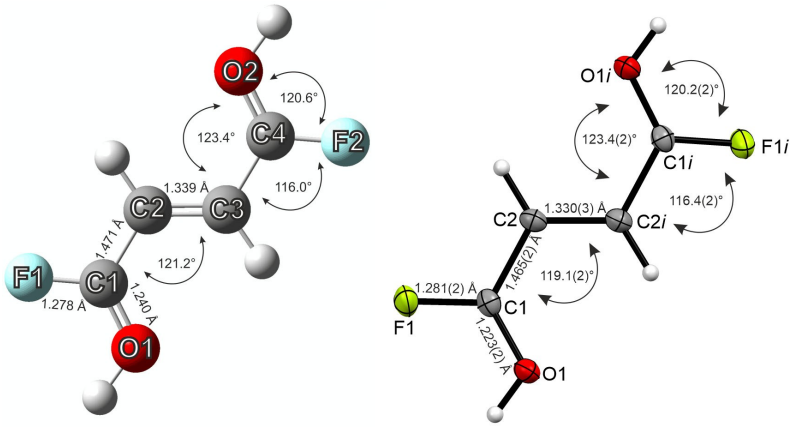

Figure 6. Calculated (left) and experimental (right) structures of $[C_4H_4F_2O_2]^{2+}$ with bond lengths and angles. The calculation was performed for $[C_4H_4F_2O_2\cdot 2\,HF]^{2+}$, but the HF molecules are omitted for clarity.

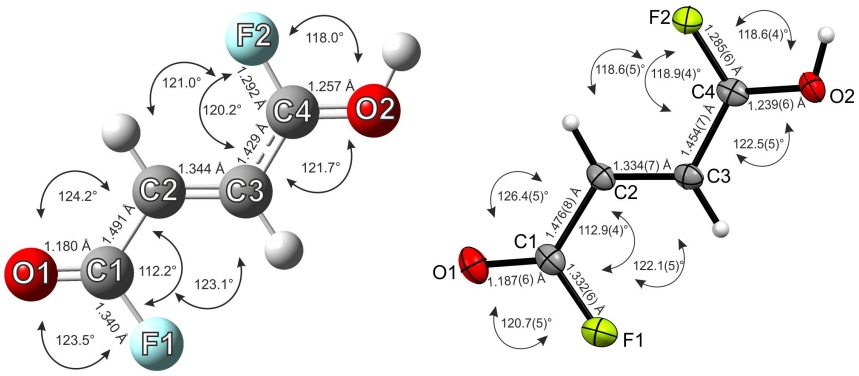

Figure 7. Calculated (left) and experimental (right) structures of $[C_4H_3F_2O_2]^+$ with bond lengths and angles. The calculation was performed for $[C_4H_3F_2O_2 \cdot HF]^+$, but the HF molecule is omitted for clarity.

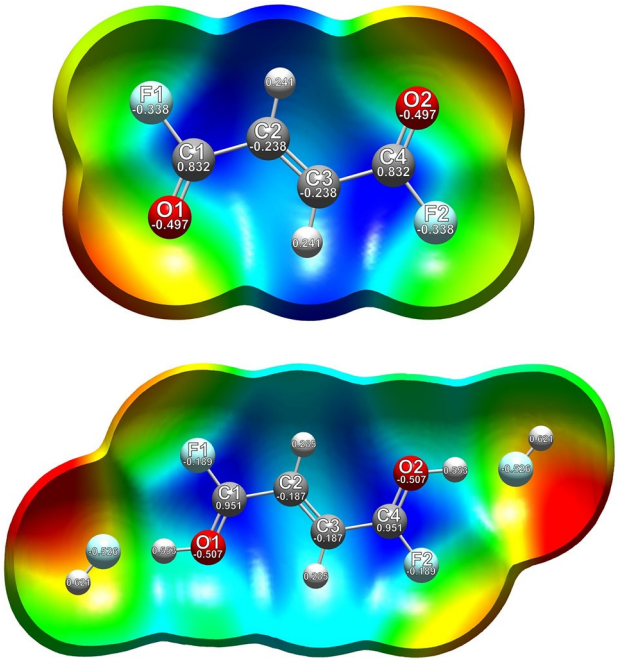

Figure 8. Top: Calculated ESP surface mapped onto an electron density isosurface value of 0.0004 bohr^{-3} with the color scale ranging from −0.029 a.u. (red) to 0.035 a.u. (blue) of *cis-cis*–$C_4H_2F_2O_2$. Bottom: calculated ESP map with an electron density isosurface value of 0.00004 bohr^{-3} and a color scale range from −0.2 a.u. (red) to 0.275 a.u. (blue) of $[C_4H_4F_2O_2 \cdot 2HF]^{2+}$. The NPA charges are given in [a.u.].

positive charge density on the carbon atom, owing to the high electronegativity of fluorine.[1] The electrostatic attraction between $F^{\delta-}$ and $(O{=}C^{\delta+})$ reduces the C–F bond distance,[1] in comparison to regular C–F bond lengths (1.36 Å).[14] The diprotonation of fumaryl fluoride results in a rearrangement of the electrostatic potential distribution. The positive electrostatic potential in the ESP map of $[C_4H_4F_2O_2 \cdot 2HF]^{2+}$ is located on the carbonyl fluoride moiety. In comparison to the reactant, the positive NPA charges of the C1 and C4 atoms in the diprotonated species increase. This leads to the assumption, that the positive charges are delocalized over the carbonyl fluoride groups. By comparing the NPA charges of fumaryl fluoride with the NPA charges of the HF complex of the dication, the negative charges of the oxygen atoms increase slightly, whereas the negative charges of the fluorine atoms decrease considerably. The electron distribution shifts from the fluorine atom, which is inductively electron withdrawing but electron donating by resonance (+M effect) despite its high electronegativity,[28–32] to the C–F bond in the diprotonated cation. This resonance effect, that opposes the inductive effect, generating a more electropositive carbon, is established in literature as +R effect,[33,34] which is illustrated in Scheme 1. The bond between carbon and fluorine reveals a low double bond character, which is described in the literature for several organofluorine compounds.[28–34] To draw comparisons of diprotonated fumaryl fluoride with organofluorine species, which are already related to resonance effects based on fluorine, the C–F bond lengths of CHF_3[35] and CF_3Cl[36] are consulted. The carbon fluorine bond distances in CHF_3 (1.326(13) Å)[35] and CF_3Cl (1.328(2) Å)[36] are considerably shortened in comparison to regular C–F bond lengths (1.36 Å).[14] This strengthening of the C–F bond is explained by a decreasing ionic character of the bond.[34] The great resonance-electron-donating ability of fluorine leads to C=F double bond structures gaining increased importance.[28,34] Notably, the C–F bond distance in **1** is even shorter than those of CHF_3[35] and CF_3Cl,[36] and therefore the contributing structure with the C=F double bond is of higher importance. Finally, we assume that the strongest bond in organic chemistry[1] is further strengthened due to the protonation of the acyl fluoride moiety, based on the resonance stabilization of the carbon–fluorine bond. This

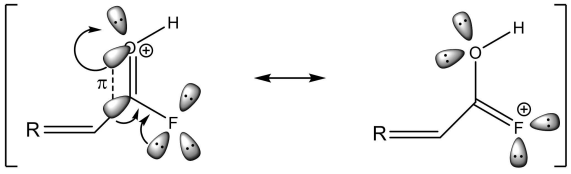

Scheme 1. Illustration of the +R effect by using the example of a protonated acyl fluoride moiety.

is especially reinforced for analogous diprotonated superelectrophiles.[37]

Conclusions

Fumaryl fluoride has been examined in the superacidic systems XF/MF_5 (X=H, D; M=As, Sb) for the first time. The salts of the monoprotonated and diprotonated fumaryl fluoride represent the first examples of a protonated acyl fluoride moiety. They were isolated and characterized by low-temperature vibrational spectroscopy. Single-crystal X-ray structure analyses and low-temperature NMR spectroscopy were performed for $[C_4H_3F_2O_2]^+[SbF_6]^-$ and for $[C_4H_4F_2O_2]^{2+}([MF_6]^-)_2$ (M=As, Sb). The experimental results have been discussed together with quantum chemical calculations on the cations $[C_4H_4F_2O_2\cdot 2\,HF]^{2+}$ and $[C_4H_3F_2O_2\cdot HF]^+$ at the B3LYP/aug-cc-pVTZ level of theory. The vibrational spectra and single-crystal X-ray structure analyses showed that the protonation results in an elongation of the C=O bonds, whereas the C–F bond lengths are considerably reduced. In order to investigate the electron distribution and the charge-related properties of the diprotonated species, electrostatic potential (ESP) maps combined with natural population analysis (NPA) charges were calculated. The electron distribution shifts from the fluorine atom, which is inductively electron withdrawing, although it is electron donating by resonance,[28–32] to the C–F bond in the diprotonated cation, known in literature as the +R effect.[33] In the NMR spectra of diprotonated fumaryl fluoride, the enhanced resonance-electron-donating ability is observed in the increased proton–fluorine coupling constants. The bond between carbon and fluorine reveals a low double-bond character in the diprotonated cation. We conclude that the strongest bond in organic chemistry[1] is further strengthened by the protonation of the acyl fluoride moiety on account of the +R effect.

Experimental Section

CAUTION! Any contact with the components must be avoided. SbF_5, AsF_5 and the reported salts can produce HF upon contact with water, burning the skin and causing irreparable injury. Adequate precautionary measures must be taken when handling these materials.

Syntheses of $[C_4H_4F_2O_2]^{2+}([AsF_6]^-)_2$ (1), $[C_4H_3F_2O_2]^+[AsF_6]^-$ (3) and $[C_4H_2D_2F_2O_2]^{2+}([AsF_6]^-)_2$ (5): At first, fumaryl fluoride (100 mg, 0.83 mmol) was condensed into a FEP reactor vessel at −196 °C. Additionally, arsenic pentafluoride (595 mg, 3.5 mmol **1**, **5**; 280 mg, 1.65 mmol **3**) and approximately 2 mL anhydrous hydrogen fluoride (*a*HF; **1**, **3**) deuterium fluoride (*a*DF; **5**), respectively, were condensed into the FEP reactor vessel at −196 °C. The reaction mixture was warmed up to −30 °C and homogenzied until the solution was clear. In dynamic vacuum excess HF was removed at −78 °C. The compounds were obtained as colorless crystalline solids with decomposition temperatures of 15 °C for **1**, **5** and −10 °C for **3**. The rector was left in an ethanol bath at −50 °C for crystallization of **1**.

Syntheses of $[C_4H_4F_2O_2]^{2+}([SbF_6]^-)_2$ (2), $[C_4H_3F_2O_2]^+[SbF_6]^-$ (4) and $[C_4H_2D_2F_2O_2]^{2+}([SbF_6]^-)_2$ (6): Antimony pentafluoride (310 mg, 1.43 mmol) was condensed into a FEP reactor vessel at −196 °C. In addition, fumaryl fluoride (40 mg, 0.33 mmol **2**, **6**; 156 mg, 1.3 mmol **4**) and 2 mL of *a*HF (**2**, **4**) or *a*DF (**6**), respectively, were condensed into the reactor vessel at −196 °C. The reaction mixture was warmed up to −30 °C and homogenized until the formed salt was dissolved thoroughly. Excess HF was removed in dynamic vacuum at −78 °C. The compounds were obtained as colorless crystalline solids with decomposition temperatures of 15 °C for **2**, **6** and −10 °C for **4**. The rector was left in an ethanol bath at −50 °C for crystallization of **2** and at −40 °C for crystallization of **4**.

Deposition Numbers 2065273 (for **1**), 2065274 (for **2**) and 2065275 (for**4**) contain the supplementary crystallographic data for this paper. These data are provided free of charge by the joint Cambridge Crystallographic Data Centre and Fachinformationszentrum Karlsruhe Access Structures service.

Acknowledgements

We gratefully acknowledge the financial support of the Department of Chemistry of the Ludwig-Maximilians-Universität (LMU), the Deutsche Forschungsgemeinschaft (DFG) and the F-Select GmbH. Open Access funding enabled and organized by Projekt DEAL.

Conflict of Interest

The authors declare no conflict of interests.

Data Availability Statement

The data that support the findings of this study are available in the supplementary material of this article.

Keywords: fluorides · quantum chemical calculations · +R effect · superacids · vibrational spectroscopy · X-ray structure analyses

[1] D. O'Hagan, *Chem. Soc. Rev.* **2008**, *37*, 308.
[2] P. Kirsch, *Modern Fluoroorganic Chemistry. Synthesis, Reactivity, Applications*, Wiley-VCH, Weinheim, **2004**.
[3] Y. Ogiwara, N. Sakai, *Angew. Chem. Int. Ed.* **2020**, *59*, 574.
[4] a) M. Gonay, C. Batisse, J.-F. Paquin, *J. Org. Chem.* **2020**, *85*, 10253; b) Y. Ogiwara, Y. Maegawa, D. Sakino, N. Sakai, *Chem. Lett.* **2016**, *45*, 790; c) Y. Liang, A. Taya, Z. Zhao, N. Saito, N. Shibata, *Beilstein J. Org. Chem.* **2020**, *16*, 3052.
[5] a) F. Seel, *Z. Anorg. Allg. Chem.* **1943**, *250*, 331; b) G. A. Olah, *Angew. Chem. Int. Ed. Engl.* **1973**, *12*, 173.
[6] G. A. Olah, S. J. Kuhn, W. S. Tolgyesi, E. B. Baker, *J. Am. Chem. Soc.* **1962**, *84*, 2733.
[7] G. A. Olah, M. B. Comisarow, *J. Am. Chem. Soc.* **1966**, *88*, 3313.
[8] M. C. Bayer, C. Jessen, A. J. Kornath, *Z. Anorg. Allg. Chem.* **2021**, *647*, 258.
[9] J. W. Larsen, P. A. Bouis, *J. Org. Chem.* **1973**, *38*, 1415.
[10] M. C. Bayer, C. Jessen, A. J. Kornath, *Z. Anorg. Allg. Chem.* **2020**, *646*, 333.
[11] G. A. Olah, A. M. White, *J. Am. Chem. Soc.* **1967**, *89*, 4752.
[12] M. Schickinger, F. Zischka, K. Stierstorfer, A. Kornath, *Eur. J. Org. Chem.* **2019**, *2019*, 1876.
[13] G. A. Olah, G. K. Prakash, J. Sommer, *Science* **1979**, *206*, 13.
[14] A. F. Holleman, E. Wiberg, N. Wiberg, G. Fischer, *Anorganische Chemie*, De Gruyter, Berlin, **2017**.

[15] a) G. Gafner, G. J. Kruger, *Acta Crystallogr.* **1974**, *B30*, 250; b) R. Minkwitz, F. Neikes, U. Lohmann, *Eur. J. Inorg. Chem.* **2002**, *2002*, 27.
[16] G. A. Jeffrey, *An Introduction to Hydrogen Bonding, Topics in Physical Chemistry*, Oxford University Press, New York, **1997**.
[17] A. Bondi, *J. Phys. Chem.* **1964**, *68*, 441.
[18] R. Minkwitz, C. Hirsch, T. Berends, *Eur. J. Inorg. Chem.* **1999**, *1999*, 2249.
[19] M. Schickinger, T. Saal, F. Zischka, J. Axhausen, K. Stierstorfer, Y. Morgenstern, A. J. Kornath, *ChemistrySelect* **2018**, *3*, 12396.
[20] R. Minkwitz, S. Schneider, *Angew. Chem.* **1999**, *111*, 229.
[21] J. Weidlein, U. Müller, K. Dehnicke, *Schwingungsspektroskopie*, Thieme, Stuttgart, **1988**.
[22] D. F. Koster, T. P. Vasileff, G. L. Carlson, *Spectrochim. Acta Part A* **1971**, *27*, 1633.
[23] T. Soltner, N. R. Goetz, A. Kornath, *Eur. J. Inorg. Chem.* **2011**, *2011*, 3076.
[24] T. P. Vasileff, D. F. Koster, *J. Org. Chem.* **1970**, *35*, 2461.
[25] J. Eills, G. Stevanato, C. Bengs, S. Glöggler, S. J. Elliott, J. Alonso-Valdesueiro, G. Pileio, M. H. Levitt, *J. Magn. Reson.* **2017**, *274*, 163.
[26] H. J. Reich, J. E. Holladay, T. G. Walker, J. L. Thompson, *J. Am. Chem. Soc.* **1999**, *121*, 9769.
[27] H. Friebolin, *Ein- und Zweidimensionale NMR-Spektroskopie: Eine Einführung*, Wiley-VCH, Weinheim, **2013**.
[28] G. A. Olah, C. A. Cupas, M. B. Comisarow, *J. Am. Chem. Soc.* **1966**, *88*, 362.
[29] B. E. Smart, *J. Fluorine Chem.* **2001**, *109*, 3.
[30] K. O. Christe, X. Zhang, R. Bau, J. Hegge, G. A. Olah, G. K. S. Prakash, J. A. Sheehy, *J. Am. Chem. Soc.* **2000**, *122*, 481.
[31] G. A. Olah, G. K. S. Prakash, G. Rasul, *Proc. Natl. Acad. Sci. USA* **2013**, *110*, 8427.
[32] E. Kraka, D. Cremer, *ChemPhysChem* **2009**, *10*, 686.
[33] T. Hiyama, *Organofluorine Compounds, Chemistry and Applications*, Springer, Berlin, **2000**.
[34] L. H. Meyer, H. S. Gutowsky, *J. Phys. Chem.* **1953**, *57*, 481.
[35] O. R. Gilliam, H. D. Edwards, W. Gordy, *Phys. Rev.* **1949**, *75*, 1014.
[36] L. S. Bartell, L. O. Brockway, *J. Chem. Phys.* **1955**, *23*, 1860.
[37] M. Artault, K. Vitse, A. Martin-Mingot, S. Thibaudeau, *Chem. Eur. J.* **2021**, *27*, 1.

Manuscript received: February 4, 2022
Accepted manuscript online: January 26, 2022
Version of record online: February 10, 2022

Chemistry—A European Journal

Supporting Information

Strengthening of the C—F Bond in Fumaryl Fluoride with Superacids

Marie C. Bayer, Christoph Kremser, Christoph Jessen, Alexander Nitzer, and Andreas J. Kornath*

Figure S1: Formula unit of $[C_4H_4F_2O_2]^{2+}([AsF_6]^-)_2$ (displacement ellipsoids with 50% probability). Symmetry operations: *i = 1–x, y, 0.5–z.*

Table S1: Selected bond lengths and angles of $[C_4H_4F_2O_2]^{2+}([AsF_6]^-)_2$ **(1)**. The estimated standard deviation is marked in parentheses. Symmetry operations: *i = 1–x, y, 0.5–z; iii = 1–x, 1–y, 1–z; iv = 1–x, –y, 1–z.*

Figure S2: Projection of the interatomic contacts in $[C_4H_4F_2O_2]^{2+}([AsF_6]^-)_2$ **(1)** (displacement ellipsoids 50% probability). Symmetry operations: *i = 1–x, y, 0.5–z; ii = x, 1–y, –0.5+z; iii = 1–x, 1–y, 1–z; iv = 1–x, –y, 1–z; v = x, –y, –0.5+z.* Interatomic contacts are drawn as dashed lines.

Figure S3: Detail of the crystal structure of $[C_4H_4F_2O_2]^{2+}([AsF_6]^-)_2$ **(1)** (displacement ellipsoids with 50% probability). Interatomic contacts are drawn as dashed lines.

Figure S4: Formula unit of $[C_4H_4F_2O_2]^{2+}([SbF_6]^-)_2$ (displacement ellipsoids with 50% probability). Symmetry operations: *i = 2–x, –y, 1–z.*

Table S2: Selected bond lengths and angles of $[C_4H_4F_2O_2]^{2+}([SbF_6]^-)_2$ **(2)**. The estimated standard deviation is marked in parentheses. Symmetry operations: *i = 2–x, –y, 1–z; ii = 2–x, 1–y, 1–z; iii = 1+x, –1+y, z.*

Figure S5: Projection of the interatomic contacts in $[C_4H_4F_2O_2]^{2+}([SbF_6]^-)_2$ **(2)** (displacement ellipsoids 50% probability). Symmetry operations: *i = 2–x, –y, 1–z; ii = 2–x, 1–y, 1–z; iii = 1+x, –1+y, z; iv = x, –1+y, z; v = 1–x, 1–y, 1–z.* Interatomic contacts are drawn as dashed lines.

Figure S6: Asymmetric unit of $[C_4H_3F_2O_2]^+[SbF_6]^-$ (displacement ellipsoids with 50% probability).

Table S3: Selected bond lengths and angles of $[C_4H_3F_2O_2]^+[SbF_6]^-$ **(4)**. The estimated standard deviation is marked in parentheses. Symmetry operations: *i = 0.5+x, 1.5–y, –0.5+z; iii = –1+x, 1–y, 0.5+z.*

Figure S7: Projection of the interatomic contacts in $[C_4H_3F_2O_2]^+[SbF_6]^-$ **(4)** (displacement ellipsoids 50% probability). Symmetry operations: *i = 0.5+x, 1.5–y, –0.5+z; ii = –0.5+x, 1.5–y, 0.5+z; iii = –1+x, 1–y, 0.5+z.* Interatomic contacts are drawn as dashed lines.

Figure S8: Detail of the crystal structure of $[C_4H_3F_2O_2]^+[SbF_6]^-$ **(4)** (displacement ellipsoids with 50% probability). Interatomic contacts are drawn as dashed lines.

Figure S9: Low-temperature IR and Raman spectra of $[C_4H_2D_2F_2O_2]^{2+}([AsF_6]^-)_2$ **(5)**, $[C_4H_2D_2F_2O_2]^{2+}([SbF_6]^-)_2$ **(6)** and fumaryl fluoride.[1]

Table S4: Experimental vibrational frequencies [cm^{-1}] of $[C_4H_4F_2O_2]^{2+}([MF_6]^-)_2$ (M = As, Sb) and calculated vibrational frequencies [cm^{-1}] of $[C_4H_4F_2O_2 \cdot 2\ HF]^{2+}$.

Table S5: Experimental vibrational frequencies [cm^{-1}] of $[C_4H_2D_2F_2O_2]^{2+}([MF_6]^-)_2$ (M = As, Sb) and calculated vibrational frequencies [cm^{-1}] of $[C_4H_2D_2F_2O_2 \cdot 2\ HF]^{2+}$.

Table S6: Experimental vibrational frequencies [cm^{-1}] of $[C_4H_3F_2O_2]^+[MF_6]^-$ (M = As, Sb) and calculated vibrational frequencies [cm^{-1}] of $[C_4H_3F_2O_2 \cdot HF]^+$.

Table S7: Observed ^1H, ^{13}C and ^{19}F chemical shifts [ppm] and spin-spin coupling constants [Hz] of fumaryl fluoride in $CDCl_3$.

Table S8: Selected observed ^1H, ^{13}C and ^{19}F NMR chemical shifts [ppm] and spin-spin coupling constants [Hz] of $C_4H_2F_2O_2$ in $CDCl_3$ as well as $C_4H_2F_2O_2$, **1**, **2** and **4** in *a*HF (external solvent Acetone-D_6), respectively.

Figure S10: Stacked ^1H NMR spectra of $C_4H_2F_2O_2$ dissolved in $CDCl_3$ and $C_4H_2F_2O_2$, $[C_4H_4F_2O_2]^{2+}([AsF_6]^-)_2$ **(1)**, $[C_4H_4F_2O_2]^{2+}([SbF_6]^-)_2$ **(2)** and $[C_4H_3F_2O_2]^+[SbF_6]^-$ **(4)** in *a*HF.

Figure S11: ^1H NMR spectrum of $C_4H_2F_2O_2$ at 26 °C in $CDCl_3$.

Figure S12: Detail of the ^1H NMR spectrum of $C_4H_2F_2O_2$ at 26 °C in $CDCl_3$.

Figure S13: ^{19}F NMR spectrum of $C_4H_2F_2O_2$ at 26 °C in $CDCl_3$.

Figure S14: Detail of the ^{19}F NMR spectrum of $C_4H_2F_2O_2$ at 26 °C in $CDCl_3$.

Figure S15: ^{13}C NMR spectrum of $C_4H_2F_2O_2$ at 26 °C in $CDCl_3$.

Figure S16: ^1H NMR spectrum of $C_4H_2F_2O_2$ at –41 °C in *a*HF and Acetone-D_6 as external solvent.

Figure S17: ^{19}F NMR spectrum of $C_4H_2F_2O_2$ at –41 °C in *a*HF and Acetone-D_6 as external solvent.

Figure S18: ^{13}C NMR spectrum of $C_4H_2F_2O_2$ at –41 °C in *a*HF and Acetone-D_6 as external solvent.

Figure S19: ^{1}H NMR spectrum of $[C_4H_4F_2O_2]^{2+}([AsF_6]^-)_2$ **(1)**, at –40 °C in *a*HF and Acetone-D_6 as external solvent.

Figure S20: ^{19}F NMR spectrum of $[C_4H_4F_2O_2]^{2+}([AsF_6]^-)_2$ **(1)**, at –40 °C in *a*HF and Acetone-D_6 as external solvent.

Figure S21: ^{13}C NMR spectrum of $[C_4H_4F_2O_2]^{2+}([AsF_6]^-)_2$ **(1)**, at –40 °C in *a*HF and Acetone-D_6 as external solvent.

Figure S22: ^{1}H NMR spectrum of $[C_4H_4F_2O_2]^{2+}([SbF_6]^-)_2$ **(2)**, at –40 °C in *a*HF and Acetone-D_6 as external solvent.

Figure S23: ^{19}F NMR spectrum of $[C_4H_4F_2O_2]^{2+}([SbF_6]^-)_2$ **(2)**, at –40 °C in *a*HF and Acetone-D_6 as external solvent.

Figure S24: ^{13}C NMR spectrum of $[C_4H_4F_2O_2]^{2+}([SbF_6]^-)_2$ **(2)**, at –35 °C in *a*HF and Acetone-D_6 as external solvent.

Figure S25: ^{1}H NMR spectrum of $[C_4H_3F_2O_2]^+[SbF_6]^-$ **(4)**, at –40 °C in *a*HF and Acetone-D_6 as external solvent.

Figure S26: ^{19}F NMR spectrum of $[C_4H_3F_2O_2]^+[SbF_6]^-$ **(4)**, at –40 °C in *a*HF and Acetone-D_6 as external solvent.

Figure S27: ^{13}C NMR spectrum of $[C_4H_3F_2O_2]^+[SbF_6]^-$ **(4)**, at –40 °C in *a*HF and Acetone-D_6 as external solvent.

Table S9: Calculated bond lengths and angles of the free cation $[C_4H_4F_2O_2]^{2+}$ and the HF complex of the cation $[C_4H_4F_2O_2 \cdot 2\,HF]^{2+}$ in comparison with the experimental structural parameters of $[C_4H_4F_2O_2]^{2+}([AsF_6]^-)_2$ **(1)**. The estimated standard deviation is marked in parentheses. Symmetry operations: *i = 1–x, y, 0.5–z*.

Table S10: Selected experimental vibrational frequencies [cm^{-1}] of $[C_4H_4F_2O_2]^{2+}([AsF_6]^-)_2$ **(1)** and calculated vibrational frequencies [cm^{-1}] of $[C_4H_4F_2O_2]^{2+}$ and $[C_4H_4F_2O_2 \cdot 2\,HF]^{2+}$.

Table S11: Calculated bond lengths and angles of the free cation $[C_4H_3F_2O_2]^+$ and the HF complex of the cation $[C_4H_3F_2O_2 \cdot HF]^+$ in comparison with the experimental structural parameters of $[C_4H_3F_2O_2]^+[SbF_6]^-$ **(4)**. The estimated standard deviation is marked in parentheses.

Table S12: Crystal data and structure refinement of $[C_4H_4F_2O_2]^{2+}([AsF_6]^-)_2$ **(1)**, $[C_4H_4F_2O_2]^{2+}([SbF_6]^-)_2$ **(2)** and $[C_4H_3F_2O_2]^+[SbF_6]^-$ **(4)**.

Table S13: Cartesian coordinates of calculated minimum structures of $[C_4H_4F_2O_2 \cdot 2\,HF]^{2+}$ at the B3LYP/aug-cc-pVTZ level of theory.

Table S14: Cartesian coordinates of calculated minimum structures of $[C_4H_4F_2O_2]^{2+}$ at the B3LYP/aug-cc-pVTZ level of theory.

Table S15: Cartesian coordinates of calculated minimum structures of $[C_4H_2D_2F_2O_2 \cdot 2\,HF]^{2+}$ at the B3LYP/aug-cc-pVTZ level of theory.

Table S16: Cartesian coordinates of calculated minimum structures of $[C_4H_3F_2O_2 \cdot HF]^+$ at the B3LYP/aug-cc-pVTZ level of theory.

Table S17: Cartesian coordinates of calculated minimum structures of $[C_4H_3F_2O_2]^+$ at the B3LYP/aug-cc-pVTZ level of theory.

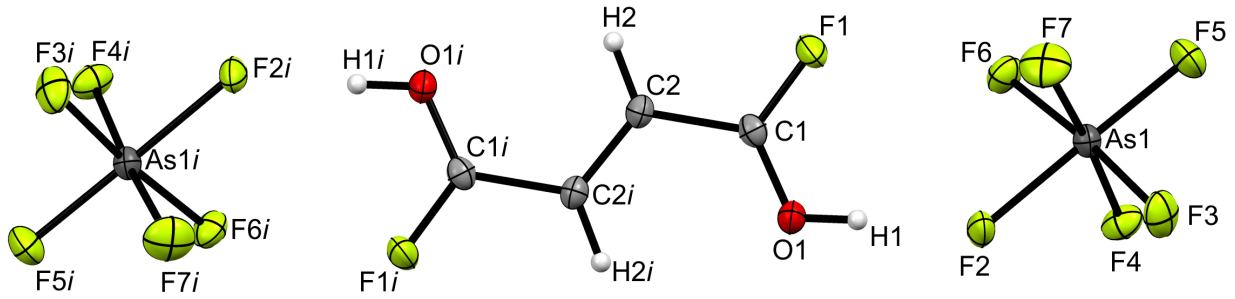

Figure S1: Formula unit of $[C_4H_4F_2O_2]^{2+}([AsF_6]^-)_2$ (displacement ellipsoids with 50% probability). Symmetry operations: *i = 1–x, y, 0.5–z.*

Table S1: Selected bond lengths and angles of $[C_4H_4F_2O_2]^{2+}([AsF_6]^-)_2$ (1). The estimated standard deviation is marked in parentheses. Symmetry operations: *i = 1–x, y, 0.5–z; iii = 1–x, 1–y, 1–z; iv = 1–x, –y, 1–z.*

Bond length [Å]	
C2–C2*i* (C=C)	1.330(3)
C1–C2 (C–C)	1.465(2)
C1–O1	1.223(2)
C1–F1	1.281(2)
Bond angle [°]	
O1–C1–F1	120.2(2)
O1–C1–C2	123.4(2)
F1–C1–C2	116.4(2)
C1–C2–C2*i*	119.1(2)
Angle of torsion [°]	
O1–C1–C2–C2*i*	9.5(3)
F1–C1–C2–C2*i*	–169.7(2)
C1–C2–C2*i*–C1*i*	177.9(1)
Interatomic contact [Å]	
O1–H1···F2	2.429(2)
C1···F4*iii*	2.614(2)
C1···F3*iv*	2.868(2)

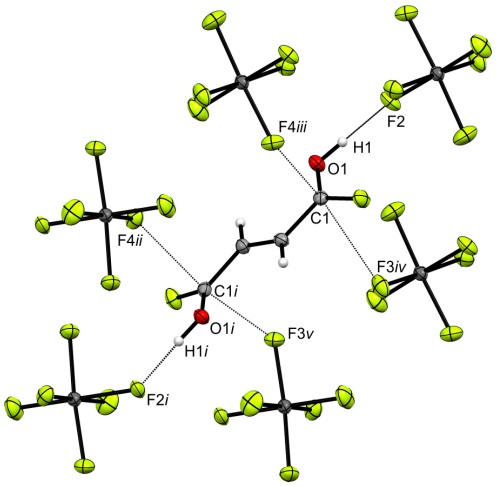

Figure S2: Projection of the interatomic contacts in $[C_4H_4F_2O_2]^{2+}([AsF_6]^-)_2$ (1) (displacement ellipsoids 50% probability). Symmetry operations: *i = 1–x, y, 0.5–z; ii = x, 1–y, –0.5+z; iii = 1–x, 1–y, 1–z; iv = 1–x, –y, 1–z; v = x, –y, –0.5+z*. Interatomic contacts are drawn as dashed lines.

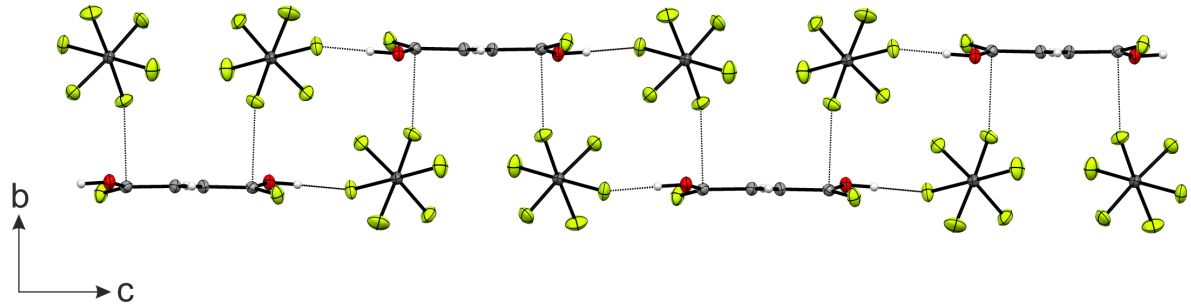

Figure S3: Detail of the crystal structure of $[C_4H_4F_2O_2]^{2+}([AsF_6]^-)_2$ (1) (displacement ellipsoids with 50% probability). Interatomic contacts are drawn as dashed lines.

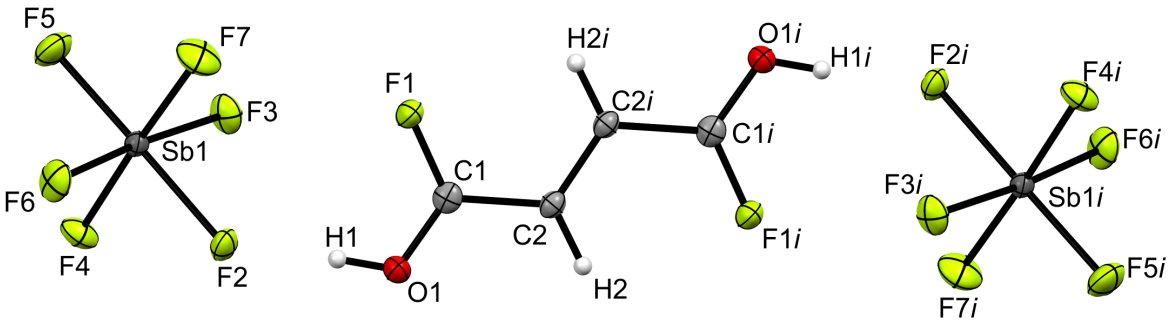

Figure S4: Formula unit of $[C_4H_4F_2O_2]^{2+}([SbF_6]^-)_2$ (displacement ellipsoids with 50% probability). Symmetry operations: *i = 2–x, –y, 1–z.*

Table S2: Selected bond lengths and angles of $[C_4H_4F_2O_2]^{2+}([SbF_6]^-)_2$ (2). The estimated standard deviation is marked in parentheses. Symmetry operations: *i = 2–x, –y, 1–z; ii = 2–x, 1–y, 1–z; iii = 1+x, –1+y, z.*

Bond length [Å]	
C2–C2*i* (C=C)	1.336(5)
C1–C2 (C–C)	1.461(4)
C1–O1	1.223(4)
C1–F1	1.287(4)
Bond angle [°]	
O1–C1–F1	120.6(3)
O1–C1–C2	121.1(3)
F1–C1–C2	118.2(3)
C1–C2–C2*i*	120.1(3)
Angle of torsion [°]	
O1–C1–C2–C2*i*	174.9(3)
F1–C1–C2–C2*i*	–6.0(5)
C1–C2–C2*i*–C1*i*	–180.0(3)
Interatomic contact [Å]	
O1–H1···F2	2.426(3)
C2–H2···F5*iii*	3.072(4)
C1···F3*ii*	2.578(4)

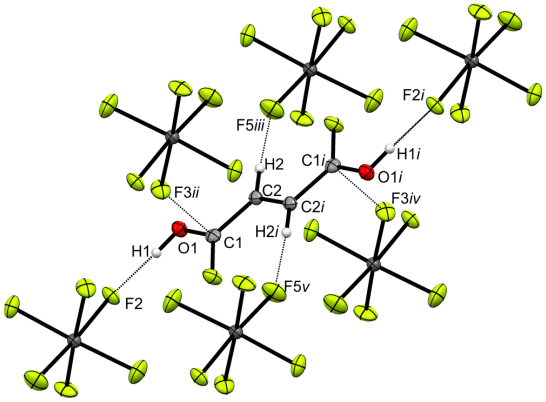

Figure S5: Projection of the interatomic contacts in $[C_4H_4F_2O_2]^{2+}([SbF_6]^-)_2$ (2) (displacement ellipsoids 50% probability). Symmetry operations: *i = 2–x, –y, 1–z; ii = 2–x, 1–y, 1–z; iii = 1+x, –1+y, z; iv = x, –1+y, z; v = 1–x, 1–y, 1–z*. Interatomic contacts are drawn as dashed lines.

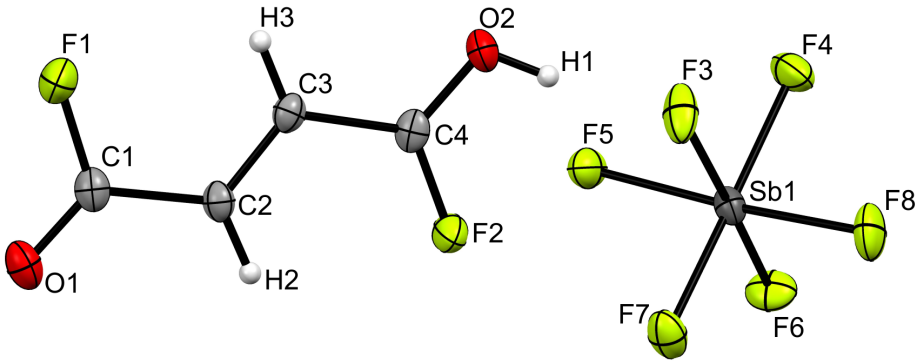

Figure S6: Asymmetric unit of $[C_4H_3F_2O_2]^+[SbF_6]^-$ (displacement ellipsoids with 50% probability).

Table S3: Selected bond lengths and angles of $[C_4H_3F_2O_2]^+[SbF_6]^-$ (4). The estimated standard deviation is marked in parentheses. Symmetry operations: *i = 0.5+x, 1.5–y, –0.5+z; iii = –1+x, 1–y, 0.5+z.*

Bond length [Å]	
C2–C3 (C=C)	1.334(7)
C1–C2 (C–C)	1.476(8)
C3–C4 (C–C)	1.454(7)
C1–O1 (C=O)	1.187(6)
C4–O2	1.239(6)
C1–F1	1.332(6)
C4–F2	1.285(6)
Bond angle [°]	
O1–C1–F1	120.7(5)
O2–C4–F2	118.6(4)
O1–C1–C2	126.4(5)
O2–C4–C3	122.5(5)
F1–C1–C2	112.9(4)
F2–C4–C3	118.9(4)
C1–C2–C3	122.1(5)
C4–C3–C2	118.6(5)
Angle of torsion [°]	
O1–C1–C2–C3	–174.5(5)
O2–C4–C3–C2	172.1(5)
F1–C1–C2–C3	7.1(7)
F2–C4–C3–C2	–6.2(7)
C1–C2–C3–C4	–177.1(5)
Interatomic contact [Å]	
O2–H1···F3	2.470(5)
C4···O1*i*	2.809(6)
C2···F8*iii*	2.839(7)

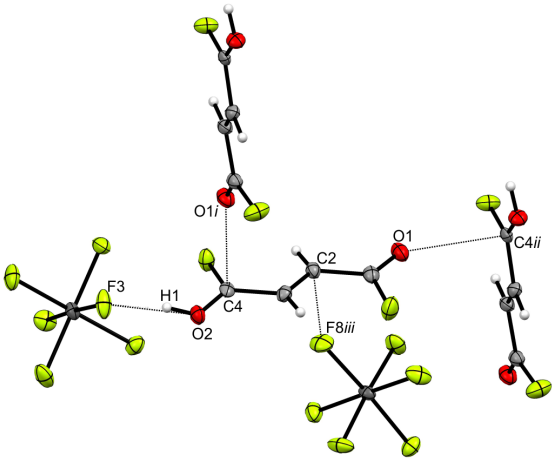

Figure S7: Projection of the interatomic contacts in $[C_4H_3F_2O_2]^+[SbF_6]^-$ (4) (displacement ellipsoids 50% probability). Symmetry operations: *i = 0.5+x, 1.5–y, –0.5+z; ii = –0.5+x, 1.5–y, 0.5+z; iii = –1+x, 1–y, 0.5+z*. Interatomic contacts are drawn as dashed lines.

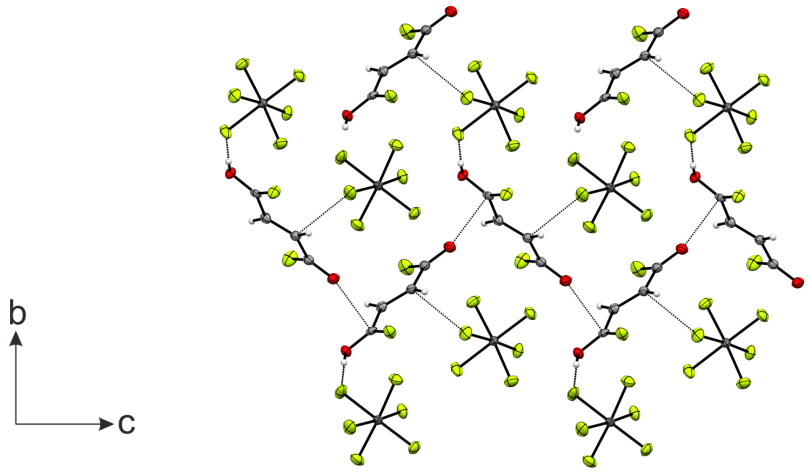

Figure S8: Detail of the crystal structure of $[C_4H_3F_2O_2]^+[SbF_6]^-$ (4) (displacement ellipsoids with 50% probability). Interatomic contacts are drawn as dashed lines.

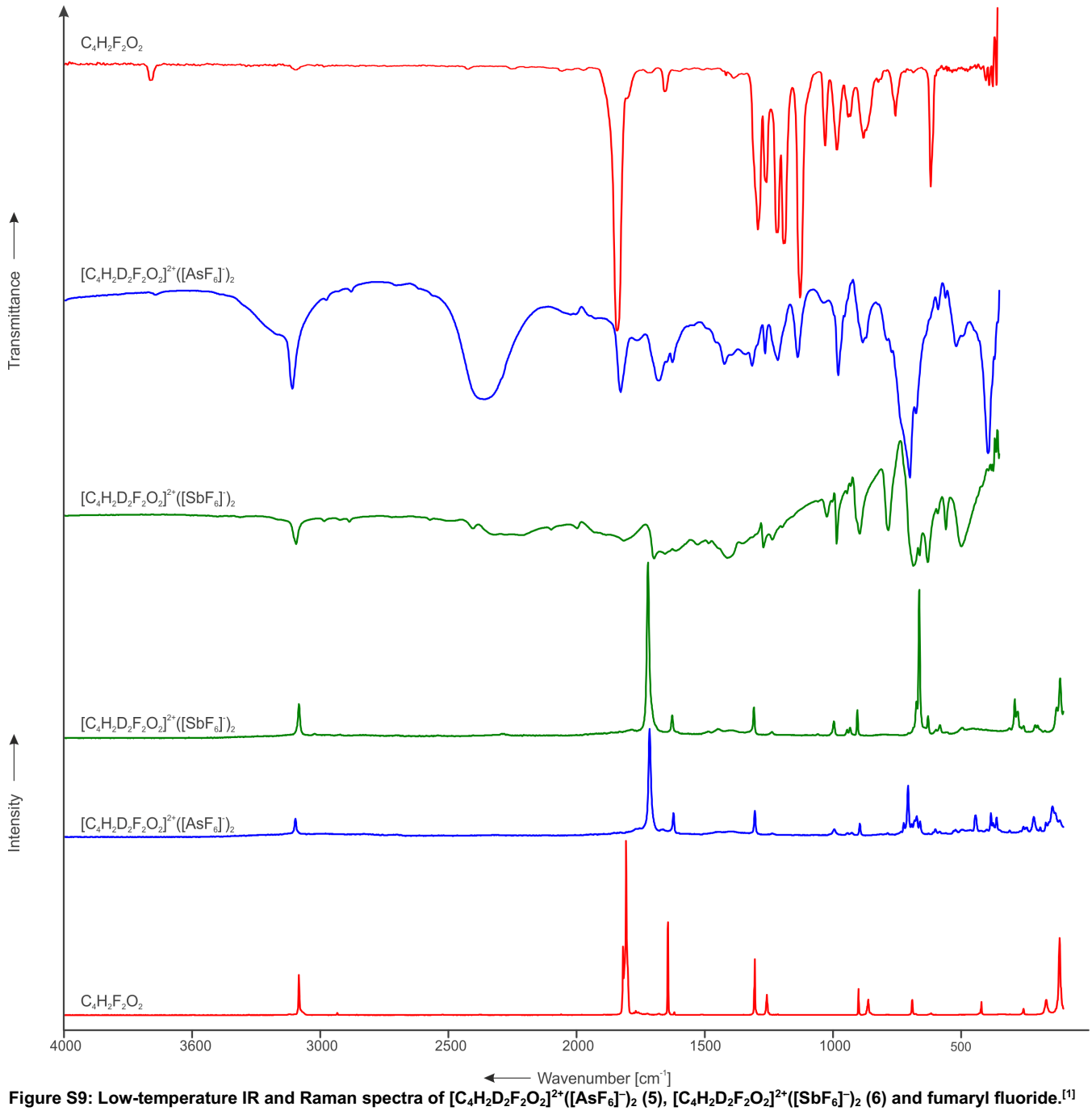

Figure S9: Low-temperature IR and Raman spectra of $[C_4H_2D_2F_2O_2]^{2+}([AsF_6]^-)_2$ (5), $[C_4H_2D_2F_2O_2]^{2+}([SbF_6]^-)_2$ (6) and fumaryl fluoride.[1]

Table S4: Experimental vibrational frequencies [cm^{-1}] of $[C_4H_4F_2O_2]^{2+}([MF_6]^-)_2$ (M = As, Sb) and calculated vibrational frequencies [cm^{-1}] of $[C_4H_4F_2O_2 \cdot 2\ HF]^{2+}$.

$[C_4H_4F_2O_2]^{2+}([AsF_6]^-)_2$ **(1)** exp.[a]		$[C_4H_4F_2O_2]^{2+}([SbF_6]^-)_2$ **(2)** exp.[a]		$[C_4H_4F_2O_2 \cdot 2\ HF]^{2+}$ calc.[b]	Assignment		
IR	Raman	IR	Raman	IR/Raman			
3109 vs		3094 vs		3190 (60/0)	ν_{21}	B_u	ν_{as}(C–H)
	3098 (24)		3085 (9)	3188 (0/79)	ν_1	A_g	ν_s(C–H)
3074 s							[c]
				2536 (3/246)	ν_2	A_g	ν_s(O–H)
3182 vs		3217 vs		2490 (7585/0)	ν_{22}	B_u	ν_{as}(O–H)
1880 w		1880 s					[c]
1823 m		1817 vs					[c]
	1717 (49)		1726 (21)	1713 (0/8)	ν_3	A_g	ν_s(C=O)
	1625 (42)		1629 (13)	1685 (0/384)	ν_4	A_g	ν(C=C)
1641 m		1666 vs		1681 (816/0)	ν_{23}	B_u	ν_{as}(C=O)
1450 m		1452 s		1485 (717/0)	ν_{24}	B_u	ν_{as}(C–F)
	1441 (8)		1445 (4)	1454 (0/4)	ν_5	A_g	ν_s(C–F)
1423 m		1423 s					[c]
1338 w		1365 s					[c]
	1304 (38)		1307 (19)	1337 (0/7)	ν_6	A_g	δ_s(CCH)
1317 w		1302 s		1302 (323/0)	ν_{25}	B_u	δ_{as}(CCH)
	1244 (20)	1246 s	1246 (10)	1280 (0/38)	ν_7	A_g	δ_s(COH)
1263 m		1273 s		1252 (216/0)	ν_{26}	B_u	δ_{as}(COH)
		1227 s					[c]
1217 m		1211 s					[c]
1153 w		1149 s		1023 (240/0)	ν_{12}	A_u	γ_{as}(COH)
		1022 vs		1022 (14/0)	ν_{17}	B_g	γ_s(COH)
999 w		982 vs		1020 (12/0)	ν_{13}	A_u	γ_{as}(HCCH)
974 m							[c]
	946 (24)		946 (18)	995 (0/6)	ν_8	A_g	ν_s(C–C)
	896 (23)		904 (15)	948 (0/4)	ν_{18}	B_g	γ_s(HCCH)
939 w							[c]
926 w		930 vs		933 (127/0)	ν_{27}	B_u	ν_{as}(C–C)
		887 s					[c]
		756 m		784 (12/0)	ν_{14}	A_u	γ_{as}(CCOF)
	693 (19)		692 (12)	712 (0/11)	ν_9	A_g	δ_s(COF)
	683 (11)		681 (19)				[c]
673 m		677 vs		647 (56/0)	ν_{28}	B_u	δ_{as}(COF)
	608 (8)		612 (4)	625 (0/1)	ν_{19}	B_g	γ_s(CCOF)
	589 (11)		588 (10)				[c]
554 vw		559 s		554 (46/0)	ν_{29}	B_u	δ_{as}(CCF)
	478 (7)		486 (5)	374 (0/2)	ν_{10}	A_g	δ_s(CCF)
	256 (16)		255 (6)	365 (0/2)	ν_{11}	A_g	δ_s(CCC)
	217 (33)		211 (6)				[c]
				190 (142/0)	ν_{15}	A_u	γ_{as}(CCC)
				136 (5/0)	ν_{30}	B_u	δ_{as}(CCC)
	133 (42)		129 (17)	132 (0/2)	ν_{20}	B_g	γ_s(CCC)
	115 (25)		113 (41)				[c]
				49 (15/0)	ν_{16}	A_u	τ(COF)
Vibrations of anions MF_6^- (M = As, Sb)							
	749 (9)						$[AsF_6]^-$
698 vs	708 (100)						$[AsF_6]^-$
	669 (47)	662 vs	662 (100)				$[AsF_6]^-$, $[SbF_6]^-$
625 m		629 vs	631 (12)				$[AsF_6]^-$, $[SbF_6]^-$
	594 (10)	592 m					$[AsF_6]^-$, $[SbF_6]^-$
501 w	500 (7)	498 s					$[AsF_6]^-$, $[SbF_6]^-$
390 s	384 (36)	440 m					$[AsF_6]^-$, $[SbF_6]^-$
368 w	374 (17)						$[AsF_6]^-$
	361 (29)	359 m	310 (5)				$[AsF_6]^-$, $[SbF_6]^-$
			290 (23)				$[SbF_6]^-$
			278 (15)				$[SbF_6]^-$
	247 (8)		266 (5)				$[AsF_6]^-$, $[SbF_6]^-$
			201 (7)				$[SbF_6]^-$
	145 (50)		172 (3)				$[AsF_6]^-$, $[SbF_6]^-$

[a] Abbrevations for IR intensities: v = very, s = strong, m = medium, w = weak. IR intensities in km/mol; Raman intensities in Å^4/u. Experimental Raman activities are relative to a scale of 1 to 100.

[b] Calculated on the B3LYP/aug-cc-pVTZ level of theory.

[c] Very probably combination tones/ overtones.

Table S5: Experimental vibrational frequencies [cm^{-1}] of $[C_4H_2D_2F_2O_2]^{2+}([MF_6]^-)_2$ (M = As, Sb) and calculated vibrational frequencies [cm^{-1}] of $[C_4H_2D_2F_2O_2 \cdot 2\ HF]^{2+}$.

$[C_4H_2D_2F_2O_2]^{2+}([AsF_6]^-)_2$ **(5)** exp.[a]		$[C_4H_2D_2F_2O_2]^{2+}([SbF_6]^-)_2$ **(6)** exp.[a]		$[C_4H_2D_2F_2O_2 \cdot 2\ HF]^{2+}$ calc.[b]	Assignment		
IR	Raman	IR	Raman	IR/Raman			
3109 m		3094 vs		3189 (60/0)	ν_{21}	B_u	ν_{as}(C–H)
	3098 (17)		3084 (19)	3187 (0/78)	ν_1	A_g	ν_s(C–H)
		2984 s					[c]
		2887 s					[c]
	2307 (2)	2403 s	2293 (2)	1869 (0/70)	ν_2	A_g	ν_s(O–D)
2359 s		2318 s		1830 (3909/0)	ν_{22}	B_u	ν_{as}(O–D)
		2098 s					[c]
		1996 s					[c]
1826 m		1815 vs					[c]
1763 w							[c]
	1715 (100)		1721 (100)	1712 (0/13)	ν_3	A_g	ν_s(C=O)
1678 m		1697 vs		1678 (927/0)	ν_{23}	B_u	ν_{as}(C=O)
1647 m	1662 (7)	1653 vs					[c]
1626 m	1622 (22)	1610 vs	1627 (13)	1676 (0/409)	ν_4	A_g	ν(C=C)
		1527 vs					[c]
		1483 vs	1486 (4)				[c]
	1447 (5)		1448 (5)				[c]
1421 m		1412 vs		1425 (703/0)	ν_{24}	B_u	ν_{as}(C–F)
	1403 (5)		1403 (4)	1402 (0/24)	ν_5	A_g	ν_s(C–F)
1313 m		1354 vs					[c]
	1304 (24)		1307 (18)	1320 (0/28)	ν_6	A_g	δ_s(CCH)
1263 w		1269 vs		1270 (56/0)	ν_{25}	B_u	δ_{as}(CCH)
1213 m	1237 (3)	1234 vs	1237 (4)				[c]
1136 w		1196 s					[c]
		1057 m	1058 (2)	1038 (0/6)	ν_7	A_g	δ_s(COD)
1034 vw		1022 s		1032 (57/0)	ν_{26}	B_u	δ_{as}(COD)
978 m		1001 m		1021 (53/0)	ν_{12}	A_u	γ_{as}(HCCH)
	995 (7)		996 (10)	962 (0/7)	ν_8	A_g	ν_s(C–C)
953 vw		984 vs					[c]
	942 (4)	943 m	944 (5)	948 (0/4)	ν_{17}	B_g	γ_s(HCCH)
	927 (4)	930 m	932 (6)				[c]
881 w	895 (12)	895 s	904 (16)	894 (223/0)	ν_{27}	B_u	ν_{as}(C–C)
870 w							[c]
	815 (3)						[c]
787 w	787 (4)	781 s		807 (84/0)	ν_{13}	A_u	γ_{as}(CCOF)
				759 (0/0)	ν_{18}	B_g	γ_s(COD)
770 w				720 (32/0)	ν_{14}	A_u	γ_{as}(COD)
	673 (19)		674 (21)	684 (0/9)	ν_9	A_g	δ_s(COF)
588 vw		590 s		629 (79/0)	ν_{28}	B_u	δ_{as}(COF)
	626 (4)		629 (12)	609 (0/1)	ν_{19}	B_g	γ_s(CCOF)
559 vw		557 s		552 (47/0)	ν_{29}	B_u	δ_{as}(CCF)
	582 (5)		582 (7)				[c]
	559 (4)		558 (3)				[c]
	496 (7)		495 (6)				[c]
393 vs	399 (7)	392 w		370 (0/2)	ν_{10}	A_g	δ_s(CCF)
366 w		361 vw					[c]
	309 (6)		310 (6)	360 (0/2)	ν_{11}	A_g	δ_s(CCC)
	256 (10)		255 (7)				[c]
	191 (9)		192 (5)	188 (150/0)	ν_{15}	A_u	γ_{as}(CCC)
	169 (13)		172 (4)	135 (5/0)	ν_{30}	B_u	δ_{as}(CCC)
	132 (23)		126 (17)	132 (0/2)	ν_{20}	B_g	γ_s(CCC)
	115 (16)		114 (34)	48 (15/0)	ν_{16}	A_u	τ(COF)
Vibrations of anions MF_6^- (M = As, Sb)							
	734 (5)						$[AsF_6]^-$
	723 (13)						$[AsF_6]^-$
	707 (48)						$[AsF_6]^-$
698 vs	691 (12)						$[AsF_6]^-$
673 s	681 (16)	685 vs					$[AsF_6]^-$, $[SbF_6]^-$
	659 (15)	660 vs	662 (84)				$[AsF_6]^-$, $[SbF_6]^-$
	600 (7)	629 vs	598 (5)				$[AsF_6]^-$, $[SbF_6]^-$
	529 (6)						$[AsF_6]^-$
517 w	522 (7)						$[AsF_6]^-$
	465 (7)	498 vs	456 (5)				$[AsF_6]^-$, $[SbF_6]^-$
	442 (20)						$[AsF_6]^-$
	421 (6)						$[AsF_6]^-$
	383 (22)	380 w					$[AsF_6]^-$, $[SbF_6]^-$
	375 (13)	372 w					$[AsF_6]^-$, $[SbF_6]^-$
	361 (18)		290 (22)				$[AsF_6]^-$, $[SbF_6]^-$
	248 (9)		279 (15)				$[AsF_6]^-$, $[SbF_6]^-$
	243 (9)		268 (6)				$[AsF_6]^-$, $[SbF_6]^-$
	216 (19)		211 (7)				$[AsF_6]^-$, $[SbF_6]^-$
	143 (28)		200 (7)				$[AsF_6]^-$, $[SbF_6]^-$

[a] Abbrevations for IR intensities: v = very, s = strong, m = medium, w = weak. IR intensities in km/mol; Raman intensities in Å^4/u. Experimental Raman activities are relative to a scale of 1 to 100.

[b] Calculated on the B3LYP/aug-cc-pVTZ level of theory.

[c] Very probably combination tones/ overtones.

Table S6: Experimental vibrational frequencies [cm^{-1}] of $[C_4H_3F_2O_2]^+[MF_6]^-$ (M = As, Sb) and calculated vibrational frequencies [cm^{-1}] of $[C_4H_3F_2O_2 \cdot HF]^+$.

$[C_4H_3F_2O_2]^+[AsF_6]^-$ **(3)** exp.[a]		$[C_4H_3F_2O_2]^+[SbF_6]^-$ **(4)** exp.[a]		$[C_4H_3F_2O_2 \cdot HF]^+$ calc.[b]	Assignment		
IR	Raman	IR	Raman	IR/Raman			
		3337 vs					[c]
		3109 vs		3212 (26/29)	ν_1	*A'*	ν(C–H)[d]
	3090 (17)		3084 (11)	3199 (6/54)	ν_2	*A'*	ν(C–H)
3196 vs		3203 vs		3061 (2649/166)	ν_3	*A'*	ν(O–H)[d]
1803 m	1823 (37)	1813 s	1825 (97)	1872 (180/260)	ν_4	*A'*	ν(C=O)
	1637 (56)		1647 (54)	1675 (636/227)	ν_5	*A'*	ν(C=C)
1770 m	1761 (100)	1770 w	1757 (60)	1621 (181/2)	ν_6	*A'*	ν(C=O)[d]
			1739 (55)				[c]
	1378 (14)		1354 (17)	1489 (195/12)	ν_7	*A'*	ν(C–F)[d]
	1304 (41)		1305 (28)	1316 (7/29)	ν_8	*A'*	δ(CCH)
1290 m	1284 (10)	1292 w	1281 (13)	1280 (22/1)	ν_9	*A'*	δ(CCH)
1261 m	1265 (8)	1261 w	1252 (8)	1259 (205/24)	ν_{10}	*A'*	δ(COH)[d]
1205 m		1209 m	1227 (5)	1213 (433/9)	ν_{11}	*A'*	ν(C–F)
1188 m		1186 m					[c]
1121 w		1121 w					[c]
1040 m		1038 w		1026 (32/1)	ν_{20}	*A"*	γ(HCCH)
987 w	981 (7)	987 w	982 (4)	956 (27/12)	ν_{12}	*A'*	ν(C–C)[d]
	962 (5)		946 (6)	944 (0/3)	ν_{21}	*A"*	γ(HCCH)
922 m	935 (13)	920 m	936 (7)	916 (122/0)	ν_{22}	*A"*	γ(COH)[d]
885 w	899 (24)	887 w	898 (26)	882 (34/13)	ν_{13}	*A'*	ν(C–C)
874 w			879 (6)				[c]
			856 (5)				[c]
	764 (6)	756 w	763 (4)	775 (12/1)	ν_{23}	*A"*	γ(CCOF)
	712 (23)		715 (18)				[c]
	691 (43)		691 (11)	687 (6/8)	ν_{14}	*A'*	δ(COF)
619 s		621 s	620 (5)	618 (22/0)	ν_{15}	*A'*	δ(COF)
	588 (12)		587 (4)	614 (5/1)	ν_{24}	*A"*	γ(CCOF)
548 w		546 vw		553 (18/1)	ν_{16}	*A'*	δ(CCF)
	263 (11)		266 (10)	252 (6/2)	ν_{17}	*A'*	δ(CCF)
			216 (12)	222 (20/1)	ν_{18}	*A'*	δ(CCC)
			170 (18)	170 (8/1)	ν_{25}	*A"*	γ(CCC)
	135 (52)		144 (39)	149 (32/0)	ν_{26}	*A"*	γ(CCC)
			108 (57)	127 (6/0)	ν_{19}	*A'*	δ(CCC)
				38 (1/0)	ν_{27}	*A"*	τ(COF)
Vibrations of anions MF_6^- (M = As, Sb)							
698 vs	699 (32)						$[AsF_6]^-$
	682 (48)		681 (9)				$[AsF_6]^-$, $[SbF_6]^-$
677 vs		671 s	671 (17)				$[AsF_6]^-$, $[SbF_6]^-$
			662 (19)				$[SbF_6]^-$
			648 (100)				$[SbF_6]^-$
			575 (9)				$[SbF_6]^-$
			566 (7)				$[SbF_6]^-$
			418 (6)				$[SbF_6]^-$
390 s	393 (11)	397 w					$[AsF_6]^-$, $[SbF_6]^-$
		384 w					$[SbF_6]^-$
	370 (27)	372 w					$[AsF_6]^-$, $[SbF_6]^-$
359 vw		365 vw					$[AsF_6]^-$, $[SbF_6]^-$
	309 (8)		296 (16)				$[AsF_6]^-$, $[SbF_6]^-$
			284 (25)				$[SbF_6]^-$
			279 (23)				$[SbF_6]^-$

[a] Abbrevations for IR intensities: v = very, s = strong, m = medium, w = weak. IR intensities in km/mol; Raman intensities in Å^4/u. Experimental Raman activities are relative to a scale of 1 to 100.
[b] Calculated on the B3LYP/aug-cc-pVTZ level of theory.
[c] Very probably combination tones/ overtones.
[d] protonated acyl fluoride moiety.

Table S7: Observed ^{1}H, ^{13}C and ^{19}F chemical shifts [ppm] and spin-spin coupling constants [Hz] of fumaryl fluoride in $CDCl_3$.

NMR Nucleus	Substance	Solvent	Temperature	Spectrometer Frequency	Chemical Shift δ [ppm] (Multiplicity, Coupling Constant, Integral, Assignment)
^{1}H	$C_4H_2F_2O_2$	$CDCl_3$	26 °C	400 MHz	6.97 (ddd, $^{3}J_{HH}$ = 12.6 Hz, $^{3}J_{HF}$ = 4.5 Hz, $^{4}J_{HF}$ = 2.7 Hz, 2H) ^{13}C-Satellites: **Pair 1:** 7.21 ppm (d, $^{5}J_{FF}$ = 7.3 Hz) and 6.77 ppm (d, $^{5}J_{FF}$ = 7.3 Hz) **Pair 2:** 7.17 ppm (d, $^{5}J_{FF}$ = 7.2 Hz) and 6.73 ppm (d, $^{5}J_{FF}$ = 7.3 Hz) $^{1}J(^{13}C,^{1}H)$ = 175.5 Hz $^{2}J(^{13}C,^{1}H)$ = 33.2 Hz
^{13}C	$C_4H_2F_2O_2$	$CDCl_3$	26 °C	101 MHz	153.57 (dd, $^{1}J_{CF}$ = 345.7 Hz, $^{4}J_{CF}$ = 1.5 Hz) 133.45 (dd, $^{2}J_{CF}$ = 71.3 Hz, $^{3}J_{CF}$ = 4.3 Hz)
^{19}F	$C_4H_2F_2O_2$	$CDCl_3$	26 °C	377 MHz	31.42 (dd, $^{3}J_{HF}$ = 4.5 Hz, $^{4}J_{HF}$ = 2.6 Hz) ^{13}C-Satellites: **Pair 1:** 32.24 ppm (d, $^{5}J_{FF}$ = 7.4 Hz) and 30.32 ppm (d, $^{5}J_{FF}$ = 8.1 Hz) **Pair 2:** 31.76 ppm (dd, $^{3}J_{HF}$ = 4.6 Hz, $^{4}J_{HF}$ = 2.9 Hz) and 30.84 ppm (dd, $^{3}J_{HF}$ = 4.5 Hz, $^{4}J_{HF}$ = 2.7 Hz) $^{2}J(^{13}C,^{1}H)$ = 33.2 Hz

Table S8: Selected observed ^{1}H, ^{13}C and ^{19}F NMR chemical shifts [ppm] and spin-spin coupling constants [Hz] of $C_4H_2F_2O_2$ in $CDCl_3$ as well as $C_4H_2F_2O_2$, 1, 2 and 4 in *a*HF (external solvent Acetone-D_6), respectively.

	$C_4H_2F_2O_2$ (in $CDCl_3$)	$C_4H_2F_2O_2$ (in *a*HF, external solvent Acetone-D_6)	**1** (in *a*HF, external solvent Acetone-D_6)	**2** (in *a*HF, external solvent Acetone-D_6)	**4** (in *a*HF, external solvent Acetone-D_6)
^{1}H Chemical Shift δ [ppm] (Multiplicity, Coupling Constant, Assignment)	6.97 (ddd, $^{3}J_{HH}$ = 12.6 Hz, $^{3}J_{HF}$ = 4.5 Hz, $^{4}J_{HF}$ = 2.7 Hz, 2H)	6.70 (s, 2H)	9.99 (s, OH) 7.20 (dd, $^{3}J_{HF}$ = 6.4 Hz, $^{4}J_{HF}$ = 2.9 Hz, 2H)	10.05 (s, OH) 7.29 (dd, $^{3}J_{HF}$ = 6.5 Hz, $^{4}J_{HF}$ = 2.9 Hz, 2H)	9.99 (s, OH) 7.26 (dd, $^{3}J_{HF}$ = 6.5 Hz, $^{4}J_{HF}$ = 2.9 Hz, 2H)
^{13}C Chemical Shift δ [ppm] (Multiplicity, Coupling Constant, Assignment)	153.57 (dd, $^{1}J_{CF}$ = 345.7 Hz, $^{4}J_{CF}$ = 1.5 Hz, **C**OF) 133.45 (dd, $^{2}J_{CF}$ = 71.3 Hz, $^{3}J_{CF}$ = 4.3 Hz, **C**H)	157.81 (d, $^{1}J_{CF}$ = 349.0 Hz, **C**OF) 133.49 (dd, $^{2}J_{CF}$ = 64.1 Hz, $^{3}J_{CF}$ = 5.2 Hz, **C**H)	166.33 (d, $^{1}J_{CF}$ = 359.6 Hz, **C**(OH)F) 136.50 (dd, $^{2}J_{CF}$ = 49.1 Hz, $^{3}J_{CF}$ = 7.5 Hz, **C**H)	166.66 (d, $^{1}J_{CF}$ = 359.7 Hz, **C**(OH)F) 136.60 (dd, $^{2}J_{CF}$ = 48.7 Hz, $^{3}J_{CF}$ = 7.6 Hz, **C**H)	166.83 (d, $^{1}J_{CF}$ = 360.1 Hz, **C**(OH)F) 136.59 (dd, $^{2}J_{CF}$ = 48.4 Hz, $^{3}J_{CF}$ = 7.6 Hz, **C**H)
^{19}F Chemical Shift δ [ppm] (Multiplicity, Coupling Constant, Assignment)	31.42 (dd, $^{3}J_{HF}$ = 4.5 Hz, $^{4}J_{HF}$ = 2.6 Hz)	27.77 (s)	30.71 (s)	30.65 (s) –125.24 (s,br, $[SbF_6]^-$)	30.74 (s) –126.70 (s, br, $[SbF_6]^-$)

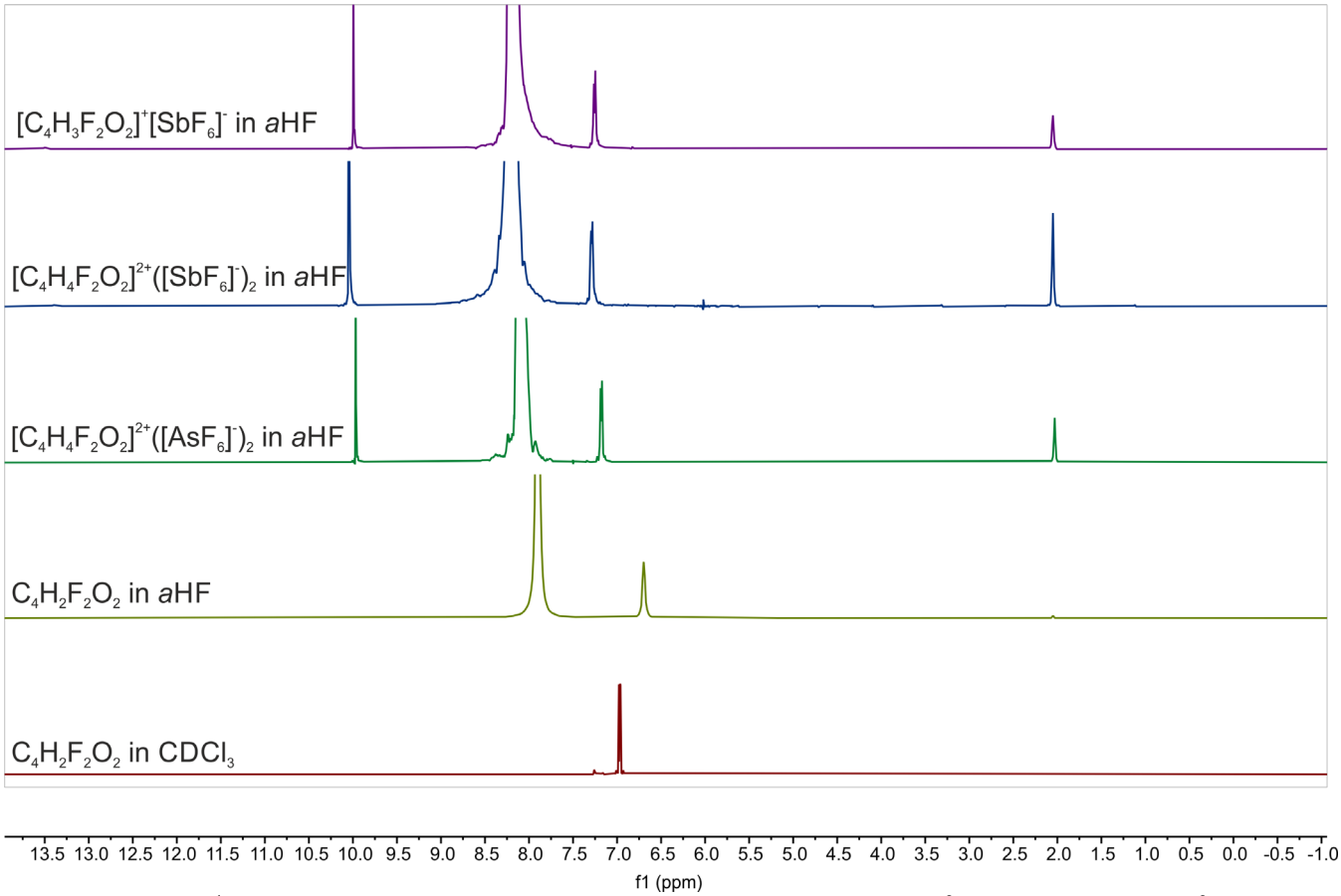

Figure S10: Stacked ^{1}H NMR spectra of $C_4H_2F_2O_2$ dissolved in $CDCl_3$ and $C_4H_2F_2O_2$, $[C_4H_4F_2O_2]^{2+}([AsF_6]^-)_2$ (1), $[C_4H_4F_2O_2]^{2+}([SbF_6]^-)_2$ (2) and $[C_4H_3F_2O_2]^+[SbF_6]^-$ (4) in *a*HF.

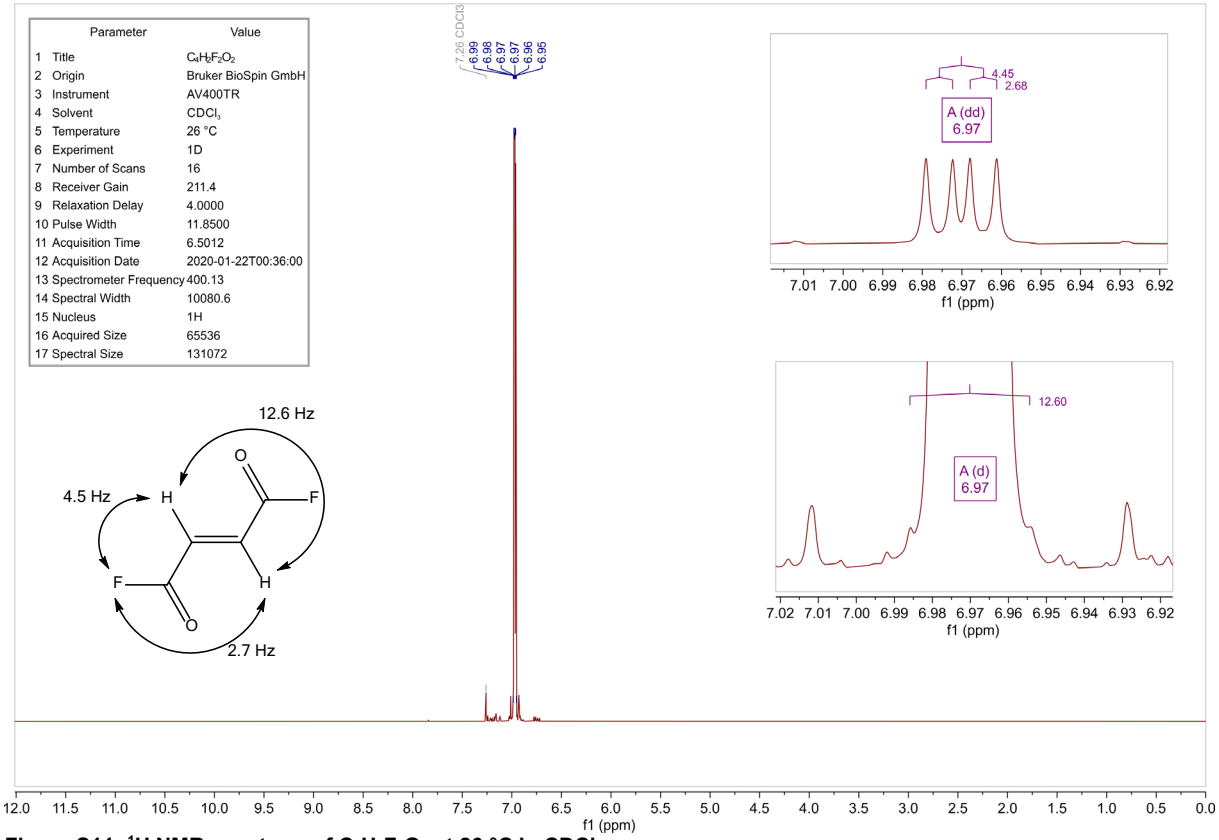

Figure S11: ^{1}H NMR spectrum of $C_4H_2F_2O_2$ at 26 °C in $CDCl_3$.

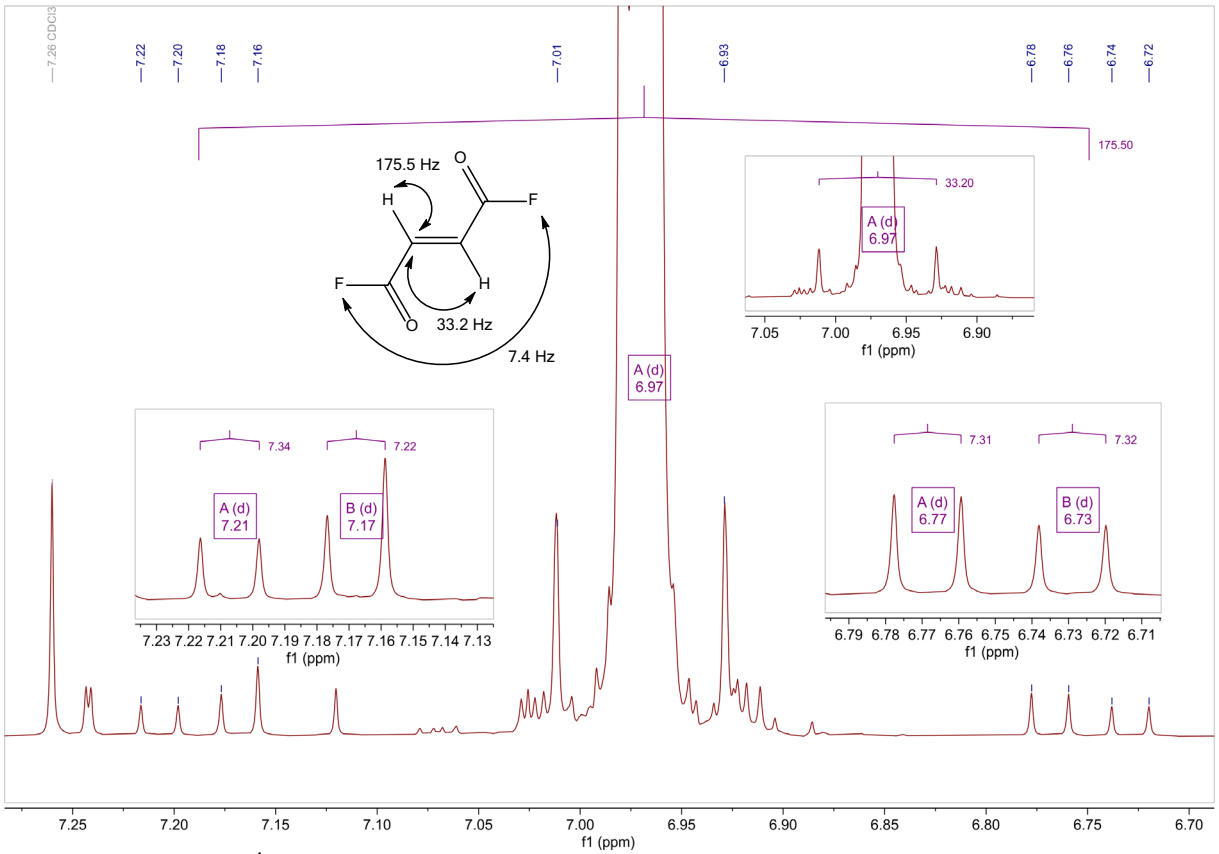

Figure S12: Detail of the ^{1}H NMR spectrum of $C_4H_2F_2O_2$ at 26 °C in $CDCl_3$.

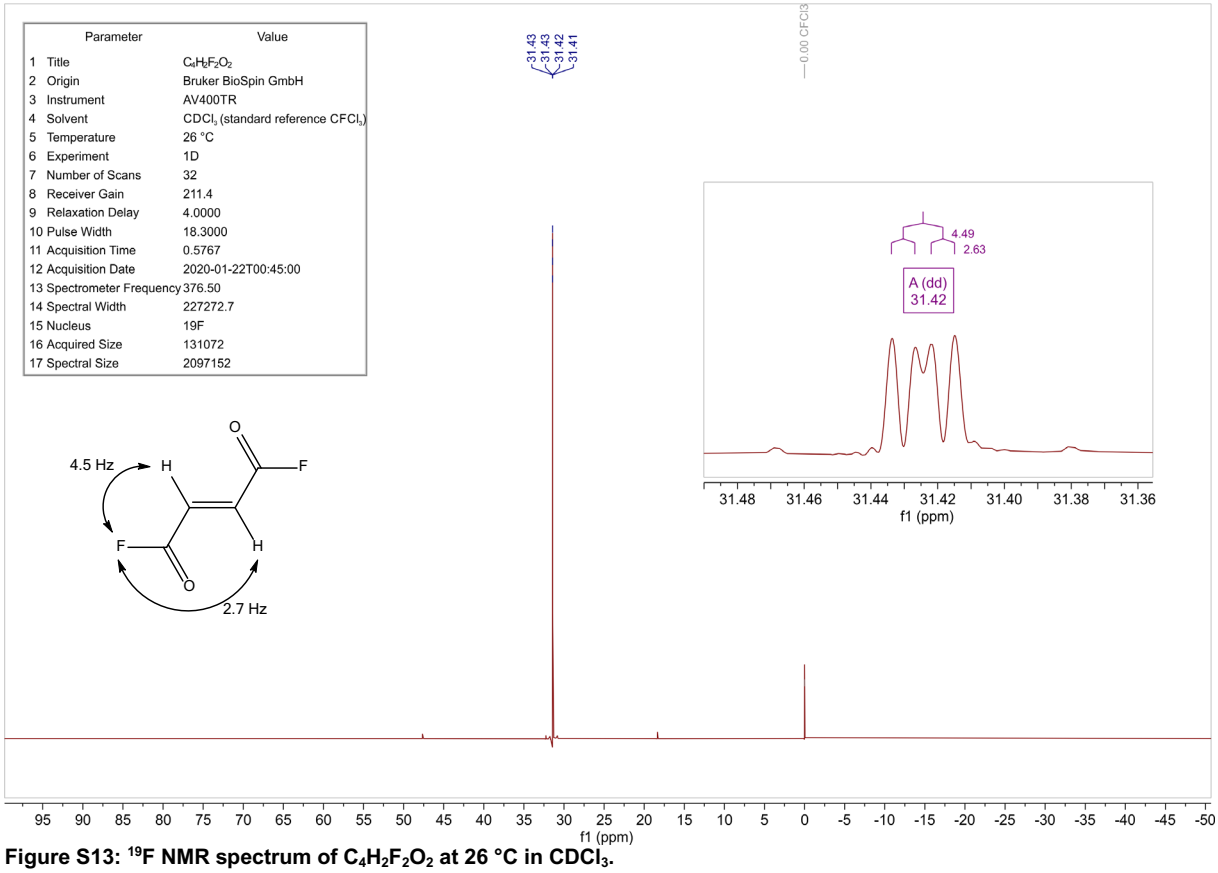

Figure S13: ^{19}F NMR spectrum of $C_4H_2F_2O_2$ at 26 °C in $CDCl_3$.

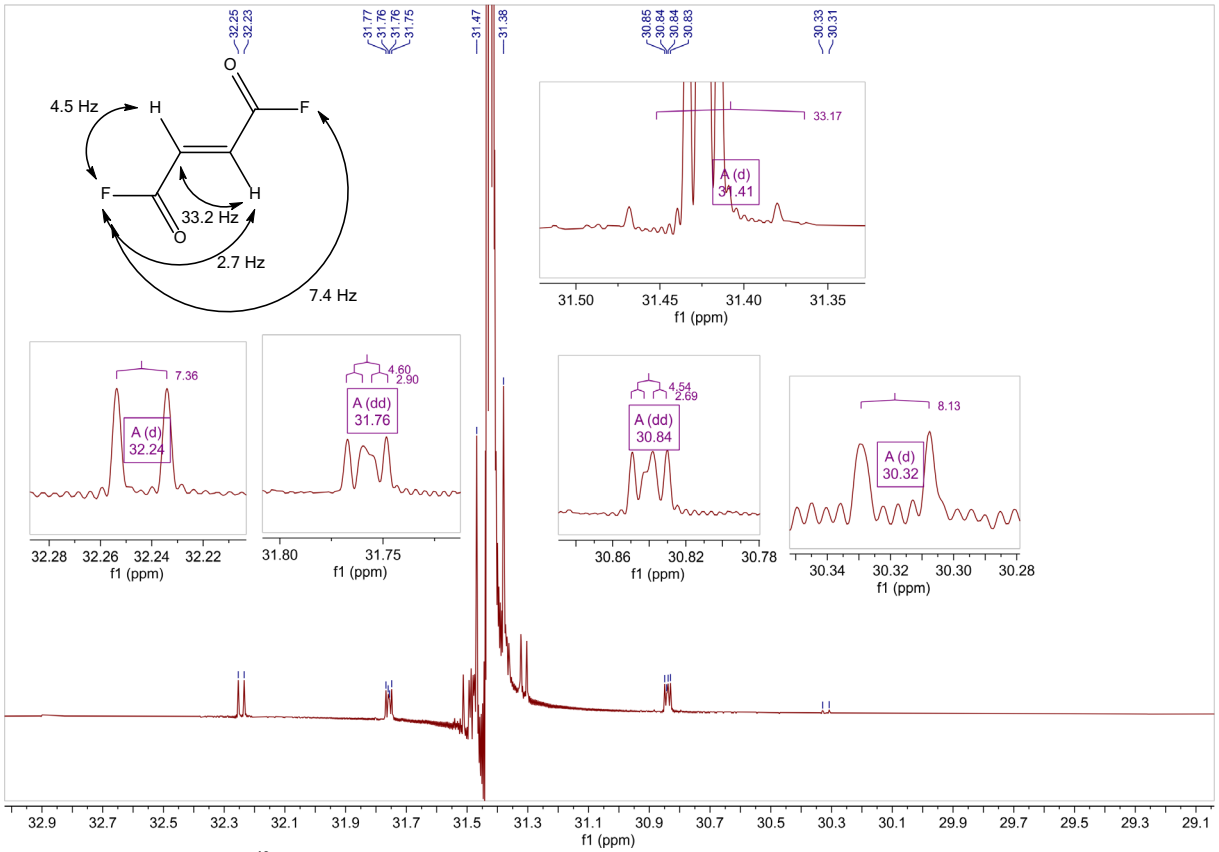

Figure S14: Detail of the ^{19}F NMR spectrum of $C_4H_2F_2O_2$ at 26 °C in $CDCl_3$.

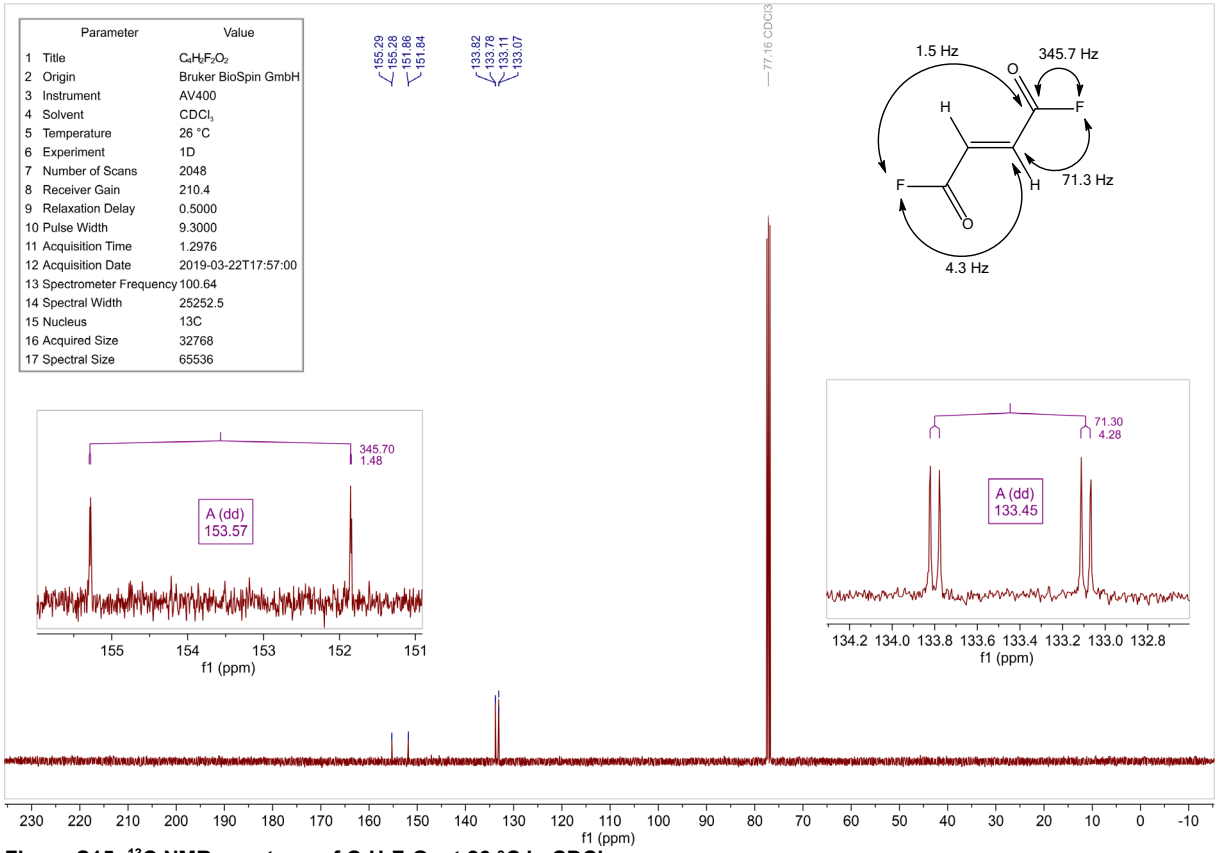

Figure S15: ^{13}C NMR spectrum of $C_4H_2F_2O_2$ at 26 °C in $CDCl_3$.

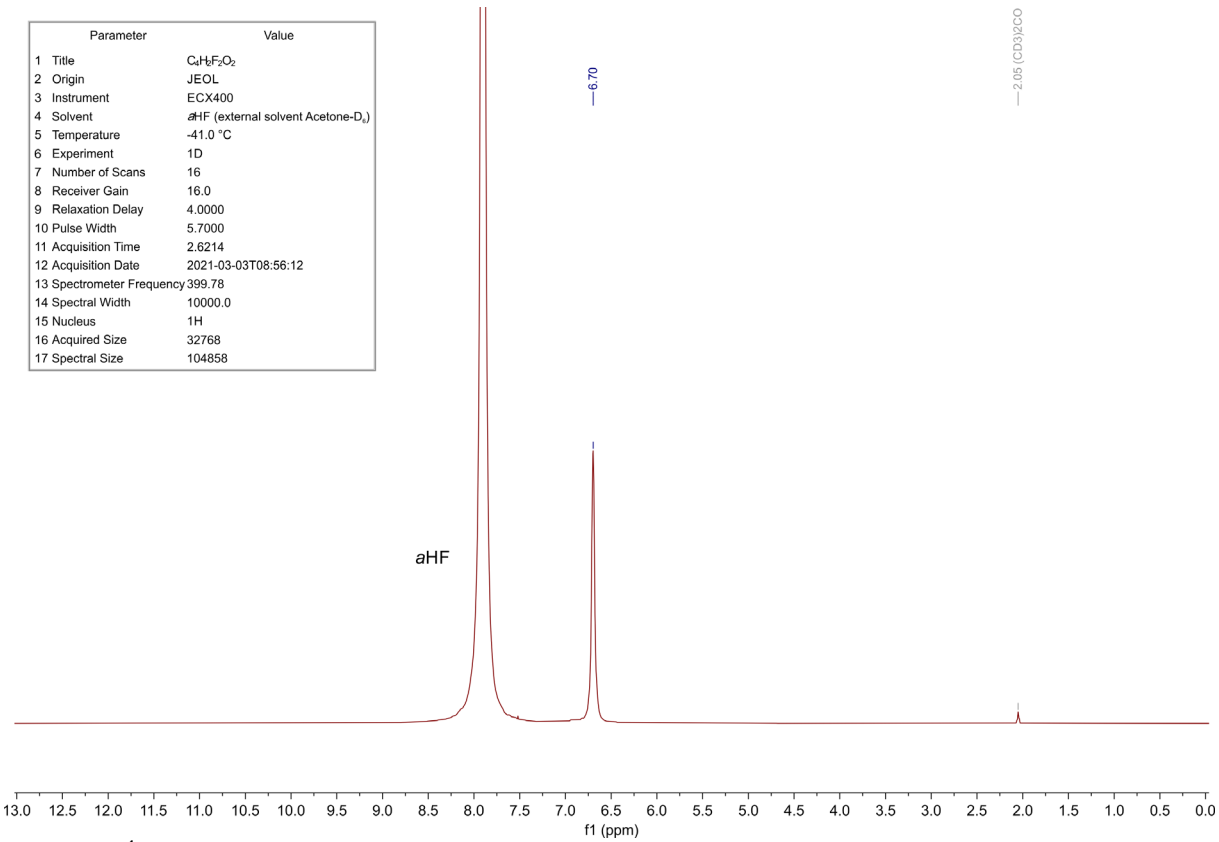

Figure S16: ^{1}H NMR spectrum of $C_4H_2F_2O_2$ at –41 °C in *a*HF and Acetone-D_6 as external solvent.

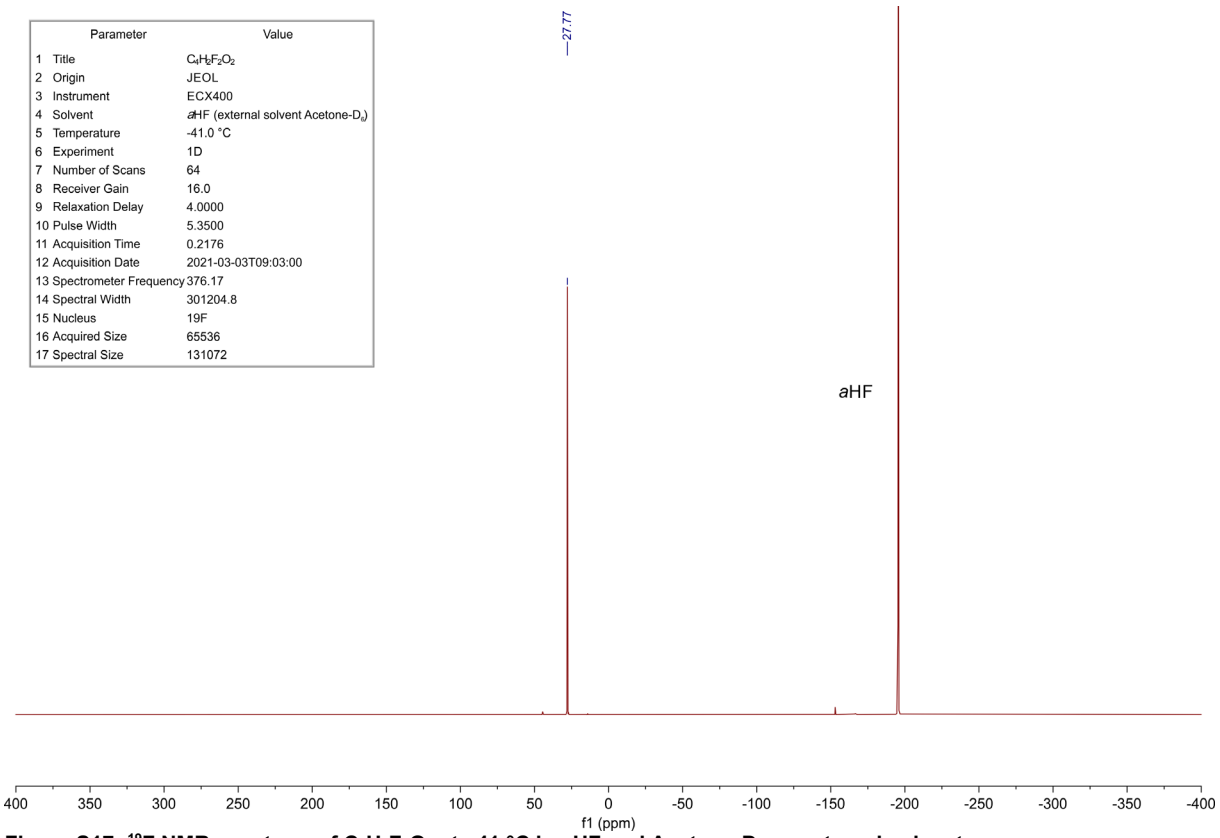

Figure S17: ^{19}F NMR spectrum of $C_4H_2F_2O_2$ at –41 °C in *a*HF and Acetone-D_6 as external solvent.

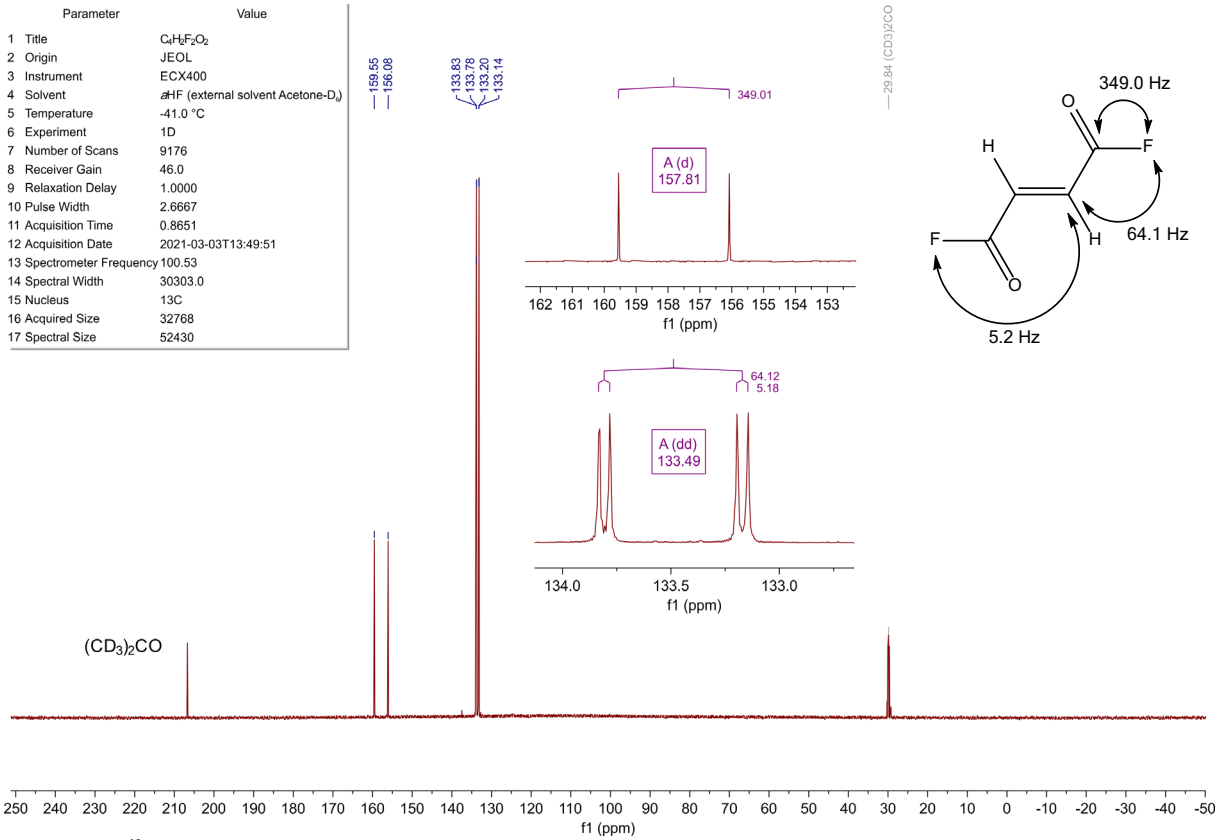

Figure S18: ^{13}C NMR spectrum of $C_4H_2F_2O_2$ at –41 °C in *a*HF and Acetone-D_6 as external solvent.

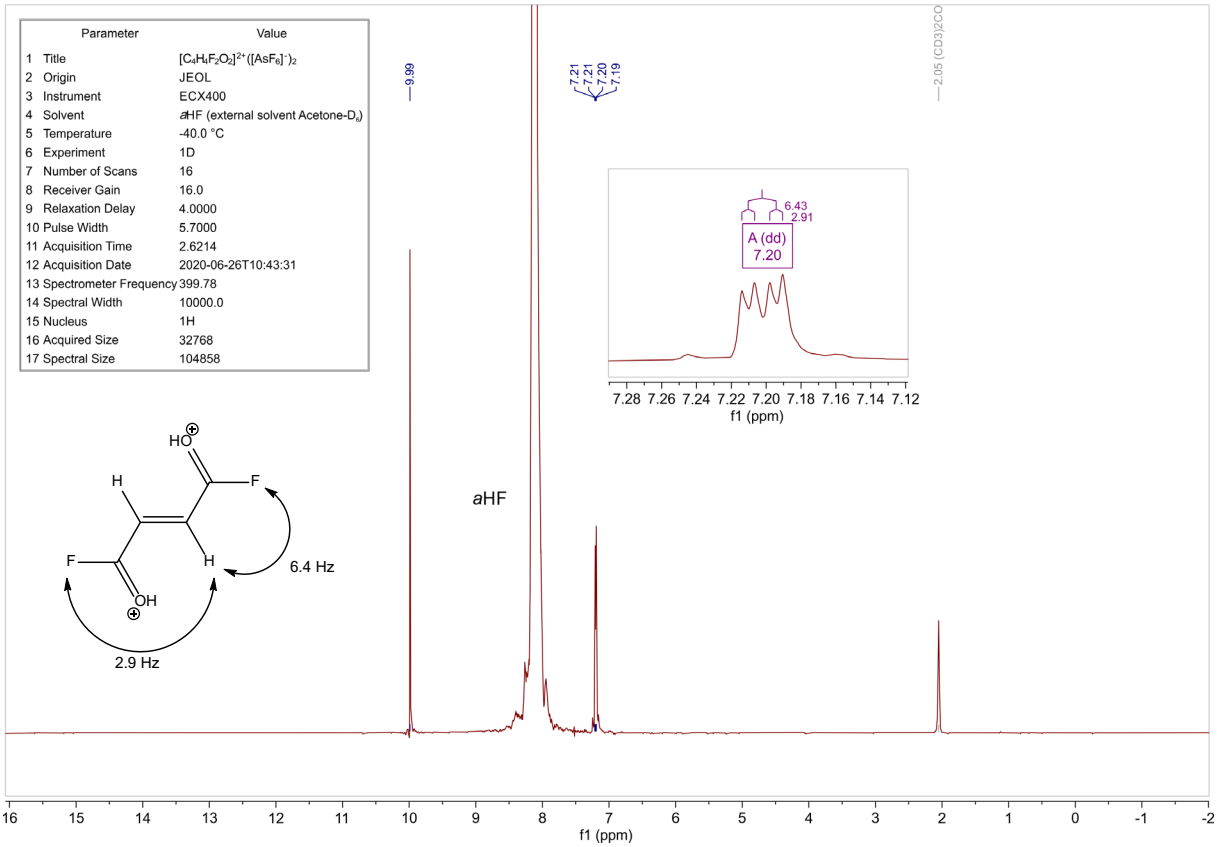

Figure S19: ^{1}H NMR spectrum of $[C_4H_4F_2O_2]^{2+}([AsF_6]^{-})_2$ (1), at –40 °C in *a*HF and Acetone-D_6 as external solvent.

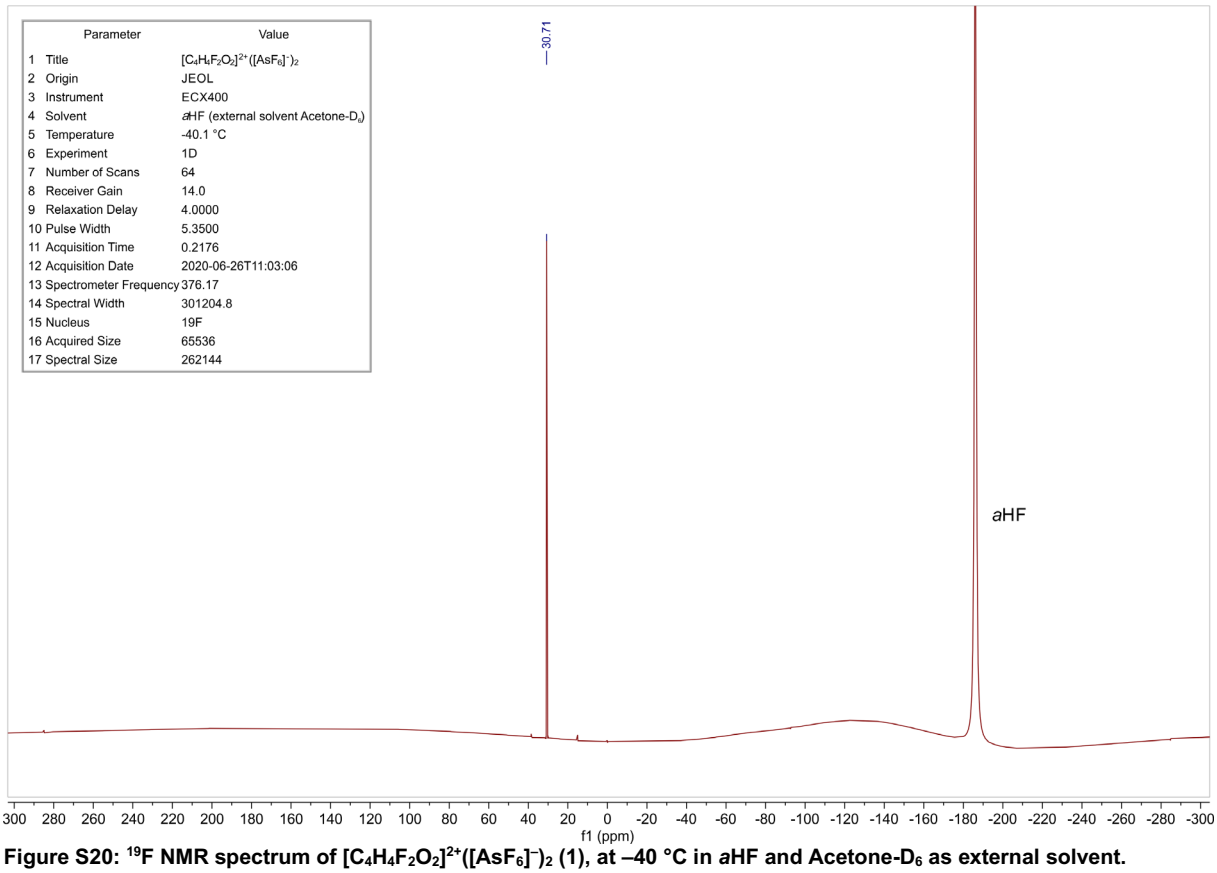

Figure S20: ^{19}F NMR spectrum of $[C_4H_4F_2O_2]^{2+}([AsF_6]^{-})_2$ (1), at –40 °C in *a*HF and Acetone-D_6 as external solvent.

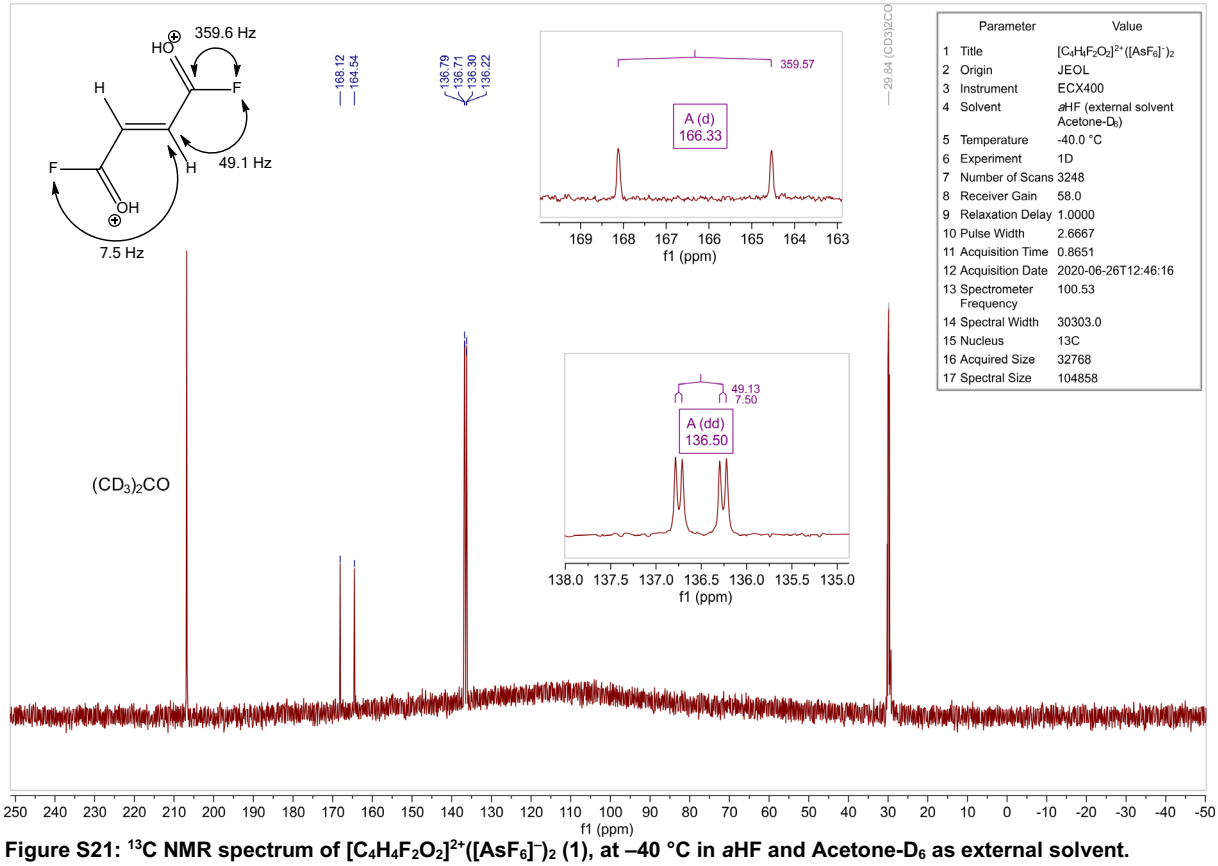

	Parameter	Value
1	Title	$[C_4H_4F_2O_2]^{2+}([AsF_6]^-)_2$
2	Origin	JEOL
3	Instrument	ECX400
4	Solvent	*a*HF (external solvent Acetone-D_6)
5	Temperature	-40.0 °C
6	Experiment	1D
7	Number of Scans	3248
8	Receiver Gain	58.0
9	Relaxation Delay	1.0000
10	Pulse Width	2.6667
11	Acquisition Time	0.8651
12	Acquisition Date	2020-06-26T12:46:16
13	Spectrometer Frequency	100.53
14	Spectral Width	30303.0
15	Nucleus	13C
16	Acquired Size	32768
17	Spectral Size	104858

Figure S21: ^{13}C NMR spectrum of $[C_4H_4F_2O_2]^{2+}([AsF_6]^-)_2$ (1), at –40 °C in *a*HF and Acetone-D_6 as external solvent.

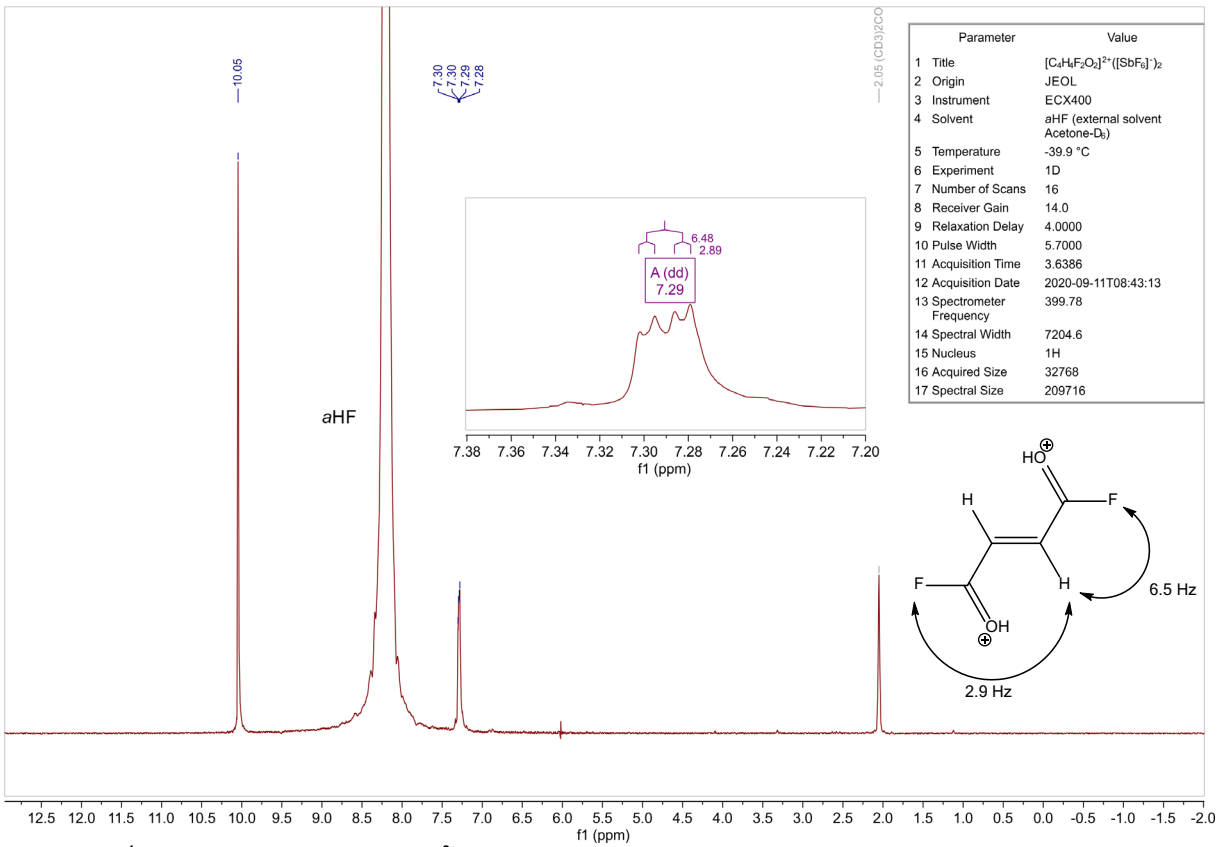

Figure S22: ^{1}H NMR spectrum of $[C_4H_4F_2O_2]^{2+}([SbF_6]^{-})_2$ (2), at –40 °C in *a*HF and Acetone-D$_6$ as external solvent.

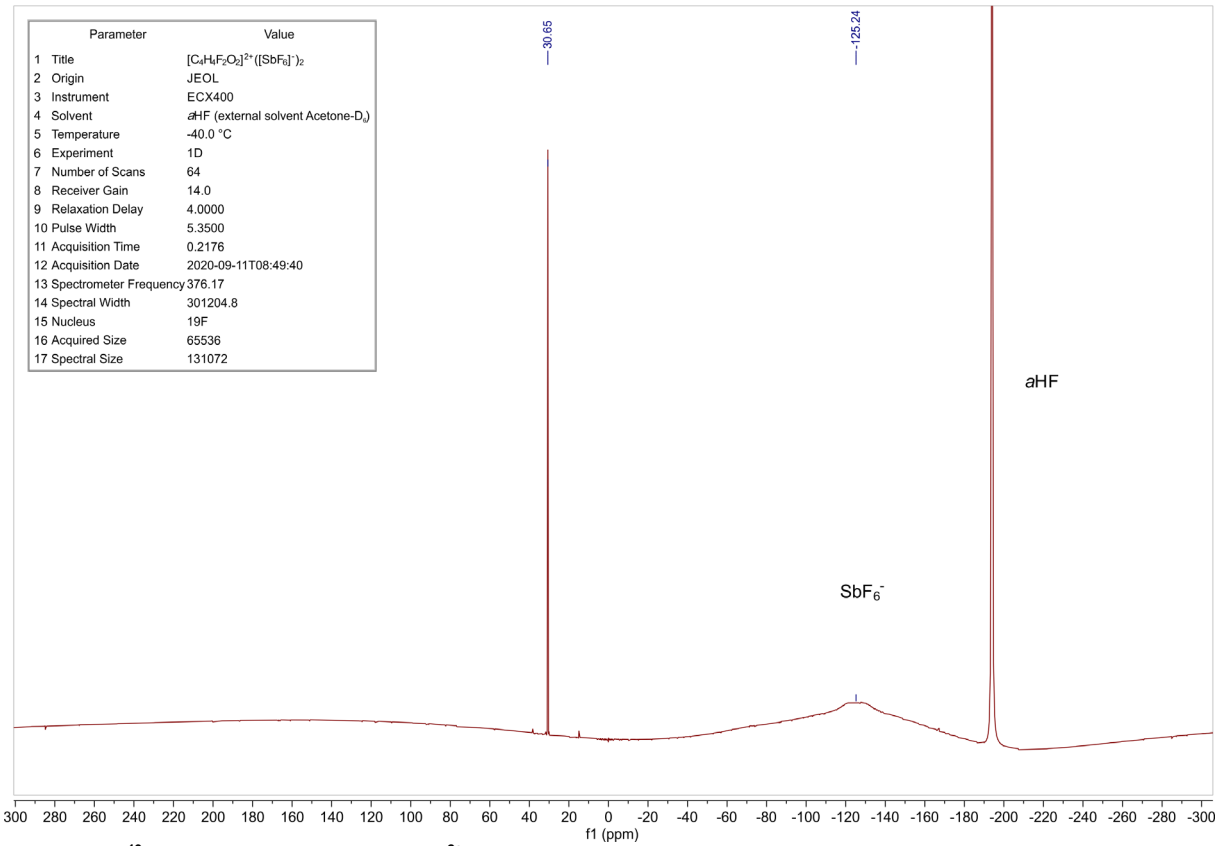

Figure S23: ^{19}F NMR spectrum of $[C_4H_4F_2O_2]^{2+}([SbF_6]^{-})_2$ (2), at –40 °C in *a*HF and Acetone-D$_6$ as external solvent.

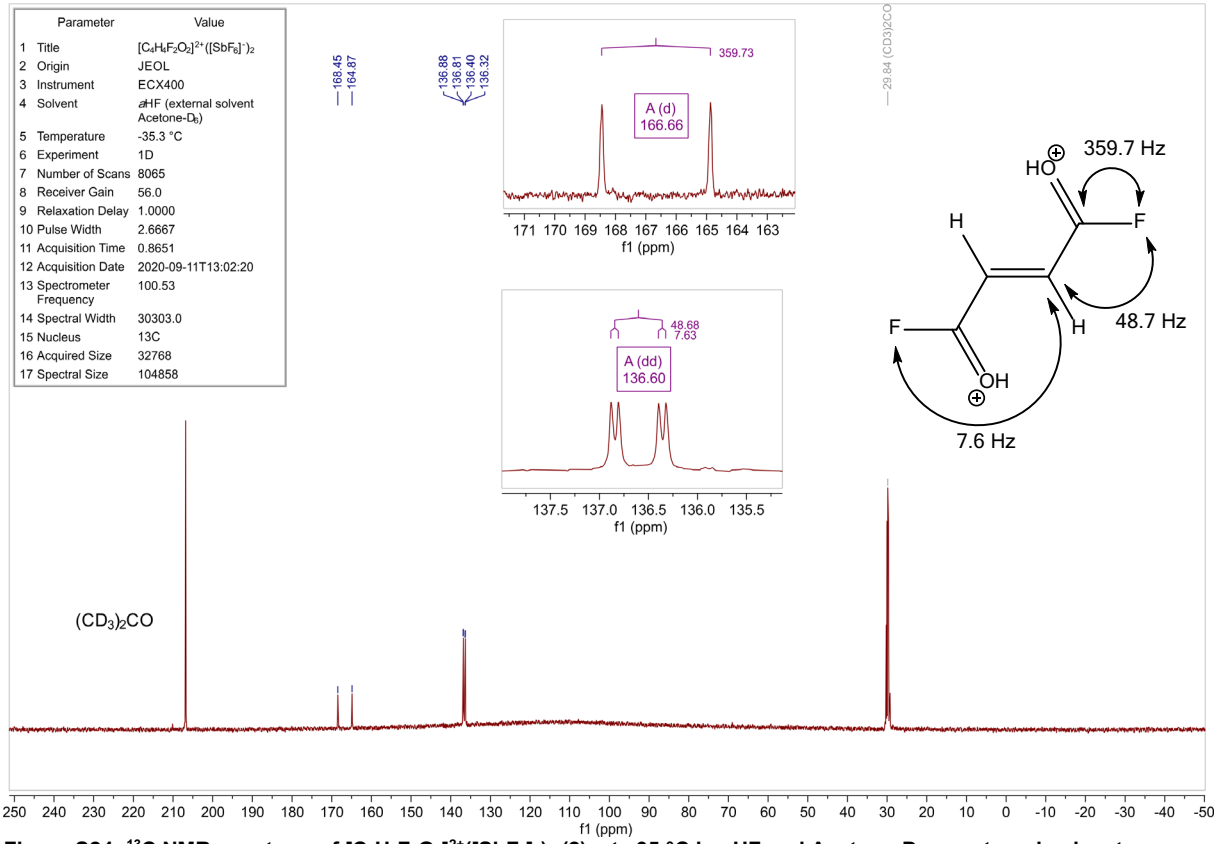

Figure S24: ^{13}C NMR spectrum of $[C_4H_4F_2O_2]^{2+}([SbF_6]^-)_2$ (2), at –35 °C in *a*HF and Acetone-D_6 as external solvent.

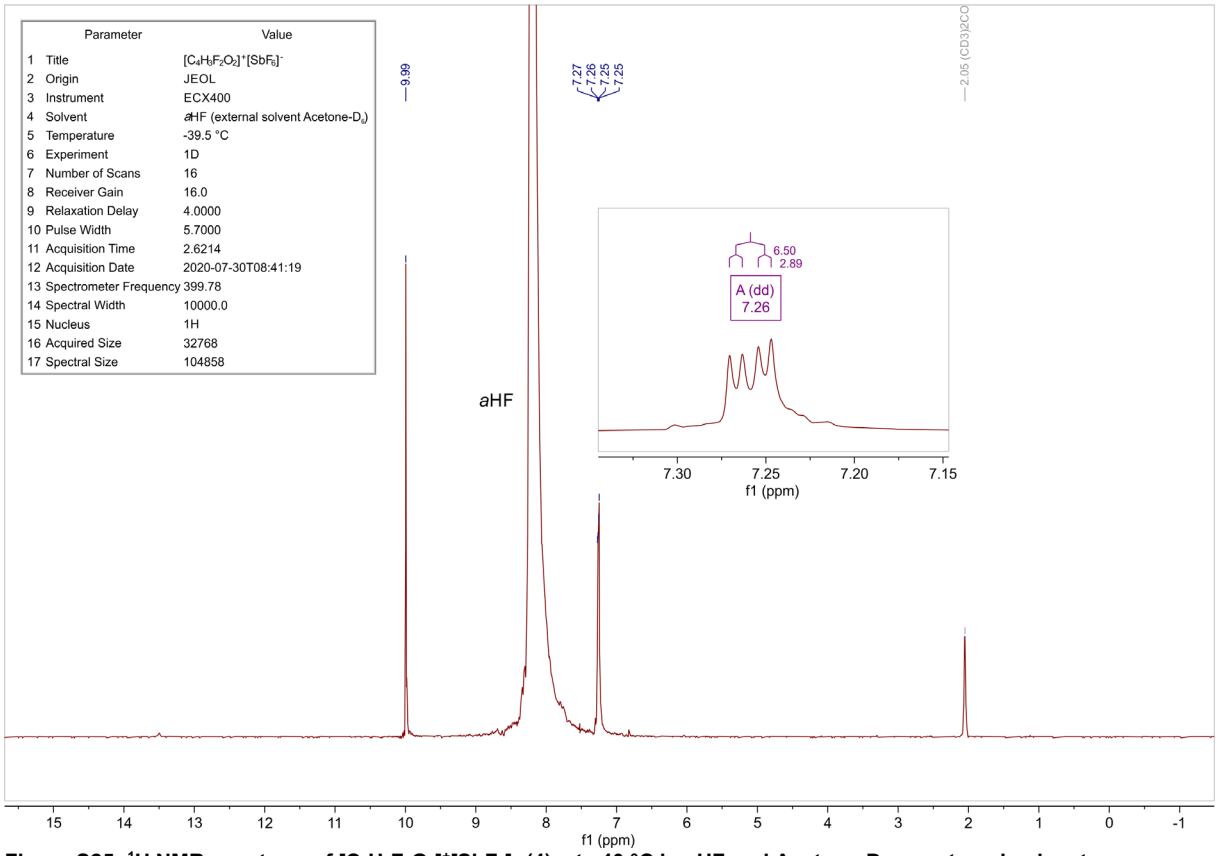

Figure S25: ^{1}H NMR spectrum of $[C_4H_3F_2O_2]^+[SbF_6]^-$ (4), at –40 °C in *a*HF and Acetone-D_6 as external solvent.

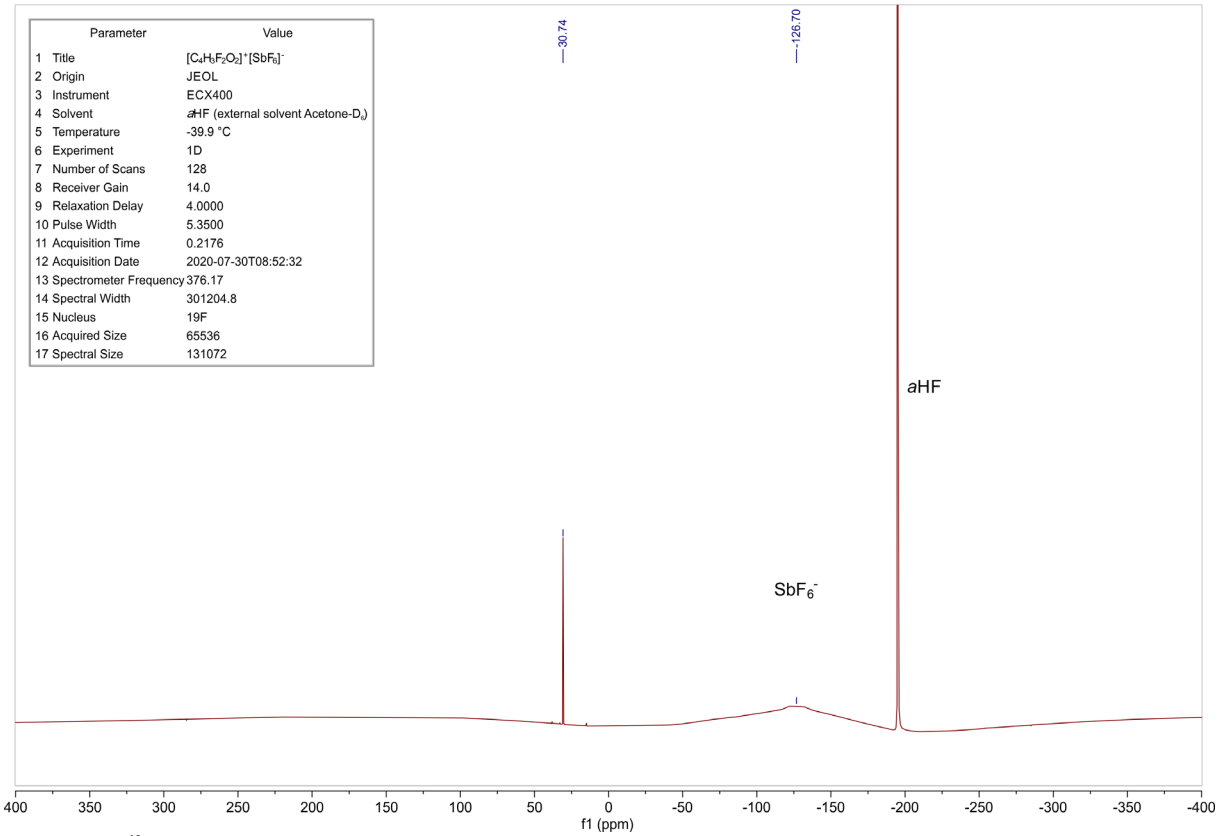

Figure S26: ^{19}F NMR spectrum of $[C_4H_3F_2O_2]^+[SbF_6]^-$ (4), at –40 °C in *a*HF and Acetone-D_6 as external solvent.

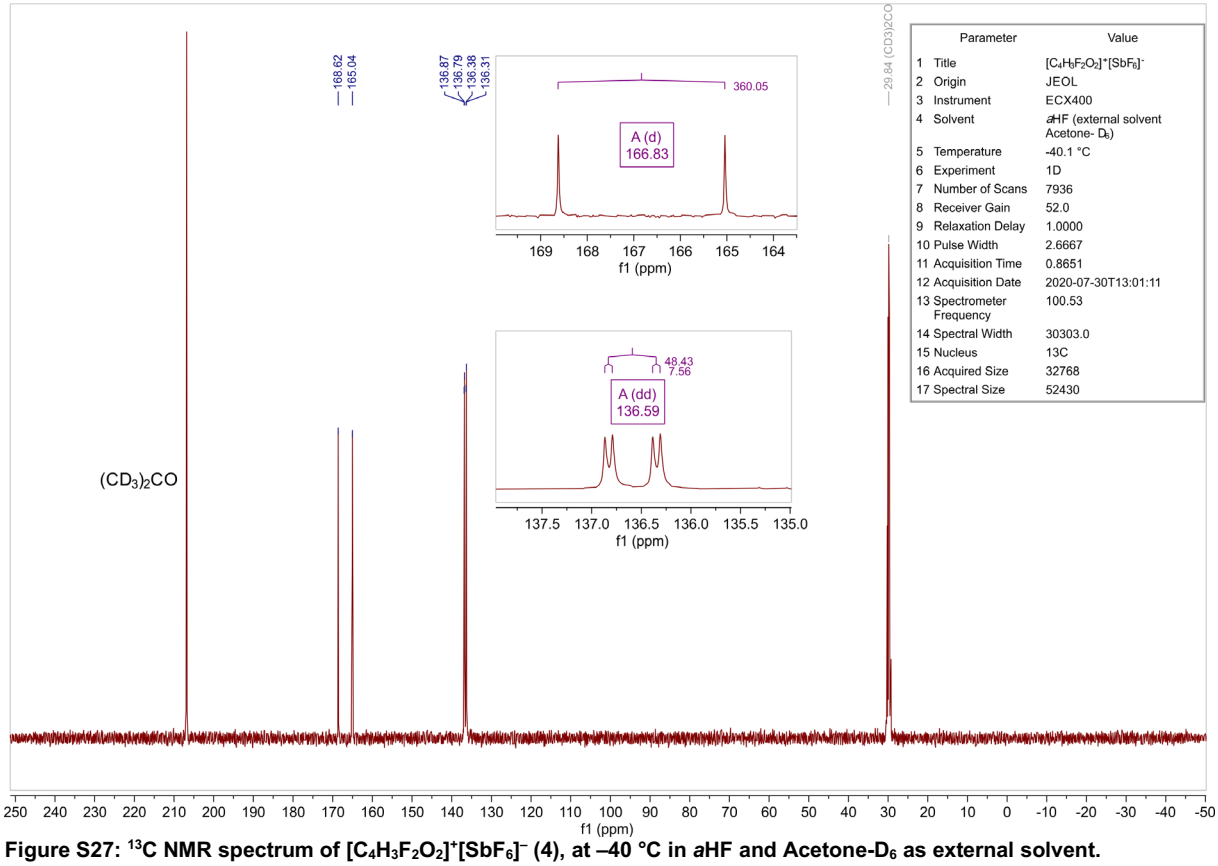

Figure S27: ^{13}C NMR spectrum of $[C_4H_3F_2O_2]^+[SbF_6]^-$ (4), at –40 °C in *a*HF and Acetone-D_6 as external solvent.

Table S9: Calculated bond lengths and angles of the free cation $[C_4H_4F_2O_2]^{2+}$ and the HF complex of the cation $[C_4H_4F_2O_2 \cdot 2\ HF]^{2+}$ in comparison with the experimental structural parameters of $[C_4H_4F_2O_2]^{2+}([AsF_6]^-)_2$ (1). The estimated standard deviation is marked in parentheses. Symmetry operations: *i = 1–x, y, 0.5–z*.

	Free cation[a] $[C_4H_4F_2O_2]^{2+}$	HF complex of the cation[a] $[C_4H_4F_2O_2 \cdot 2\ HF]^{2+}$	Crystal structure of $[C_4H_4F_2O_2]^{2+}([AsF_6]^-)_2$ **(1)**	
Bond length [Å]				
C1–F1	1.267	1.278	C1–F1 (C–F)	1.281(2)
C1–O1	1.254	1.240	C1–O1 (C=O)	1.223(2)
C1–C2	1.471	1.471	C1–C2 (C–C)	1.465(2)
C2–C3	1.342	1.339	C2–C2*i* (C=C)	1.330(3)
C3–C4	1.471	1.471		
C4–F2	1.267	1.278		
C4–O2	1.254	1.240		
Bond angle [°]				
O1–C1–F1	120.5	120.6	O1–C1–F1	120.2(2)
O1–C1–C2	122.3	123.4	O1–C1–C2	123.4(2)
F1–C1–C2	117.2	116.0	F1–C1–C2	116.4(2)
C1–C2–C3	121.3	121.2	C1–C2–C2*i*	119.1(2)
O2–C4–F2	120.5	120.6		
O2–C4–C3	122.3	123.4		
F2–C4–C3	117.2	116.0		
C2–C3–C4	121.3	121.2		
Angle of torsion [°]				
O1–C1–C2–C3	0.0	0.0	O1–C1–C2–C2*i*	9.5(2)
F1–C1–C2–C3	–180.0	–180.0	F1–C1–C2–C2*i*	–169.7(1)
O2–C4–C3–C2	0.0	0.0		
F2–C4–C3–C2	–180.0	–180.0		

[a] Calculated at the B3LYP/aug-cc-pVTZ level of theory.

Table S10: Selected experimental vibrational frequencies [cm^{-1}] of $[C_4H_4F_2O_2]^{2+}([AsF_6]^-)_2$ (1) and calculated vibrational frequencies [cm^{-1}] of $[C_4H_4F_2O_2]^{2+}$ and $[C_4H_4F_2O_2 \cdot 2\ HF]^{2+}$.

$[C_4H_4F_2O_2]^{2+}([AsF_6]^-)_2$ **(1)** exp.[a]		$[C_4H_4F_2O_2]^{2+}$ calc.[b]	$[C_4H_4F_2O_2 \cdot 2\ HF]^{2+}$ calc.[b]	Assignment
IR	Raman	IR/Raman	IR/Raman	
3109 vs		3181 (82/0)	3190 (60/0)	ν_{as}(C–H)
	3098 (24)	3179 (0/74)	3188 (0/79)	ν_s(C–H)
3182 vs		3494 (1286/0)	2490 (7585/0)	ν_{as}(O–H)
	1717 (49)	1654 (0/222)	1713 (0/8)	ν_s(C=O)
	1625 (42)	1696 (0/81)	1685 (0/384)	ν(C=C)
1641 m		1646 (510/0)	1681 (816/0)	ν_{as}(C=O)
1450 m		1486 (1020/0)	1485 (717/0)	ν_{as}(C–F)
	1441 (8)	1470 (0/3)	1454 (0/4)	ν_s(C–F)
	1304 (38)	1328 (0/18)	1337 (0/7)	δ_s(CCH)
1317 w		1284 (33/0)	1302 (323/0)	δ_{as}(CCH)
	1244 (20)	1140 (0/24)	1280 (0/38)	δ_s(COH)
1263 m		1130 (307/0)	1252 (216/0)	δ_{as}(COH)
1153 w		703 (201/0)	1023 (240/0)	γ_{as}(COH)
	946 (24)	987 (0/7)	995 (0/6)	ν_s(C–C)
	896 (23)	947 (0/3)	948 (0/4)	γ_s(HCCH)
926 w		920 (85/0)	933 (127/0)	ν_{as}(C–C)
	693 (19)	649 (0/9)	712 (0/11)	δ_s(COF)
673 m		575 (83/0)	647 (56/0)	δ_{as}(COF)
	608 (8)	593 (0/0)	625 (0/1)	γ_s(CCOF)

[a] Abbrevations for IR intensities: v = very, s = strong, m = medium, w = weak. IR intensities in km/mol; Raman intensities in Å^4/u. Experimental Raman activities are relative to a scale of 1 to 100.

[b] Calculated on the B3LYP/aug-cc-pVTZ level of theory.

Table S11: Calculated bond lengths and angles of the free cation $[C_4H_3F_2O_2]^+$ and the HF complex of the cation $[C_4H_3F_2O_2 \cdot HF]^+$ in comparison with the experimental structural parameters of $[C_4H_3F_2O_2]^+[SbF_6]^-$ (4). The estimated standard deviation is marked in parentheses.

	Free cation[a] $[C_4H_3F_2O_2]^+$	HF complex of the cation[a] $[C_4H_3F_2O_2 \cdot HF]^+$	Crystal structure of $[C_4H_3F_2O_2]^+[SbF_6]^-$ **(4)**	
Bond length [Å]				
C2–C3	1.347	1.344	C2–C3	1.334(7)
C1–C2	1.492	1.491	C1–C2	1.476(8)
C3–C4	1.422	1.429	C3–C4	1.454(7)
C1–O1	1.180	1.180	C1–O1	1.187(6)
C4–O2	1.269	1.257	C4–O2	1.239(6)
C1–F1	1.337	1.340	C1–F1	1.332(6)
C4–F2	1.288	1.292	C4–F2	1.285(6)
Bond angle [°]				
O1–C1–F1	123.9	123.5	O1–C1–F1	120.7(5)
O2–C4–F2	117.6	118.0	O2–C4–F2	118.6(4)
O1–C1–C2	123.9	124.2	O1–C1–C2	126.4(5)
O2–C4–C3	121.2	121.7	O2–C4–C3	122.5(5)
F1–C1–C2	112.2	112.2	F1–C1–C2	112.9(4)
F2–C4–C3	121.3	120.2	F2–C4–C3	118.9(4)
C1–C2–C3	123.0	123.1	C1–C2–C3	122.1(5)
C4–C3–C2	120.7	121.0	C4–C3–C2	118.6(5)
Angle of torsion [°]				
O1–C1–C2–C3	179.9	–180.0	O1–C1–C2–C3	–174.5(5)
O2–C4–C3–C2	180.0	–180.0	O2–C4–C3–C2	172.1(5)
F1–C1–C2–C3	–0.1	0.0	F1–C1–C2–C3	7.1(7)
F2–C4–C3–C2	–0.0	0.0	F2–C4–C3–C2	–6.2(7)
C1–C2–C3–C4	–180.0	180.0	C1–C2–C3–C4	–177.1(5)

[a] Calculated at the B3LYP/aug-cc-pVTZ level of theory.

Table S12: Crystal data and structure refinement of $[C_4H_4F_2O_2]^{2+}([AsF_6]^-)_2$ (1), $[C_4H_4F_2O_2]^{2+}([SbF_6]^-)_2$ (2) and $[C_4H_3F_2O_2]^+[SbF_6]^-$ (4).

	$[C_4H_4F_2O_2]^{2+}([AsF_6]^-)_2$ **(1)**	$[C_4H_4F_2O_2]^{2+}([SbF_6]^-)_2$ **(2)**	$[C_4H_3F_2O_2]^+[SbF_6]^-$ **(4)**
Molecular Formula	$C_4H_4As_2F_{14}O_2$	$C_4H_4F_{14}O_2Sb_2$	$C_4H_3F_8O_2Sb$
M_r[g·mol^{-1}]	499.91	593.57	356.82
Crystal size [mm^3]	0.44 x 0.18 x 0.04	0.18 x 0.15 x 0.14	0.309 x 0.261 x 0.136
Crystal system	orthorhombic	monoclinic	monoclinic
Space group	*Pbcn*	$P2_1/c$	*Cc*
a [Å]	9.4255(3)	5.3576(2)	5.5007(5)
b [Å]	7.6954(2)	8.0884(3)	17.9058(13)
c [Å]	17.0276(6)	15.3046(6)	8.9660(6)
α [°]	90	90	90
β [°]	90	97.603(4)	96.007(7)
γ [°]	90	90	90
V [A^3]	1235.06(7)	657.39(4)	878.25(12)
Z	4	2	4
ρ_{calc} [g·cm^{-3}]	2.689	2.999	2.699
μ [mm^{-1}]	5.595	4.282	3.254
$\lambda_{MoK\alpha}$ [Å]	0.71073	0.71073	0.71073
F(000)	944	544	664
T [K]	109(2)	112(2)	293(2)
h, k, l range	–13:14; –11:11; –24:24	–7:7; –12:12; –19:22	–8:8; –27:26; –13:13
Measured reflexes	11992	6711	8944
Unique reflexes	2087	2188	2950
R_{int}	0.0266	0.0342	0.0300
Parameters	103	103	138
R(F)/wR(F^2)[a)] (all data)	0.0286/0.0510	0.0432/0.0702	0.0297/0.0556
Weighting scheme[b)]	0.021000/0.760500	0.030100	0.027300/0.235600
S (Gof)[c)]	1.065	1.087	1.049
Residual density [e·Å^{-3}]	0.555/–0.545	2.978/–0.859	0.763/–0.470
Device	Oxford XCalibur	Oxford XCalibur	Oxford XCalibur
CCDC	2065273	2065274	2065275

[a)] $R_1 = \Sigma||F_o|-|F_c||/\Sigma|F_o|$;
[b)] $wR_2 = [\Sigma[w(F_o^2-F_c^2)^2]/\Sigma[w(F_o)^2]]^{1/2}$; $w = [\sigma_c^2(F_o^2)+(xP)^2+yP]^{-1}$; $P = (F_o^2+2F_c^2)/3$
[c)] GoF = $\{\Sigma[w(F_o^2-F_c^2)^2]/(n-p)\}^{1/2}$ (n = number of reflexions; p = total number of parameters).

Table S13: Cartesian coordinates of calculated minimum structures of $[C_4H_4F_2O_2 \cdot 2\ HF]^{2+}$ at the B3LYP/aug-cc-pVTZ level of theory.

Atom	x	y	z
F	0.000013377	–0.000000413	0.000042976
F	–0.000003126	–0.000004837	–0.000004708
O	–0.000029351	–0.000015410	–0.000039845
C	0.000025460	0.000015901	0.000022157
C	0.000021739	–0.000000957	0.000003606
H	–0.000015723	–0.000000449	–0.000007002
H	0.000009037	0.000003322	0.000022123
F	–0.000000030	0.000005764	0.000005868
O	0.000036465	0.000017531	0.000000629
C	–0.000034905	–0.000004712	–0.000032434
C	–0.000020536	–0.000005824	0.000001747
H	0.000015001	0.000000877	0.000006768
H	0.000007038	–0.000017021	0.000027575
F	0.000001120	0.000005147	–0.000010942
H	–0.000024590	0.000002658	–0.000037630
H	–0.000000977	–0.000001577	–0.000000888

Table S14: Cartesian coordinates of calculated minimum structures of $[C_4H_4F_2O_2]^{2+}$ at the B3LYP/aug-cc-pVTZ level of theory.

Atom	x	y	z
F	0.000008196	0.000000586	–0.000022814
O	–0.000015896	0.000001265	0.000199621
C	0.000055132	0.000000972	0.000060027
C	0.000282106	–0.000005391	–0.000002706
H	–0.000195442	0.000005197	–0.000071303
H	–0.000024940	–0.000002629	–0.000228923
F	–0.000008196	0.000000586	0.000022814
O	0.000015896	0.000001265	–0.000199621
C	–0.000055132	0.000000972	–0.000060027
C	–0.000282106	–0.000005391	0.000002706
H	0.000195442	0.000005197	0.000071303
H	0.000024940	–0.000002629	0.000228923

Table S15: Cartesian coordinates of calculated minimum structures of $[C_4H_2D_2F_2O_2 \cdot 2\ HF]^{2+}$ at the B3LYP/aug-cc-pVTZ level of theory.

Atom	x	y	z
F	0.000013507	0.000017541	0.000002734
F	–0.000001060	0.000002156	–0.000000597
O	–0.000009266	–0.000012576	0.000007513
C	0.000007268	0.000007375	0.000006902
C	0.000001417	0.000008364	–0.000004810
H	–0.000001451	–0.000005016	–0.000000170
D	0.000000848	0.000006839	–0.000012522
F	0.000001605	–0.000001406	–0.000001038
O	0.000003976	0.000017293	–0.000008303
C	–0.000012506	–0.000015302	0.000001512
C	0.000000882	–0.000007256	0.000002060
H	0.000001266	0.000004649	–0.000000600
D	0.000001035	–0.000005295	0.000008761
F	0.000002482	–0.000000823	–0.000002388
H	–0.000009827	–0.000013328	0.000000627
H	–0.000000177	–0.000003216	0.000000318

Table S16: Cartesian coordinates of calculated minimum structures of $[C_4H_3F_2O_2 \cdot HF]^+$ at the B3LYP/aug-cc-pVTZ level of theory.

Atom	x	y	z
F	–0.000004615	–0.000026454	0.000062575
F	0.000002273	0.000002094	0.000002459
F	0.000000584	–0.000001197	–0.000001043
O	0.000000556	–0.000029763	0.000123924
H	–0.000000662	0.000051268	–0.000194542
O	0.000002181	–0.000000945	0.000002396
C	0.000000366	–0.000007563	–0.000007871
C	0.000002634	0.000000807	0.000002265
C	–0.000003282	–0.000002258	–0.000003301
H	0.000004871	–0.000000044	0.000000677
C	0.000001780	0.000004404	0.000006324
H	–0.000002177	0.000002173	–0.000001037
H	–0.000004509	0.000007477	0.000007172

Table S17: Cartesian coordinates of calculated minimum structures of $[C_4H_3F_2O_2]^+$ at the B3LYP/aug-cc-pVTZ level of theory.

Atom	x	y	z
C	0.000001589	0.000011539	0.000020116
H	0.000006770	0.000000449	–0.000002211
C	0.000002711	0.000000591	–0.000057211
H	0.000002476	0.000005970	0.000022150
C	0.000008598	–0.000032851	–0.000008687
C	0.000042868	–0.000076509	0.000010641
O	–0.000013294	0.000029042	0.000002599
F	–0.000009391	–0.000000637	0.000003279
F	–0.000030296	0.000058047	0.000004921
O	–0.000006734	0.000017732	0.000004546
H	–0.000005297	–0.000013371	–0.000000142

[1] M. C. Bayer, C. Jessen, A. J. Kornath, *Z. Anorg. Allg. Chem.* **2021**, *647*, 258.